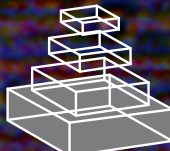


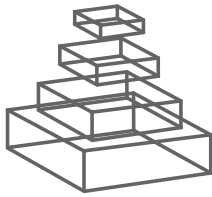
frontiers RESEARCH TOPICS

PROTEIN ENGINEERING AND
OTHER BIO-SYNTHETIC ROUTES
FOR BIO-BASED MATERIALS:
CURRENT USES AND POTENTIAL
APPLICATIONS

Topic Editor
Carissa M. Soto



frontiers in
CHEMISTRY



FRONTIERS COPYRIGHT STATEMENT

© Copyright 2007-2014
Frontiers Media SA.
All rights reserved.

All content included on this site, such as text, graphics, logos, button icons, images, video/audio clips, downloads, data compilations and software, is the property of or is licensed to Frontiers Media SA ("Frontiers") or its licensees and/or subcontractors. The copyright in the text of individual articles is the property of their respective authors, subject to a license granted to Frontiers.

The compilation of articles constituting this e-book, wherever published, as well as the compilation of all other content on this site, is the exclusive property of Frontiers. For the conditions for downloading and copying of e-books from Frontiers' website, please see the Terms for Website Use. If purchasing Frontiers e-books from other websites or sources, the conditions of the website concerned apply.

Images and graphics not forming part of user-contributed materials may not be downloaded or copied without permission.

Individual articles may be downloaded and reproduced in accordance with the principles of the CC-BY licence subject to any copyright or other notices. They may not be re-sold as an e-book.

As author or other contributor you grant a CC-BY licence to others to reproduce your articles, including any graphics and third-party materials supplied by you, in accordance with the Conditions for Website Use and subject to any copyright notices which you include in connection with your articles and materials.

All copyright, and all rights therein, are protected by national and international copyright laws.

The above represents a summary only. For the full conditions see the Conditions for Authors and the Conditions for Website Use.

ISSN 1664-8714
ISBN 978-2-88919-395-0
DOI 10.3389/978-2-88919-395-0

ABOUT FRONTIERS

Frontiers is more than just an open-access publisher of scholarly articles: it is a pioneering approach to the world of academia, radically improving the way scholarly research is managed. The grand vision of Frontiers is a world where all people have an equal opportunity to seek, share and generate knowledge. Frontiers provides immediate and permanent online open access to all its publications, but this alone is not enough to realize our grand goals.

FRONTIERS JOURNAL SERIES

The Frontiers Journal Series is a multi-tier and interdisciplinary set of open-access, online journals, promising a paradigm shift from the current review, selection and dissemination processes in academic publishing.

All Frontiers journals are driven by researchers for researchers; therefore, they constitute a service to the scholarly community. At the same time, the Frontiers Journal Series operates on a revolutionary invention, the tiered publishing system, initially addressing specific communities of scholars, and gradually climbing up to broader public understanding, thus serving the interests of the lay society, too.

DEDICATION TO QUALITY

Each Frontiers article is a landmark of the highest quality, thanks to genuinely collaborative interactions between authors and review editors, who include some of the world's best academicians. Research must be certified by peers before entering a stream of knowledge that may eventually reach the public - and shape society; therefore, Frontiers only applies the most rigorous and unbiased reviews.

Frontiers revolutionizes research publishing by freely delivering the most outstanding research, evaluated with no bias from both the academic and social point of view.

By applying the most advanced information technologies, Frontiers is catapulting scholarly publishing into a new generation.

WHAT ARE FRONTIERS RESEARCH TOPICS?

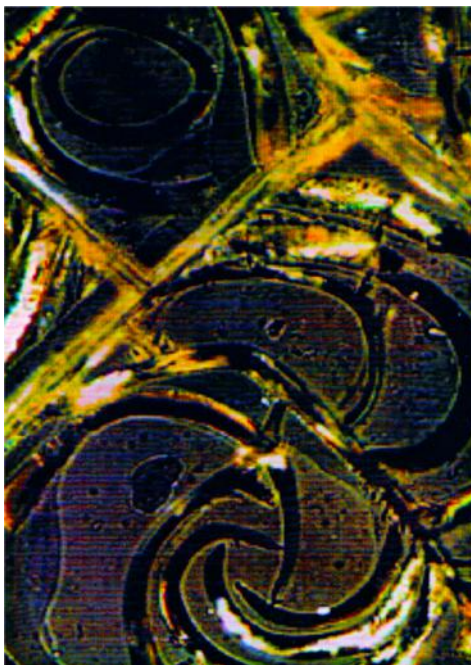
Frontiers Research Topics are very popular trademarks of the Frontiers Journals Series: they are collections of at least ten articles, all centered on a particular subject. With their unique mix of varied contributions from Original Research to Review Articles, Frontiers Research Topics unify the most influential researchers, the latest key findings and historical advances in a hot research area!

Find out more on how to host your own Frontiers Research Topic or contribute to one as an author by contacting the Frontiers Editorial Office: researchtopics@frontiersin.org

PROTEIN ENGINEERING AND OTHER BIO-SYNTHETIC ROUTES FOR BIO-BASED MATERIALS: CURRENT USES AND POTENTIAL APPLICATIONS

Topic Editor:

Carissa M. Soto, Center for Bio/Molecular Science and Engineering, U. S. Naval Research Laboratory, USA



Polarized optical micrograph of monodisperse poly(β -benzyl α , L-aspartate).

In the past 20 years protein engineering has been used for the production of proteins mostly for biological applications. The incorporation of artificial amino acids and chemical handles into proteins had made possible the design and production of protein-based materials like hybrid inorganic-organic materials, smart/responsive materials, monodisperse polymers, and nanoscale assemblies. In the current topic, we cover current uses and envision future applications of materials generated using protein engineering and biosynthesis techniques.

I would like to acknowledge the U.S. Office of Naval Research for financial support and Dr. Cherise Bernard for her contributions during the early stages of the Research Topic.

Table of Contents

- 04 Protein Engineering and Other Bio-Synthetic Routes for Bio-Based Materials: Current Uses and Potential Applications**
Carissa M. Soto
- 06 Basic Research Opportunities Focused on Bio-Based and Bio-Inspired Materials and Potential Applications**
Stephanie A. Nick McElhinny and Jennifer J. Becker
- 09 Controlling Topological Entanglement in Engineered Protein Hydrogels with a Variety of Thiol Coupling Chemistries**
Shengchang Tang and Bradley D. Olsen
- 20 Transient Dynamic Mechanical Analysis of Resilin-Based Elastomeric Hydrogels**
Linqing Li and Kristi L. Kiick
- 33 Engineered Recombinant Bacterial Collagen as an Alternative Collagen-Based Biomaterial for Tissue Engineering**
Bo An, David L. Kaplan and Barbara Brodsky
- 38 Three-Layer Microfibrous Peripheral Nerve Guide Conduit Composed of Elastin-Laminin Mimetic Artificial Protein and Poly(L-Lactic Acid)**
Sachiro Kakinoki, Midori Nakayama, Toshiyuki Moritan and Tetsuji Yamaoka
- 46 RGD-Conjugated Rod-Like Viral Nanoparticles on 2D Scaffold Improved Bone Differentiation of Mesenchymal Stem Cells**
Pongkwan Sitasuwan, L. Andrew Lee, Kai Li, Huong Giang Nguyen and Qian Wang
- 54 Covalent Modification of a Ten-Residue Cationic Antimicrobial Peptide with Levofloxacin**
Carlos A. Rodriguez, Emilios A. Papanastasiou, Melanie Juba and Barney Bishop
- 66 Magnetic Biocatalysts and their Uses to Obtain Biodiesel and Biosurfactants**
Carmen López, Álvaro Cruz-Izquierdo, Enrique A. Picó, Teresa García-Bárcena, Noelia Villarroel, María J. Llama and Juan L. Serra
- 77 Development of Organophosphate Hydrolase Activity in a Bacterial Homolog of Human Cholinesterase**
Patricia M. Legler, Susanne M. Boisvert, Jaimee R. Compton and Charles B. Millard
- 92 The Emergence of Clostridium Thermocellum as a High Utility Candidate for Consolidated Bioprocessing Applications**
Hannah Akinoshio, Kelsey Yee, Dan Close and Arthur Ragauskas
- 110 Delivery of Chemical Cargo to Endogenous Proteins on Live Cells**
James J. Chambers
- 114 Non-Standard Amino Acid Incorporation into Proteins Using Escherichia Coli Cell-Free Protein Synthesis**
Seok Hoon Hong, Yong-Chan Kwon and Michael C. Jewett



Protein engineering and other bio-synthetic routes for bio-based materials: current uses and potential applications

Carissa M. Soto *

U. S. Naval Research Laboratory, Center for Bio/Molecular Science and Engineering, Washington, DC, USA

*Correspondence: carissa.soto@nrl.navy.mil

Edited by:

John Wade, Florey Institute of Neuroscience and Mental Health, Australia

Reviewed by:

Laszlo Otvos, OLPE, LLC, USA

Keywords: hydrogels, biocatalysis, human cholinesterase, bacterial collagen, biomass degradation

Since the pioneer work of Stanley Cohen, Herbert Boyer and their collaborators almost 40 years ago (Cohen et al., 1973), genetic engineering had advanced greatly. The tools and resources available to the genetic engineer open new opportunities in genome engineering (Carr and Church, 2009) and synthetic biology (Lu et al., 2009). But still much needs to be done to build and control biological systems. In the current Research Topic, we focus on the synthesis of bio-based materials employing the basic principles of genetic engineering. The rationale of utilizing biosynthesis as a route for material production relies on the capability of the biological machinery to produce macromolecules of well-defined sequence, stereochemistry, and size. The specific location of the chemical groups in a given bio-macromolecule is critical to its structure and ultimately its biological function. Protein engineering has emerged as a strong tool to produce proteins in large scale with high fidelity. In the context of the current Research Topic we refer to such protein products as bio/macromolecules, nanostructures, biologicals or precursors produced in a bio-based environment. The topic is designed to present several approaches to biosynthesis, not limited to the production of a target protein in a bacterial host.

At first, I would like to direct the readers to an opinion article that presents a broad perspective of the field of bio-based and bio-inspired materials (Nick McElhinny and Becker, 2014). Following their theme, most of the articles in the current Research Topic fit in the category of *Using Biology as a Material*. For example, several original research papers report the utilization of genetically-engineered proteins to obtain materials for various applications such as: tunable hydrogels (Tang and Olsen, 2014), hydrogels for mechanically active tissues (Li and Kiick, 2014), bacterial collagen for tissue engineering (An et al., 2014), and microfibers for nerve guide conduits (Kakinoki et al., 2014). Plant viruses (Pongkwan et al., 2014) and antimicrobial peptides (Rodriguez et al., 2014) are the starting bio-based materials to incorporate new functionalities by well-known chemical methods. In the field of biocatalysis, immobilized enzymes are used for industry-scale production of bioproducts (López et al., 2014) and bacterial homologs of human cholinesterase (Legler et al., 2014) are engineered in the

laboratory setting with the aim of using them as a therapeutic enzyme.

From the materials science perspective, one can easily envision using a biological organism guided by well-established biotechnology techniques to generate a single product. However, the biological environment still has more to offer. An example is described in the review article where *Clostridium thermocellum* is presented as a strong candidate in bioprocessing applications. The system attributes are due to its unique, multivariate enzyme cellulosome complex and its role during biomass degradation (Akinoshio et al., 2014). Studies of complex cellular processes without disturbing natural biological events (Chambers, 2014) are needed to expand our knowledge and ultimately to facilitate the engineering of biological systems for our benefit. Lastly, a new paradigm is presented in which bio-building blocks and non-standard amino acids are utilized in a cell-free environment (Hong et al., 2014). While others incorporate artificial amino acids into protein products using cell-based biosynthesis strategies, having a cell-free environment offers alternatives to new applications where a cell-free environment is more desirable. We can imagine using a cell-free environment for the biosynthesis of more complex systems where biomacromolecules are produced in a concerted way to control synthesis and/or assembly.

There is no doubt that bio-based products provide a rich toolbox with a great potential for a wide variety of applications as presented in the current Research Topic. Taking a multidisciplinary approach, combining knowledge from biology, chemistry, and materials science to produce complex materials is crucial to succeed in this field. Still challenges exist for the utilization of bio-based materials in main stream industrial production. Public acceptance and cost effectiveness will be key elements in engaging the industry into adapting these new biosynthetic strategies as alternatives to classical chemical synthetic routes. For example, one general public concern on using plants to produce materials is the limitation in arable land and fresh water which are needed to fulfill future demands on food for a constantly increasing population (Ronald, 2011). Furthermore, genetic engineering can be of a great concern if the engineered systems are delivered to the environment causing a spread of un-desirable traits

or antibiotic resistant bacterial strains. In spite of such concerns, major advances in the production of biopolymers at the industrial scale are already implemented by major bioplastics producers (Smith, 2012). Proper engineer controls must be implemented to avoid *biological contamination* similarly as chemicals production is tightly regulated. As the field advances and we increase our understanding of biological synthetic platforms and our ability to engineer those systems improves, we should be able to generate materials previously not imaginable.

ACKNOWLEDGMENTS

The author acknowledges the Office of Naval Research for financial support under 6.1 NRL internal basic research funds and Dr. Walter Dressick for his comments on the editorial note.

REFERENCES

- Akinoshio, H., Yee, K., Close, D., and Ragauskas, A. (2014). The emergence of *Clostridium thermocellum* as a high utility candidate for consolidated bioprocessing applications. *Front. Chem.* 2:66. doi: 10.3389/fchem.2014.00066
- An, B., Kaplan, D. L., and Brodsky, B. (2014). Engineered recombinant bacterial collagen as an alternative collagen-based biomaterial for tissue engineering. *Front. Chem.* 2:40. doi: 10.3389/fchem.2014.00040
- Carr, P. A., and Church, G. M. (2009). Genome engineering. *Nat. Biotechnol.* 27, 1151. doi: 10.1038/nbt1590
- Chambers, J. J. (2014). Delivery of chemical cargo to endogenous proteins on live cells. *Front. Chem.* 2:11. doi: 10.3389/fchem.2014.00011
- Cohen, S. N., Chang, A. C. Y., Boyer, H. W., and Helling, R. B. (1973). Construction of biologically functional bacterial plasmids *in vitro*. *Proc. Natl. Acad. Sci. U.S.A.* 70, 3240–3244.
- Hong, S. H., Kwon, Y.-C., and Jewett, M. C. (2014). Non-standard amino acid incorporation into proteins using *Escherichia coli* cell-free protein synthesis. *Front. Chem.* 2:34. doi: 10.3389/fchem.2014.00034
- Kakinoki, S., Nakayama, M., Moritan, T., and Yamaoka, T. (2014). Three-layer microfibrous peripheral nerve guide conduit composed of elastin-laminin mimetic artificial protein and poly(L-lactic acid). *Front. Chem.* 2:52. doi: 10.3389/fchem.2014.00052
- Legler, P. M., Boisvert, S. M., Compton, J. R., and Millard, C. B. (2014). Development of organophosphate hydrolase activity in a bacterial homolog of human cholinesterase. *Front. Chem.* 2:46. doi: 10.3389/fchem.2014.00046
- Li, L., and Kiick, K. L. (2014). Transient dynamic mechanical analysis of resilin-based elastomeric hydrogels. *Front. Chem.* 2:21. doi: 10.3389/fchem.2014.00021
- López, C., Cruz-Izquierdo, Á., Picó, E. A., García-Bárcena, T., Villarroel, N., Llama, M. J., et al. (2014). Magnetic biocatalysts and their uses to obtain biodiesel and biosurfactants. *Front. Chem.* 2:72. doi: 10.3389/fchem.2014.00072
- Lu, T. K., Khalil, A. S., and Collins, J. J. (2009). Next-generation synthetic gene networks. *Nat. Biotechnol.* 27, 1139. doi: 10.1038/nbt1591
- Nick McElhinny, S. A., and Becker, J. J. (2014). Basic research opportunities focused on bio-based and bio-inspired materials and potential applications. *Front. Chem.* 2:24. doi: 10.3389/fchem.2014.00024
- Pongkwan, S., Lee, L. A., Li, K., Nguyen, H. G., and Wang, Q. (2014). RGD-conjugated rod-like viral nanoparticles on 2D scaffold improve bone differentiation of mesenchymal stem cells. *Front. Chem.* 2:31. doi: 10.3389/fchem.2014.00031
- Rodriguez, C. A., Papanastasiou, E. A., Juba, M., and Bishop, B. (2014). Covalent modification of a ten-residue cationic antimicrobial peptide with levofloxacin. *Front. Chem.* 2:71. doi: 10.3389/fchem.2014.00071
- Ronald, P. (2011). Plant genetics, sustainable agriculture and global food security. *Genetics* 188, 11. doi: 10.1534/genetics.111.128553
- Smith, C. (2012). Why green plastics are here to stay. *Compound. World*. Available online at: <http://content.yudu.com/A1xfaf2/CompoundinWorldJun12/resources/44.htm>
- Tang, S., and Olsen, B. D. (2014). Controlling topological entanglement in engineered protein hydrogels with a variety of thiol coupling chemistries. *Front. Chem.* 2:23. doi: 10.3389/fchem.2014.00023

Conflict of Interest Statement: The author declares that the research was conducted in the absence of any commercial or financial relationships that could be construed as a potential conflict of interest.

Received: 04 September 2014; accepted: 19 September 2014; published online: 13 October 2014.

Citation: Soto CM (2014) Protein engineering and other bio-synthetic routes for bio-based materials: current uses and potential applications. *Front. Chem.* 2:83. doi: 10.3389/fchem.2014.00083

This article was submitted to Chemical Biology, a section of the journal *Frontiers in Chemistry*.

Copyright © 2014 Soto. This is an open-access article distributed under the terms of the Creative Commons Attribution License (CC BY). The use, distribution or reproduction in other forums is permitted, provided the original author(s) or licensor are credited and that the original publication in this journal is cited, in accordance with accepted academic practice. No use, distribution or reproduction is permitted which does not comply with these terms.



Basic research opportunities focused on bio-based and bio-inspired materials and potential applications

Stephanie A. Nick McElhinny* and **Jennifer J. Becker**

U.S. Army Research Office, Research Triangle Park, NC, USA

*Correspondence: stephanie.a.mcelhinny.civ@mail.mil

Edited by:

Carissa M. Soto, Naval Research Laboratory, USA

Reviewed by:

Vincent Conticello, Emory University, USA

Keywords: bio-based materials, bio-inspired materials, hybrid materials, biomimetic systems, basic research

The U.S. Army Research Office (ARO) serves as the Army's premier extramural basic research agency in the engineering, physical, information and life sciences. ARO drives the national basic research agenda and programs in these areas to create new scientific discoveries and increase knowledge through high-risk, high-payoff research opportunities with academia and industry. ARO also ensures that the results of these efforts are made available to the Army research and development community for the pursuit of long-term technological applications. ARO is supporting emerging research opportunities in the areas of bio-based and bio-inspired materials that focus on four primary goals: (i) Using biology to produce materials, (ii) Using biology as a material, (iii) Integrating biology with synthetic materials, and (iv) Imparting properties inherent in biological systems to materials.

USING BIOLOGY TO PRODUCE BIOLOGICAL, NON-BIOLOGICAL, AND HYBRID MATERIALS

Biological organisms have evolved complex synthetic capabilities that are often unrivaled, if not impossible, by traditional chemical approaches, with products ranging from small molecule chemicals to biological polymers to macromolecular assemblies with complex catalytic or mechanical activities to metallic and semiconductor nanoparticles. In addition to the many valuable products naturally produced by biological systems, such as the chemotherapeutic agent Taxol produced by an endophytic fungus living within the bark of the Pacific Yew tree, biological systems are also being engineered to produce

specific products of interest. From the advent of genetic engineering approaches in the 1970s to the recent emergence of the field of synthetic biology, the research community continues to push the boundaries of biological engineering and the complexity of the products that are synthesized by biological systems.

The capability to efficiently produce valuable chemicals and materials using biological systems is particularly desirable due to the mild synthesis conditions and general lack of toxic byproducts. Biological synthetic platforms are also conducive to the design and production of hybrid products that contain both biological and non-biological elements. Currently supported research is focused on engineering microorganisms to incorporate unnatural amino acids into protein polymer chains. Successful efforts could enable the production of hybrid polymers that contain strategically located biological functional groups to endow materials produced from these polymers with specific recognition or reactive functions. Such strain engineering also opens the possibility to one day produce traditional chemical polymers in a biological system with control over monomer sequence—a fundamental characteristic of biological polymers such as DNA, RNA, and proteins that has remained elusive for non-biological polymers.

The potential applications of biologically produced materials could be vast, depending on the types of materials that can be made and the quantities of these materials that can be reliably produced. Biological production platforms could be optimized to produce naturally occurring products, including therapeutic

compounds, alternative fuels or enzymes. Engineered biological systems could produce hybrid products with both biological and non-biological elements, leading to materials with both traditionally desirable properties, such as high strength and stability, as well as biological functionality, such as molecular recognition or enzymatic reactivity. Engineered biological systems also hold potential to produce entirely novel products not yet imagined, with the type of advanced genetic pathway design and assembly envisioned by the DARPA Living Foundries program.

USING BIOLOGY AS A MATERIAL

Biological molecules and macromolecular assemblies form intricate and precise architectures at the nano- and micro-scale with nanometer resolution of structural features. This level of precision is not yet accessible with traditional top-down fabrication approaches, providing an opportunity to utilize biological assemblies as materials themselves.

DNA nanotechnology enables the production of precisely designed nanometer and micron scale 2D and 3D structures with complex features including curvature and inner channels and cavities, and recent advances provide novel assembly approaches to "carve" precise 3D structures from a "molecular canvas" of DNA (Ke et al., 2012). As a material, DNA nanostructures could be used as templates to organize functional elements with control over spatial orientation at the nanometer scale or as a "mold" for the production of inorganic materials with nano scale features. A major research program is currently exploring the use of DNA nanostructures as a surrogate for the 3D

spatial control of the cellular environment to promote the activity of a biochemical pathway in an *in vitro* setting. DNA nanostructures have also been used to design molecular machines and have potential applications in molecular scale electronics and targeted drug delivery.

Proteins also assemble into organized structures that can be utilized as materials. Perhaps one of the most well-known protein-based materials is the protein fiber. Many different proteins assemble into fibers and fibrils, including collagen, elastin, silk, and amyloid proteins, with each protein fiber exhibiting unique material properties. Amyloid fibrils have been used as a nanoscaffold for enzyme immobilization and stabilization. Glucose oxidase and organophosphate hydrolase have been successfully immobilized onto amyloid fibrils and demonstrated an increase in thermal stability while maintaining activity (Pilkington et al., 2010; Raynes et al., 2011). Proteins also assemble into complex 3D structures, including viral capsids which vary dramatically in size and shape, and have potential to be used as molecular delivery vessels or templates for the ordered display of functional elements. Currently supported research is exploring the Tobacco mosaic virus as a biological building block for engineered systems. This nanotube-shaped virus may be genetically and chemically modified to tailor its physical properties and is compatible with some conventional microfabrication processes (Fan et al., 2013).

INTEGRATING BIOLOGY WITH SYNTHETIC MATERIALS

An ability to integrate biological elements with synthetic materials may enable systems that marry the specificity and reactivity of biology with the stability and predictability of synthetic material systems. Integrating these two worlds is no simple task, and major research programs are focusing on elucidating key elements that support retention of biological structure and function when these two material classes are merged.

A significant effort is focused on understanding the interactions at the interface between immobilized proteins and a chemical surface, and how the chemical and physical environment at this interface impacts biological structure and

function. Future applications that could be realized by scientific advances in this area include reactive coatings, bioactive textile treatments, advanced chemical sensors, anti-biofouling approaches, and catalysis. Another major program aims to integrate biological and biomimetic synthetic cellular elements to create novel artificial cells with unprecedented spatial and temporal control of genetic circuits and biological pathways. These hybrid biological/synthetic cells have the potential to provide a fundamentally new chassis for synthetic biology that addresses the critical challenge of instilling increased control and stability to engineered biological systems.

IMPARTING PROPERTIES INHERENT IN BIOLOGICAL SYSTEMS TO MATERIALS

For certain applications and use scenarios, a fully synthetic material or chemical system that exhibits properties inherent in biological systems, without the inclusion of biological elements, would be ideal. Living biological systems have many desirable characteristics. They can be dynamic, self-organizing, multi-functional, responsive, and complex. They can autonomously adapt to their changing environment. Novel approaches which impart these properties to non-biological synthetic chemical and material systems could enable significant new capabilities.

One property of biological systems that would provide novel functionality for synthetic material systems is the precise temporal and spatial regulation of activity. Biology has evolved complex mechanisms to tightly regulate molecular functions. This regulation can be achieved via changes in chemical, optical, electrical, and mechanical stimulation of active molecular elements. A major program will aim to understand the molecular mechanisms by which living cells regulate intracellular biochemical activity with mechanical force and to reproduce and analyze these force-activated mechanisms in virtual and synthetic materials. Scientific advances in this area could lead to sense-and-respond systems that incorporate force-activation to maximize multi-modal functionality, reactive

coatings, novel sensor paradigms, and self-healing materials.

Major research programs are also investigating methods for imparting multi-functionality and dynamic, responsive behavior into purely synthetic chemical and material systems. Potential applications of these systems include smart sensors, self-healing and self-repairing materials, reconfigurable materials, and controlled release of materials. For example, micelle/nanoparticle composite systems are possible in which different environmental stimuli (pH, temperature, oxidation) result in different material responses (Zhuang et al., 2013). In another example, micelle systems have been made in which the morphology of the micelle can be changed by environmental triggers. An enzymatic reaction or addition/removal of complimentary DNA can cause micelles to alternate between spherical and cylindrical forms resulting in bulk material changes (Randolph et al., 2012).

The revolutionary basic research ARO is supporting in the areas of bio-based and bio-inspired materials as summarized above has the potential to impact diverse applications in sensing, alternative fuels, molecular scale electronics, targeted drug delivery, and autonomously adaptive materials. This research has the potential to harness the power of biology with the control and stability of material and chemical systems to provide revolutionary scientific advances.

REFERENCES

- Fan, X. Z., Pomerantseva, E., Gnerlich, M., Brown, A., Gerasopoulos, K., McCarthy, M., et al. (2013). Tobacco mosaic virus: a biological building block for micro/nano/bio systems. *J. Vac. Sci. Technol. A* 31, 050815-1–050815-24. doi: 10.1116/1.4816584
- Ke, Y., Ong, L. L., Shih, W. M., and Yin, P. (2012). Three-dimensional structures bled from DNA bricks. *Science* 338, 1177–1183. doi: 10.1126/science.1227268
- Pilkington, S., Roberts, S., Meade, S., and Gerrard, J. A. (2010). Amyloid fibrils as a nanoscaffold for enzyme immobilization. *Biotechnol. Prog.* 26, 93–100. doi: 10.1002/btpr.309
- Randolph, L. M., Chien, M.-P., and Gianneschi, N. C. (2012). Biological stimuli and biomolecules in the assembly and manipulation of nanoscale polymeric particles. *Chem. Sci.* 3, 1363–1380. doi: 10.1039/c2sc00857b

- Raynes, J., Pearce, G., Meade, S., and Gerrard, J. A. (2011). Immobilization of organophosphate hydrolase on an amyloid fibril nanoscaffold: towards bioremediation and chemical detoxification. *Biotechnol. Prog.* 27, 360–367. doi: 10.1002/bptr.518
- Zhuang, J., Gordon, M. R., Ventura, J., Li, L., and Thayumanavan, S. (2013). Multi-stimuli responsive macromolecules and their assemblies. *Chem. Soc. Rev.* 42, 7421–7435. doi: 10.1039/C3CS600094G

Conflict of Interest Statement: The authors declare that the research was conducted in the absence of any commercial or financial relationships that could be construed as a potential conflict of interest.

Received: 18 March 2014; accepted: 22 April 2014; published online: 13 May 2014.

Citation: Nick McElhinny SA and Becker JJ (2014) Basic research opportunities focused on bio-based and bio-inspired materials and potential applications. Front. Chem. 2:24. doi: 10.3389/fchem.2014.00024

This article was submitted to Chemical Biology, a section of the journal Frontiers in Chemistry.

Copyright © 2014 Nick McElhinny and Becker. This is an open-access article distributed under the terms of the Creative Commons Attribution License (CC BY). The use, distribution or reproduction in other forums is permitted, provided the original author(s) or licensor are credited and that the original publication in this journal is cited, in accordance with accepted academic practice. No use, distribution or reproduction is permitted which does not comply with these terms.



Controlling topological entanglement in engineered protein hydrogels with a variety of thiol coupling chemistries

Shengchang Tang and Bradley D. Olsen *

Department of Chemical Engineering, Massachusetts Institute of Technology, Cambridge, MA, USA

Edited by:

Carissa M. Soto, Naval Research Laboratory, USA

Reviewed by:

Paola Laurienzo, Italian Research Council (CNR), Italy

Yanli Zhao, Nanyang Technological University, Singapore

***Correspondence:**

Bradley D. Olsen, Department of Chemical Engineering, Massachusetts Institute of Technology, 77 Massachusetts Avenue, Cambridge, MA 02139, USA

e-mail: bdolsen@mit.edu

Topological entanglements between polymer chains are achieved in associating protein hydrogels through the synthesis of high molecular weight proteins via chain extension using a variety of thiol coupling chemistries, including disulfide formation, thiol-maleimide, thiol-bromomaleimide and thiol-ene. Coupling of cysteines via disulfide formation results in the most pronounced entanglement effect in hydrogels, while other chemistries provide versatile means of changing the extent of entanglement, achieving faster chain extension, and providing a facile method of controlling the network hierarchy and incorporating stimuli responsivities. The addition of trifunctional coupling agents causes incomplete crosslinking and introduces branching architecture to the protein molecules. The high-frequency plateau modulus and the entanglement plateau modulus can be tuned by changing the ratio of difunctional chain extender to the trifunctional branching unit. Therefore, these chain extension reactions show promise in delicately controlling the relaxation and mechanical properties of engineered protein hydrogels in ways that complement their design through genetic engineering.

Keywords: engineered protein hydrogels, coiled-coil, thiol-X click chemistries, entanglement, branching

INTRODUCTION

Control of advanced mechanical properties of hydrogels is central to their applications. In many situations, such as engineering simulant materials of articular cartilage or blood vessels (Drury and Mooney, 2003), hydrogels are required to support mechanical load and maintain structural integrity. Multiple approaches have been developed to address this issue, with emphasis on increasing the network toughness and elastic moduli, such as preparing double-networks (Gong et al., 2003; Sun et al., 2012) and fabricating composite materials (Haraguchi and Takehisa, 2002; Wang et al., 2010a). In some scenarios where dynamic properties such as injectability, self-healing, shape memory, and controlled degradation/reinforcement are desirable, non-covalent crosslinks and stimuli-responsive triggers can be incorporated into gels to fulfill the application requirements (Kloxin et al., 2009; Holten-Andersen et al., 2011; Guvendiren et al., 2012; Glassman et al., 2013). However, many methods developed in synthetic polymer systems cannot be readily applied to protein hydrogels, and manipulating the mechanical response of the gels presents a new challenge. Because the function of a protein is related to its hierarchical structure and the diversity of amino acid functional groups, site-specific and orthogonal reactions are often required to preserve protein properties in the final gel. In addition, the modification reactions can usually only be performed in aqueous buffers due to the poor solubility of proteins in organic solvents.

Currently there are two main strategies for chemically modifying proteins to manipulate the mechanical properties of protein hydrogels. The first strategy is covalently crosslinking protein polymer chains by adding crosslinking reagents (Trabbi-Carlson et al., 2003; Li et al., 2011; Chung et al., 2012), catalysts (Shen et al., 2005; Lv et al., 2010) and/or enzymes (Davis et al., 2010). As

this method only modifies the amino acid residues participating in junction formation, the protein strands can retain most of their function (e.g., elasticity and stimuli responsivity). In addition, many mechanical properties at equilibrium, such as modulus and maximum swelling ratio, can be controlled by varying the dosage of the crosslinking agents according to well-known laws of hydrogel physics and network theories (Graessley, 2004; Tanaka, 2011; Kim et al., 2013). In a typical crosslinking reaction, however, the formation of network imperfections, such as dangling chains and inelastic loops, is usually uncontrollable and difficult to quantify (Zhou et al., 2012). The second strategy is coupling synthetic polymers and proteins to prepare chimeric copolymers (Jing et al., 2008; Sahin and Kiick, 2009; Wu et al., 2011; Glassman and Olsen, 2013; Glassman et al., 2013). Interactions leading to self-assembly of the polymer or protein component then create nanostructure within the hydrogel, which in some cases can be triggered by external stimuli. This method allows delicate manipulation of hydrogel mechanics, such as erosion rate, toughness and elasticity. However, preparing hybrid hydrogels adds challenges in materials synthesis and purification.

Recently, we developed a facile method for introducing entanglements into protein hydrogels through simple chain extension reactions, and we exploited this entanglement effect to engineer new mechanical responses into the materials (Tang et al., 2014). This strategy minimally modifies the protein molecules, only extending protein chains by establishing disulfide end linkages, yet it creates a drastic enhancement in many mechanical properties, including the low-frequency modulus, resistance to creep, extensibility and toughness. The disulfide linkages are redox responsive, which provides opportunities to regulate network mechanics by redox stimuli.

In addition to disulfide coupling, several other thiol chemistries are promising candidates for coupling high molar mass proteins: thiol-maleimide, thiol-bromomaleimide and thiol-ene coupling. Thiol-maleimide chemistry enables site-specific modification of cysteine residues and has been a popular route for constructing protein-based bioconjugates (Canalle et al., 2010; Stephanopoulos and Francis, 2011). Recently, the thiol-maleimide addition has been found to be reversible, offering new opportunities to control the degradation of the conjugates (Baldwin and Kiick, 2011). Thiol-dibromomaleimide conjugation has emerged as another important “click” chemistry (Smith et al., 2010; Jones et al., 2011; Robin et al., 2013), but only recently has its potential in the chain extension reaction been appreciated (Cui et al., 2013). The thiomaleimide adduct is redox responsive: the addition of reducing reagents such as β -mercaptoethanol (BME) reverses the reaction and recovers the unmodified proteins. Compared to other coupling chemistries, the thiol-ene reaction is the most rapid coupling method, with extremely high bimolecular rate constants in the thiyl-alkene addition, ranging from 10^5 to $10^7 \text{ M}^{-1} \text{ s}^{-1}$ (Northrop and Coffey, 2012), which is 4–5 orders of magnitude larger than thiol-maleimide addition (Schelté et al., 1999). Despite potential side reactions (Schöneich, 2008), there exist many successful examples demonstrating the use of thiol-ene chemistry in direct protein modification (Dondoni et al., 2009; Weinrich et al., 2010; Valkevich et al., 2012).

In this work, thiol-maleimide, thiol-bromomaleimide and thiol-ene coupling chemistries for application in protein chain extension reactions to produce entangled hydrogels are compared. In addition, the ability to use chain extension points for the modification of proteins with poly(*N*-isopropylacrylamide) (PNIPAM) side chains is established, demonstrating thermally responsive mechanical behavior. By using trifunctional chain coupling agents, branched proteins are also prepared, and the effect of the ratio of di to trifunctional chain coupling agent on entanglements is assessed. These experiments demonstrate sophisticated control of molecular structure and network mechanics in engineered protein hydrogels, yielding the ability to control chain topology, chain entanglement, and chemical functionalization all through thiol-based chain coupling chemistries.

MATERIALS AND METHODS

MATERIALS

Bismaleimide diethylene glycol (**1a**) was purchased from Thermo Fischer. Maleimide-PEG(1k)-maleimide (**1b**) was purchased from creative PEGWorks. The average molecular weight of the PEG portion determined by ^1H NMR was 1082 Da. β -cyclodextrin (β CD) and 2,2'-Azobis[2-(2-imidazolin-2-yl)propane]dihydrochloride (VA-044) were purchased from Wako USA. All other chemical reagents were purchased from commercial sources (Sigma-Aldrich and VWR) and used as received unless otherwise noted.

CHARACTERIZATION

^1H NMR spectra were recorded in CDCl_3 or $\text{DMSO}-d_6$ using a Varian Mercury 300 MHz Spectrometer in Department of

Chemistry Instrumentation Facilities at MIT. High-resolution mass spectrometry (HRMS) data was obtained on a Bruker Daltonics APEXIV 4.7 Tesla Fourier Transform Ion Cyclotron Resonance Mass Spectrometer. Matrix assisted laser desorption ionization mass spectrometry (MALDI) data was obtain on a Bruker Omniplex MALDI-TOF Mass Spectrometer. α -Cyano-4-hydroxycinnamic acid (CHCA) was used as matrix. Gel permeation chromatography (GPC) was performed on an Agilent 1260 system equipped with a Wyatt Optilab T-rEX refractive index (RI) detector and a Wyatt Mini-DAWN multi-angle light scattering (LS) detector. The mobile phase was DMF supplemented with 0.02 M LiBr and the instrument was operated at 1.0 mL/min at 70°C.

PROTEIN Cys-P₄-Cys EXPRESSION AND PURIFICATION

Protein expression and purification by ammonium sulfate purification have been described previously (Tang et al., 2014). In this study, the proteins were additionally purified by anion exchange chromatography using a HiTrap Q Sepharose HP 5 mL column (GE healthcare, WI), eluting with a gradient of 0–500 mM NaCl in 6 M urea and 20 mM Tris (pH 8.0). A typical isolation yield is 120 mg per liter culture and the protein purity was determined to be >97% by sodium dodecyl sulfate-polyacrylamide gel electrophoresis (SDS-PAGE).

CHEMICAL COMPOUND SYNTHESIS

Dibromomaleimide-alkyne

The synthesis procedure reported elsewhere (Jones et al., 2011) was slightly modified. Potassium carbonate (0.89 g, 6.50 mmol) was suspended in 20 mL acetone and 2,3-dibromomaleimide (1.5 g, 5.90 mmol) was added to the slurry in one portion and the reaction was left to stir at room temperature for 5 min. Propargyl bromide (80% in toluene, 0.72 mL, 6.50 mmol) was added drop-wise to the mixture over 10 min. After 24 h, solvent was removed under vacuum and the mixture was redissolved in DCM. Salts were filtered and the residue was loaded onto a silica gel column vacuum. The crude product was purified by flash chromatography, eluted with 0–2% MeOH in DCM (TLC R_f = 0.78, stained with KMnO_4 solution) to afford 492 mg **4** as a white powder (yield 28.5%).

^1H NMR (300 MHz, CDCl_3) δ 4.38 (d, J = 2.4 Hz, 2H), 4.83 (t, J = 2.4 Hz, 1H). DART HRMS (m/z) calcd for $\text{C}_7\text{H}_4\text{Br}_2\text{NO}_2$ [$\text{M}+\text{H}]^+$: 293.8586; found 293.8585.

Dibromomaleimide- β -CD

To a 25 mL Schlenk tube was added **4** (58.5 mg, 0.20 mmol), mono-6-deoxy-6-azido- β -cyclodextrin (Petter et al., 1990) (116.0 mg, 0.10 mmol), $\text{Cu}(\text{I})\text{Br}$ (14.3 mg, 0.10 mmol) and 5 mL DMF. The mixture was degassed through 3 freeze-pump-thaw cycles. 2,2'-Bipyridine (15.6 mg, 0.10 mmol) was added to the frozen mixture and the mixture was degassed one more time. The click reaction was performed at 30°C for 24 h. Catalyst was removed by passing through a short alumina column and the product was obtained by precipitation in acetone twice to get 63 mg **2** as a yellow powder (yield 43.4%).

^1H NMR (300 MHz, $\text{DMSO}-d_6$) δ 8.06 (s, 1H), 5.95–5.60 (m, 14H), 5.10–4.67 (m, 9H), 4.65–4.42 (m, 6H), 3.79–3.48

(m, 28H), 3.43–3.21 (m, overlaps with HOD). MALDI-TOF MS (m/z) calcd for C₄₉H₇₂Br₂N₄O₃Na [M+Na]⁺: 1473.22; found 1473.22.

Bisallyl tetraethylene glycol

Tetraethylene glycol (5.0 g, 25.7 mmol) was dissolved in 30 mL anhydrous DMF. Sodium hydride (3.5 g, 60% in mineral oil, 87.5 mmol) was added to the mixture in one portion. The mixture was cooled with a water bath and allowed to stir for 30 min at room temperature. After the reaction stopped bubbling, allyl bromide (9.5 g, 78.4 mmol) was added dropwise. After 14 h, excess NaH was quenched by adding 10 mL saturated NH₄Cl aqueous solution. The mixture was diluted with EtOAc, washed with DI water and brine, and dried over MgSO₄. Then solvent was removed under reduced pressure. The crude product was purified by silica gel column chromatography, eluted with 50% EtOAc in hexanes (TLC *R_f* = 0.41, stained with KMnO₄ solution) to afford 3.65 g **3** as a slightly yellow liquid (yield 51.8%).

¹H NMR (300 MHz, CDCl₃) δ 5.91 (d × d × t, *J* = 17.1 Hz, *J* = 10.5 Hz, ³*J* = 5.7 Hz, 2H), 5.27 (d × d × t, *J* = 17.1 Hz, *J* = 1.5 Hz, *J* = 1.5 Hz, 2H), 5.18 (d × d × t, *J* = 17.1 Hz, *J* = 1.8 Hz, *J* = 1.2 Hz, 2H), 4.02 (d × t, *J* = 5.7 Hz, *J* = 1.5 Hz, 4H), 3.68–3.58 (m, 16H). DART HRMS (m/z) calcd for C₁₄H₂₇O₅ [M+H]⁺: 275.1853; found 275.1851.

EMP-Adamantane (EMP-Ad)

The synthesis of 2-ethylsulfanylthiocarbonylsulfanyl-2-methyl-propionic acid (EMP) was performed as previously reported (Lai et al., 2002; Convertine et al., 2006). To a 25 mL round bottom flask was added EMP (179.5 mg, 0.80 mmol), 1-adamantane methanol (159.6 mg, 0.96 mmol), 4-dimethylaminopyridine (DMAP) (19.5 mg, 0.16 mmol) and 5 mL DCM. After all reagents were dissolved, *N,N'*-dicyclohexylcarbodiimide (DCC) (247.6 mg, 1.20 mmol) was added in one portion. The reaction mixture was stirred at room temperature overnight. The precipitate was filtered and the solvent was removed under vacuum. The crude product was purified by silica gel column chromatography, eluted with 30% DCM in hexanes (TLC *R_f* = 0.30, yellow or stained with KMnO₄ solution) to afford 210 mg **5** as a bright yellow solid (yield 70.5%).

¹H NMR (300 MHz, CDCl₃) δ 3.60 (s, 2H), 3.25 (q, *J* = 7.5 Hz, 2H), 1.93 (s, 3H), 1.71–1.60 (m, 12H), 1.49 (d, *J* = 2.4 Hz, 6H), 1.28 (d, *J* = 7.5 Hz, 3H). ESI HRMS (m/z) calcd for C₁₈H₂₈O₂S₃ [M+H]⁺: 373.1343; found 373.1324.

PNIPAM-Ad

N-isopropyl acrylamide (NIPAM) was freshly purified by sublimation and azobisisobutyronitrile (AIBN) was recrystallized twice from ethanol. In polymerization, NIPAM (1.09 g, 9.6 mmol), EMP-Ad (29.8 mg, 0.080 mmol), AIBN (2.63 mg, 0.016 mmol) and 4.8 mL acetonitrile were added to a 25 mL Schlenk tube. The reaction mixture was subjected to 3 cycles of freeze-pump-thaw to degas oxygen. The reaction was heated at 60°C for 4 h, after which polymers were recovered by precipitation in diethyl ether. The molar mass of the obtained polymer was 7.8 kg/mol (from GPC, dispersity *D* = 1.05), 7.4 kg/mol (from

¹H NMR endgroup analysis) and 7.0 kg/mol (from MALDI-TOF MS), respectively.

EXTENDING PROTEIN CHAINS USING DIFFERENT CYSTEINE COUPLING CHEMISTRIES (INCLUDING BRANCHING REACTIONS)

Thiol-maleimide

Protein Cys-P₄-Cys was dissolved in denaturing buffer (8 M urea and 100 mM phosphate, pH 8.0) to reach a concentration of 10% (w/v). Tris(2-carboxyethyl)phosphine (TCEP) (20 eq.) was added to the solution and the pH was adjusted to 7.5. Bismaleimide **1a** or **1b** was dissolved in DMF, and was added to the solution (1 eq.). The reaction was stirred at room temperature for 3 days, and it was then dialyzed against MilliQ water and lyophilized. The long reaction time was chosen based on experimental results to maximize endgroup conversion and entanglement in gels.

Thiol-bromomaleimide

Protein Cys-P₄-Cys was dissolved in denaturing buffer (8 M urea and 100 mM phosphate, pH 8.0) to reach a concentration of 10% (w/v). TCEP (20 eq.) was added to the solution and the pH was adjusted to 6.2. βCD functionalized dibromomaleimide **2** was dissolved in DMSO, and was added to the solution (1 eq.). The reaction was stirred at 4°C for 7 days, and it was then dialyzed against MilliQ water and lyophilized.

Thiol-ene

Protein Cys-P₄-Cys was dissolved in denaturing buffer (8 M urea and 100 mM phosphate, pH 8.0) to reach a concentration of 10% (w/v). TCEP (20 eq.) was added to the solution. The mixture was left to stir at room temperature for 4 h, and it was then dialyzed against MilliQ water and lyophilized. After reduction, >99% of the proteins were in the monomeric state, assessed by SDS-PAGE (Supplementary Figure 2). Reduced proteins were hydrated in 100 mM sodium phosphate buffer (pH 7.6), and mixed with **3** (1 eq.) and VA-044 (0.2 eq.). The final concentration was adjusted to 20% (w/v). Hydrogel samples were loaded on the rheometer after hydration for 2 days. The reaction was triggered by heating at 60°C for 3 h. The moduli were monitored at 25°C to ensure that the steady state was reached before measurement.

In branching reactions, the trifunctional crosslinker 2,4,6-triethoxy-1,3,5-triazine **6** was used in place of the bifunctional crosslinker **3**. The total number of alkene groups was kept in 1:1 molar ratio to thiol groups, while the amount of **6** was varied from 0–100% of the total mole fraction of alkene-containing oligomer.

RHEOLOGY

Rheology experiments were performed on Anton Paar MCR 301, 501, and 702 rheometers using a cone and plate geometry (25 mm diameter, 1° cone and 50 μm truncation gap) or a parallel plate geometry (10 mm diameter and 300 μm gap, only for measurement with βCD-functionalized protein hydrogels). The quantitative measurement of hydrogel mechanics was not affected by the choice of rheometers. Lyophilized proteins were hydrated in 100 mM sodium phosphate buffer (pH 7.6) to a final concentration of 20% (w/v). Hydrogels were kept at 4°C for 2 days to allow complete hydration. In order to minimize dehydration during measurement, the edges of hydrogel samples

were coated with mineral oil. After loading onto the rheometer, samples were heated from 25°C to 90°C and cooled to 25°C at 5°C/min. Unfolding of the coiled-coil domains at high temperatures allowed rapid stress relaxation within the gel to eliminate any shear history, but no sol-gel transition was observed over this temperature range (Supplementary Figure 1). Frequency sweep measurements were performed at 1% strain in the linear viscoelastic regime (LVE). In creep experiments, a 25 Pa load was exerted on hydrogels for 2 h, and the load was removed to monitor the recovery behavior for 2 h. The creep-recovery experiment was repeated at 50 Pa load to ensure the deformation was independent of the applied load.

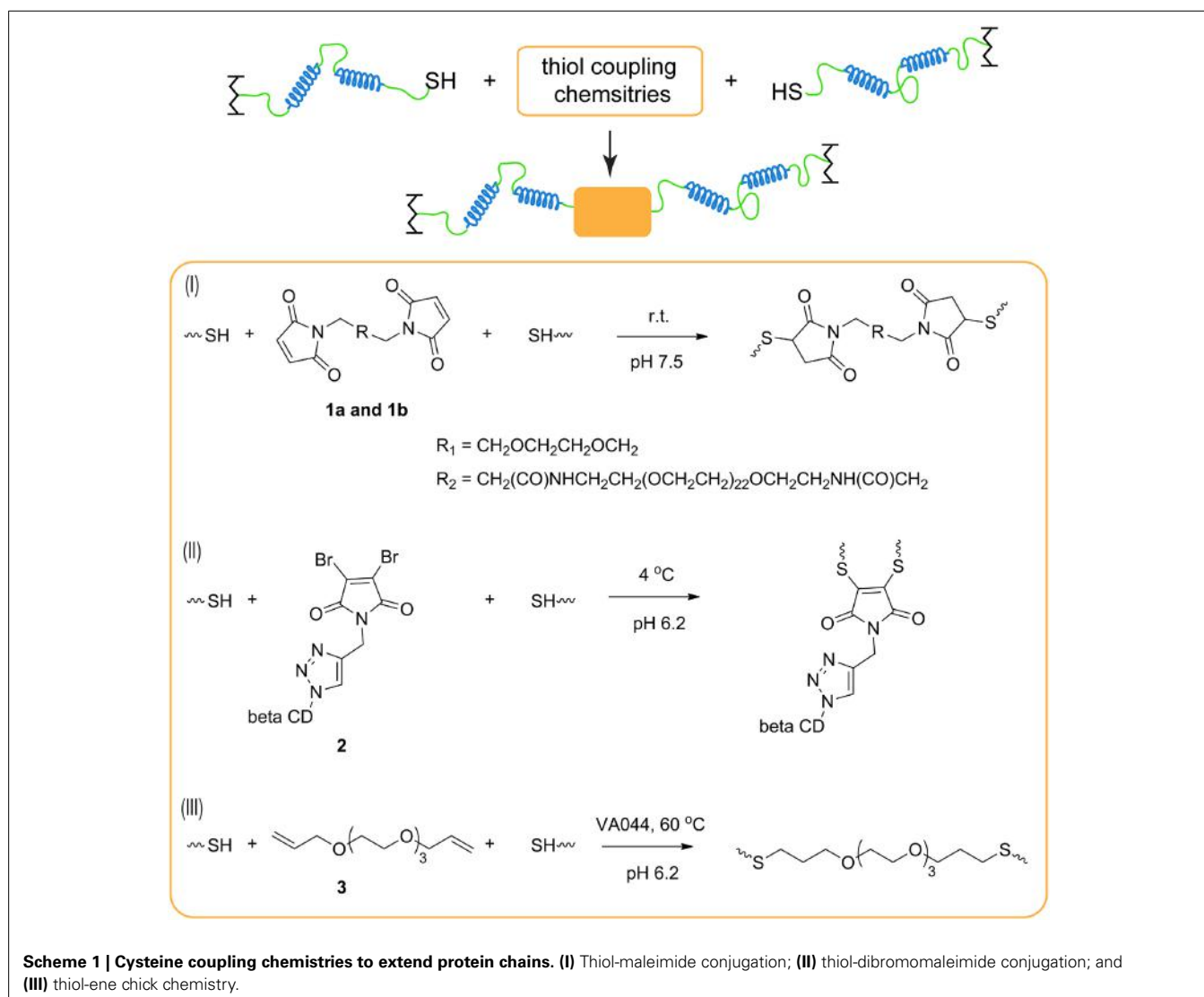
RESULTS AND DISCUSSION

COMPARISON OF VARIOUS CHEMISTRIES ON THE CHAIN EXTENSION REACTION

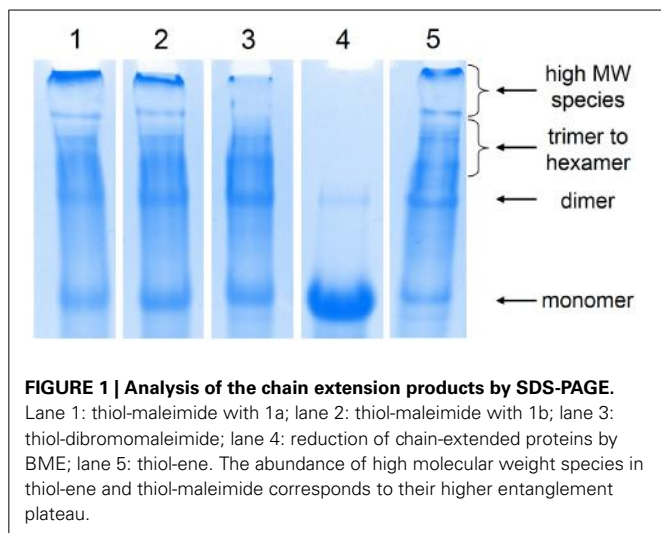
Chain extension of cysteine end-capped proteins can be achieved by applying thiol-maleimide, thiol-bromomaleimide and thiolene coupling chemistries under appropriate reaction conditions

(**Scheme 1** and **Figure 1**). All chemistries require reduction of existing disulfides to recover reactive cysteine residues. In order to achieve significant changes in mechanical properties, the conversion of these macromolecular polycondensation reactions must be relatively high to produce proteins of high molecular weights. In practice, this is achieved by controlling stoichiometry of the reacting species. A theoretical full conversion of endgroups can only be obtained when the ratio of cysteines to alkenes is 1:1. Running the reaction for extended periods is also useful to reach high conversions.

Each chemistry offers its own distinct advantages and disadvantages for chain extension. In the thiol-maleimide reaction, pH control is critical to minimize amine-maleimide coupling while achieving fast conjugation (Hermanson, 2008). In addition, dimaleimide reagents are commercially available with varying distance between the two maleimide groups, and this spacer length may affect the polycondensation reaction due to their subtle differences in solubility or by altering the propensity to form bridges or primary loops (Dutton et al., 1994). To study the effect of the



Scheme 1 | Cysteine coupling chemistries to extend protein chains. (I) Thiol-maleimide conjugation; **(II)** thiol-dibromomaleimide conjugation; and **(III)** thiol-ene click chemistry.



distance between two conjugation sites, bismaleimide with two different oligo ethylene glycol spacer lengths **1a** and **1b** are used to conduct chain extension. It is found that the spacer length does not greatly affect the chain extension when the coupling reagents can be solubilized and homogeneously dispersed in the reaction.

As for thiol-dibromomaleimide coupling, controlling the hydrolysis of the maleimide ring, especially the monothio adduct, is crucial to attain significant chain extension. If hydrolysis happens on the dithio adduct, transformation from maleimide to maleamic acid does not affect chain extension, and it only results in loss of the reversibility of the thiomaleimide adduct (Supplementary Scheme 1). In contrast, hydrolysis of the monothio adduct can potentially limit the conversion, as the number of reactive bromomaleimide functional group decreases (Supplementary Scheme 1). Maleimide hydrolysis can be regulated in many ways, including changing temperature, pH (Ryan et al., 2011) and the electron density distribution in the maleimide structure (Nathani et al., 2013). In our hands, the first two parameters are optimized: a low temperature (4°C) and a slightly acidic buffer condition (pH 6.2) are chosen to be the reaction condition, under which moderate chain extension is achieved. After chain extension, the protein is exposed to 1000-fold excess BME, and ~ 98% of the proteins are converted to the monomeric state (Figure 1), which demonstrates the reversibility of the dithiomaleimide adduct.

In the thiol-ene coupling strategy, bis allyl compound **3** is chosen as the chain extender to prevent homopolymerization of alkenes that can occur when (meth)acrylate groups are used (Hoyle and Bowman, 2010), and water soluble VA-044 is selected as the thermal initiator for its low decomposition temperature. As the thiol-ene reaction is tolerant of oxygen (Hoyle et al., 2010), no cumbersome degassing procedure is required, enabling its convenient use in applications. Upon heating at 60°C for 3 h, a large fraction of high-molecular-weight proteins is formed. While thermally initiated chain extension is used here in order to ensure homogeneous reaction through a concentrated solution, it is also possible to perform photoinitiated chain extension using this chemistry, especially in occasions when spatial and temporal

control of gel mechanics is required. TCEP needs to be removed prior to the thiol-ene reaction; otherwise the degree of chain extension is fairly low (Supplementary Figure 2). The deleterious effect of TCEP may be due to the desulfurization of cysteines catalyzed by TCEP during free-radical-based reactions, an effect that has been observed under similar reaction conditions (Wan and Danishefsky, 2007).

Cysteine coupling chemistries exhibit different performances in the chain extension reaction, and the differences in the molecular weight distribution of the chain-extended proteins result in varying extents of entanglement in the protein hydrogels. As shown in Figure 2, hydrogels prepared *via* different chemistries all show an entanglement plateau modulus in the low-frequency regime. The chain molar mass distributions extracted from gels in Figure 1 do not fit well to the Jacobson-Stockmayer distribution, likely because of challenges in controlling stoichiometry of reagents in small samples and because of difficulty in quantitatively separating the large high molar mass band, which contains a mix of proteins with a molar mass of ca. 380 kg/mol and above (6-mers and above). Therefore, the chain extension and the entanglement effect is quantitatively analyzed by the entanglement plateau moduli in the low frequency regime. The apparent entanglement molecular weight M_e can be estimated as (Larson et al., 2003)

$$M_e = \frac{4}{5} \frac{\rho \varphi R T}{G_e}$$

with ρ being the protein density, φ the protein volume fraction in the gel, R the gas constant, T the absolute temperature and G_e the entanglement plateau modulus. Although the entanglement plateau modulus should not depend on the molecular weight of the protein polymers in the high molecular weight limit, proteins formed *via* macromolecular polycondensation show very broad molecular weight distributions with a certain fraction of the protein chains below the critical entanglement length. These “small” proteins act as macromolecular diluents and lower the effective concentration of the entangled species, consistent with the concentrations investigated being in the transition from the sticky Rouse phase to the sticky reptation regime (Tang et al., 2014). Therefore, increasing chain molecular weight, particularly the low molar mass tail, can increase M_e . Consequently, differences in the degree of chain extension will yield differences in the plateau modulus of gels.

Compared to disulfide bridging investigated previously (Tang et al., 2014), the three chemistries examined here show lower degrees of chain extension. G_e and M_e are compared in Figures 3A,B. For 20% (w/v) hydrogels, disulfide coupling leads to a G_e of around 8800 Pa, approximately 2–8 times larger than the G_e 's from other chemistries. As a result, M_e is only 55 kg/mol in the disulfide coupling, even smaller than the molecular weight of a monomeric protein. The reasons for the lower entanglement molar masses in disulfide coupling are two-fold. First and most importantly, the stoichiometric imbalance between alkenes and thiols, due to inevitable experimental errors, set a practical limit of the functional group conversion in the A–A + B–B type macromolecular polycondensation that becomes more acute

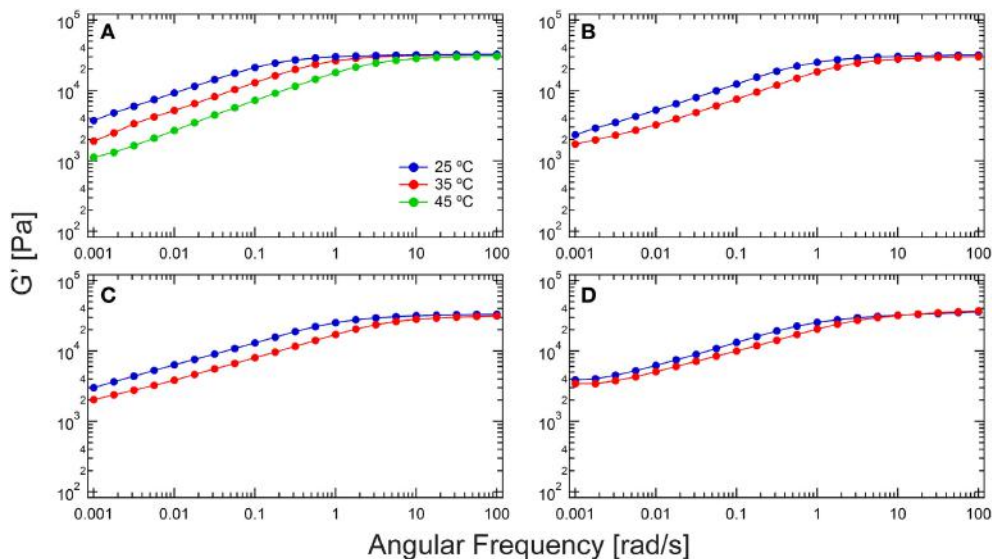


FIGURE 2 | Comparison of rheological frequency sweeps of chain extended hydrogels from various chemistries. (A) Thiol-maleimide with 1a; **(B)** thiol-maleimide with 1b; **(C)** thiol-dibromomaleimide; and **(D)** thiol-ene.

The plateau modulus in the low frequency regime down to 0.001 rad/s is the entanglement plateau. The frequency spectrum shifts to the high-frequency end at elevated temperatures.

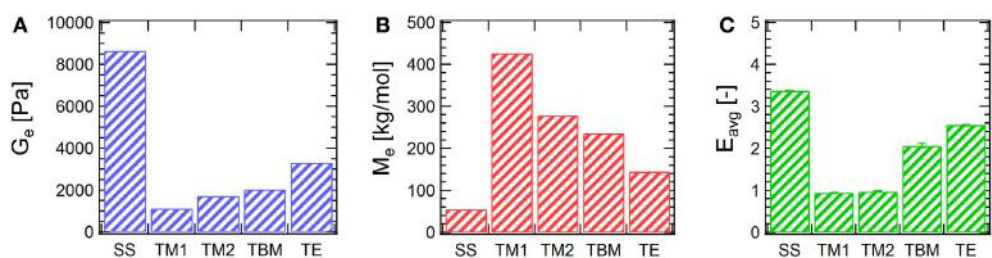


FIGURE 3 | Comparison of (A) entanglement plateau moduli, (B) the apparent entanglement molecular weights, and (C) the average entanglement densities. SS: disulfide, data from Tang et al. (2014); TM1,

thiol-maleimide with 1a; TM2, thiol-maleimide with 1b; TBM, thiol-dibromomaleimide; TE, thiol-ene. Error bars represent a 95% confidence interval.

for chemistry performed on small samples. On the contrary, the disulfide bridging chemistry has no theoretical limit in the degree of chain extension due to stoichiometry since it is an A-A type polycondensation. Second, there are various side reactions in thiol-maleimide, thiol-bromomaleimide and thiol-ene coupling, which limit their ability to reach full conversion. As mentioned previously, the primary concern is that the occurrence of side reactions may reduce the availability of the reactive functional groups (e.g., maleimide hydrolysis) or cause uncontrollable chain coupling (e.g., amine-maleimide coupling). These side reactions further exacerbate challenges in controlling the stoichiometry of A and B reactive groups in the macromolecular polycondensation. G_e not only provides clues to analyze the extent of entanglement, but also provides information on the effect of side reactions. The difference in G_e might indicate that fewer side reactions occur in the thiol-ene coupling in the three chemistries examined in the study. Interestingly, although coupling with 2 only reaches moderate chain extension and side reactions might have the most detrimental effect, G_e

from thiol-bromomaleimde coupling is larger those from thiol-maleimide chemistries. It is hypothesized that the supramolecular association between β CD and amino acid residues forms weak and dynamic crosslink junctions (with equilibrium constant $\log K$ around 2–3) (Rekharsky and Inoue, 1998), thus increasing the modulus in the low-frequency regime.

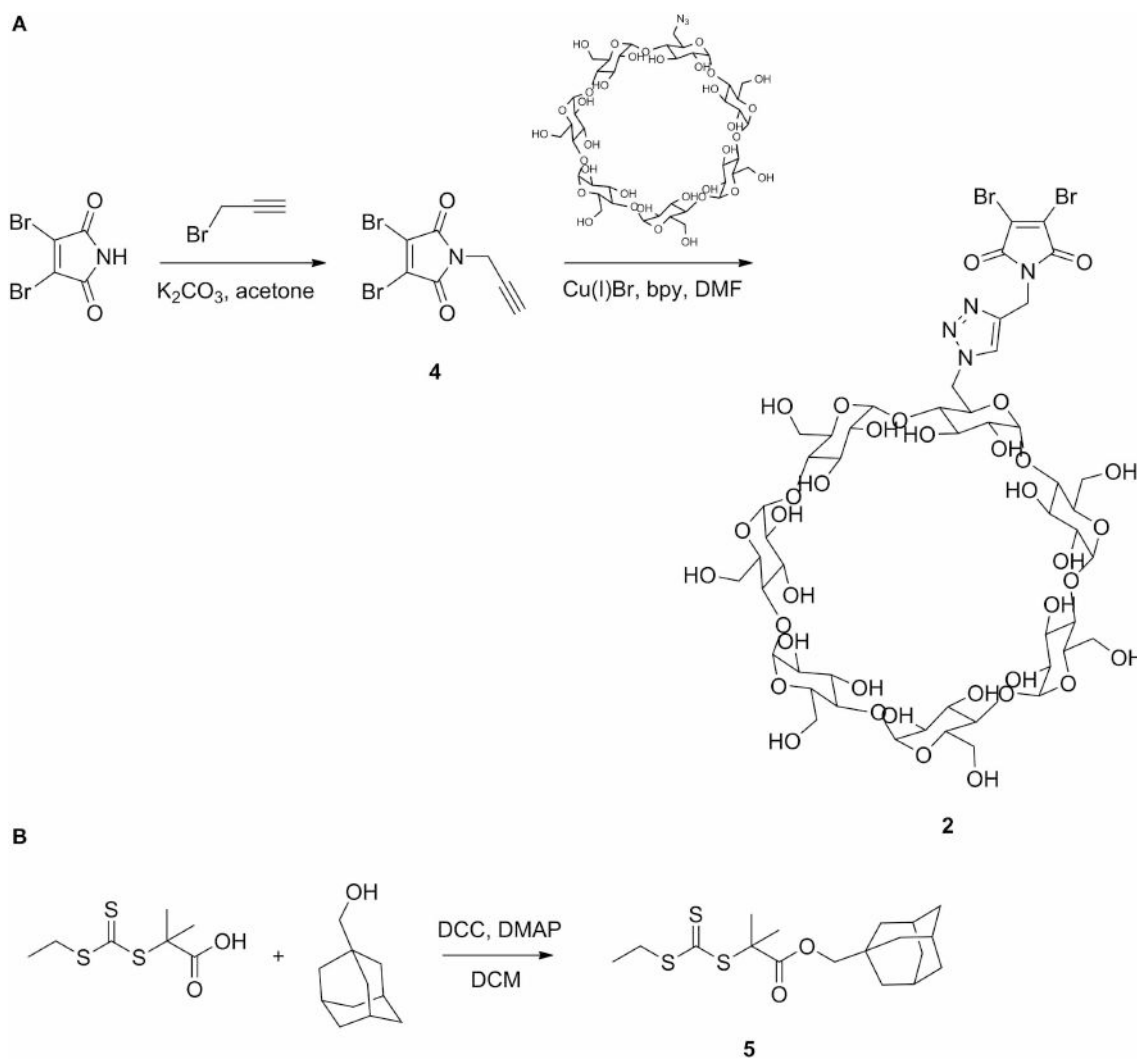
Creep experiments also provides information to compare the entanglement effects in gels prepared by different chemistries. Here, entanglement density E is used to quantify the entanglement effect, a quantity defined as the number of entanglements per molecule, namely, $E = M/M_e$ (Graessley, 2008). Strictly speaking, the definition above is used to describe the extent of entanglement of monodisperse polymers. Here the concept is borrowed to provide an estimate of the number-averaged entanglement density. In the low E limit (when $E < 6$), the average entanglement density in the chain extended protein mixtures can be calculated as

$$E_{avg} = 2.5J_e^0 G_e$$

where J_e^0 is the recoverable compliance, calculated as the extrapolated intercept from a linear fit in steady state of the J - t data (Supplementary Figure 3); G_e is the entanglement plateau modulus, as defined by Graessley (2008) differently than the definition by Larson et al. shown above by a factor of 4/5. As shown in **Figure 3C**, the low E values confirm the previous assumption that the entanglement density is not large. It is also found that the average entanglement densities of the chain-extended proteins gives the same trend as the entanglement plateau moduli in gels, namely, disulfide > thiol-ene > thiol-bromomaleimide > thiol-maleimide. For entangled gels prepared *via* thiol-maleimide coupling, E_{avg} is only approximately unity. On the contrary, E_{avg} is larger than 3 for gels prepared *via* disulfide bridging.

Because dibromomaleimide can be readily functionalized, dibromomaleimide coupling provides a facile method of incorporating biological niches into the hydrogel network and embedding additional stimuli triggers to manipulate network structure. To illustrate this concept, dibromomaleimide is first derivatized with alkyne, and is further functionalized with β CD through

copper-catalyzed azide-alkyne cycloaddition (CuAAC) to obtain **2** (**Scheme 2**). β CD is chosen because its internal cavity can host many small guest molecules, such as drugs, *via* hydrogen bonding and hydrophobic interactions (Davis and Brewster, 2004). The most widely used complexation pair is β CD-adamantane with an association constant K_a of about $5 \times 10^4 \text{ M}^{-1}$ (Harries et al., 2005). This supramolecular association may offer modification sites to attach functionalities to the protein backbone. Here, the β CD-adamantane host-guest interaction is used to demonstrate the ability to add thermoreversible association to hydrogels. Adamantane end-capped monodisperse PNIPAM is synthesized by reversible addition-fragmentation chain transfer (RAFT) polymerization using trithiocarbonate **5** as the RAFT agent (Supplementary Figure 4), and the polymer's endgroup structure is confirmed by MALDI-TOF and NMR (Supplementary Figures 5, 6, respectively). Upon complexation, the hybrid structure is hypothesized to adopt a graft-like structure: the chain-extended protein serves as backbone while the thermoresponsive polymers PNIPAM graft as side chains (**Figure 4**). Under the experimental



Scheme 2 | Synthesis of dibromomaleimide functionalized β CD (A) and adamantane functionalized trithiocarbonate RAFT agent (B).

conditions, approximately 91.8% of the PNIPAM can be attached to the proteins (see calculation details in Supplementary Materials and Supplementary Figure 7). The high-frequency plateau modulus (G' at 100 rad/s) of the hybrid gel is 10 kPa larger than the unmodified gel, and it increases moderately with increasing temperature, with a peak value at around 28°C. The entanglement modulus also increases from 2030 to 3670 Pa. The enhancement in the both moduli might originate from changes of protein architecture, and the formation of nanostructure within the gel due to segregation between the PNIPAM domain and the protein domain. Such microphase separation may even exist at low temperature, as enhancement in moduli is observed as low as 5°C. This observation is consistent with the previous finding that PNIPAM segregation takes place even when the polymers are highly solvated (Glassman and Olsen, 2013).

INFLUENCE OF BRANCHED ARCHITECTURE ON THE MECHANICAL PROPERTIES

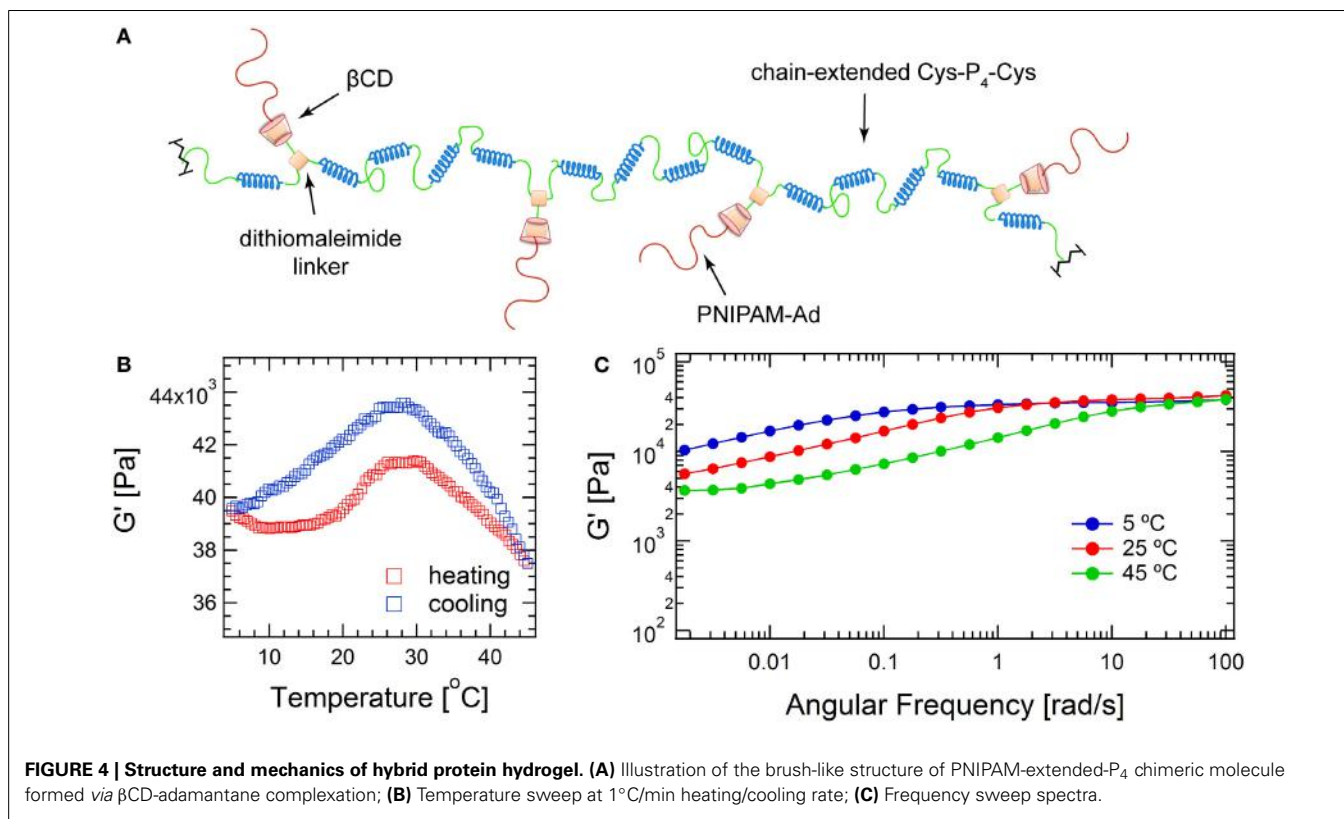
Branched polymers have attracted much interest for fundamental studies and industrial applications due to their distinct flow behaviors compared to their linear analogs (Dealy and Wissbrun, 1990; Janzen and Colby, 1999; Wood-Adams and Costeux, 2001; Lohse et al., 2002; Graessley, 2008; Wang et al., 2010b). However, few reports characterize the synthesis or properties of branched proteins, using either chemical methods or cellular machinery (Zhang et al., 2013). Here, branched proteins are synthesized with the use of multifunctional crosslinkers in the chain extension reaction, demonstrating an important means to control the mechanical properties of protein gels by modulating the chain structure. The effect of branching is examined by varying the

fraction of the trifunctional crosslinker (2,4,6-triallyloxy-1,3,5-triazine, **6**) from 0 to 100% in the total alkenes (note that the ratio of total alkenes to thiols is kept 1:1). The hydrogels are prepared by thiol-ene click chemistry *via* thermal initiation. Similar to chain extension, all branching reactions are found to reach high endgroup conversion, yielding significant fractions of high molar mass proteins from SDS-PAGE (Figure 5). Significant differences in molecular weight distribution of proteins among the 6 reactions examined cannot be measured by gel electrophoresis. An exception occurs at 100% triene, where a larger fraction of low molar mass protein is present, suggesting that the end-group conversion might be lower than those in other cases. All protein hydrogels are able to be dissolved in 6 M urea buffer post reaction, confirming the hypothesis that addition of **6** only results in branching and not crosslinking, even with 100% triene crosslinker. The gel point under each reaction condition can be calculated using the Carothers equation or the Flory-Stockmayer theory (see calculation details in Supplementary Materials and Supplementary Figure 8), which shows great dependence on the triene composition. The solubility of gels in urea suggests that the conversion of the endgroups is below the gel point in all cases.

The mechanical properties of hydrogels are influenced by the branched structure of the proteins. To better compare the entire relaxation spectra with different fractions of **6**, rheology data from creep experiments are converted to the dynamic compliance J' and J'' using a Fourier transform (Ferry, 1980),

$$J'(\omega) = J_e^0 - \omega \int_0^\omega [J_e^0 - J(t) + t/\eta_0] \sin \omega t dt$$

$$J''(\omega) = 1/\omega \eta_0 + \omega \int_0^\omega [J_e^0 - J(t) + t/\eta_0] \cos \omega t dt$$



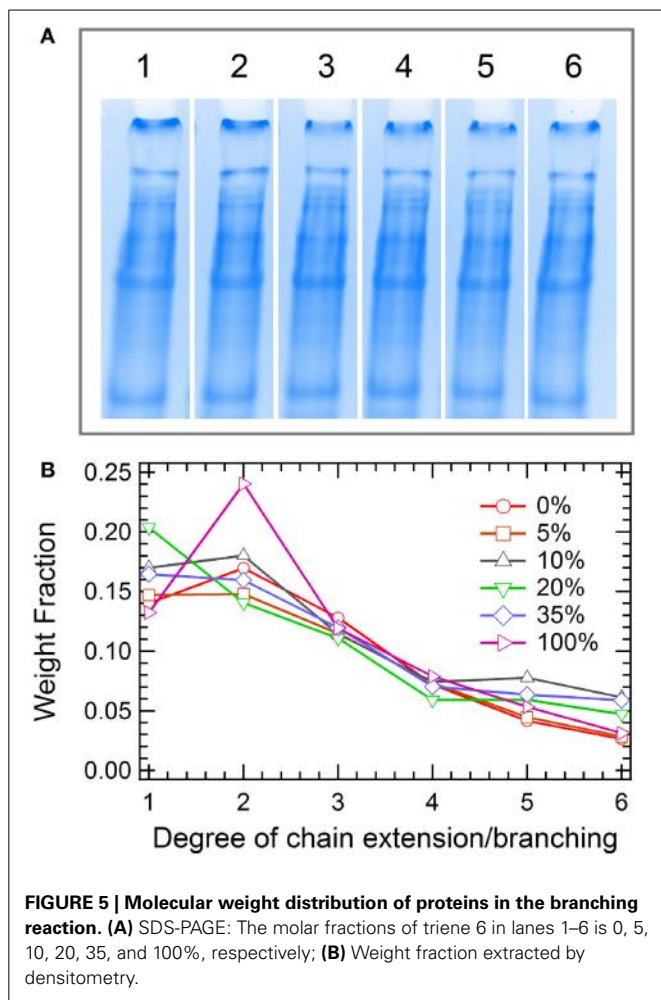


FIGURE 5 | Molecular weight distribution of proteins in the branching reaction. (A) SDS-PAGE: The molar fractions of triene 6 in lanes 1–6 is 0, 5, 10, 20, 35, and 100%, respectively; **(B)** Weight fraction extracted by densitometry.

where J_e^0 is the recoverable compliance, ω the angular frequency, η_0 the zero-shear-rate viscosity, t the experiment time. J_e^0 and η_0 are the intercept and the inverse of the slope, respectively, from a linear fit in steady-state phase of creep. The dynamic compliances are further translated into dynamic moduli G' and G'' ,

$$G' = J'/\left(J'^2 + J''^2\right)$$

$$G'' = J''/\left(J'^2 + J''^2\right)$$

The combined master curves are shown in **Figure 6**, which can be divided into three different regimes according to the relaxations present in the gels (from fast to slow): the coiled-coil regime, the entanglement regime and the terminal regime. With addition of a small amount of **6** (5 and 10%), both the high-frequency modulus (G'_∞) and the entanglement modulus (G_e) decrease. This suggests that adding a small amount of crosslinker only causes short chain branching and small drops in the backbone length of the chain-extended proteins, since this would result in a decrease in the total number of entanglements. However, at 20% triene, both G'_∞ and G_e reach their peak values, where the number density of the branch points and the branch length reach an optimal combination. In this case, the backbone length of the protein is likely to be comparable to the linear case, as the molecular weight distributions from SDS-PAGE of these two cases are not distinguishable, but the branched structure provides extra topological interactions. The introduced branches retard the reptation of the entire molecule, as it is only after arm retraction that the reptation of the chain-extended backbone is allowed to happen (Mcleish, 2002). Although the coiled-coil relaxation is only slightly affected by the molecule topology (see Supplementary Figures 9, 10), the reptation regime broadens in the frequency spectrum and extends toward the low frequency regime. This

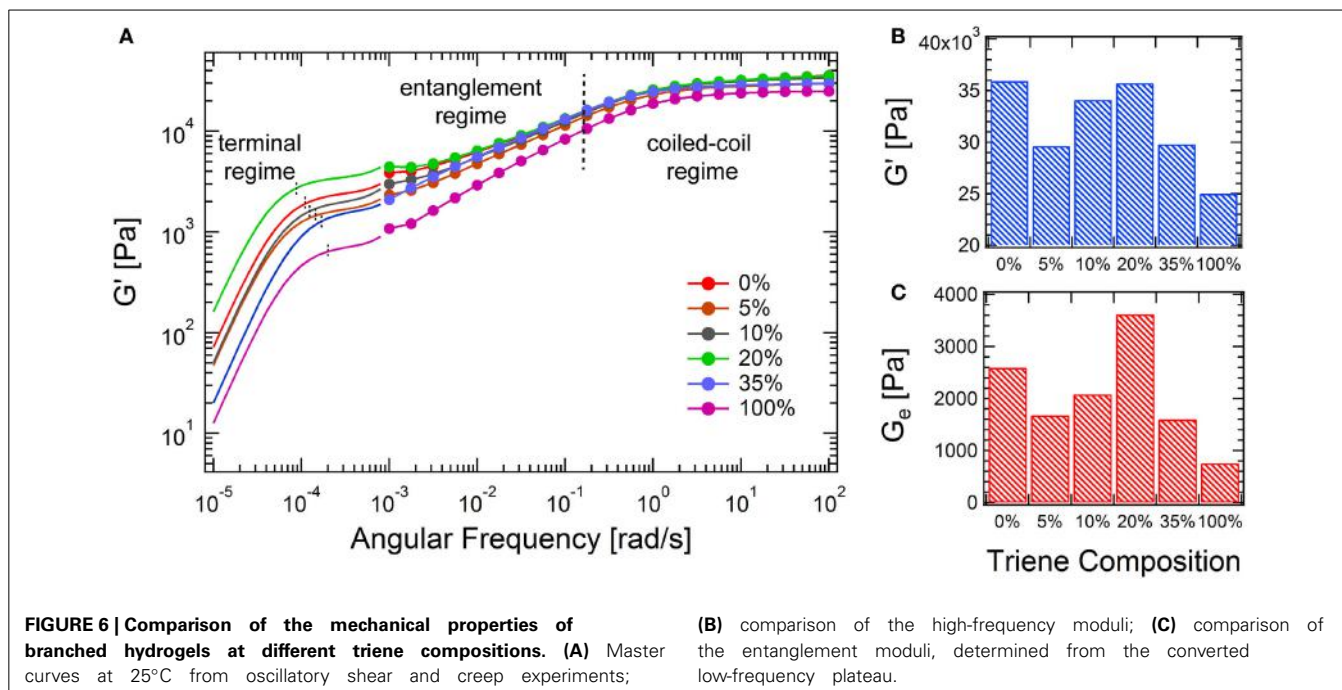


FIGURE 6 | Comparison of the mechanical properties of branched hydrogels at different triene compositions. (A) Master curves at 25°C from oscillatory shear and creep experiments;

(B) comparison of the high-frequency moduli; **(C)** comparison of the entanglement moduli, determined from the converted low-frequency plateau.

is consistent with the observation of randomly branched polymers in the melt state (Mcleish, 2002). Further increase of the triene composition leads to decreases in both G'_∞ and G_e . This is hypothesized to originate from the decreased endgroup conversion and the formation of hyperbranched molecular structures. The densely packed branches impose permanent topological barriers for different chains to entangle, which leads to much lower solution viscosities (Voit and Lederer, 2009). Recently, the viscoelasticity and the dynamic relaxation of the synthetic hydrogels is found to be essential to mimic the complex biological tissues (Mckinnon et al., 2013). The presented branching reaction in this study establishes a facile approach of tuning the network mechanics over the entire frequency window, especially in the long time relaxation, which can be useful in mimicking the properties of natural tissues.

CONCLUSION

Under appropriate conditions, thiol-maleimide, thiol-bromomaleimide and thiol-ene coupling can all result in significant chain extension. The differences in chemistries' reactivity and side reactions may cause variations in the molecular weight and its distribution of chain-extended proteins and the topological entanglement effect in gels. While thiol-maleimide conjugation is the most common and the easiest to implement, thiol-ene click chemistry can achieve high endgroup conversion fairly rapidly. Thiol-bromomaleimide shows its potential in reversibly modifying proteins, and using functionalized dibromomaleimide as a chain extender allows further control of hydrogels' properties by incorporating side chain functionalities into the protein architecture. Here, thermoresponsive changes in mechanical properties of gels are demonstrated with PNIPAM grafts. Lastly, branched proteins are prepared in $A_2 + B_2/B_3$ mixed type reactions. The entanglement plateau modulus is increased when branches are long enough to enhance topological constraints yet the added branches do not sacrifice the backbone length. In conclusion, the structure of engineered proteins and their assembly behaviors can be easily modified with the use of different chemistries, which presents a rich toolbox to tailor the structure-properties of protein materials in various applications.

ACKNOWLEDGMENTS

This research was supported by the U.S. Army Research Office through the Institute of Soldier Nanotechnologies under contract W911NF-07-D-0004. The authors would like to acknowledge Krystyn Van Vliet and Gareth McKinley for the use of rheometers, Alexander Babarti for providing training on the MCR 702 rheometer, and Muzhou Wang for assistance with FPLC.

SUPPLEMENTARY MATERIAL

The Supplementary Material for this article can be found online at: <http://www.frontiersin.org/journal/10.3389/fchem.2014.00023/abstract>

REFERENCES

- Baldwin, A. D., and Kiick, K. L. (2011). Tunable degradation of maleimide–thiol adducts in reducing environments. *Bioconjug. Chem.* 22, 1946–1953. doi: 10.1021/bc200148v
- Canalle, L. A., Lowik, D. W. P. M., and Van Hest, J. C. M. (2010). Polypeptide-polymer bioconjugates. *Chem. Soc. Rev.* 39, 329–353. doi: 10.1039/b807871h
- Chung, C., Lampe, K. J., and Heilshorn, S. C. (2012). Tetrakis(hydroxymethyl) phosphonium chloride as a covalent cross-linking agent for cell encapsulation within protein-based hydrogels. *Biomacromolecules* 13, 3912–3916. doi: 10.1021/bm3015279
- Convertine, A. J., Lokitz, B. S., Vasileva, Y., Myrick, L. J., Scales, C. W., Lowe, A. B., et al. (2006). Direct synthesis of thermally responsive DMA/NIPAM Diblock and DMA/NIPAM/DMA triblock copolymers via aqueous, room temperature RAFT Polymerization†. *Macromolecules* 39, 1724–1730. doi: 10.1021/ma0523419
- Cui, Y., Yan, Y., Chen, Y., and Wang, Z. (2013). Dibromomaleimide derivative as an efficient polymer coupling agent for building topological polymers. *Macromol. Chem. Phys.* 214, 470–477. doi: 10.1002/macp.201200614
- Davis, M. E., and Brewster, M. E. (2004). Cyclodextrin-based pharmaceuticals: past, present and future. *Nat. Rev. Drug Discov.* 3, 1023–1035. doi: 10.1038/nrd1576
- Davis, N. E., Ding, S., Forster, R. E., Pinkas, D. M., and Barron, A. E. (2010). Modular enzymatically crosslinked protein polymer hydrogels for *in situ* gelation. *Biomaterials* 31, 7288–7297. doi: 10.1016/j.biomaterials.2010.06.003
- Dealy, J. M., and Wissbrun, K. F. (1990). *Melt Rheology and Its Role in Plastics Processing: Theory and Applications*. New York, NY: Van Nostrand Reinhold.
- Dondoni, A., Massi, A., Nanni, P., and Roda, A. (2009). A new ligation strategy for peptide and protein glycosylation: photoinduced thiol–ene coupling. *Chem. Eur. J.* 15, 11444–11449. doi: 10.1002/chem.200901746
- Drury, J. L., and Mooney, D. J. (2003). Hydrogels for tissue engineering: scaffold design variables and applications. *Biomaterials* 24, 4337–4351. doi: 10.1016/S0142-9612(03)00340-5
- Dutton, S., Rolfs, H., and Stepto, R. F. T. (1994). Comparison of ahmad-rolfes-stepto theory, rate theory and monte-carlo modelling of gel point and network modulus. *Polymer* 35, 4521–4526. doi: 10.1016/0032-3861(94)90797-8
- Ferry, J. (1980). *Viscoelastic Properties of Polymers*. New York, NY: Wiley.
- Glassman, M. J., Chan, J., and Olsen, B. D. (2013). Reinforcement of shear thinning protein hydrogels by responsive block copolymer self-assembly. *Adv. Funct. Mater.* 23, 1182–1193. doi: 10.1002/adfm.201202034
- Glassman, M. J., and Olsen, B. D. (2013). Structure and mechanical response of protein hydrogels reinforced by block copolymer self-assembly. *Soft Matt.* 9, 6814–6823. doi: 10.1039/c3sm00102d
- Gong, J. P., Katsuyama, Y., Kurokawa, T., and Osada, Y. (2003). Double-network hydrogels with extremely high mechanical strength. *Adv. Mater.* 15, 1155–1158. doi: 10.1002/adma.200304907
- Graessley, W. W. (2004). *Polymeric Liquids and Networks: Structure and Properties*. New York, NY: Garland Science.
- Graessley, W. W. (2008). *Polymeric Liquids and Networks: Dynamics and Rheology*. London; New York: Garland Science.
- Guvendiren, M., Lu, H. D., and Burdick, J. A. (2012). Shear-thinning hydrogels for biomedical applications. *Soft Matt.* 8, 260–272. doi: 10.1039/c1sm06513k
- Haraguchi, K., and Takehisa, T. (2002). Nanocomposite Hydrogels: a unique organic–inorganic network structure with extraordinary mechanical, optical, and swelling/de-swelling properties. *Adv. Mater.* 14, 1120–1124. doi: 10.1002/1521-4095(20020816)14:16<1120::AID-ADMA1120>3.0.CO;2-9
- Harries, D., Rau, D. C., and Parsegian, V. A. (2005). Solutes probe hydration in specific association of cyclodextrin and adamantane. *J. Am. Chem. Soc.* 127, 2184–2190. doi: 10.1021/ja045541t
- Hermanson, G. T. (2008). *Bioconjugate Techniques, 2nd Edn*. Amsterdam: Elsevier.
- Holten-Andersen, N., Harrington, M. J., Birkedal, H., Lee, B. P., Messersmith, P. B., Lee, K. Y. C., et al. (2011). pH-induced metal-ligand cross-links inspired by mussel yield self-healing polymer networks with near-covalent elastic moduli. *Proc. Natl. Acad. Sci. U.S.A.* 108, 2651–2655. doi: 10.1073/pnas.1015862108
- Hoyle, C. E., and Bowman, C. N. (2010). Thiol–ene click chemistry. *Angewandte Chem. Int. Ed.* 49, 1540–1573. doi: 10.1002/anie.200903924
- Hoyle, C. E., Lowe, A. B., and Bowman, C. N. (2010). Thiol-click chemistry: a multifaceted toolbox for small molecule and polymer synthesis. *Chem. Soc. Rev.* 39, 1355–1387. doi: 10.1039/b901979k
- Janzen, J., and Colby, R. H. (1999). Diagnosing long-chain branching in polyethylenes. *J. Mol. Struct.* 485–486, 569–584. doi: 10.1016/S0022-2860(99)00097-6
- Jing, P., Rudra, J. S., Herr, A. B., and Collier, J. H. (2008). Self-assembling peptide-polymer hydrogels designed from the coiled coil region of fibrin. *Biomacromolecules* 9, 2438–2446. doi: 10.1021/bm800459v
- Jones, M. W., Strickland, R. A., Schumacher, F. F., Caddick, S., Baker, J. R., Gibson, M. I., et al. (2011). Polymeric dibromomaleimides as extremely efficient

- disulfide bridging bioconjugation and pegylation agents. *J. Am. Chem. Soc.* 134, 1847–1852. doi: 10.1021/ja210335f
- Kim, M., Tang, S., and Olsen, B. D. (2013). Physics of engineered protein hydrogels. *J. Polymer Sci. B Polymer Phys.* 51, 587–601. doi: 10.1002/polb.23270
- Kloxin, A. M., Kasko, A. M., Salinas, C. N., and Anseth, K. S. (2009). Photodegradable hydrogels for dynamic tuning of physical and chemical properties. *Science* 324, 59–63. doi: 10.1126/science.1169494
- Lai, J. T., Filla, D., and Shea, R. (2002). Functional polymers from novel carboxyl-terminated trithiocarbonates as highly efficient RAFT agents. *Macromolecules* 35, 6754–6756. doi: 10.1021/ma020362m
- Larson, R. G., Sridhar, T., Leal, L. G., Mckinley, G. H., Likhtman, A. E., and Mcleish, T. C. B. (2003). Definitions of entanglement spacing and time constants in the tube model. *J. Rheol.* 47, 809–818. doi: 10.1122/1.1567750
- Li, L., Teller, S., Clifton, R. J., Jia, X., and Kiick, K. L. (2011). Tunable mechanical stability and deformation response of a resilin-based elastomer. *Biomacromolecules* 12, 2302–2310. doi: 10.1021/bm200373p
- Lohse, D. J., Milner, S. T., Fetter, L. J., Xenidou, M., Hadjichristidis, N., Mendelson, R. A., et al. (2002). Well-defined, model long chain branched Polyethylene. 2. Melt rheological behavior. *Macromolecules* 35, 3066–3075. doi: 10.1021/ma0117559
- Lv, S., Dudek, D. M., Cao, Y., Balamurali, M. M., Gosline, J., and Li, H. (2010). Designed biomaterials to mimic the mechanical properties of muscles. *Nature* 465, 69–73. doi: 10.1038/nature09024
- Mckinnon, D. D., Domaille, D. W., Cha, J. N., and Anseth, K. S. (2013). Biophysically defined and cyocompatible covalently adaptable networks as Viscoelastic 3D cell culture systems. *Adv. Mater.* 26, 865–872. doi: 10.1002/adma.201303680
- Mcleish, T. C. B. (2002). Tube theory of entangled polymer dynamics. *Adv. Phys.* 51, 1379–1527. doi: 10.1080/00018730210153216
- Nathani, R. I., Chudasama, V., Ryan, C. P., Moody, P. R., Morgan, R. E., Fitzmaurice, R. J., et al. (2013). Reversible protein affinity-labelling using bromomaleimide-based reagents. *Org. Biomol. Chem.* 11, 2408–2411. doi: 10.1039/c3ob40239h
- Northrop, B. H., and Coffey, R. N. (2012). Thiol-ene click chemistry: computational and kinetic analysis of the influence of alkene functionality. *J. Am. Chem. Soc.* 134, 13804–13817. doi: 10.1021/ja305441d
- Petter, R. C., Salek, J. S., Sikorski, C. T., Kumaravel, G., and Lin, F. T. (1990). Cooperative binding by aggregated mono-6-(alkylamino)-beta-cyclodextrins. *J. Am. Chem. Soc.* 112, 3860–3868. doi: 10.1021/ja00166a021
- Rekharsky, M. V., and Inoue, Y. (1998). Complexation thermodynamics of cyclodextrins. *Chem. Rev.* 98, 1875–1918. doi: 10.1021/cr970015o
- Robin, M. P., Wilson, P., Mabire, A. B., Kiviah, J. K., Raymond, J. E., Haddleton, D. M., et al. (2013). Conjugation-induced fluorescent labeling of proteins and polymers using dithiomaleimides. *J. Am. Chem. Soc.* 135, 2875–2878. doi: 10.1021/ja3105494
- Ryan, C. P., Smith, M. E. B., Schumacher, F. F., Grohmann, D., Papaioannou, D., Waksman, G., et al. (2011). Tunable reagents for multi-functional bioconjugation: reversible or permanent chemical modification of proteins and peptides by control of maleimide hydrolysis. *Chem. Commun.* 47, 5452–5454. doi: 10.1039/c1cc11114k
- Sahin, E., and Kiick, K. L. (2009). Macromolecule-induced assembly of coiled-coils in alternating multiblock polymers. *Biomacromolecules* 10, 2740–2749. doi: 10.1021/bm900474k
- Schelté, P., Boeckler, C., Frisch, B., and Schuber, F. (1999). Differential reactivity of maleimide and bromoacetyl functions with thiols: application to the preparation of liposomal diepitope constructs. *Bioconjug. Chem.* 11, 118–123. doi: 10.1021/bc990122k
- Schöneich, C. (2008). Mechanisms of protein damage induced by cysteine thiol radical formation. *Chem. Res. Toxicol.* 21, 1175–1179. doi: 10.1021/tx800005u
- Shen, W., Lammertink, R. G. H., Sakata, J. K., Kornfield, J. A., and Tirrell, D. A. (2005). Assembly of an artificial protein hydrogel through leucine zipper aggregation and disulfide bond formation. *Macromolecules* 38, 3909–3916. doi: 10.1021/ma048348s
- Smith, M. E. B., Schumacher, F. F., Ryan, C. P., Tedaldi, L. M., Papaioannou, D., Waksman, G., et al. (2010). Protein modification, bioconjugation, and disulfide bridging using bromomaleimides. *J. Am. Chem. Soc.* 132, 1960–1965. doi: 10.1021/ja908610s
- Stephanopoulos, N., and Francis, M. B. (2011). Choosing an effective protein bioconjugation strategy. *Nat. Chem. Biol.* 7, 876–884. doi: 10.1038/nchembio.720
- Sun, J.-Y., Zhao, X., Illeperuma, W. R. K., Chaudhuri, O., Oh, K. H., Mooney, D. J., et al. (2012). Highly stretchable and tough hydrogels. *Nature* 489, 133–136. doi: 10.1038/nature11409
- Tanaka, F. (2011). *Polymer Physics: Applications to Molecular Association and Thermoreversible Gelation*. Cambridge: Cambridge University Press. doi: 10.1017/CBO9780511975691
- Tang, S., Glassman, M. J., Li, S., Socrate, S., and Olsen, B. D. (2014). Oxidatively responsive chain extension to entangle engineered protein hydrogels. *Macromolecules* 47, 791–799. doi: 10.1021/ma401684w
- Trabbic-Carlson, K., Setton, L. A., and Chilkoti, A. (2003). Swelling and mechanical behaviors of chemically cross-linked hydrogels of elastin-like polypeptides. *Biomacromolecules* 4, 572–580. doi: 10.1021/bm025671z
- Valkevich, E. M., Guenette, R. G., Sanchez, N. A., Chen, Y.-C., Ge, Y., and Strieter, E. R. (2012). Forging isopeptide bonds using thiol-ene chemistry: site-specific coupling of ubiquitin molecules for studying the activity of isopeptidases. *J. Am. Chem. Soc.* 134, 6916–6919. doi: 10.1021/ja300500a
- Voit, B. I., and Lederer, A. (2009). Hyperbranched and highly branched polymer architectures—synthetic strategies and major characterization aspects. *Chem. Rev.* 109, 5924–5973. doi: 10.1021/cr900068q
- Wan, Q., and Danishefsky, S. J. (2007). Free-radical-based, specific desulfurization of cysteine: a powerful advance in the synthesis of polypeptides and glycopolypeptides. *Angewandte Chem. Int. Ed.* 46, 9248–9252. doi: 10.1002/anie.200704195
- Wang, Q., Mynar, J. L., Yoshida, M., Lee, E., Lee, M., Okuro, K., et al. (2010a). High-water-content mouldable hydrogels by mixing clay and a dendritic molecular binder. *Nature* 463, 339–343. doi: 10.1038/nature08693
- Wang, Z., Chen, X., and Larson, R. G. (2010b). Comparing tube models for predicting the linear rheology of branched polymer melts. *J. Rheol.* (1978–present) 54, 223–260. doi: 10.1122/1.3301246
- Weinrich, D., Lin, P.-C., Jonkheijm, P., Nguyen, U. T. T., Schröder, H., Niemeyer, C. M., et al. (2010). Oriented immobilization of farnesylated proteins by the thiol-ene reaction. *Angewandte Chem. Int. Ed.* 49, 1252–1257. doi: 10.1002/anie.200906190
- Wood-Adams, P., and Costeux, S. (2001). Thermorheological behavior of polyethylene: effects of microstructure and long chain branching. *Macromolecules* 34, 6281–6290. doi: 10.1021/ma0017034
- Wu, L. C., Yang, J., and Kopeček, J. (2011). Hybrid hydrogels self-assembled from graft copolymers containing complementary β -sheets as hydroxyapatite nucleation scaffolds. *Biomaterials* 32, 5341–5353. doi: 10.1016/j.biomaterials.2011.04.014
- Zhang, W.-B., Sun, F., Tirrell, D. A., and Arnold, F. H. (2013). Controlling macromolecular topology with genetically encoded sputag-spycatcher chemistry. *J. Am. Chem. Soc.* 135, 13988–13997. doi: 10.1021/ja4076452
- Zhou, H., Woo, J., Cok, A. M., Wang, M., Olsen, B. D., and Johnson, J. A. (2012). Counting primary loops in polymer gels. *Proc. Natl. Acad. Sci. U.S.A.* 109, 19119–19124. doi: 10.1073/pnas.1213169109
- Conflict of Interest Statement:** The authors declare that the research was conducted in the absence of any commercial or financial relationships that could be construed as a potential conflict of interest.
- Received:** 03 March 2014; **accepted:** 22 April 2014; **published online:** 14 May 2014.
- Citation:** Tang S and Olsen BD (2014) Controlling topological entanglement in engineered protein hydrogels with a variety of thiol coupling chemistries. *Front. Chem.* 2:23. doi: 10.3389/fchem.2014.00023
- This article was submitted to Chemical Biology, a section of the journal Frontiers in Chemistry.
- Copyright © 2014 Tang and Olsen. This is an open-access article distributed under the terms of the Creative Commons Attribution License (CC BY). The use, distribution or reproduction in other forums is permitted, provided the original author(s) or licensor are credited and that the original publication in this journal is cited, in accordance with accepted academic practice. No use, distribution or reproduction is permitted which does not comply with these terms.



Transient dynamic mechanical properties of resilin-based elastomeric hydrogels

Linqing Li¹ and Kristi L. Kiick^{1,2,3*}

¹ Department of Materials Science and Engineering, University of Delaware, Newark, DE, USA

² Biomedical Engineering, University of Delaware, Newark, DE, USA

³ Delaware Biotechnology Institute, Newark, DE, USA

Edited by:

Carissa M. Soto, Naval Research Laboratory, USA

Reviewed by:

Paola Laurienzo, Italian Research Council (CNR), Italy

Chao Zhang, University of Southern California, USA

***Correspondence:**

Kristi L. Kiick, Department of Materials Science and Engineering, University of Delaware, 212 DuPont Hall, Newark, DE 19716, USA

e-mail: kiick@udel.edu

The outstanding high-frequency properties of emerging resilin-like polypeptides (RLPs) have motivated their development for vocal fold tissue regeneration and other applications. Recombinant RLP hydrogels show efficient gelation, tunable mechanical properties, and display excellent extensibility, but little has been reported about their transient mechanical properties. In this manuscript, we describe the transient mechanical behavior of new RLP hydrogels investigated via both sinusoidal oscillatory shear deformation and uniaxial tensile testing. Oscillatory stress relaxation and creep experiments confirm that RLP-based hydrogels display significantly reduced stress relaxation and improved strain recovery compared to PEG-based control hydrogels. Uniaxial tensile testing confirms the negligible hysteresis, reversible elasticity and superior resilience (up to 98%) of hydrated RLP hydrogels, with Young's modulus values that compare favorably with those previously reported for resilin and that mimic the tensile properties of the vocal fold ligament at low strain (<15%). These studies expand our understanding of the properties of these RLP materials under a variety of conditions, and confirm the unique applicability, for mechanically demanding tissue engineering applications, of a range of RLP hydrogels.

Keywords: resilin-like polypeptide, elastomer, hydrogel, biomaterials, vocal fold

INTRODUCTION

Elastomeric biomaterials have long been targets for application in the engineering of mechanically active tissues, and recently introduced resilin-like polypeptides (RLPs) may have unique suitability for such applications. In particular, our laboratories have been developing RLPs for application in the treatment of vocal fold pathologies. Human phonation occurs in the larynx by airflow-induced, self-sustained oscillation of a layered connective tissue called the vocal fold lamina propria (LP), which is the major vibratory tissue activated during phonation (Titze, 1984, 1989; Jiang and Tao, 2007). The vibration of the vocal folds is controlled actively by an aerodynamic driving force (e.g., lung pressure), vocal fold positioning, and non-linear interactions, but most importantly depends on the viscoelasticity of the connective tissue of the vocal fold LP; (Riede et al., 2011) these mechanical properties are important both in terms of short transient responses and longer time-dependent behavior (Titze, 1988; Chan and Titze, 1999, 2000; Chan, 2004; Klemuk and Titze, 2004). Two distinct types of forces are involved in human phonation: oscillatory shear force generated from the vibration of the vocal mucosa and longitudinal stretching force derived from elongation of the vocal ligament at high pitch or large tissue deformation (Titze, 1988; Min et al., 1995; Chan and Titze, 1999, 2000). The viscoelastic properties of the vocal mucosa under shear deformation contribute to key parameters of phonation, such as the fundamental frequency, the amplitude of oscillation, and phonation threshold pressure. Titze and co-workers showed that phonation threshold pressure is directly related to the

viscoelasticity of vocal fold mucosa under small amplitude oscillation (Titze, 1988). Min et al. reported mechanical properties of the human vocal ligament under longitudinal force, including the Young's modulus (33 kPa at low-strain and 600 kPa at high-strain), non-linear tensile elasticity, and hysteresis along the direction of tissue fibers (Min et al., 1995).

Mechanical stress from excessive phonation, deleterious environmental factors, and pathological conditions can disrupt the natural pliability of the vocal folds, resulting in a wide spectrum of vocal disorders and causing significant implications for individual health, social productivity, and occupational function (Zeitels et al., 2002). Surgical approaches for vocal fold augmentation or mucosal reconstruction have employed a variety of either injectable or implantable synthetic and biological materials (Hallén et al., 2001; Hirano et al., 2008; Jahan-Parwar et al., 2008; Kwon and Lee, 2008; Kishirnoto et al., 2009; Kutty and Webb, 2009b). Although improvements in voice production have been reported, limitations such as implant migration, foreign body reaction, stiffness, immunological consequences, and the need of multi-stage procedures largely have prevented restoration of functional vocal fold tissue. Recent studies aimed at the regeneration of vocal fold LP highlighted the importance of mechanical stimulation, which is directly related to the minimum subglottic air pressure needed to initiate vocal fold oscillation, and regulation of the subsequent matrix composition (Jiao et al., 2009; Kutty and Webb, 2009a; Teller et al., 2012).

Knowledge of the mechanical properties of materials targeted for vocal fold therapies is important clinically in terms of the

surgical management of vocal fold disorders. However, the introduction of injectable or implantable biomaterials into the vocal fold can change the mechanical properties of the vocal fold and thus alter the mechanics of vocal fold oscillation. This is an issue of considerable clinical importance, as pathologic changes in the biomedical properties of vocal fold ECM could severely impair normal vocal fold oscillation and potentially cause severe phonation difficulties. This is particularly true in small amplitude oscillation like phonation onset and offset (Chan and Titze, 1999, 2000; Chan, 2001); these oscillations involve a surface mucosal shear wave, and frequent vibrational and shear forces are thus applied to vocal fold connective tissue. The mechanical properties of implantable/injectable biomaterials under shear are therefore particularly significant when intended for these applications.

We and others have previously reported the outstanding mechanical properties of emerging RLPs for the production of new elastomeric biomaterials, and we have been interested in coupling the biological activity of a matrix with useful high-frequency mechanical behavior for vocal fold tissue regeneration (Elvin et al., 2005; Charati et al., 2009; Li et al., 2010, 2011; Li and Kiick, 2013). The modular, recombinantly synthesized RLPs can be rapidly cross-linked via a Mannich-type condensation reaction to yield hydrogels with mechanical properties—storage shear moduli (500 Pa to 10 kPa), Young's moduli (15–35 kPa), resilience values (>90%), and storage shear moduli at high frequency (1000–2000 Pa)—that are consistent with the reported mechanical properties of native vocal fold tissues (Jiao et al., 2009; Teller et al., 2012). These RLPs also exhibit enzymatic-triggered degradation, facilitate the 2D adhesion and spreading of various cell types, and support the 3D encapsulation and survival of hMSCs *in vitro*, offering opportunities for fabricating either implantable or injectable scaffolds for vocal fold tissue therapies (Charati et al., 2009; Li et al., 2011, 2013; McGann et al., 2013).

To date, efforts have been conducted on matching the shear modulus and Young's modulus of various materials with those of natural vocal fold tissues (Thibeault et al., 2009, 2011); however, transient mechanical responses have not commonly been characterized for the materials that are proposed for vocal fold tissue engineering, particularly via oscillatory rheology methods. The investigation of transient biomechanical responses is highly relevant, however, as Zhang et al. demonstrated that the transient mechanical response of the vocal fold tissue can influence phonation processes. (Zhang et al., 2009) Given this lack of information on the dynamic transient mechanical analysis of materials proposed for vocal fold therapies, this manuscript describes both sinusoidal oscillatory shear deformation and uniaxial tensile stress-strain mechanical characterization of RLP-based hydrogels, and in particular the transient and time-dependent behavior that is of relevance for the vocal fold mucosa and vocal ligament tissues during phonation (Min et al., 1995; Zhang et al., 2007, 2009). Stress relaxation and creep experiments via oscillatory shear rheology were characterized to investigate the reduction of shear stress at a constant strain and the response of strain at a constant stress; relaxation rates were calculated from the stress relaxation data (Lv et al., 2010; Chen et al., 2012). The behavior of the RLP-based hydrogels was experimentally compared to that of polymeric PEG hydrogels. Uniaxial tensile testing of the

RLP hydrogels, including stress relaxation and cyclic stress-strain deformation up to 10 cycles, was explored to determine Young's modulus, investigate hysteresis, and calculate resilience.

MATERIALS AND METHODS

MATERIALS

Chemically competent cells of *E. coli* strain M15[pREP4] (for transformation of recombinant plasmids) and Ni-NTA agarose resin (for protein purification) were purchased from Qiagen (Valencia, CA). The tri-functional cross-linker tris(hydroxymethyl phosphine) (THP) was purchased from Strem Chemicals (Newburyport, MA). 20 kDa, amine-terminated, 4-arm PEG was purchased from Creative PEG Works (Winston Salem, NC). All other chemicals were obtained from Sigma-Aldrich (St. Louis, MO) or Fisher Scientific (Waltham, MA) and were used as received unless otherwise noted. Water was deionized and filtered through a NANOpure Diamond water purification system (Dubuque, IO).

EXPRESSION AND PURIFICATION OF RLP

Genes encoding the RLP polypeptide(s) were produced as described in our previous reports (Li et al., 2013); RLP protein expression and purification was also conducted as previously described (Charati et al., 2009; Li et al., 2011, 2013). The purity and molecular weight of the protein were confirmed *via* high performance liquid chromatography (HPLC), sodium dodecyl sulfate polyacrylamide gel electrophoresis (SDS-PAGE), and matrix-assisted laser desorption/ionization-time of flight mass spectrometry (MALDI-TOF-MS); the composition of the RLPs were probed via amino acid analysis. Approximately 20–30 mg of polypeptide per liter of cell culture was obtained after dialysis and lyophilization.

RLP AND PEG HYDROGEL FORMATION AND OSCILLATORY RHEOLOGY

The formation of RLP-based hydrogels was monitored on a stress-controlled rheometer (ARG2, TA Instruments, New Castle, DE), with a 20 mm diameter cone-on-plate geometry and a 1° cone angle with a 25 mm gap distance at 37°C. Various amounts (2, 4, and 8 mg) of RLP were dissolved in pH 7.4 PBS to attain final concentrations of 50, 100, and 200 mg mL⁻¹ respectively. Stock solutions of both the RLP and the cross-linker THP (100 mg mL⁻¹) were chilled on ice before mixing in order to slow the rate of the cross-linking reaction, preventing cross-linking during handling. 0.7, 1.3, and 2.6 μL THP stock solution was added to 39.3, 38.7, and 37.4 μL of RLP stock solutions, respectively, to yield a final solution volume of 40 μL and 5, 10, and 20 wt% hydrogels with a 1:1 cross-linking ratio (molar ratio of lysine residues to reactive hydroxymethylphosphine (HMP) groups). For control samples, 4 mg 20 kDa, 4-arm, amine-functionalized PEG was dissolved in pH 7.4 PBS followed by the addition of 0.5 μL of THP stock solution (1:1 cross-linking ratio) to achieve the final 40 μL 10 wt% PEG hydrogel. To ensure homogeneous mixing, the mixture was vortexed gently for less than 5 s after the addition of the THP, and then followed by careful pipetting onto the rheometer Peltier plate for *in situ* rheological characterization. Time sweep studies were performed at a constant frequency (6 rad s⁻¹) while frequency sweeps were conducted from 0.1 to

100 rad s⁻¹ at a fixed strain amplitude of 1%. Strain sweeps were collected from 0.1 to 1000% strain at a constant frequency of 6 rad s⁻¹ to determine the strain-to-break value in shear mode. Light mineral oil was applied to the perimeter of the sample to prevent evaporation of buffer over the course of the experiment. Experiments were repeated with four samples and representative data are presented.

OSCILLATORY STRESS RELAXATION AND CREEP EXPERIMENTS

After the hydrogels were formed as described above, stress relaxation and creep analysis were performed on RLP hydrogels (5, 10, and 20 wt%) and 10 wt% PEG hydrogels as controls. Four replicates for each testing condition were prepared for both characterization methods. For stress relaxation, the shear stress was monitored over 10 min at a constant strain (15, 45, and 90%) for each RLP and PEG hydrogel, and the data was fitted to an exponential decay function to calculate the relaxation rate. For creep experiments, shear strain was monitored the first 20 min after a shear stress (ranging from 50 to 4000 Pa) was applied, and followed by another 20 min when the shear stress was removed, to explore the percentage of strain recovered upon removal of applied stress.

UNIAXIAL TENSILE TESTING

RLP films for uniaxial mechanical testing were prepared in contact lens molds (Bausch and Lomb, Rochester, NY) by the addition of desired amounts of THP to 20 wt% RLP in PBS buffer. The hydrogel films were cross-linked at 37°C for 2 h. Before the measurements, hydrogel films were hydrated in PBS overnight to reach equilibrium and cut into dog-bone specimens with a stainless steel mold (width 2 mm; length 6 mm). (The PEG hydrogels could not be characterized via tensile testing owing to the poor mechanical properties of the PEG hydrogels.) The test samples were mounted on an Instron 4502 mechanical tester equipped with a 250 g mechanical load cell and were tested at room temperature under hydrated conditions, utilizing a tank containing saline buffer around the grips. For stress relaxation experiments, three replicates of RLP hydrogel samples were stretched to 15, 30, 60, and 100% strain at a constant strain rate of 5 mm/min, and then the stress was monitored over 10 min at each fixed strain. For cyclic loading and unloading experiments, stress-strain data were recorded at the same strain rate and the hydrogel films were subjected to three cycles each to strains of 30, 60, and 100%, and then to failure. Resilience values were obtained by dividing the area under the unloading curves by the area under the loading curves at each fixed cycle; average values were obtained from at least three replicate samples. Young's modulus values were calculated from the linear region (5–15%) of the stress-strain curve.

RESULTS AND DISCUSSION

EXPRESSION AND PURIFICATION OF RLPs

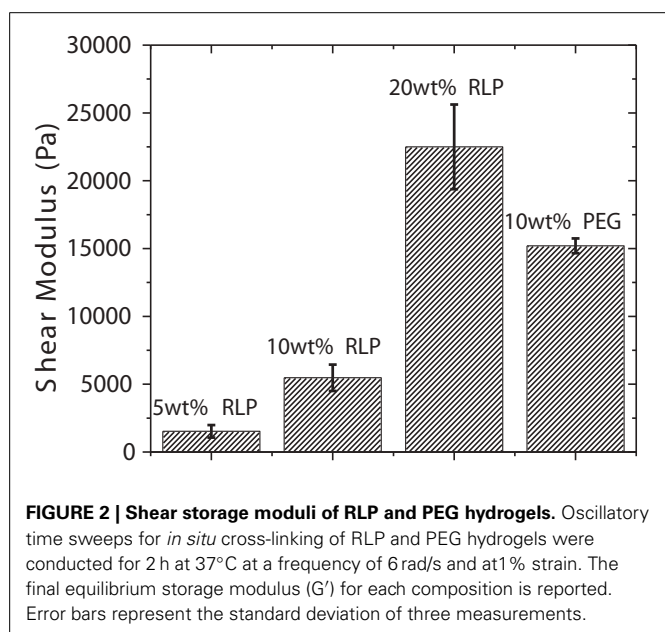
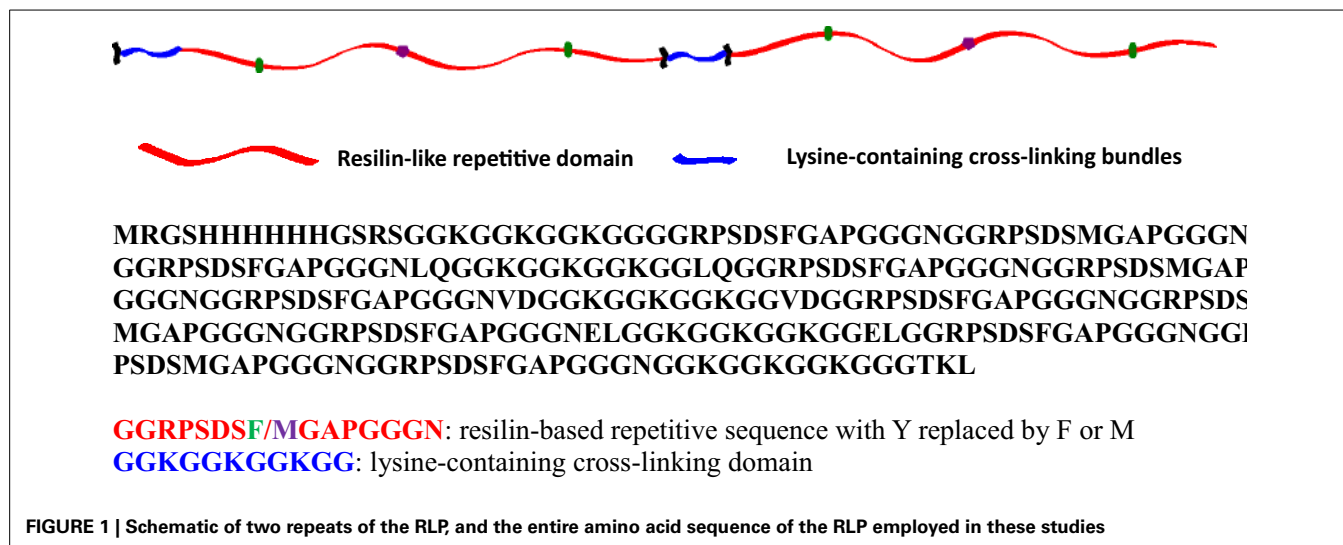
The detailed amino acid sequence of the RLP is presented in **Figure 1**. Twelve repeats of the pro-resilin putative consensus sequence (GGRPSDSFGAPGGGN, derived from the first exon of *Drosophila melanogaster* CG15920) was employed (Charati et al., 2009; Li et al., 2011, 2013; McGann et al., 2013). Five lysine-containing GGKGGKGGGG cross-linking bundles were

incorporated and placed evenly along the polypeptide chain, with 45 amino acids in between, to mimic the cross-link density in natural resilin (ca. 30–60 amino acids between di- and tri-tyrosine crosslinks) (Andersen, 1964; Elliott et al., 1965). The expression of RLP, via traditional IPTG induction, yielded 20–30 mg/L protein per liter of cell culture. Cell pellets were lysed under native conditions, followed by washing steps and elution from a Ni-NTA column in native buffer, followed by dialysis against DI H₂O to remove salts before lyophilization. The molecular weight (23 kDa), purity (>95%), and final composition of the RLP samples were confirmed via SDS-PAGE, MALDI-TOF MS, HPLC, and amino acid analysis (Li et al., 2013).

OSCILLATORY RHEOLOGICAL CHARACTERIZATION OF RLP AND PG HYDROGELS

In situ oscillatory shear rheology was employed to monitor the viscoelastic properties of the RLP hydrogels and provided a practical approach to characterize the impact of crosslinking conditions on gelation kinetics, gel stability and ultimate equilibrium shear moduli of hydrogels. Guided by the vocal fold ECM composition and distribution *in vivo*, we chose RLP hydrogels at 5, 10, and 20 wt% material concentrations, and characterized the RLP materials under physiologically relevant strain (15–90%) and stress (50–4000 Pa) ranges (Jiang et al., 2000; Kutty and Webb, 2009b). The hydrogels were cross-linked under mild aqueous conditions via the Mannich-type condensation reaction of THP with primary amines from the lysine residues of polypeptide. Protein and polymer solutions were pre-vortexed with THP solutions, to ensure homogeneous mixing, at room temperature before deposition of the solution onto the Peltier plate to form hydrogels, at an equimolar ratio of reactive lysines to HMP groups.

The shear mechanical moduli of cross-linked RLPs were characterized *in situ* via dynamic oscillatory shear mode rheometry using a cone-on-plate geometry after cross-linking the hydrogels under physiologically relevant conditions. Samples tested using two cone-on-plate geometries with different cone-angles resulted in similar gelation times, times to plateau, and final storage moduli, confirming the lack of slip during these dynamic oscillatory shear rheological experiments. Both RLP- and PEG-hydrogels were characterized in time sweep, frequency sweep, and strain sweep modes; the equilibrium shear storage moduli (G') and strain sweep profiles for the various hydrogels are presented in **Figure S1**, **Figures 2, 3**. During the time sweep experiment, all polypeptide solutions exhibited fast gelation, at 37°C, upon mixing with THP cross-linker at 1:1 stoichiometric ratio; shear storage moduli reached an equilibrium value within 10 min with 50–100-fold differences (data not shown) between the storage modulus (G') and loss modulus (G''), indicating the formation of solid elastic hydrogels. Increasing protein concentration increased the rate of gelation and also resulted in increased final storage modulus values, as expected; RLP hydrogels of concentrations at 5, 10, and 20 wt% yielded storage modulus values of 1, 5, and 20 kPa, while a 10 wt% PEG control hydrogels yielded a storage modulus of 15 kPa (**Figure 2**). The 10 wt% PEG hydrogel was chosen not only to match the polymer concentration of the 10 wt% RLP hydrogel, but also to achieve a G' value between those of the 10 and 20 wt% RLP hydrogels.



Dynamic oscillatory frequency sweeps ranging from 0.1 to 100 rad/s were then employed to assess the stability of RLP- and PEG-hydrogels; the insensitivity of shear moduli over the frequency range investigated confirmed the hydrogels behave as elastic solid-like materials derived from permanently cross-linked networks (data not shown). Finally, oscillatory shear strain sweeps from 0.1 to 1000% at 6 rad/s were characterized to illustrate the yield behavior of RLP- and PEG-hydrogels over various compositions; the results of these experiments are summarized in **Figure 3**. As shown in the figure, the linear regime extends to approximately 30, 60, 100, and 1000% strain for 5, 10, 20 wt% RLP hydrogels and the 10 wt% 4-arm PEG hydrogel, respectively (**Figures 3A–D**). For the RLP-based hydrogels, further increases in strain amplitude result in an increase in both the storage (G')

and loss moduli (G'') until they cross-over ($G'' > G'$), with a sharp overall decrease in the stress response resulting from failure of the gel network. The strain stiffening observed in these hydrogels is consistent with that observed in multiple other biological hydrogels (including native vocal folds) as well as in other synthetic networks (Xu and Craig, 2011; Xu et al., 2012); strain stiffening in biological tissues may serve as a means to prevent tissue damage from exposure to large deformation (Storm et al., 2005; Erk et al., 2010). Quantitatively, the average oscillatory shear strain-to-break values are $240 \pm 30\%$, $190 \pm 20\%$, and $160 \pm 20\%$ for the 5, 10, and 20 wt% RLP hydrogels, respectively. The PEG hydrogels did not exhibit a sharp decrease in the amplitude of the shear stress [even though G'' exceeds G' (**Figure 3D**)], suggesting slipping of materials under large strain. All subsequent stress relaxation and creep experiments were conducted well below 100% strain, where no significant slip was indicated. The hydrogels were also tested under continuous shear in steady shear flow, strain-to-break experiments; the data from these experiments are shown in **Figure 3E**. Although these conditions do not mimic the mechanical environment of human vocal folds *in vivo*, the data provide additional information to compare strain-to-break properties of RLP hydrogels to the data acquired from oscillatory experiments. As shown in the figure, the strain-to-break values for RLPs are $220 \pm 7\%$, $200 \pm 6\%$, and $150 \pm 20\%$ at 5, 10, and 20 wt% polypeptide concentrations, which are in good agreement with results from dynamic shear strain sweeps.

OSCILLATORY SHEAR STRESS RELAXATION

The time-dependent mechanical properties of tissues are important to their function and repair. For example, the repair of vocal fold tissue should benefit from the match of stress-relaxation behavior to that of native tissue, especially during phonation, to permit stimulation of appropriate cellular behavior with desired matrix deposition. In matrices intended for drug delivery, the application of controlled mechanical strain over select periods of time can be useful for regulating the release of drugs (Titze, 1988; Chan and Titze, 1999, 2000; Zhang et al., 2009; Xiao et al.,

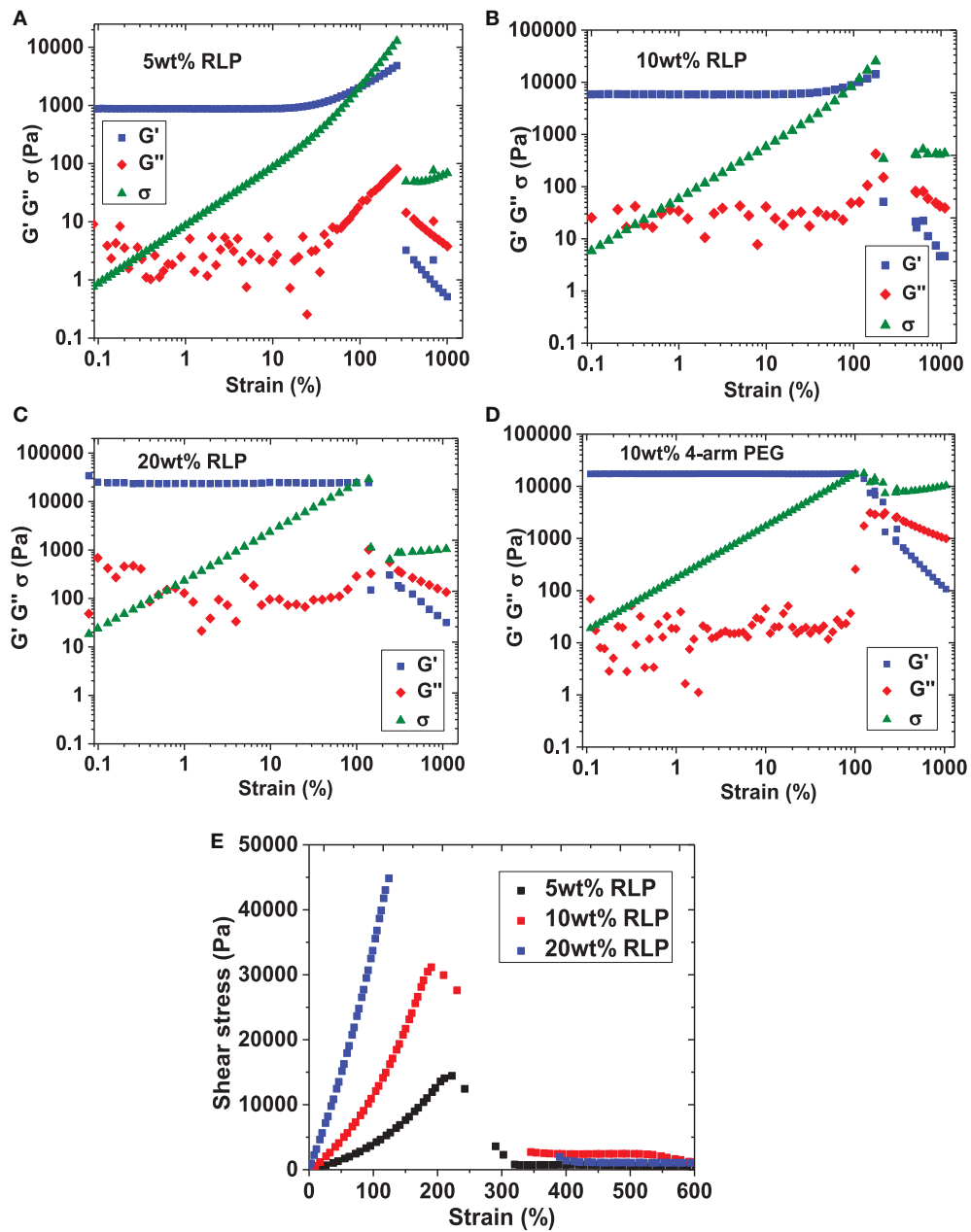


FIGURE 3 | Strain sweeps of RLP hydrogels at (A) 5wt%, (B) 10wt%, and (C) 20wt% polypeptide concentrations and (D) 10wt% 4-arm PEG hydrogels. (E) Summary of steady shear flow, strain-to-break experiments on

all RLP compositions, yielding similar strain-to-break values compared to those collected under oscillatory mode (5 wt%: $220 \pm 7\%$; 10 wt%: $200 \pm 6\%$; 20 wt%: $150 \pm 20\%$).

2013). In order to further explore the energy dissipation behavior of RLP-based hydrogels, the oscillatory shear stress relaxation of *in situ* cross-linked RLP hydrogels was characterized; the relaxation behavior of these materials is relevant owing to the importance of transient mechanical responses of the vocal fold tissue in phonation.

Shear stress relaxation experiments were conducted on 5, 10, and 20 wt% RLP hydrogels and the 10 wt% PEG control hydrogel. After hydrogel formation was complete (indicated by G'

reaching a plateau), each sample was subjected, consecutively, to 15%, then 45%, and finally 90% strain values, for 10 min at each strain. The oscillatory shear stress was monitored over time; representative data are shown in Figure 4. When the cross-linked RLP hydrogels were deformed to 15, 45, and 90% strain, the shear stress quickly increased and reached a maximum value; this behavior was observed across all polypeptide concentrations and applied strains (Figures 4A–C). This essentially instantaneous increase of shear stress demonstrates the highly elastic response

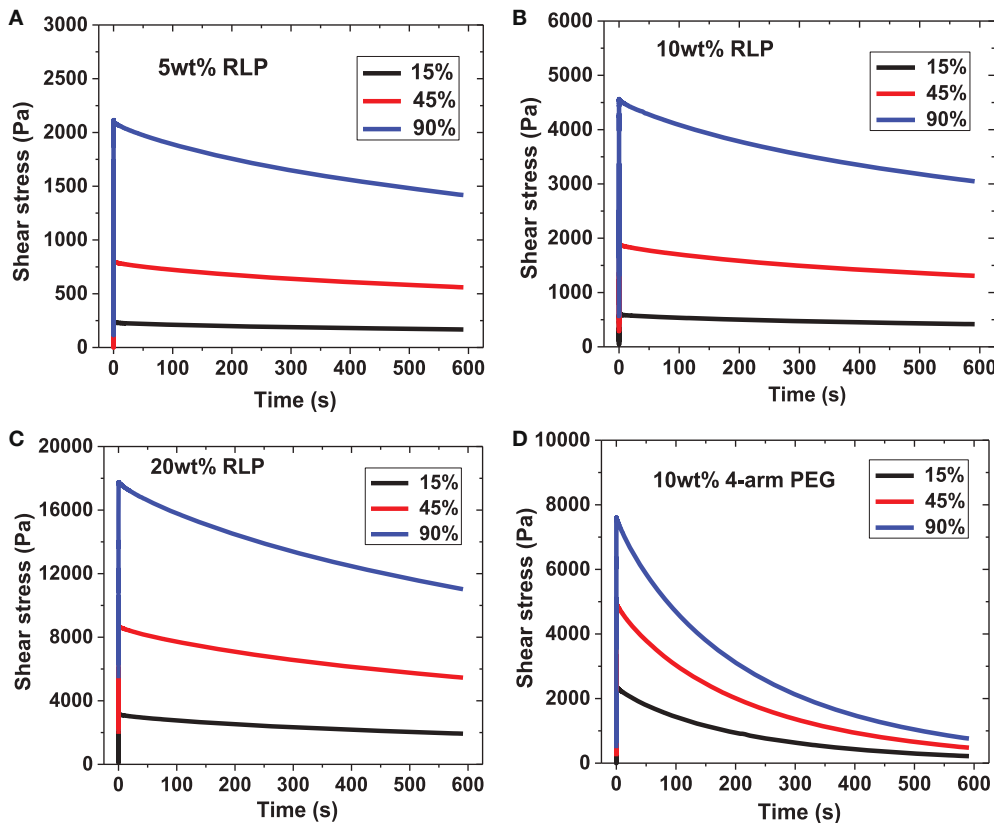


FIGURE 4 | Representative oscillatory stress relaxation data. (A) 5 wt% RLP, **(B)** 10 wt% RLP, **(C)** 20 wt% RLP and **(D)** 10 wt% 4-arm PEG cross-linked hydrogels at 15, 45, and 90% strain.

of RLP-hydrogels to external energy input, as anticipated for an ideal rubber. The shear stress was then monitored as a function of time for 10 min under constant strain; this time period was chosen based upon the fact that the time scale is long enough to observe any stress relaxation from dynamic protein chain movements as well as to maintain experimental conditions similar to those reported for other recombinant or natural proteins. The 5, 10, and 20 wt% RLP hydrogels exhibited similar stress relaxation behavior (Figures 4A–C), with a largely elastic response with relatively minor stress relaxation after each incremental strain. This behavior is similar to the stress relaxation response reported for canine vocalis muscle tissue (Alipour-Haghghi and Titze, 1985). The stress relaxation of the 10 wt% PEG hydrogel (Figure 4D), however, was markedly different. Although the PEG hydrogels also exhibited an immediate increase in stress similar to that observed for the RLP hydrogels (as expected for the chemically cross-linked network), the PEG hydrogel network was not able to hold the energy input over time and displayed a significant decrease in shear stress under the same experimental conditions. These differences are suggested to arise from the intrinsic disparities in the properties of the polymer chains of these two systems, given that the crosslinking densities and chemistries are similar between the PEG control and the RLP hydrogels. Among the RLP hydrogels, a slight increase in stress relaxation is observed with an increase in RLP concentration, suggesting that

the higher-concentration samples are less elastomeric, consistent with the reported importance of hydration in the elastomeric behavior of RLPs (Gosline et al., 2002; Truong et al., 2011).

In order to facilitate comparison of the data, the shear stresses for all materials recorded at time 0, 100, and 600 s were tabulated. The stresses at later time-points were compared to the initial stress and the percentage of shear stress lost was calculated; the averaged data are listed in Table S1 and illustrated graphically in Figure 5. The short-scale (100 s) and long-time (600 s) intervals were chosen to facilitate the comparison to reported stress relaxation properties of other previously reported materials. The initial shear stress ($t = 0$ s) upon input of elastic energy increased with an increase in applied strain, and with RLP hydrogel concentration, as expected. The RLP hydrogels exhibited a relatively minor reduction in stress compared to the initial shear stress, with reductions of approximately 10% at 100 s (Figure 5A) and 35% at 600 s (Figure 5B), over all three RLP hydrogel concentrations and all applied strains. In contrast, the PEG hydrogels exhibited almost 35 and 90% reduction in shear stress at 100 and 600 s. Although select other PEG-based materials have shown less stress relaxation than observed here, the reduced stress relaxation was observed in systems of higher polymer concentrations, different cross-linking chemistries, and tightly cross-linked networks mixed with multiple components (Snyders et al., 2007; Roberts et al., 2011; Cui et al., 2012).

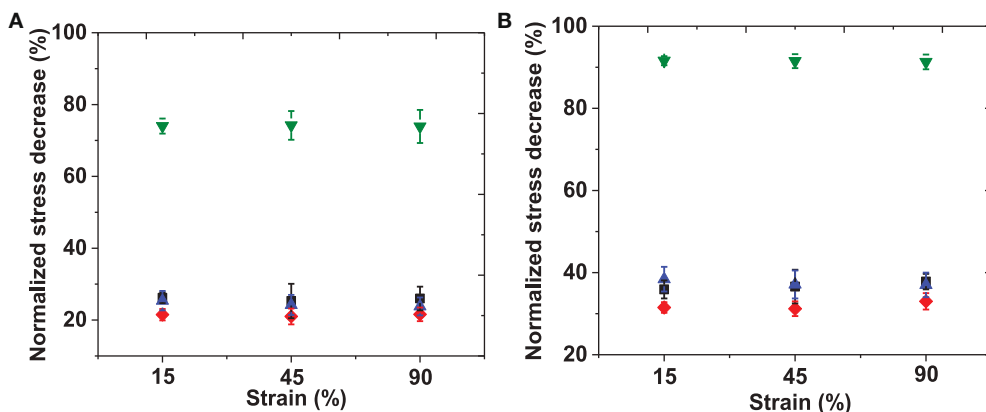


FIGURE 5 | Percentage of normalized shear stress decreased at (A) 100s and (B) 600s. Shear stresses at each strain were normalized to the shear stress at $t = 0$ min of 5 wt% (black), 10 wt% (red), 20 wt% (blue)

RLPs and 10 wt% 4-arm PEG hydrogels (green) at 15, 45, and 90% constant strains. Error bars represent the standard deviation of three measurements.

In order to quantitatively analyze the stress relaxation, the stress relaxation curves of RLP and PEG hydrogels were fit to a single exponential equation: $\sigma(t) = \sigma_0 + A^* \exp(-tk)$, where σ_0 is the offset shear stress, A is the decay amplitude, and k is the relaxation rate. Representative stress relaxation curves and fits for the 10 wt% RLP and 10 wt% PEG hydrogels are shown in Figure 6A, illustrating the good fit of the data to a single exponential decay. The relaxation rate constants for all hydrogels are compared in Figure 6B. For RLP hydrogels, the relaxation rates fall within the range of $0.001\text{--}0.002\text{ s}^{-1}$ across all hydrogel concentrations and applied strains, while the relaxation rates for the PEG hydrogel are twice as fast (approximately 0.0045 s^{-1}). The relaxation rates for the RLP-based hydrogels reported here are 10-fold slower than those reported for GB1-RLP multi-domain proteins, which feature a folded streptococcal B1 immunoglobulin-binding domain of protein G (GB1 domain) alternating with random-coil resilin domains, in order to mimic the muscle protein titin (Cao and Li, 2007; Lv et al., 2010). This difference is likely due to the fact that the RLP hydrogels lack folded protein domains; in the GB1-RLP materials, single RLP consensus motifs are intercepted by multiple GB1 folded domains. The rapid response of the RLP hydrogels with an immediate increase in shear stress, followed by a minor loss in shear stress, demonstrates the efficient response to energy input of the RLP materials, with low energy dissipation. This behavior is similar to that observed in ideal rubbers and vocal fold tissues (Alipour-Haghghi and Titze, 1985; Urry et al., 2002), and substantially different than that observed for PEG-control hydrogels and other reported polysaccharide-based and ELP-based hydrogels (Cloyd et al., 2007; Shazly et al., 2008; Wu et al., 2008; Riede et al., 2011; Roberts et al., 2011; Krishna et al., 2012; Razavi-Nouri, 2012).

OSCILLATORY CREEP MEASUREMENTS

Time-dependent changes in strain response to stress are influenced by the density and pore size of a 3D network, its hydration, as well as the chemical nature of the cross-links. For example, it has been reported that ELP-based biomaterials show substantially different deformation responses depending on the conditions

under which they are tested. Variations in temperature, solvent, and preconditioning steps have been shown to influence their deformation. Specifically, ELP-films cast below the transition temperature or in 2,2,2-trifluoroethanol (TFE) solvent displayed limited creep response (<10%) compared to films cast above the transition temperature in water (creep >60%) (Wu et al., 2008). Creep analysis under oscillatory rheology conditions was conducted on RLP and PEG hydrogels to explore the transient dynamic mechanical responses; both the instant and total strain deformation (at 20 min) and strain recovery (after 20 min, $\sigma = 0\text{ Pa}$) under various constant shear stresses were characterized. Representative data from the hydrogels are shown in Figure 7. We note that although the strain deformation was kept similar across the various samples to permit comparisons of strain recovery, the applied stresses were different for the various RLP and PEG hydrogels, as higher stresses were necessary to achieve the same strain deformation on hydrogels with a higher shear modulus. For example, approximately 45% instant strain was observed for a 5 wt% RLP hydrogel upon application of a shear stress of 500 Pa; however, application of a shear stress of 2000 Pa was required in order to obtain percentage similar strain deformation for the 10 wt% PEG hydrogel.

The creep data for RLP hydrogels at 5, 10, and 20 wt% concentrations are shown in Figures 7A–C, with summaries of the data given in Figure 8, and Table S2. The various hydrogels exhibit similar creep behaviors, with large instantaneous deformation followed by a slow increase in strain over 20 min with constant applied shear stress. Significant strain recovery was observed for all hydrogels when the applied shear stress was removed; the hydrogels continued to recover over the next 20 min with total strain recovery of approximately 70, 60, and 50% for the 5, 10, and 20 wt% RLP hydrogels, respectively. In comparison, the 10 wt% PEG-based hydrogel control (Figure 7D) displayed a lower instant strain deformation followed by a sharper increase of strain over 20 min at constant applied shear stress. Moreover, minimal strain recovery was observed upon the removal of the applied shear stress, with only small strain recovery (15%) over the following 20 min. Generally speaking, the RLP and PEG

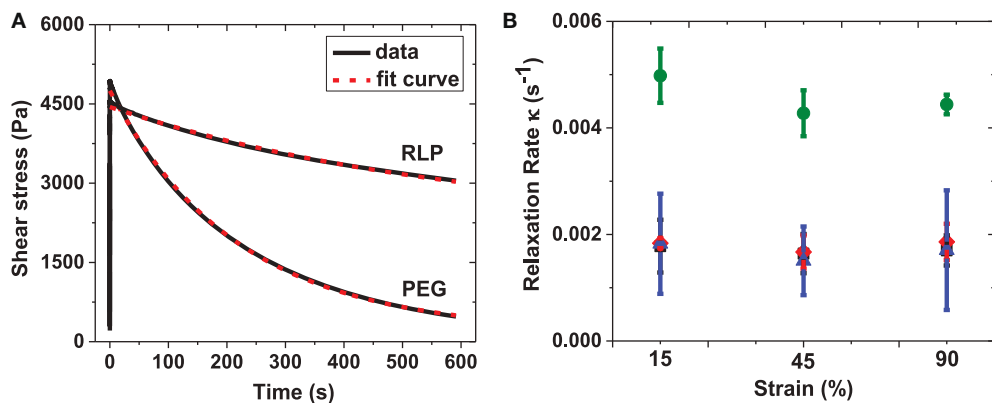


FIGURE 6 | (A) Representative fitting curves for 10 wt% RLP and 10 wt% 4-arm PEG hydrogels; **(B)** summary of relaxation rate of 5 wt% (square), 10 wt% (diamond) and 20 wt% (triangle) RLP and 10 wt% 4-arm PEG (circle) hydrogels at 15, 45, and 90% constant strains. The stress

relaxation behavior was fitted to an exponential equation: $\sigma(t) = \sigma_0 + A * \exp(-\kappa t)$, where σ_0 is the offset shear stress, A is the decay amplitude and κ is the relaxation rate. Error bars represent the standard deviation of three measurements.

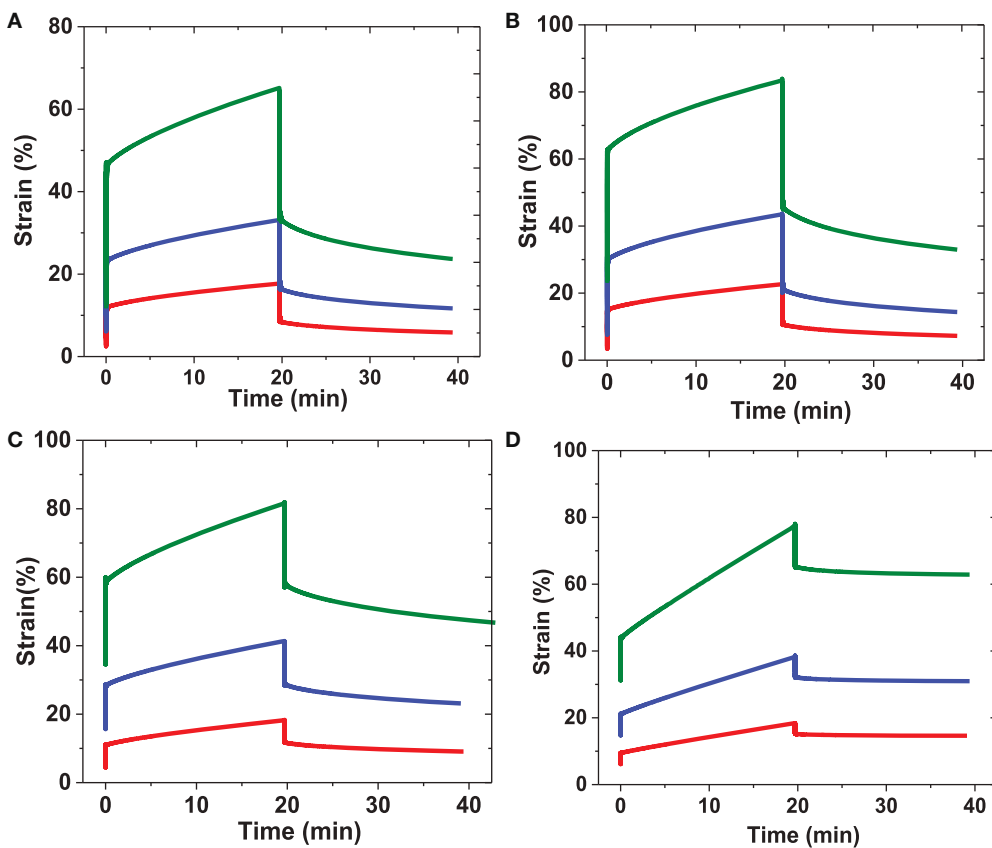


FIGURE 7 | Representative creep behavior for RLP and PEG hydrogels. Samples were subjected to applied constant shear stresses for 20 min followed by removing the applied shear stresses and monitoring strain change over another 20 min. **(A)** 5 wt% RLP at constant shear stress 100 Pa (red), 200 Pa (blue), and 500 Pa (green);

(B) 10 wt% RLP at constant shear stress 500 Pa (red), 1000 Pa (blue), and 2000 Pa (green); **(C)** 20 wt% RLP at constant shear stress 1000 Pa (red), 2000 Pa (blue), and 4000 Pa (green) and **(D)** 10 wt% 4-arm PEG cross-linked hydrogels at constant shear stress 500 Pa (red), 1000 Pa (blue), and 2000 Pa (green).

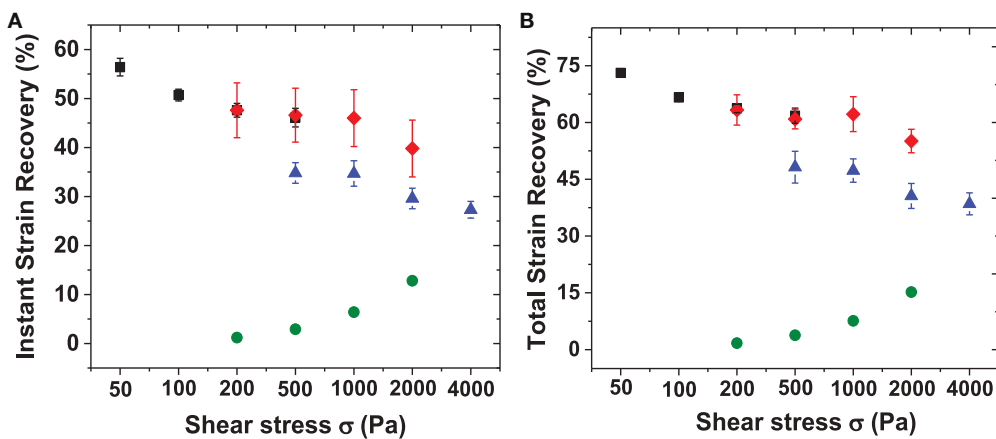


FIGURE 8 | Summary of instant and total strain recovery for RLP and PEG hydrogels upon removing the applied shear stresses. Both instant and total strain recoveries were normalized to the highest strain reached before removal of the applied shear stresses. **(A)** Instant stain recovery at

20 min and **(B)** total strain recovery at 40 min for 5 wt% (square), 10 wt% (diamond), 20 wt% (triangle) RLP-based hydrogels and 10 wt% 4-arm PEG-hydrogels (circle) with applied constant shear stresses ranging from 50 to 4000 Pa.

hydrogels exhibited creep behavior typical of viscoelastic materials, although show distinct differences in immediate and total strain recovery (Figure 8 and Table S2). The highly dynamic behavior of the flexible RLP chains is reported to be derived from hydrogen bond exchange, charge interactions, and the high polarity of the side chains; the elastomeric properties of the RLP-based materials here is consistent with this behavior (Kappiyoor et al., 2011). The applied shear stresses (50–4000 Pa) in our experiments, selected for deformation of the RLP-based hydrogels to physiologically relevant strains, are significantly lower than those applied (30 KPa–0.8 MPa) in the characterization of elastin-like polypeptide- (ELP) and silk-elastin like polypeptide(SEL-P)-based biomaterials (McPherson et al., 1992; Wu et al., 2008; Qiu et al., 2009, 2010; Teng et al., 2009), owing to the fact that the RLP-based hydrogels are more soft and extensible than the previously reported materials.

UNIAXIAL TENSILE TESTING

Repeated loading and unloading strain cycles in standard tensile testing format were employed to probe the deformation response, analyze hysteresis, determine the longitudinal elasticity, and calculate the resilience of hydrated RLP-based hydrogels comprising polypeptide sequences and numbers of cycles that are distinct from those of our previous reports. Twenty wt% RLP hydrogel films were the only samples employed in the uniaxial tensile testing experiments due to practical limitations in the handling of the softer RLP and PEG hydrogels; representative data from these experiments are shown in Figure 9.

For each sample, three consecutive loading and unloading cycles were applied at each strain, first to 30% (three cycles), then to 60% (three cycles), and then to 100% strain (three cycles); only the third cycles at each strain are shown in Figure 9A for simplicity. Resilience values were calculated by dividing the area under the unloading curves by the area under the loading curves at each cycle. The overlap of the stress-strain curves during loading and unloading confirms the negligible hysteresis of these RLP

hydrogels, indicating their reversible recovery and excellent elasticity even up to 100% strain over many types of compositions (Elvin et al., 2005; Charati et al., 2009; Lyons et al., 2009; Li et al., 2011; Qin et al., 2011). A non-linear dependence of stress with applied strain is observed, similar to previously reported data for both human vocal ligament and the vocal fold cover (Min et al., 1995; Zhang et al., 2006; Chan et al., 2007). Ten consecutive loading and unloading cycles were conducted to 100% strain; only the first and the 10th cycle are plotted for comparison in Figure 9B. The two stress-strain curves overlap almost perfectly with resilience values approaching 95%, indicating the excellent recovery and fatigue resistance of the RLP hydrogel films, confirming the elastic storage and release of the energy introduced during the repeated extension process, and demonstrating that negligible energy was dissipated as heat during the deformation.

For the stress relaxation experiment, RLP hydrogels were stretched to 15, 30, 60 and 100% strain at a 5 mm/min strain rate. The length of the sample remained constant while the stress was monitored as a function of time; representative data are shown in Figure 9C. The stress increased rapidly once the strain was applied to the hydrogels, indicating instantaneous deformation, as in the oscillatory experiments. Essentially negligible stress-relaxation, consistent with the behavior of an ideal rubber, was observed for 20 wt% RLP hydrogels at the various strains tested, in sharp contrast to the significant stress relaxation observed for previously reported ELP-based hydrogels and GB1-RLP proteins, (Wu et al., 2008; Teng et al., 2009; Lv et al., 2010). The significant stress relaxation in the latter materials results from irreversible unfolding of the protein chains with applied stress, suggesting the absence of such folding/unfolding in the cross-linked RLP hydrogels (Lv et al., 2010).

Strain-to-break experiments on these RLP hydrogels were also conducted to determine the longitudinal elasticity and Young's modulus. As shown in Figure 9D, hydrated RLP films show an average extension-to-break value of approximately 190% with an average Young's modulus value of approximately 30 kPa. The

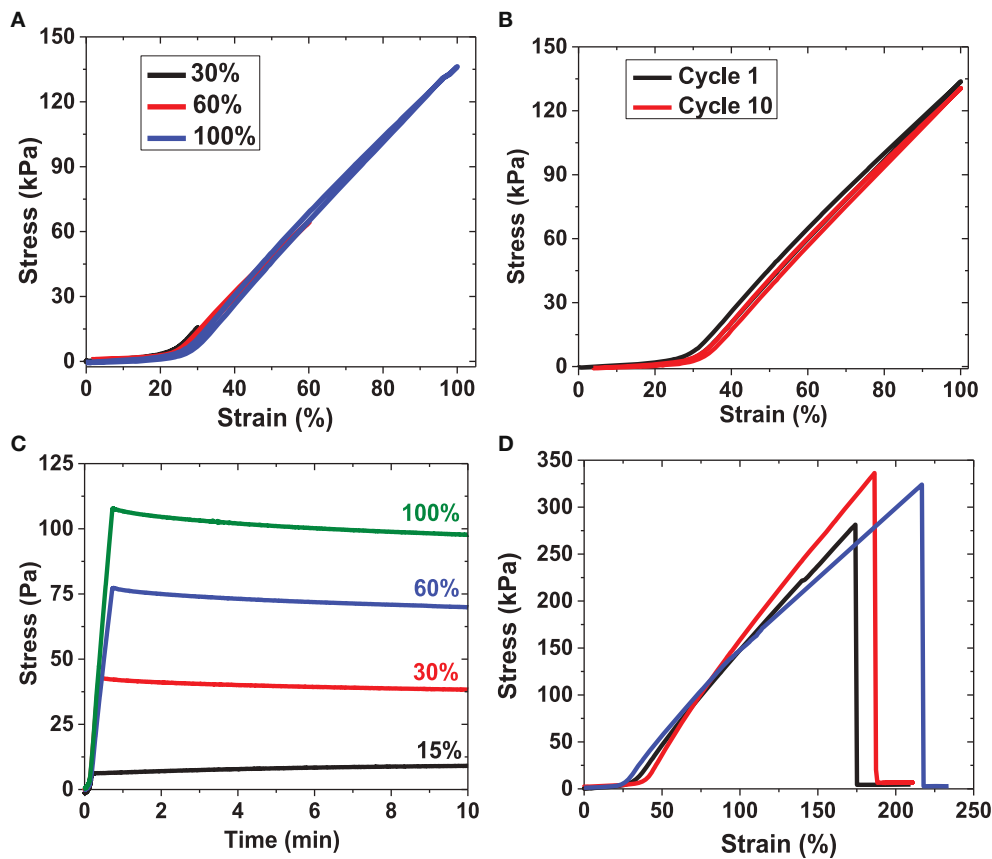


FIGURE 9 | Uniaxial tensile testing experiments for RLP hydrogels. (A) Third cycle of strain-loading and unloading up to 30, 60, and 100% strain for RLP hydrogel; **(B)** first cycle and tenth cycle of cyclic loading and unloading at 100% strain of RLP hydrogel; **(C)** stress relaxation of RLP hydrogel at 15, 30,

60, and 100% constant strains; **(D)** three repeats of strain-to-break tensile testing experiment on RLP hydrogels. All materials characterized in tensile testing experiments are 20 wt% hydrated RLP hydrogels at 1:1 cross-linking ratio.

RLP-based hydrogels exhibited linear stress-strain behavior at low strain (0–15%) and non-linear behavior at high strain, similar to the tensile behavior observed for human vocal ligaments, (Min et al., 1995; Kutty and Webb, 2009a).

A detailed summary of the results from the tensile testing, including resilience values, Young's modulus, and average strain-to-break values, is provided in **Table S3**. The average strain-to-break values ($190 \pm 20\%$) for the RLP hydrogel (cross-linking efficiency of ca. 40% and water content of ca. 80%), are consistent with the properties reported for natural resilin and other recombinantly synthesized RLPs characterized under similar strain rates (Weis-Fogh, 1960; Elvin et al., 2005; Wu et al., 2008; Charati et al., 2009; Lyons et al., 2009; Lv et al., 2010; Li et al., 2011, 2013; Qin et al., 2011; Renner et al., 2012; McGann et al., 2013). The Young's modulus of the RLP-based hydrogel films is approximately 30 kPa, which compares favorably to those of human vocal fold tissues (20–40 kPa) and other RLPs (25.5 kPa). The RLP-based hydrogels displayed high resilience values ranging exceeding 95% over repeated strain cycles, which also is consistent with natural resilin and previously reported resilin-based polypeptides, and improved over available data reported for ELP-based hydrogels (Daamen et al., 2007; Wu et al., 2008; Krishna et al.,

2012). Slight hysteresis between the first and subsequent cycles is often observed, and is likely due to stabilization of load-induced changes in microstructure, such as the dissociation of entanglements, after initial stretching (Nagapudi et al., 2005; Wu et al., 2008). The heterogeneity in the strain-to-break values might arise from sample specific local defects, micro-cracks, sample gripping, loading, and variations of sample thickness. The hydrated RLP hydrogels exhibited improved elastomeric properties over those for the hydrogels formed *in situ* in the oscillatory rheology experiments; this is probably due to the fact that water behaves as a lubricant for the RLP polymer networks by enhancing the exchange of hydrogen bonds and reducing charge interactions between polar amino acid side chains thus increasing chain flexibility. These dynamic features of the polypeptide chain promote conformational changes that further dissipate the energy input, lowering the stiffness and providing a higher resistance to fracture (Gosline et al., 2002; Nairn et al., 2008; Woody, 2009; Kappiyoor et al., 2011; Truong et al., 2011). Taken together, the outstanding elastomeric mechanical properties of the RLP hydrogels, under various loading conditions, recommend the potential use of RLP-based hydrogels for vocal fold tissue regeneration applications.

CONCLUSIONS

Given the excellent mechanical properties of naturally occurring resilin, recombinant RLPs have been designed and studied for vocal fold tissue engineering applications. This modular RLP allows efficient gelation upon mixing with the cross-linker THP, and exhibits mechanical stability and extensibility. Facile tuning of mechanical properties (e.g., storage modulus) can be achieved by changing the RLP concentrations of hydrogels. *In situ* oscillatory shear stress relaxation experiments illustrated that RLP-based hydrogels showed substantially improved energy storage over that observed for PEG-based hydrogels. Similarly, oscillatory creep experiments demonstrated that RLP-based hydrogels exhibited larger deformation and subsequently more strain recovery compared to those of PEG-based hydrogels. Uniaxial tensile testing showed negligible hysteresis, reversible elasticity, and superior resilience (up to 98%) of hydrated RLP hydrogels, with Young's modulus values comparing favorably with those previously reported for resilin and mimicking the tensile properties of the vocal fold ligament at low strain. Together, the data presented here highlight the relevance of the dynamic mechanical properties of these RLP-based materials, which are highly comparable to those of targeted vocal fold tissue, and illustrate the opportunities for creating scaffolds of unique applicability to vocal fold tissue engineering.

ACKNOWLEDGMENTS

We would like to acknowledge support from the National Center for Research Resources (NCRR), a component of the National Institutes of Health [P20-RR017716 (Kristi L. Kiick)] and the National Institute on Deafness and Other Communication Disorders (NIDCD RO1 DC011377A to Kristi L. Kiick). Spencer Szczesny is acknowledged for assistance with the discussion and analysis of exponential fitting of oscillatory stress relaxation data.

SUPPLEMENTARY MATERIAL

The Supplementary Material for this article can be found online at: <http://www.frontiersin.org/journal/10.3389/fchem.2014.00021/abstract>

Figure S1 | Dynamic oscillatory shear storage moduli of RLP hydrogels at 5, 10, and 20 wt% concentrations. Oscillatory time sweeps were conducted for 2 h at 37°C at a frequency of 6 rad/s and at 1% strain.

Table S1 | Summary of average shear stress and normalized decrease in shear stress at $t = 0, 100, 600$ s with constant strain at $\epsilon = 15, 45$, and 90% amplitude for 5, 10, 20 wt% RLP and 10 wt% 4-arm PEG hydrogel compositions. Errors reported are the standard deviation from a minimum of four measurements.

Table S2 | Summary of average strain deformation and normalized strain recovery upon release of applied shear stress. Average strains (@ $t = 0$ min and 20 min) upon deformation with applied shear stress ranging from 50 to 4000 Pa were calculated from the data of multiple samples. Normalized percentages of strain recovery after 20 min (immediate recovery) and 40 min (total recovery) were calculated for 5, 10, 20 wt% RLP and 10 wt% 4-arm PEG hydrogel compositions. Errors are reported as the standard deviation from a minimum of four measurements.

Table S3 | Summary of general properties and resilience values for 20 wt% RLP hydrogels.

REFERENCES

- Alipour-Haghghi, F., and Titze, I. R. (1985). Viscoelastic modeling of canine vocalis muscle in relaxation. *J. Acoust. Soc. Am.* 78, 1939–1943. doi: 10.1121/1.392701
- Andersen, S. O. (1964). The cross-links in resilin identified as dityrosine + triptyrosine. *Biochim. Biophys. Acta* 93, 213–215. doi: 10.1016/0304-4165(64)90289-2
- Cao, Y., and Li, H. B. (2007). Polyprotein of GB1 is an ideal artificial elastomeric protein. *Nat. Mater.* 6, 109–114. doi: 10.1038/nmat1825
- Chan, R. W. (2001). Estimation of viscoelastic shear properties of vocal-fold tissues based on time—temperature superposition. *J. Acoust. Soc. Am.* 110, 1548–1561. doi: 10.1121/1.1387094
- Chan, R. W. (2004). Measurements of vocal fold tissue viscoelasticity: approaching the male phonatory frequency range. *J. Acoust. Soc. Am.* 115, 3161–3170. doi: 10.1121/1.1736272
- Chan, R. W., Fu, M., Young, L., and Tirunagari, N. (2007). Relative contributions of collagen and elastin to elasticity of the vocal fold under tension. *Ann. Biomed. Eng.* 35, 1471–1483. doi: 10.1007/s10439-007-9314-x
- Chan, R. W., and Titze, I. R. (1999). Viscoelastic shear properties of human vocal fold mucosa: measurement methodology and empirical results. *J. Acoust. Soc. Am.* 106, 2008–2021. doi: 10.1121/1.427947
- Chan, R. W., and Titze, I. R. (2000). Viscoelastic shear properties of human vocal fold mucosa: theoretical characterization based on constitutive modeling. *J. Acoust. Soc. Am.* 107, 565–580. doi: 10.1121/1.428354
- Charati, M. B., Ifkovits, J. L., Burdick, J. A., Linhardt, J. G., and Kiick, K. L. (2009). Hydrophilic elastomeric biomaterials based on resilin-like polypeptides. *Soft Matter* 5, 3412–3416. doi: 10.1039/b910980c
- Chen, D. L., Yang, P. F., and Lai, Y. S. (2012). A review of three-dimensional viscoelastic models with an application to viscoelasticity characterization using nanoindentation. *Microelectron. Reliab.* 52, 541–558. doi: 10.1016/j.microrel.2011.10.001
- Cloyd, J. M., Malhotra, N. R., Weng, L., Chen, W., Mauck, R. L., and Elliott, D. M. (2007). Material properties in unconfined compression of human nucleus pulposus, injectable hyaluronic acid-based hydrogels and tissue engineering scaffolds. *Eur. Spine J.* 16, 1892–1898. doi: 10.1007/s00586-007-0443-6
- Cui, J., Lackey, M. A., Madkour, A. E., Saffer, E. M., Griffin, D. M., Bhatia, S. R., et al. (2012). Synthetically simple, highly resilient hydrogels. *Biomacromolecules* 13, 584–588. doi: 10.1021/bm300015s
- Daamen, W. F., Veerkamp, J. H., van Hest, J. C. M., and van Kuppevelt, T. H. (2007). Elastin as a biomaterial for tissue engineering. *Biomaterials* 28, 4378–4398. doi: 10.1016/j.biomaterials.2007.06.025
- Elliott, G. F., Huxley, A. F., and Weis-Fogh, T. (1965). On the structure of resilin. *J. Mol. Biol.* 13, 791–795. doi: 10.1016/S0022-2836(65)80144-9
- Elvin, C. M., Carr, A. G., Huson, M. G., Maxwell, J. M., Pearson, R. D., Vuocolo, T., et al. (2005). Synthesis and properties of crosslinked recombinant pro-resilin. *Nature* 437, 999–1002. doi: 10.1038/nature04085
- Erk, K. A., Henderson, K. J., and Shull, K. R. (2010). Strain stiffening in synthetic and biopolymer networks. *Biomacromolecules* 11, 1358–1363. doi: 10.1021/bm100136y
- Gosline, J., Lillie, M., Carrington, E., Guerette, P., Ortlepp, C., and Savage, K. (2002). Elastic proteins: biological roles and mechanical properties. *Philos. Trans. R. Soc. Lond. B Biol. Sci.* 357, 121–132. doi: 10.1098/rstb.2001.1002
- Hallén, L., Testad, P., Sederholm, E., Dahlqvist, Å., and Laurent, C. (2001). DiHA (dextransomers in hyaluronan) injections for treatment of insufficient closure of the vocal folds: early clinical experiences. *Laryngoscope* 111, 1063–1067. doi: 10.1097/00005537-200106000-00025
- Hirano, S., Kishimoto, Y., Suehiro, A., Kanemaru, S., and Ito, J. (2008). Regeneration of aged vocal fold: first human case treated with fibroblast growth factor. *Laryngoscope* 118, 2254–2259. doi: 10.1097/MLG.0b013e3181845720
- Jahan-Parwar, B., Chhetri, D. K., Ye, M., Hart, S., and Berke, G. S. (2008). Hylian B gel restores structure and function to laser-ablated canine vocal folds. *Ann. Otol. Rhinol. Laryngol.* 117, 703–707.
- Jiang, J., Lin, E., and Hanson, D. G. (2000). Vocal fold physiology *Otolaryngol. Clin. North Am.* 33, 699–718. doi: 10.1016/S0030-6665(05)70238-3

- Jiang, J. J., and Tao, C. (2007). The minimum glottal airflow to initiate vocal fold oscillation. *J. Acoust. Soc. Am.* 121, 2873–2881. doi: 10.1121/1.2710961
- Jiao, T., Farran, A., Jia, X., and Clifton, R. J. (2009). High frequency measurements of viscoelastic properties of hydrogels for vocal fold regeneration. *Exp. Mech.* 49, 235–246. doi: 10.1007/s11340-008-9126-4
- Kappiyoor, R., Balasubramanian, G., Dudek, D. M., and Puri, I. K. (2011). Elastomechanical properties of resilin. *Soft Matter* 7, 11006–11009. doi: 10.1039/C1SM06163A
- Kishirnoto, Y., Hirano, S., Kojima, T., Kanemaru, S., and Ito, J. (2009). Implantation of an atelocollagen sheet for the treatment of vocal fold scarring and sulcus vocalis. *Ann. Otol. Rhinol. Laryngol.* 118, 613–620.
- Klemuk, S. A., and Titze, I. R. (2004). Viscoelastic properties of three vocal-fold injectable biomaterials at low audio frequencies. *Laryngoscope* 114, 1597–1603. doi: 10.1097/00005537-200409000-00018
- Krishna, U. M., Martinez, A. W., Caves, J. M., and Chaikof, E. L. (2012). Hydrazone self-crosslinking of multiphase elastin-like block copolymer networks. *Acta Biomater.* 8, 988–997. doi: 10.1016/j.actbio.2011.11.024
- Kutty, J. K., and Webb, K. (2009a). Mechanomimetic hydrogels for vocal fold lamina propria regeneration. *J. Biomater. Sci. Polym. Ed.* 20, 737–756. doi: 10.1163/156856209X426763
- Kutty, J. K., and Webb, K. (2009b). Tissue engineering therapies for the vocal fold lamina propria. *Tissue Eng. Part B Rev.* 15, 249–262. doi: 10.1089/ten.teb.2008.0588
- Kwon, S. K., and Lee, B. J. (2008). The combined effect of autologous mesenchymal stem cells and hepatocyte growth factor on vocal fold regeneration and fibrosis in vocal fold wound. *Tissue Eng. Regen. Med.* 5, 735–742.
- Li, L., and Kiick, K. L. (2013). Resilin-based materials for biomedical applications. *ACS Macro Lett.* 2, 635–640. doi: 10.1021/mz4002194
- Li, L. Q., Charati, M. B., and Kiick, K. L. (2010). Elastomeric polypeptide-based biomaterials. *Polym. Chem.* 1, 1160–1170. doi: 10.1039/b9py00346k
- Li, L. Q., Teller, S., Clifton, R. J., Jia, X. Q., and Kiick, K. L. (2011). Tunable mechanical stability and deformation response of a resilin-based elastomer. *Biomacromolecules* 12, 2302–2310. doi: 10.1021/bm200373p
- Li, L. Q., Tong, Z. X., Jia, X. Q., and Kiick, K. L. (2013). Resilin-like polypeptide hydrogels engineered for versatile biological function. *Soft Matter* 9, 665–673. doi: 10.1039/c2sm26812d
- Lv, S., Dudek, D. M., Cao, Y., Balamurali, M. M., Gosline, J., and Li, H. B. (2010). Designed biomaterials to mimic the mechanical properties of muscles. *Nature* 465, 69–73. doi: 10.1038/nature09024
- Lyons, R. E., Nairn, K. M., Huson, M. G., Kim, M., Dumsday, G., and Elvin, C. M. (2009). Comparisons of recombinant resilin-like proteins: repetitive domains are sufficient to confer resilin-like properties. *Biomacromolecules* 10, 3009–3014. doi: 10.1021/bm900601h
- McGann, C. L., Levenson, E. A., and Kiick, K. L. (2013). Resilin-based hybrid hydrogels for cardiovascular tissue engineering. *Macromol. Chem. Phys.* 214, 203–213. doi: 10.1002/macp.201200412
- McPherson, D. T., Morrow, C., Minehan, D. S., Wu, J. G., Hunter, E., and Urry, D. W. (1992). Production and purification of a recombinant elastomeric polypeptide, G-(VPGVG)₁₉-VPGV, from Escherichia Coli. *Biotechnol. Progr.* 8, 347–352. doi: 10.1021/bp00016a012
- Min, Y. B., Titze, I. R., and Alipouraghahighi, F. (1995). Stress-strain response of the human vocal ligament. *Ann. Otol. Rhinol. Laryngol.* 104, 563–569.
- Nagapudi, K., Brinkman, W. T., Leisen, J., Thomas, B. S., Wright, E. R., Haller, C., et al. (2005). Protein-based thermoplastic elastomers. *Macromolecules* 38, 345–354. doi: 10.1021/ma0491199
- Nairn, K. M., Lyons, R. E., Mulder, R. J., Mudie, S. T., Cookson, D. J., Lesieur, E., et al. (2008). A synthetic resilin is largely unstructured. *Biophys. J.* 95, 3358–3365. doi: 10.1529/biophysj.107.119107
- Qin, G. K., Rivkin, A., Lapidot, S., Hu, X., Preis, I., Arinus, S. B., et al. (2011). Recombinant exon-encoded resilins for elastomeric biomaterials. *Biomaterials* 32, 9231–9243. doi: 10.1016/j.biomaterials.2011.06.010
- Qiu, W., Huang, Y., Teng, W., Cohn, C. M., Cappello, J., and Wu, X. (2010). Complete recombinant silk-elastinlike protein-based tissue scaffold. *Biomacromolecules* 11, 3219–3227. doi: 10.1021/bm100469w
- Qiu, W., Teng, W., Cappello, J., and Wu, X. (2009). Wet-spinning of recombinant silk-elastin-like protein polymer fibers with high tensile strength and high deformability. *Biomacromolecules* 10, 602–608. doi: 10.1021/bm801296r
- Razavi-Nouri, M. (2012). Creep and stress relaxation behavior of polypropylene, metallocene-prepared polyethylene and their blends. *Iran. J. Chem. Eng.* 9, 60–68.
- Renner, J. N., Cherry, K. M., Su, R. S. C., and Liu, J. C. (2012). Characterization of resilin-based materials for tissue engineering applications. *Biomacromolecules* 13, 3678–3685. doi: 10.1021/bm301129b
- Riede, T., York, A., Furst, S., Müller, R., and Seelecke, S. (2011). Elasticity and stress relaxation of a very small vocal fold. *J. Biomech.* 44, 1936–1940. doi: 10.1016/j.biomech.2011.04.024
- Roberts, J. J., Earnshaw, A., Ferguson, V. L., and Bryant, S. J. (2011). Comparative study of the viscoelastic mechanical behavior of agarose and poly(ethylene glycol) hydrogels. *J. Biomed. Mater. Res. B-Appl. Biomater.* 99B, 158–169. doi: 10.1002/jbm.b.31883
- Shazly, T. M., Artzi, N., Boehning, F., and Edelman, E. R. (2008). Viscoelastic adhesive mechanics of aldehyde-mediated soft tissue sealants. *Biomaterials* 29, 4584–4591. doi: 10.1016/j.biomaterials.2008.08.032
- Snyders, R., Shingel, K. I., Zabeida, O., Roberge, C., Faure, M.-P., Martinu, L., et al. (2007). Mechanical and microstructural properties of hybrid poly(ethylene glycol)-soy protein hydrogels for wound dressing applications. *J. Biomed. Mater. Res. A* 83A, 88–97. doi: 10.1002/jbm.a.31217
- Storm, C., Pastore, J. J., MacKintosh, F. C., Lubensky, T. C., and Janmey, P. A. (2005). Nonlinear elasticity in biological gels. *Nature* 435, 191–194. doi: 10.1038/nature03521
- Teller, S. S., Farran, A. J. E., Xiao, L. X., Jiao, T., Duncan, R. L., Clifton, R. J., et al. (2012). High-frequency viscoelastic shear properties of vocal fold tissues: implications for vocal fold tissue engineering. *Tissue Eng. Part A* 18, 2008–2019. doi: 10.1089/ten.tea.2012.0023
- Teng, W., Cappello, J., and Wu, X. (2009). Recombinant silk-elastinlike protein polymer displays elasticity comparable to elastin. *Biomacromolecules* 10, 3028–3036. doi: 10.1021/bm900651g
- Thibeault, S. L., Klemuk, S. A., Chen, X., and Quinchia Johnson, B. H. (2011). In vivo engineering of the vocal fold ECM with injectable HA hydrogels—late effects on tissue repair and biomechanics in a rabbit model. *J. Voice* 25, 249–253. doi: 10.1016/j.jvoice.2009.10.003
- Thibeault, S. L., Klemuk, S. A., Smith, M. E., Leugers, C., and Prestwich, G. (2009). In vivo comparison of biomimetic approaches for tissue regeneration of the scarred vocal fold. *Tissue Eng. Part A* 15, 1481–1487. doi: 10.1089/ten.tea.2008.0299
- Titze, I. (1988). The physics of small-amplitude oscillation of the vocal folds. *J. Acoust. Soc. Am.* 83, 1536–1552. doi: 10.1121/1.395910
- Titze, I. R. (1984). Parameterization of the glottal area, glottal flow, and vocal fold contact area. *J. Acoust. Soc. Am.* 75, 570–580. doi: 10.1121/1.390530
- Titze, I. R. (1989). On the relation between subglottal pressure and fundamental frequency in phonation. *J. Acoust. Soc. Am.* 85, 901–906. doi: 10.1121/1.397562
- Truong, M. Y., Dutta, N. K., Choudhury, N. R., Kim, M., Elvin, C. M., Nairn, K. M., et al. (2011). The effect of hydration on molecular chain mobility and the viscoelastic behavior of resilin-mimetic protein-based hydrogels. *Biomaterials* 32, 8462–8473. doi: 10.1016/j.biomaterials.2011.07.064
- Urry, D. W., Hugel, T., Seitz, M., Gaub, H. E., Sheiba, L., Dea, J., et al. (2002). Elastin: a representative ideal protein elastomer. *Philos. Trans. R. Soc. Lond. B Biol. Sci.* 357, 169–184. doi: 10.1098/rstb.2001.1023
- Weis-Fogh, T. (1960). A rubber-like protein in insect cuticles. *J. Exp. Biol.* 37, 889–907.
- Woody, R. W. (2009). Circular dichroism spectrum of peptides in the poly(Pro)II conformation. *J. Am. Chem. Soc.* 131, 8234–8245. doi: 10.1021/ja901218m
- Wu, X. Y., Sallach, R. E., Caves, J. M., Conticello, V. P., and Chaikof, E. L. (2008). Deformation responses of a physically cross-linked high molecular weight elastin-like protein polymer. *Biomacromolecules* 9, 1787–1794. doi: 10.1021/bm800012x
- Xiao, L., Tong, Z., Chen, Y., Pochan, D. J., Sabanayagam, C. R., and Jia, X. (2013). Hyaluronic acid-based hydrogels containing covalently integrated drug depots: implication for controlling inflammation in mechanically stressed tissues. *Biomacromolecules* 14, 3808–3819. doi: 10.1021/bm4011276
- Xu, D., Asai, D., Chilkoti, A., and Craig, S. L. (2012). Rheological properties of cysteine-containing elastin-like polypeptide solutions and hydrogels. *Biomacromolecules* 13, 2315–2321. doi: 10.1021/bm300760s

- Xu, D., and Craig, S. L. (2011). Strain hardening and strain softening of reversibly cross-linked supramolecular polymer networks. *Macromolecules* 44, 7478–7488. doi: 10.1021/ma201386t
- Zeitels, S. M., Hillman, R. E., Mauri, M., Desloge, R., and Doyle, P. B. (2002). Phonometricsurgery in singers and performing artists: treatment outcomes, management theories, and future directions. *Ann. Otol. Rhinol. Laryngol.* 111, 21–40.
- Zhang, K., Siegmund, T., and Chan, R. W. (2006). A constitutive model of the human vocal fold cover for fundamental frequency regulation. *J. Acoust. Soc. Am.* 119, 1050–1062. doi: 10.1121/1.2159433
- Zhang, K., Siegmund, T., and Chan, R. W. (2007). A two-layer composite model of the vocal fold lamina propria for fundamental frequency regulation. *J. Acoust. Soc. Am.* 122, 1090–1101. doi: 10.1121/1.2749460
- Zhang, K., Siegmund, T., and Chan, R. W. (2009). Modeling of the transient responses of the vocal fold lamina propria. *J. Mech. Behav. Biomed. Mater.* 2, 93–104. doi: 10.1016/j.jmbbm.2008.05.005

Conflict of Interest Statement: The authors declare that the research was conducted in the absence of any commercial or financial relationships that could be construed as a potential conflict of interest.

Received: 14 February 2014; accepted: 07 April 2014; published online: 28 April 2014.

Citation: Li L and Kiick KL (2014) Transient dynamic mechanical properties of resilin-based elastomeric hydrogels. *Front. Chem.* 2:21. doi: 10.3389/fchem.2014.00021

This article was submitted to Chemical Biology, a section of the journal Frontiers in Chemistry.

Copyright © 2014 Li and Kiick. This is an open-access article distributed under the terms of the Creative Commons Attribution License (CC BY). The use, distribution or reproduction in other forums is permitted, provided the original author(s) or licensor are credited and that the original publication in this journal is cited, in accordance with accepted academic practice. No use, distribution or reproduction is permitted which does not comply with these terms.



Engineered recombinant bacterial collagen as an alternative collagen-based biomaterial for tissue engineering

Bo An, David L. Kaplan * and Barbara Brodsky *

Department of Biomedical Engineering, Tufts University, Medford, MA, USA

*Correspondence: david.kaplan@tufts.edu; barbara.brodsky@tufts.edu

Edited by:

Carissa M. Soto, Naval Research Laboratory, USA

Reviewed by:

Lisa Fitzgerald, Naval Research Laboratory, USA

Keywords: collagen, triple helix, recombinant expression, biomaterials, tissue engineering

The key structural and signaling roles of collagen in the extracellular matrix (ECM) make it an attractive biomaterial for tissue engineering, but there are limitations in the standardization and purity of natural collagen sources currently available for such applications (Ruggiero and Koch, 2008; Werkmeister and Ramshaw, 2012). Significant effort has been made to produce human collagen in recombinant systems, such as yeast, insect cells and plants (Ruggiero et al., 2000; Myllyharju, 2009). However, the requirement for post-translational proline hydroxylation has proven to be a significant obstacle in achieving large scale production. Recent findings of collagen-like proteins in bacteria suggest these may represent alternative biosynthetic collagen materials which may complement current sources.

Over the past 10 years, collagen-like proteins have been identified from numerous bacterial genomes database based on the signature (Gly-Xaa-Yaa)_n repeating amino acid sequence characteristic of the collagen triple-helix (Rasmussen et al., 2003; Yu et al., 2014). Some of these collagen-like molecules may function as virulence factors by bacteria to evade the immune system of higher animals or to interact with surface receptors or with other ECM molecules necessary to promote host cell invasion (Humtsoe et al., 2005). More than 100 putative collagen-like proteins have been identified in bacterial genomes, of which eight have been recombinantly expressed in *Escherichia coli* (see Yu et al., 2014 for review). All eight expressed bacterial

collagens were shown to form stable triple-helices with $T_m \sim 35\text{--}39^\circ\text{C}$. *E. coli* and most bacteria lack prolyl hydroxylase, so this high stability is attained in the absence of hydroxyproline (Hyp), a post-translationally modified amino acid known to be critical to the thermal stability of mammalian collagens. Initial interest in bacterial collagen-like proteins focused on their roles in pathogenesis. However, recent work has focused on one specific bacterial collagen protein, designated Scl2, to demonstrate the utility of recombinant bacterial collagen as a tool for defining collagen sequence/structure/function relationships and for establishing a class of novel collagen-based biomaterials.

The gram positive bacterium *Streptococcus pyogenes* contains two collagen-like proteins, Scl1 and Scl2, which have been well characterized in terms of structure and functional properties (Lukomski et al., 2001; Xu et al., 2002; Mohs et al., 2007; Caswell et al., 2008). The Scl2 protein includes an N-terminal globular trimerization domain adjacent to a (Gly-Xaa-Yaa)₇₉ core collagen-like domain. It has been possible to generate constructs in a recombinant *E. coli* system with various sequence modifications of Scl2 and to establish large scale production methods. Based on recent progress, we suggest that the Scl2 recombinant bacterial collagen system has advantages compared to recombinant human collagen strategies for large scale production and biomedical applications, and may serve as a prototype for engineering novel collagen-based biomaterials.

STABLE TRIPLE HELICAL PROTEIN WITHOUT HYDROXYPROLINE

The recombinant Scl2 protein and its modified variants are able to form a triple helix with stability similar to that of mammalian collagens ($T_m \sim 37^\circ\text{C}$) even though there is no Pro hydroxylation. In animal collagens, Pro residues in the Y positions of the repeating Gly-X-Y sequence are hydroxylated to Hyp, and this hydroxylation is required to stabilize the triple-helix: T_m of hydroxylated collagen = 37°C , while T_m of unhydroxylated collagen = 26°C (Berg and Prockop, 1973; Jimenez et al., 1973). The bacterial collagen appears to compensate for the absence of Hyp with electrostatic interactions (Mohs et al., 2007). In yeast, plants, and other expression systems for human collagens, the genes for the alpha and beta subunits of human prolyl hydroxylase (P4H) must be introduced to form stable collagen molecules (Ruggiero et al., 2000; Myllyharju, 2009; Xu et al., 2011; Shoseyov et al., 2014). However, P4H activity and hydroxylation levels are highly dependent on expression conditions, such as the gene copy ratio of collagen to hydroxylase, concentration of cofactors, induction time, and sequence (Chan et al., 2012), so generating optimal hydroxylation to model native human collagen has been challenging in systems with inserted P4H genes and even in mammalian cell expression systems. The bacterial collagen-like proteins are highly compatible with expression in *E. coli*, and the lack of requirement for any post-translational modifications presents the

potential for producing large quantities of recombinant stable triple-helical proteins for biomaterials applications.

MIX AND MATCH FUNCTIONAL MODULAR UNITS

In addition to production advantages, the ability to express the collagen-like protein in *E. coli* allows easy manipulation of the sequence to enhance biomaterial properties. Insertion of known human collagen binding sites within Scl2 presents the possibility of designing collagen-like materials with defined biological properties. The native human collagen sequence contains more than 40 binding sites which interact with other biologically functional molecules, including cell receptors, other ECM proteins and collagenases (MMPs) (Kadler, 1994). Examination of the Scl2 recombinant protein suggests that this particular bacterial collagen-like protein lacks any known biologically active sites, making it a convenient blank slate for the introduction of human collagen ligand binding sites (Caswell et al., 2008; Cosgriff-Hernandez et al., 2010). Various human-derived collagen short amino acid sequences (2–6 triplets) with identified bioactive sites have been inserted into the Scl2 collagen-like domain, including sites for binding integrin $\alpha 2\beta 1$ (Seo et al., 2010), fibronectin (An et al., 2014), heparin (Peng et al., 2013), and MMPs (Yu et al., 2012). The inserted sequences have conferred the expected biological activities on the Scl2 protein based on *in vitro* binding, cleavage, and cell culture assays. The Scl2 sequence will apparently fold the short human collagen insert into a triple helix, while the correctly folded human collagen sequence imparts the corresponding biological function to the chimeric protein. The introduction of the integrin and fibronectin binding sites promoted the growth of different types of mammalian cells *in vitro*, while Scl2 molecules with MMP cleavage sites show enzyme cleavage at the native position. More collagen bioactive sites are being identified each year primarily through synthetic collagen mimetic Toolkit peptides (Farndale et al., 2008), providing an increasing pool of candidates for a recombinant chimeric bacteria-human library with human collagen functions. Such a recombinant library is particularly useful

for applying a synthetic biology “plug and play” concept to future biomaterial designs (Figure 1). Only those collagen biological functions that are required for a particular application will be selected and incorporated into a final product, leading to precise tuning for each application.

MOLECULAR AND HIGHER ORDER STRUCTURE

With recombinant DNA technologies, it has been possible to manipulate the Scl2 protein, studying individual fragments of the triple-helix (Yu et al., 2011) or duplicating the entire triple-helix portion (Yoshizumi et al., 2009), while maintaining secondary structure and stability. Scl2 is a homotrimer, serving as a model for homotrimeric collagens such as type II collagen in cartilage. To better mimic heterotrimeric collagens such as the dominant type I collagen in bone and tendon or type IV collagen in basement membrane, it may be possible to replace the natural trimerization V domain with a heterotrimeric coiled coil (Nautiyal et al., 1995) or an electrostatic interaction chain selection mechanism (Jalan et al., 2013).

While facile manipulation of the Scl2 protein can optimize molecular and biological properties, successful biomaterial applications will require optimization of material properties as well. The most abundant animal collagens self-associate into characteristic periodic cross-linked fibrils, which provide the mechanical properties for tissues and biomaterials. Thus far, Scl2 exhibits limited ability to form fibrillar structures (Yoshizumi et al., 2009). The Scl2 triple-helix is only about 1/5 of the length of the human fibrillar collagen triple-helix, and it is possible that increasing its length will promote self-association. The *E. coli* system usually has an upper threshold for the size of the recombinant protein it can produce, but it may be possible to transfer the Scl2 expression system into yeast or insect cells to further increase its chain length. Crystal structures on small collagen model peptides and studies on recombinant tobacco type I collagen suggest Hyp may be essential for collagen fibril formation (Kramer et al., 2000; Perret et al., 2001). Thus, it may be necessary to introduce P4H genes into the bacterial system in order to induce fibril formation, even though the Hyp is

not necessary to form the stable triple-helix. Alternative approaches to attaining an optimal self-supporting material from Scl2 include chemical modifications such as glutaraldehyde vapor or 1-ethyl-3-(3-dimethylaminopropyl)carbodiimide or crosslinking by poly(ethylene glycol) diacrylate to form interchain networks (Cosgriff-Hernandez et al., 2010; Peng et al., 2010). Chemical modifications are simple and effective, but the level of crosslinking maybe difficult to control, especially in large 3D scaffolds, and a high degree of cross-linking may limit accessibility to biologically active sites within the collagen material. Another strategy recently reported involved non-covalent binding of Scl2 constructs with fibronectin and integrin interaction sites to solid silk protein material, generating porous silk scaffolds with improved support of cell growth (An et al., 2013) (Figure 1).

PURIFICATION, SCALABILITY, AND PROJECTED COST

Animal extracted collagens are produced in large quantity and are generally inexpensive. However, difficulties in developing standardized preparations of these collagens and in producing minor types of collagens that are free of collagen I and biological contaminants are major limitations. Potential infectious and allergic risks of animal collagen products are also a concern. The recombinant bacterial collagens have attached tags, such as His-tag and Strep II tags to simplify standardized chromatographic purification. A high-throughput batch purification methodology for Scl2 has also been developed (Peng et al., 2014). Native triple helical sequences are resistant to digestion by non-specific enzymes such as trypsin and chymotrypsin, and trypsin treatment of acidified cell lysate resulted in purified triple helical bacterial collagen. Enzymatic digestion during the purification process ensures the final product will be free of non-triple helical contaminants, which is important for quality control for industrial production. Recombinant expression of proteins in *E. coli* is a mature industrial process with excellent scalability. This has already been demonstrated for Scl2 production (Peng et al., 2012) with an average yield of 0.2–0.3 g/L of purified collagen protein in traditional shaking flask

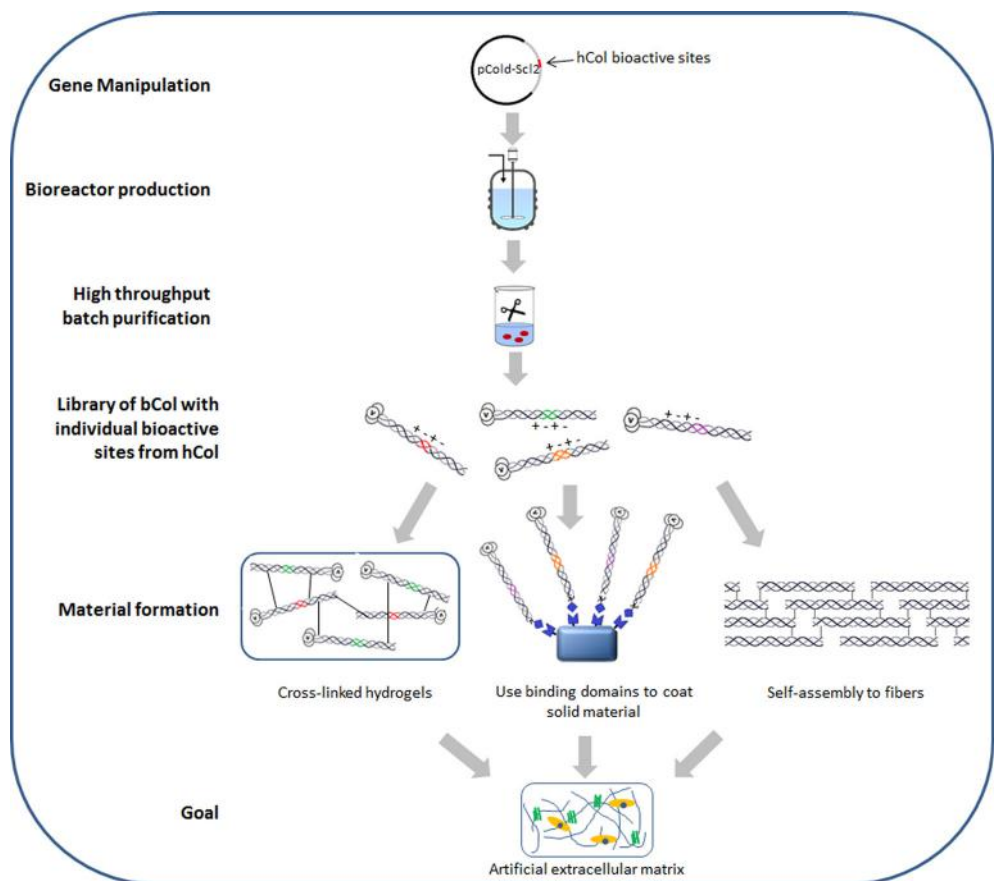


FIGURE 1 | Schematic diagram of recombinant bacterial collagen production method and material fabrication strategies. hCol, human collagen; bCol, recombinant bacterial collagen Scl2.

culture and up to 9.5 g/L in high density fed-batch culture. With the ease of generating different Scl2 constructs through molecular cloning, the overall resource cost for producing this highly tunable bacterial collagen material will likely be lower than recombinant collagen obtained from mammalian cell or even transgenic systems.

TOWARD IN VIVO APPLICATIONS

Translational science remains a less explored area for recombinant collagens. Recombinant human collagens obtained from systems with high scalability, such as *Pichia* and *Nicotiana*, have been formulated into hydrogels and explored for their potential as artificial cornea (Merrett et al., 2008) and wound dressings (Shilo et al., 2013), respectively. In terms of bacterial collagen, Scl2 has been shown to be non-immunogenic, non-cytotoxic and non-thrombogenic (Peng et al., 2010).

Recently, poly(ethylene glycol) crosslinked bioactive Scl2 hydrogels have been reinforced with an electrospun polyurethane mesh to achieve suitable biomechanical property for vascular grafts (Browning et al., 2012). The rate of cell migration is tunable through altering protein concentration in the material. Further investigation, especially the degradation and turnover time of Scl2 material *in vivo* is needed to evaluate its suitability as medical implants.

CRITICAL PROPERTIES FOR A SUCCESSFUL COLLAGEN PRODUCTION STRATEGY

Figure 1 illustrates the current production method and material fabrication strategies for recombinant bacterial collagen Scl2. Large amounts of bioactive collagen molecules can be produced with simple gene manipulation, large scale production and high throughput purification.

Functional collagen proteins could then be cross-linked into hydrogels or used as coating on other solid materials. Conditions and sequence manipulations which would trigger Scl2 self-assembly into large fibers are currently under investigation. Such fabricated materials could lead to the ultimate goal of designing and developing artificial extracellular matrices, an objective important for tissue engineering as well as biomedical fields. With its high tunability and scalability accompanied by low complexity and cost, we believe the Scl2 recombinant bacterial collagen system has clear advantages which could not only circumvent the difficulties seen for recombinant human collagens, but also open up a brand new pathway for collagen production.

LONG TERM PROSPECTS

Extracted bovine collagen is likely to remain a staple for biomaterial

construction due to its low cost and useful material properties, but challenges in standardization and concerns for bioburdens, as well as a desire to modify collagen sequence and function, will lead to continued interest in research and applications with recombinant collagens. As described here for the specific Scl2 protein from *S. pyogenes*, bacterial collagens represent a biosynthetic ground up approach, where a triple-helical non-animal collagen molecule with no specific bioactivity can be designed to include desired interactions and regulated degradation. Although research has focused on Scl2, the approach could be extended to other collagen-like proteins from bacteria and viruses, which may bring new properties and variations useful for biomaterials. Fundamental studies on Scl2 and other bacterial collagens will continue to elucidate basic features of collagen, with a focus on chemistry, sequence, biological activity, and self-assembly. The success of the bacterial collagen approach toward biomaterial applications will depend on developing the capacity to generate biomaterials with desirable biomechanical properties useful for *in vivo* applications.

ACKNOWLEDGMENT

The authors thank the support from NIH grant#EB011620 (to Barbara Brodsky and David L. Kaplan) for this work.

REFERENCES

- An, B., Abbonante, V., Yigit, S., Balduini, A., Kaplan, D. L., and Brodsky, B. (2014). Definition of the native and denatured Type II collagen binding site for fibronectin using a recombinant collagen system. *J. Biol. Chem.* 289, 4941–4951. doi: 10.1074/jbc.M113.530808
- An, B., DesRochers, T. M., Qin, G., Xia, X., Thiagarajan, G., Brodsky, B., et al. (2013). The influence of specific binding of collagen, *Aisilk* chimeras to silk biomaterials on hMSC behavior. *Biomaterials* 34, 402–412. doi: 10.1016/j.biomaterials.2012.09.085
- Berg, R. A., and Prockop, D. J. (1973). The thermal transition of a non-hydroxylated form of collagen. Evidence for a role for hydroxyproline in stabilizing the triple-helix of collagen. *Biochem. Biophys. Res. Commun.* 52, 115–120. doi: 10.1016/0006-291X(73)90961-3
- Browning, M. B., Dempsey, D., Guiza, V., Becerra, S., Rivera, J., Russell, B., et al. (2012). Multilayer vascular grafts based on collagen-mimetic proteins. *Acta Biomater.* 8, 1010–1021. doi: 10.1016/j.actbio.2011.11.015
- Caswell, C. C., Barczyk, M., Keene, D. R., Lukomska, E., Gullberg, D. E., and Lukomski, S. (2008). Identification of the first prokaryotic collagen sequence motif that mediates binding to human collagen receptors, integrins alpha2beta1 and alpha11beta1. *J. Biol. Chem.* 283, 36168–36175. doi: 10.1074/jbc.M806865200
- Chan, S. W., Greaves, J., Da Silva, N. A., and Wang, S. W. (2012). Assaying proline hydroxylation in recombinant collagen variants by liquid chromatography-mass spectrometry. *BMC Biotechnol.* 12:51. doi: 10.1186/1472-6750-12-51
- Cosgriff-Hernandez, E., Hahn, M. S., Russell, B., Wilems, T., Munoz-Pinto, D., Browning, M. B., et al. (2010). Bioactive hydrogels based on designer collagens. *Acta Biomater.* 6, 3969–3977. doi: 10.1016/j.actbio.2010.05.002
- Farndale, R. W., Lisman, T., Bihani, D., Hamaia, S., Smerling, C. S., Pugh, N., et al. (2008). Cell-collagen interactions: the use of peptide Toolkits to investigate collagen-receptor interactions. *Biochem. Soc. Trans.* 36(Pt 2), 241–250. doi: 10.1042/BST0360241
- Humtsoe, J. O., Kim, J. K., Xu, Y., Keene, D. R., Hook, M., Lukomski, S., et al. (2005). A streptococcal collagen-like protein interacts with the alpha2beta1 integrin and induces intracellular signaling. *J. Biol. Chem.* 280, 13848–13857. doi: 10.1074/jbc.M410605200
- Jalan, A. A., Demeler, B., and Hartgerink, J. D. (2013). Hydroxyproline-free single composition ABC collagen heterotrimer. *J. Am. Chem. Soc.* 135, 6014–6017. doi: 10.1021/ja402187t
- Jimenez, S., Harsch, M., and Rosenblom, J. (1973). Hydroxyproline stabilizes the triple helix of chick tendon collagen. *Biochem. Biophys. Res. Commun.* 52, 106–114. doi: 10.1016/0006-291X(73)90960-1
- Kadler, K. (1994). Extracellular matrix. 1: fibrill-forming collagens. *Protein Profile* 1, 519–638.
- Kramer, R. Z., Venugopal, M. G., Bella, J., Mayville, P., Brodsky, B., and Berman, H. M. (2000). Staggered molecular packing in crystals of a collagen-like peptide with a single charged pair. *J. Mol. Biol.* 301, 1191–1205. doi: 10.1006/jmbi.2000.4017
- Lukomski, S., Nakashima, K., Abdi, I., Cipriano, V. J., Shelvin, B. J., Graviss, E. A. (2001). Identification and characterization of a second extracellular collagen-like protein made by group A Streptococcus: control of production at the level of translation. *Infect. Immun.* 69, 1729–1738. doi: 10.1128/IAI.69.3.1729-1738.2001
- Merrett, K., Fagerholm, P., McLaughlin, C. R., Dravida, S., Lagali, N., Shinozaki, N., et al. (2008). Tissue-engineered recombinant human collagen-based corneal substitutes for implantation: performance of type I versus type III collagen. *Invest. Ophthalmol. Vis. Sci.* 49, 3887–3894. doi: 10.1167/iovs.07-1348
- Mohs, A., Silva, T., Yoshida, T., Amin, R., Lukomski, S., Inouye, M. et al. (2007). Mechanism of stabilization of a bacterial collagen triple helix in the absence of hydroxyproline. *J. Biol. Chem.* 282, 29757–29765. doi: 10.1074/jbc.M703991200
- Myllyharju, J. (2009). Recombinant collagen trimers from insect cells and yeast. *Methods Mol. Biol.* 522, 51–62. doi: 10.1007/978-1-59745-413-1_3
- Nautiyal, S., Woolfson, D. N., King, D. S., and Alber, T. (1995). A designed heterotrimeric coiled coil. *Biochemistry* 34, 11645–11651. doi: 10.1021/bi00037a001
- Peng, Y. Y., Howell, L., Stoichevska, V., Werkmeister, J. A., Dumsday, G. J., and Ramshaw, J. A. (2012). Towards scalable production of a collagen-like protein from *Streptococcus pyogenes* for biomedical applications. *Microb. Cell Fact.* 11, 146. doi: 10.1186/1475-2859-11-146
- Peng, Y. Y., Stoichevska, V., Madsen, S., Howell, L., Dumsday, G. J., Werkmeister, J. A., et al. (2014). A simple cost-effective methodology for large-scale purification of recombinant non-animal collagens. *Appl. Microbiol. Biotechnol.* 98, 1807–1815. doi: 10.1007/s00253-013-5475-8
- Peng, Y. Y., Stoichevska, V., Schacht, K., Werkmeister, J. A., and Ramshaw, J. A. (2013). Engineering multiple biological functional motifs into a blank collagen-like protein template from *Streptococcus pyogenes*. *J. Biomed. Mater. Res. A* 102, 2189–2196. doi: 10.1002/jbm.a.34898
- Peng, Y. Y., Yoshizumi, A., Danon, S. J., Glattauer, V., Prokopenko, O., Mirochnitchenko, O., et al. (2010). A *Streptococcus pyogenes* derived collagen-like protein as a non-cytotoxic and non-immunogenic cross-linkable biomaterial. *Biomaterials* 31, 2755–2761. doi: 10.1016/j.biomaterials.2009.12.040
- Perret, S., Merle, C., Bernocco, S., Berland, P., Garrone, R., Hulmes, D. J., et al. (2001). Unhydroxylated triple helical collagen I produced in transgenic plants provides new clues on the role of hydroxyproline in collagen folding and fibril formation. *J. Biol. Chem.* 276, 43693–43698. doi: 10.1074/jbc.M105507200
- Rasmussen, M., Jacobsson, M., and Bjork, L. (2003). Genome-based identification and analysis of collagen-related structural motifs in bacterial and viral proteins. *J. Biol. Chem.* 278, 32313–32316. doi: 10.1074/jbc.M304709200
- Ruggiero, F., Exposito, J. Y., Bournat, P., Gruber, V., Perret, S., Comte, J., et al. (2000). Triple helix assembly and processing of human collagen produced in transgenic tobacco plants. *FEBS Lett.* 469, 132–136. doi: 10.1016/S0014-5793(00)01259-X
- Ruggiero, F., and Koch, M. (2008). Making recombinant extracellular matrix proteins. *Methods* 45, 75–85. doi: 10.1016/j.ymeth.2008.01.003
- Seo, N., Russell, B. H., Rivera, J. J., Liang, X., Xu, X., Afshar-Kharghan, V., et al. (2010). An engineered alpha1 integrin-binding collagenous sequence. *J. Biol. Chem.* 285, 31046–31054. doi: 10.1074/jbc.M110.151357
- Shilo, S., Roth, S., Amzel, T., Harel-Adar, T., Tamir, E., Grynspan, F., et al. (2013). Cutaneous wound healing after treatment with plant-derived human recombinant collagen flowable gel. *Tissue Eng. Part A* 19, 1519–1526. doi: 10.1089/ten.tea.2012.0345
- Shoseyov, O., Posen, Y., and Grynspan, F. (2014). Human collagen produced in plants: more than just another molecule. *Bioengineered* 5, 49–52. doi: 10.4161/bioe.26002
- Werkmeister, J. A., and Ramshaw, J. A. (2012). Recombinant protein scaffolds for tissue engineering. *Biomed. Mater.* 7:012002. doi: 10.1088/1748-6041/7/1/012002
- Xu, X., Gan, Q., Clough, R. C., Pappu, K. M., Howard, J. A., Baez, J. A., et al. (2011). Hydroxylation of recombinant human collagen type I alpha 1 in

- transgenic maize co-expressed with a recombinant human prolyl 4-hydroxylase. *BMC Biotechnol.* 11:69. doi: 10.1186/1472-6750-11-69
- Xu, Y., Keene, D. R., Bujnicki, J. M., Höök, M., and Lukomski, S. (2002). Streptococcal Scl1 and Scl2 proteins form collagen-like triple helices. *J. Biol. Chem.* 277, 27312–27318. doi: 10.1074/jbc.M201163200
- Yoshizumi, A., Yu, Z., Silva, T., Thiagarajan, G., Ramshaw, J. A., Inouye, M., et al. (2009). Self-association of streptococcus pyogenes collagen-like constructs into higher order structures. *Protein Sci.* 18, 1241–1251. doi: 10.1002/pro.134
- Yu, Z., An, B., Ramshaw, J. A., and Brodsky, B. (2014). Bacterial collagen-like proteins that form triple-helical structures. *J. Struct. Biol.* 186, 451–461. doi: 10.1016/j.jsb.2014.01.003
- Yu, Z., Brodsky, B., and Inouye, M. (2011). Dissecting a bacterial collagen domain from *Streptococcus pyogenes*: sequence and length-dependent variations in triple helix stability and folding. *J. Biol. Chem.* 286, 18960–18968. doi: 10.1074/jbc.M110.217422
- Yu, Z., Visse, R., Inouye, M., Nagase, H., and Brodsky, B. (2012). Defining requirements for collagenase cleavage in collagen Type III using a bacterial collagen system. *J. Biol. Chem.* 287, 22988–22997. doi: 10.1074/jbc.M112.348979

Received: 21 March 2014; accepted: 04 June 2014; published online: 23 June 2014.

Citation: An B, Kaplan DL and Brodsky B (2014) Engineered recombinant bacterial collagen as an alternative collagen-based biomaterial for tissue engineering. *Front. Chem.* 2:40. doi: 10.3389/fchem.2014.00040

This article was submitted to Chemical Biology, a section of the journal *Frontiers in Chemistry*.

Copyright © 2014 An, Kaplan and Brodsky. This is an open-access article distributed under the terms of the Creative Commons Attribution License (CC BY). The use, distribution or reproduction in other forums is permitted, provided the original author(s) or licensor are credited and that the original publication in this journal is cited, in accordance with accepted academic practice. No use, distribution or reproduction is permitted which does not comply with these terms.



Three-layer microfibrous peripheral nerve guide conduit composed of elastin-laminin mimetic artificial protein and poly(L-lactic acid)

Sachiro Kakinoki¹, Midori Nakayama^{1,2}, Toshiyuki Moritan² and Tetsuji Yamaoka^{1*}

¹ Department of Biomedical Engineering, National Cerebral and Cardiovascular Center Research Institute, Suita, Japan

² Department of Clinical Engineering, Faculty of Medical Engineering, Suzuka University of Medical Science, Suzuka, Japan

Edited by:

Carissa M. Soto, Naval Research Laboratory, USA

Reviewed by:

Henrique De Amorim Almeida,
Polytechnic Institute of Leiria,
Portugal

Hongyan Sun, City University of
Hong Kong, Hong Kong

***Correspondence:**

Tetsuji Yamaoka, Department of
Biomedical Engineering, National
Cerebral and Cardiovascular Center
Research Institute, 5-7-1 Fujishirodai,
Suita, Osaka 565-8565, Japan
e-mail: yamtet@ncvc.go.jp

We developed a microfibrous poly(L-lactic acid) (PLLA) nerve conduit with a three-layered structure to simultaneously enhance nerve regeneration and prevent adhesion of surrounding tissue. The inner layer was composed of PLLA microfiber containing 25% elastin-laminin mimetic protein (AG73-(VPGIG)₃₀) that promotes neurite outgrowth. The thickest middle layer was constructed of pure PLLA microfibers that impart the large mechanical strength to the conduit. A 10% poly(ethylene glycol) was added to the outer layer to prevent the adhesion with the surrounding tissue. The AG73-(VPGIG)₃₀ compositing of an elastin-like repetitive sequence (VPGIG)₃₀ and a laminin-derived sequence (RKRLQVQLSIRT: AG73) was biosynthesized using *Escherichia coli*. The PLLA microfibrous conduits were fabricated using an electrospinning procedure. AG73-(VPGIG)₃₀ was successfully mixed in the PLLA microfibers, and the PLLA/AG73-(VPGIG)₃₀ microfibers were stable under physiological conditions. The PLLA/AG73-(VPGIG)₃₀ microfibers enhanced adhesion and neurite outgrowth of PC12 cells. The electrospun microfibrous conduit with a three-layered structure was implanted for bridging a 2.0-cm gap in the tibial nerve of a rabbit. Two months after implantation, no adhesion of surrounding tissue was observed, and the action potential was slightly improved in the nerve conduit with the PLLA/AG73-(VPGIG)₃₀ inner layer.

Keywords: poly(L-lactic acid), elastin-laminin mimetic protein, electrospun microfiber, nerve conduit, tissue adhesion prevention

INTRODUCTION

Traumatic nerve injuries in which direct suturing of the proximal and distal stumps is difficult due to the long nerve gap are generally treated with nerve autografts. However, autologous nerve grafting has several disadvantages, such as size mismatch and permanent loss of donor function due to the extraction of normal nerve. As an alternative, artificial nerve conduits have become widely accepted for bridging gaps between nerve stumps (Ichihara et al., 2008; Lohmeyer et al., 2009; Sieminow and Brzezicki, 2009).

Artificial nerve conduits constructed of numerous polymeric materials such as silicone (Lundborg et al., 1982), collagen (Archibald et al., 1995), chitosan (Freier et al., 2005; Ao et al., 2006), hyaluronic acid (Wang et al., 1998), poly(caprolactone) (PCL), poly(glycolic acid) (PGA), and poly(lactic acid) (PLA) (Nakamura et al., 2004; Yoshitani et al., 2007) have been investigated. Recently, an artificial nerve conduit composed of poly(lactic-co-glycolic acid) (PLGA) mesh filled with animal-derived collagen has been put into clinical use and has shown good performance (Nakamura et al., 2004). PLGA is hydrolyzed and metabolized *in vivo*, and thus the PLGA conduit is absorbed during nerve regeneration over the course of several months (Mainil-Varlet et al., 1996). Because PLGA does not possess any biological activity, collagen is used for promoting nerve

regeneration. Collagen is a major component of the basement membrane of nerve tissue and plays a key role in the reconstruction of the axon network by Schwann cells (Thomas, 1964; Chernousov et al., 2008). Although collagen strongly enhances nerve regeneration, animal-derived materials raise concerns about viral infection and immune responses (Lynn et al., 2004). The mesh structure of this conduit is effective for inhibiting the intrusion of surrounding connective tissues and for allowing the permeation of liquid factors and small molecules. However, the mesh structure promotes adherence with surrounding tissues and can cause painful traction neuropathies (Smit et al., 2004). Hence, the ideal conduits for promoting nerve regeneration and preventing tissue adhesion would not include animal-derived materials.

To avoid the use of animal-derived materials, short peptide sequences isolated from extracellular matrix proteins can be used, because they show biological activity equal to that of full-length proteins. For example, the RGD sequence of fibronectin provides excellent cell adhesive properties (Hersel et al., 2003). Focusing on nerve regeneration, the IKVAV (Tashiro et al., 1989), YIGSR (Iwamoto et al., 1987), and RKRLQVQLSIRT (AG73) (Nomizu et al., 1996) sequences derived from laminin have been well studied in the activation of neural cells. These small peptides are

easily synthesized chemically or biologically and are useful for imparting nerve regenerative activity to polymeric materials (Rao and Winter, 2009; Kakinoki and Yamaoka, 2010). Suzuki et al. prepared IKVAV- or YIGSR-immobilized tendon chitosan tubes and demonstrated the efficacy of peptide immobilization for assisting nerve regeneration in a rat model of nerve injury (Suzuki et al., 2003a). Previously, we reported that poly(L-lactic acid) (PLLA) nerve conduits modified with laminin-derived AG73 peptides and a polyethylene glycol (PEG)-containing outer layer are effective for preventing the adhesion of surrounding tissue (Kakinoki et al., 2011). The AG73 peptide was immobilized onto PLLA microfibers using oligo(D-lactic acid) (ODLA)-AG73 conjugates. The microfibers were fabricated by electrospinning of a mixed solution containing PLLA and the ODLA-AG73 conjugate, resulting in stable immobilization of the AG73 peptide via stereocomplex formation between the PLLA and the ODLA. Regeneration of functional nerve tissue was observed in AG73-immobilized microfibrous nerve conduit in the rat model of nerve injury, but it required a long period of time, approximately 6 months. Thus, the efficiency of AG73-immobilized microfibers is insufficient for nerve regeneration. We speculated that the efficacy of AG73 immobilization was decreased immediately after implantation by release of the low-molecular weight PDLA-AG73 conjugates from the microfibers *in vivo*.

To fabricate a more effective biological material for nerve regeneration, we designed and biosynthesized a high molecular weight elastin-laminin mimetic protein. The basement membrane of nerve tissue is primarily constructed with collagen, laminin, and elastin (Rutka et al., 1988). These proteins cooperatively support the process of nerve regeneration. Specifically, collagen and laminin function in axon extension, and elastin provides elasticity for the tissue structure (Toyota et al., 1990). We previously biosynthesized an elastin-laminin mimetic protein and used it for the functionalization of PLLA scaffolds (Kakinoki and Yamaoka, 2014). This protein is composed of 30 repeats of an elastin-like VPGIG repetitive sequence and a laminin-derived AG73 sequence (AG73-(VPGIG)₃₀). AG73-(VPGIG)₃₀ showed temperature-dependent coacervation in phosphate buffered saline (PBS) solution at approximately 14°C. Because the AG73-(VPGIG)₃₀ was insoluble at body temperature, this protein was expected to serve as a suitable scaffold for nerve regeneration. Our results showed that the adhesion and neurite outgrowth of PC12 cells were enhanced on the AG73-(VPGIG)₃₀ adsorbed PLLA films *in vitro*.

In this study, we prepared PLLA microfibrous nerve conduit with a three-layered structure that promoted nerve regeneration and prevented tissue adhesion. The therapeutic efficacy of peripheral nerve regeneration was evaluated using a rabbit model of nerve injury. Microfibrous conduits composed of a PLLA, PLLA/AG73, or PLLA/AG73-(VPGIG)₃₀ inner layer, a PLLA middle layer, and a PLLA/PEG outer layer were fabricated using an electrospinning procedure. Adhesion and neurite outgrowth of PC12 cells on PLLA microfibers containing AG73-(VPGIG)₃₀ were studied *in vitro*. Nerve autografts and microfibrous conduits were implanted in rabbits to bridge a 2-cm tibial nerve gap. Two months after implantation, nerve regeneration was evaluated by electrophysiological measurements.

MATERIALS AND METHODS

EXPRESSION AND PURIFICATION OF THE ELASTIN-LAMININ MIMETIC PROTEIN

The elastin-laminin mimetic protein (AG73-(VPGIG)₃₀) was expressed by *Escherichia coli* BL21(DE3)pLysS (Life Technologies Corporation, Carlsbad, CA, USA) that had been transformed with the pET28(+) vector (Merck KGaA, Darmstadt, Germany) encoding AG73-(VPGIG)₃₀, as described previously (Kakinoki and Yamaoka, 2014). AG73-(VPGIG)₃₀ expression was automatically induced using an Overnight Express™ Autoinduction System (Merck KGaA). Briefly, *E. coli* cells were incubated in 2 × YT medium supplemented with 34 µg/mL of kanamycin and the reagents of the Overnight Express™ Autoinduction System at 30°C for 24 h. *E. coli* was harvested by centrifugation at 3500 × g at 4°C for 15 min. Bacterial pellets were resuspended in lysis solution (8 M urea) and frozen at -80°C. After thawing, bacteria were disrupted by sonication on ice. Insoluble debris was removed by centrifugation at 10,000 × g at 4°C for 15 min, and the supernatant was purified on a His-tag affinity column (COSMOGEL His-Accept, Nacalai Tesque, Kyoto, Japan).

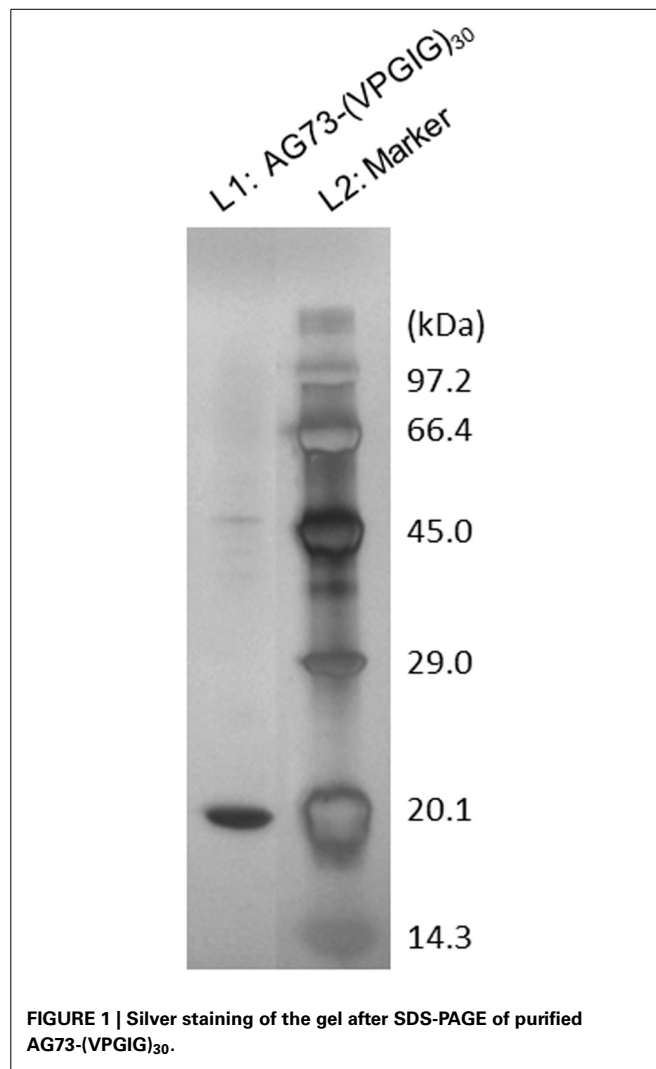


FIGURE 1 | Silver staining of the gel after SDS-PAGE of purified AG73-(VPGIG)₃₀.

Following dialysis (MwCo = 10,000 Da) in deionized water at 4°C, purified AG73-(VPGIG)₃₀ was obtained by lyophilization. The purity of the AG73-(VPGIG)₃₀ was confirmed by sodium dodecyl sulfate-polyacrylamide gel electrophoresis (SDS-PAGE) analysis with silver staining.

FABRICATION OF PLLA/AG73-(VPGIG)₃₀ NON-WOVEN MICROFIBERS

A PLLA/AG73-(VPGIG)₃₀ solution with a concentration of 20w% was prepared by dissolving PLLA (Mw: 106,000, Mn: 60,000, Mw/Mn: 1.77) (Musashino Chemical Laboratory, Inc., Tokyo, Japan) and AG73-(VPGIG)₃₀ in hexafluoroisopropanol (HFIP) at a weight ratio of 4:1. This solution was electrospun using a plastic syringe equipped with a stainless steel needle (length = 15.0 mm, diameter = 20 G) at a constant feed rate of 4 mL/h. An aluminum plate was used as a target and the distance between the target and the needle tip was 100 mm. The solution was electrospun at a high voltage (15 kV) for 5 min. Non-woven PLLA/AG73-(VPGIG)₃₀ microfibers were collected and cut for subsequent experiments. Non-woven PLLA and PLLA/AG73 microfibers were prepared using a similar procedure. The concentration of the AG73 peptide (Purity > 82.6%; Sigma-Aldrich, Inc.) in the PLLA/AG73 solution was adjusted to the same molarity as that of the AG73-(VPGIG)₃₀ in the non-woven PLLA/AG73-(VPGIG)₃₀ microfibers. After immersion in PBS for 24 h at 37°C, the structure of the non-woven microfibers was observed by scanning electron microscopy (SEM; JCM-5700, JEOL, Tokyo, Japan).

NEURITE OUTGROWTH ASSAY

A neurite outgrowth assay was performed using rat adrenal pheochromocytoma (PC12) cells (RIKEN BioResource Center, Ibaraki, Japan), which are widely used as a model for neural stem cells. PC12 cells were maintained in Dulbecco's modified Eagles medium (DMEM) supplemented with 100 units/mL penicillin, 100 µg/mL streptomycin (Life Technologies Corporation, Carlsbad, CA, USA), 10% fetal bovine serum (FBS; MP Biomedicals, Inc., Solon, OH, USA), and 7.5% horse serum (HS; Sigma-Aldrich, Inc., St. Louis, MO, USA). PC12 cells were cultured in poly-D-lysine-coated cell culture dishes (Asahi Glass Co., Ltd., Tokyo, Japan) and maintained at 37°C in a 5% CO₂ atmosphere. Prior to the neurite growth assay, PC12 cells were cultivated in DMEM/F12 medium (Life Technologies Corporation, Carlsbad, CA, USA) with 100 ng/mL nerve growth factor (NGF; Sigma-Aldrich, Inc.) for 24 h on polystyrene cell culture dishes. The medium was refreshed with normal culture medium, and cells were incubated for 30 min at 37°C in a 5% CO₂ atmosphere. Cells were harvested by gentle agitation and resuspended in advanced DMEM/F12 containing 5 mg/mL insulin (Life Technologies Corporation, Carlsbad, CA, USA), 100 ng/mL NGF, 20 nM progesterone, 100 mg/mL transferrin, and 30 nM sodium selenite (Na₂SeO₃) (Nacalai Tesque, Inc., Kyoto, Japan), and seeded on non-woven microfibers fixed with Cell Crown (Scaffdex Ltd., Tampere, Finland) in 24-well cell culture plates at a density of 2.0 × 10⁴ cells/sample. After 48 h incubation at 37°C in a 5% CO₂ atmosphere,

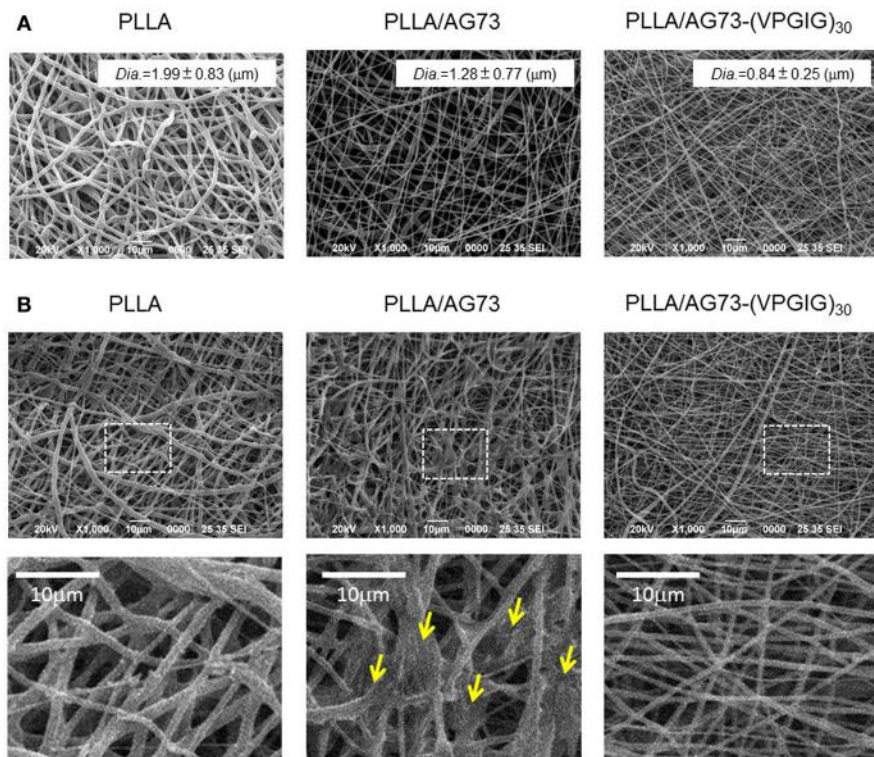


FIGURE 2 | SEM images of electrospun PLLA, PLLA/AG73, and PLLA/AG73-(VPGIG)₃₀ micro-fibers (A) before and (B) after immersion in PBS for 24 h at 37°C. Yellow arrows indicate fusion points.

cells adherent to the non-woven fibers were fixed with 10% formalin and stained with 4% crystal violet/methanol solution. The number of adherent cells observed in the stained images were counted and categorized according to neurite length.

FABRICATION OF PLLA/AG73-(VPGIG)₃₀ MICROFIBROUS CONDUIT

We designed the electrospun microfibrous conduits with 3 layer structure, PLLA, PLLA/AG73, or PLLA/AG73-(VPGIG)₃₀ inner layer, PLLA middle layer, and PLLA/polyethylene glycol (PEG) outer layer. For fabricating conduits, a rotating stainless steel tube (outer diameter = 2.0 mm, speed = 1500 rpm) was used as a target. Other conditions for electrospinning were completely same to nonwovens. First, inner layer (PLLA, PLLA/AG73, or PLLA/AG73-(VPGIG)₃₀) was electrospun as described previously for 5 min. Middle layer was electrospun with 20w% of PLLA solution for 30 min. Then, the mixed solution at 20w% containing PLLA and PEG (9:1) was electrospun for 10 min as an outer layer. The matrices mass for inner, middle, and outer layer were adjusted to 1: 6: 2 for covering inner and outer surface of the mechanically strong middle layer. Microfibrous conduits were cut to length of 22 mm, and immersed in 70%-ethanol for the sterilization. After drying *in vacuo*, conduits were used for animal experiment.

IMPLANTATION OF MICROFIBROUS CONDUITS

Electrospun microfibrous conduits were implanted into 2.0-cm gaps in the left tibial nerve of a total of 12 New Zealand white

rabbits (3.0–3.5 kg, male) (Oriental Yeast Co., Ltd., Tokyo, Japan). This study was performed in accordance with the animal experimental guidelines of the National Cerebral and Cardiovascular Center Research Institute. Rabbits were anesthetized by intramuscular injection of 0.1 mL/kg of Selactar (Bayer Yakuhin, Ltd., Osaka, Japan) and anesthesia was maintained by inhalation of 3% Escain isoflurane (Mylan Inc., Canonsburg, PA, USA). Under an operating microscope, the left tibial nerve was exposed and a 2.0-cm segment was removed. A section of microfibrous conduit was filled with physiological saline solution and sutured with 10-0 vicryl (Ethicon, Somerville, NJ, USA) to bridge the gap between the proximal and distal stumps. Both nerve stumps were pulled 1.0 mm inside the conduits. In addition, the removed nerve tissue was inverted on its proximal-distal axis and implanted as an auto-graft control. Muscle and skin were closed with 3-0 silk sutures (Ethicon), and the rabbits were allowed to recover in a controlled environment.

ELECTROPHYSIOLOGICAL ANALYSIS

Two months after implantation, nerve regeneration was evaluated by electrophysiological analysis. Rabbits were anesthetized in the same manner as for transplantation of the microfibrous conduits, and the implanted site was exposed from the proximal to the distal portions. In order to record electromyograms at the implantation site, a pair of stimulating and recording electrodes was attached to the proximal and distal portions, respectively. Both electrodes were connected to an electric stimulator (SEN-3401, Nihon Kohden, Tokyo, Japan) and a data acquisition system

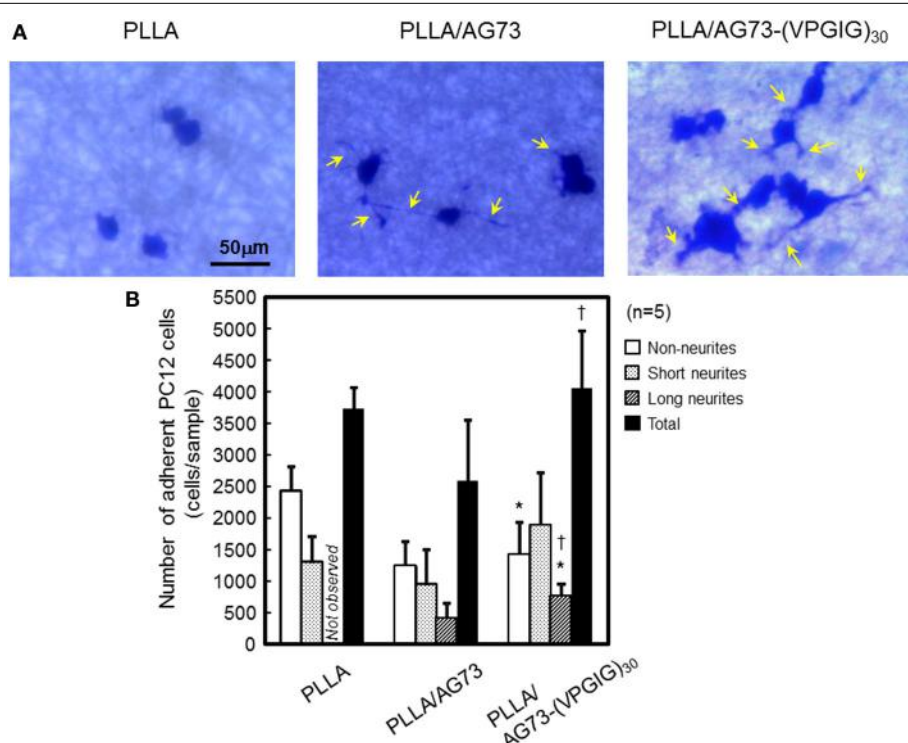


FIGURE 3 | Adhesion and neurite outgrowth of NGF-treated PC12 cells on electrospun nanofibers. **(A)** Morphology of NGF-treated PC12 cells 48 h after seeding. Yellow arrows indicate neurites. **(B)** The number of adherent

PC12 cells categorized as non-neurites, short neurites (< 50 μ m), and long neurites ($\geq 50 \mu$ m). * and † indicate statistically significant differences, $p < 0.05$ vs. PLLA and PLLA/AG73, respectively (Student's *t*-test).

(PowerLab 8/30, ADInstruments, Colorado Springs, CO, USA). The stimulation parameters were as follows: strength = 1 V, current = 1 mA, duration = 10 s, pulse width = 0.1 ms. The active potential was amplified using a PowerLab system (ADInstruments, Burlingame, CA, USA), and recorded as the average of 50 traces.

RESULTS AND DISCUSSION

EXPRESSION AND PURIFICATION OF ELASTIN-LAMININ MIMETIC PROTEIN

SDS-PAGE analysis of purified AG73-(VPGIG)₃₀ is shown in **Figure 1**. A single band was observed at 17–18 kDa, which is concordant with the theoretical molecular weight. Sixty milligrams of high-purity AG73-(VPGIG)₃₀ was successfully obtained from 1 L of culture medium. As previously reported, PBS solution containing AG73-(VPGIG)₃₀ demonstrated temperature-dependent coacervation at 14°C, indicating that the protein is insoluble at 37°C in a physiological environment (Kakinoki and Yamaoka, 2014).

MORPHOLOGY AND STABILITY OF ELECTROSPUN NON-WOVEN MICROFIBERS

SEM images of PLLA, PLLA/AG73, and PLLA/AG73-(VPGIG)₃₀ non-woven microfibers before and after PBS immersion are shown in **Figure 2**. The diameter of the PLLA microfibers was approximately 2.0 μm (**Figure 2A**). When AG73 or AG73-(VPGIG)₃₀ was mixed with the PLLA, the diameter of the

microfibers decreased to approximately 1.3 and 0.9 μm, respectively. The diameter of electrospun microfibers is known to be influenced by solution viscosity and electronic charge (Huang et al., 2003). The PLLA concentration was decreased by the addition of the AG73 and AG73-(VPGIG)₃₀, thus decreasing the viscosity of the solution. Furthermore, the electronic charge of the solution should be positive because AG73 is positive due to its Arg and Lys residues. We assumed that the diameter of the microfibers was decreased by the changes in solution viscosity and electronic charge with the addition of the AG73 and AG73-(VPGIG)₃₀. The surfaces of the PLLA/AG73 and PLLA/AG73-(VPGIG)₃₀ were smooth, without phase separation, suggesting that the AG73 and AG73-(VPGIG)₃₀ were homogeneously mixed.

The morphology of the microfibers following immersion in PBS for 24 h is shown in **Figure 2B**. The shape of the PLLA microfibers did not differ before and after immersion in PBS. However, the morphology of PLLA/AG73 microfibers became rough and some fusion appeared (**Figure 2B**; indicated with yellow arrows) after PBS immersion. These morphological changes suggested that the PLLA/AG73 microfibers partially dissolved in PBS. In contrast, the morphology of PLLA/AG73-(VPGIG)₃₀ microfibers did not change after PBS immersion, indicating that the PLLA/AG73-(VPGIG)₃₀ microfibers were stable in a physiological environment.

NEURITE OUTGROWTH OF PC12 CELLS ON NON-WOVEN MICROFIBERS

The morphology and number of PC12 cells adherent on non-woven microfibers are shown in **Figure 3**. On PLLA, the rate of adherence of PC12 cells was approximately 3750/sample. Most of the adherent cells were non-neurites, and cells with long neurites were not observed. On PLLA/AG73, a similar number of adherent cells was observed, but neurite outgrowth was slightly enhanced in comparison to PLLA. PC12 cells have been reported to adhere to AG73-immobilized substrates through syndecans and the NGF pathway has been reported to be activated, resulting in neurite outgrowth (Suzuki et al., 2003b). Thus, AG73 must be stably immobilized on a substrate to express its biological function. The AG73 was removed from the surface of the PLLA/AG73 microfibers in culture medium, resulting in poor enhancement of adhesion and neurite outgrowth of PC12 cells. On PLLA/AG73-(VPGIG)₃₀ microfibers, the adhesion and neurite outgrowth of PC12 cells was significantly accelerated compared to PLLA and PLLA/AG73. Because the hydrophobicity of the (VPGIG)₃₀ region renders AG73-(VPGIG)₃₀ insoluble in PBS, it was stably bound to the PLLA. The hydrophilic AG73 region was available to contact PC12 cells at the outermost surface of the microfibers, resulting in promotion of adhesion and neurite outgrowth of PC12 cells.

NERVE REGENERATION IN THE RABBIT MODEL OF NERVE INJURY

The electrospun microfibrous conduits had a three-layered structure, including a PLLA/PEG outer layer, a PLLA middle layer, and a PLLA, PLLA/AG73, or PLLA/AG73-(VPGIG)₃₀ inner layer, as shown in **Figure 4**. PEG was used in the outer layer to prevent the adhesion of surrounding tissues, because the adhesion of surrounding tissues to nerves causes painful traction

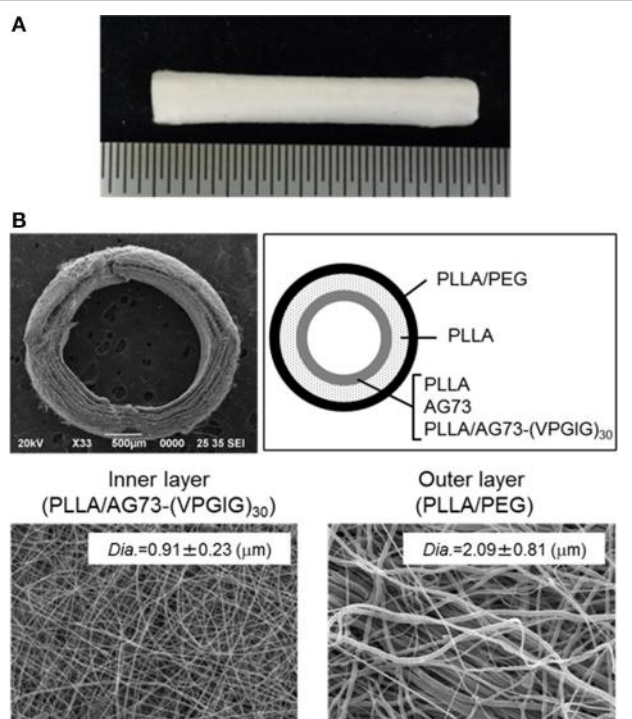


FIGURE 4 | Micro-fibrous nerve conduit with a three-layered structure. **(A)** Whole image, **(B)** SEM images of cross-sections and inner and outer layers.

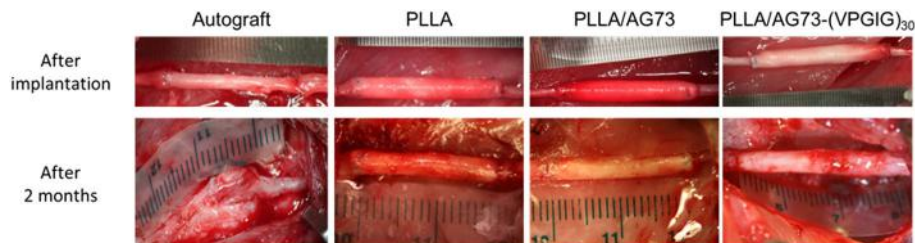


FIGURE 5 | Intraoperative photographs of autograft and micro-fibrous conduits (A) immediately after implantation and (B) 2 months after implantation. The proximal side is shown on the left.

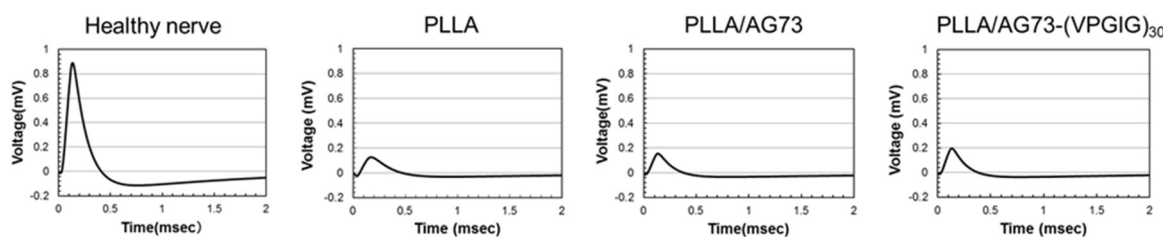


FIGURE 6 | Active potential of healthy nerve and PLLA micro-fibrous conduits 2 months after implantation.

Table 1 | Peak time and intensity of active potentials determined using electrophysiological analysis.

Experimental group	Peak of active potential	N			Average	SD
		1	2	3		
PLLA	Time (ms)	0.21	0.19	0.17	0.19	0.02
	Intensity (mV)	0.11	0.03	0.12	0.09	0.05
PLUVAG73	Time (ms)	0.16	0.17	0.16	0.16	0.01
	Intensity (mV)	0.28	0.13	0.08	0.16	0.10
PLUVAG73-(VPGIG) ₃₀	Time (ms)	0.17	0.15	0.14	0.15	0.02
	Intensity (mV)	0.24	0.19	0.19	0.21	0.03

neuropathies (Tashiro et al., 1989). The microfibrous conduits were approximately 500-μm thick, and the diameter of the PLLA/PEG microfiber outer layer was approximately 2.0 μm. Intraoperative photographs of the autografts and the microfibrous conduits in the rabbit tibial nerve gap were taken immediately after the implantation, and are shown in **Figure 5**. The conduits possessed sufficient strength for suturing and maintained their tubular shape after implantation. Two months after implantation, the nerve autografts were strongly adhered to the surrounding tissue and muscle, as shown in **Figure 5**. In contrast, the microfibrous conduits were easily located because the PEG in the PLLA microfibers of the outer layer had suppressed tissue adhesion. All conduits maintained their tubular structure during the 2 months, due to the slow degradation of the high molecular weight PLLA.

Reinnervation by nerve autografts or conduit implantation was analyzed by electrophysiological detection of active potentials

(**Figure 6**). The action potential of healthy tibial nerve was 0.9 mV at 0.12 ms. The intensity and peak time of the action potential are summarized in **Table 1**. No action potential was detected in implanted nerve autografts, due to the abnormal adhesion of surrounding tissues, but action potentials were reproducibly detected for PLLA microfibrous conduits. In unmodified PLLA conduit, the time and intensity of the action potential were 0.19 ms and 0.09 mV, respectively. Mixing the AG73 peptide in the inner layers lightly improved the action potential, to 0.16 mV at 0.16 ms. The microfibrous conduit with a PLLA/AG73-(VPGIG)₃₀ inner layer carried an action potential of 0.15 ms at 0.21 mV. This recovery is far from functional reinnervation, but nerve regeneration was slightly enhanced by mixing PLLA with AG73-(VPGIG)₃₀, compared to PLLA and PLLA/AG73 nerve conduits due to the stable interaction of AG73-(VPGIG)₃₀ with PLLA microfibers.

CONCLUSION

PLLA microfibers containing the AG73 peptide or the elastin-laminin mimetic protein AG73-(VPGIG)₃₀ were fabricated using an electrospinning procedure. AG73-(VPGIG)₃₀ was homogeneously mixed in PLLA microfibers, and the fibers were insoluble in a physiological environment. Neurite outgrowth of PC12 cells was promoted on the PLLA/AG73-(VPGIG)₃₀ non-woven microfibers compared to that on the PLLA and PLLA/AG73 non-woven microfibers. In addition, we prepared electrospun microfibrous conduits with a three-layered structure: a PLLA/PEG outer layer, a PLLA middle layer, and a PLLA, PLLA/AG73, or PLLA/AG73-(VPGIG)₃₀ inner layer. When microfibrous conduits were implanted into a 2.0-cm gap in an injured rabbit tibial nerve, their tubular structure was maintained after suturing. Although nerve autografts strongly adhered to the

surrounding tissue, PLLA microfibrous conduits did not, owing to PEG mixed in the outer layer. The active potential was slightly improved in PLLA/AG73-(VPGIG)₃₀ microfibrous conduit compared to PLLA and PLLA/AG73 microfibrous conduits. However, this recovery was insufficient to achieve functional reinnervation. Microfiber orientation has been reported to influence the differentiation and proliferation of neural stem cell (Bashur et al., 2006; Ghasemi-Mobarakeh et al., 2008). In this study, the structure of the AG73-(VPGIG)₃₀ microfibers of the inner layer was random. Alignment of the inner-layer fibers of conduits is expected to enhance reinnervation. The results of this study demonstrate that the electrospun PLLA microfiber conduit with a PEG-mixed outer layer and an AG73-(VPGIG)₃₀-mixed inner layers shows excellent potential for enhancing nerve regeneration.

ACKNOWLEDGMENTS

This work was partially supported by a Grant-in-Aid from the Comprehensive Research on Disability Health and Welfare Program, the Ministry of Health, Labor and Welfare of Japan, the S-innovation Research Program for the “Development of the biofunctional materials for realization of innovative medicine,” Japan Science and Technology Agency (JST), and Intramural Research Fund of National Cerebral and Cardiovascular Center.

REFERENCES

- Ao, Q., Wang, A., Cao, W., Zhang, L., Kong, L., He, Q., et al. (2006). Manufacture of multimicrotubule chitosan nerve conduits with novel molds and characterization *in vitro*. *J. Biomed. Mater. Res. A* 77A, 11–18. doi: 10.1002/jbm.a.30593
- Archibald, S. J., Shefner, J., Krarup, C., and Madison, R. D. (1995). Monkey median nerve repaired by nerve graft or collagen nerve guide tube. *J. Neurosci.* 15, 4109–4123.
- Bashur, C. A., Dahlgren, L. A., and Goldstein, A. S. (2006). Effect of fiber diameter and orientation on fibroblast morphology and proliferation on electro-spun poly(D,L-lactic-co-glycolic acid) meshes. *Biomaterials* 27, 5681–5688. doi: 10.1016/j.biomaterials.2006.07.005
- Chernousov, M. A., Yu, W., Chen, Z., Carey, D. J., and Strickland, S. (2008). Regulation of schwann cell function by the extracellular matrix. *GLIA* 56, 1498–1507. doi: 10.1002/glia.20740
- Freier, T., Montenegro, R., Koh, H. S., and Shoichet, M. S. (2005). Chitin-based tubes for tissue engineering in the nervous system. *Biomaterials* 26, 4624–4632. doi: 10.1016/j.biomaterials.2004.11.040
- Ghasemi-Mobarakeh, L., Prabhakaran, M. P., Morshed, M., Nasr-Esfahani, M.-H., and Ramakrishna, S. (2008). Electrospun poly(ε-caprolactone)/gelatin nanofibrous scaffolds for nerve tissue engineering. *Biomaterials* 29, 4532–4539. doi: 10.1016/j.biomaterials.2008.08.007
- Hersel, U., Dahmen, C., and Kessler, H. (2003). RGD modified polymers: biomaterials for stimulated cell adhesion and beyond. *Biomaterials* 24, 4385–4415. doi: 10.1016/S0142-9612(03)00343-0
- Huang, Z., Zhang, Y. Z., Kotaki, M., and Ramakrishna, S. (2003). A review on polymer nanofibers by electrospinning and their applications in nanocomposites. *Compos. Sci. Technol.* 63, 2223–2253. doi: 10.1016/S0266-3538(03)00178-7
- Ichihara, S., Inada, Y., and Nakamura, T. (2008). Artificial nerve tubes and their application for repair of peripheral nerve injury: an update of current concepts, ainjury. *Injury* 39(Suppl. 4), S29–S39. doi: 10.1016/j.injury.2008.08.029
- Iwamoto, Y., Robey, F. A., Graf, J., Sasaki, M., Kleinman, H. K., Yamada, Y., et al. (1987). YIGSR, a synthetic laminin pentapeptide, inhibits experimental metastasis formation. *Science* 238, 1132–1134. doi: 10.1126/science.2961059
- Kakinoki, S., Uchida, S., Ehashi, T., Murakami, A., and Yamaoka, T. (2011). Surface modification of poly(L-lactic acid) nanofiber with oligo(D-Lactic acid) bioactive-peptide conjugates for peripheral nerve regeneration. *Polymers* 3, 820–832. doi: 10.3390/polym3020820
- Kakinoki, S., and Yamaoka, T. (2010). Stable modification of poly(lactic acid) surface with neurite outgrowth-promoting peptides via hydrophobic collagen-like sequence. *Acta Biomater.* 6, 1925–1930. doi: 10.1016/j.actbio.2009.12.001
- Kakinoki, S., and Yamaoka, T. (2014). Thermoresponsive elastin/laminin mimicking artificial protein for modifying PLLA scaffolds in nerve regeneration. *J. Mat. Chem. B*. doi: 10.1039/c4tb00305e
- Lohmeyer, J. A., Siemers, F., Machens, H.-G., and Mailänder, P. (2009). The clinical use of artificial nerve conduits for digital nerve repair: a prospective cohort study and literature review. *J. Reconstr. Microsurg.* 25, 55–61. doi: 10.1055/s-0028-1103505
- Lundborg, G., Dahlén, L. B., Danielsen, N., Gelberman, R. H., Longo, F. M., Powell, H. C., et al. (1982). Nerve regeneration in silicone chambers: influence of gap length and of distal stump components. *Exp. Neurol.* 76, 361–375. doi: 10.1016/0014-4886(82)90215-1
- Lynn, S. K., Yannas, I. V., and Bonfield, W. (2004). Antigenicity and immunogenicity of collagen. *J. Biomed. Mater. Res.* 71B, 343–354. doi: 10.1002/jbm.b.30096
- Mainil-Varlet, P., Gogolewski, S., and Nieuwenhuis, P. (1996). Long-term soft tissue reaction to various polylactides and their *in vivo* degradation. *J. Mater. Sci. Mater. Med.* 7, 713–721. doi: 10.1007/BF00121406
- Nakamura, T., Inada, Y., Fukuda, S., Yoshitani, M., Nakada, A., Itoi, S., et al. (2004). Experimental study on the regeneration of peripheral nerve gaps through a polyglycolic acid-collagen (PGA-collagen) tube. *Brain Res.* 1027, 18–29. doi: 10.1016/j.brainres.2004.08.040
- Nomizu, M., Song, S. Y., Kuratomi, Y., Tanaka, M., Kim, W. H., Kleinman, H. K., et al. (1996). Active peptides from the carboxyl-terminal globular domain of laminin alpha2 and Drosophila alpha chains. *FEBS Lett.* 396, 37–42. doi: 10.1016/0014-5793(96)01060-5
- Rao, S. S., and Winter, J. O. (2009). Adhesion molecule-modified biomaterials for neural tissue engineering. *Front. Neuroeng.* 2:6. doi: 10.3389/neuro.16.006.2009
- Rutka, J. T., Apodaca, G., Stern, R., and Rosenblum, M. (1988). The extracellular matrix of the central and peripheral nervous systems: structure and function. *J. Neurosurg.* 69, 155–170. doi: 10.3171/jns.1988.69.2.0155
- Sieminow, M., and Brzezicki, G. (2009). Current techniques and concepts in peripheral nerve repair. *Int. Rev. Neurobiol.* 87, 141–172. doi: 10.1016/S0074-7742(09)87008-6
- Smit, X., van Neck, J. W., Afoko, A., and Hovius, S. E. R. (2004). Reduction of neural adhesions by biodegradable autocrosslinked hyaluronic acid gel after injury of peripheral nerves: an experimental study. *J. Neurosurg.* 101, 648–652. doi: 10.3171/jns.2004.101.4.0648
- Suzuki, M., Itoh, S., Yamaguchi, I., Takakuda, K., Kobayashi, H., Shinomiya, K., et al. (2003a). Tendon chitosan tubes covalently coupled with synthesized laminin peptides facilitate nerve regeneration *in vivo*. *J. Neurosci. Res.* 72, 646–659. doi: 10.1002/jnr.10589
- Suzuki, N., Ichikawa, N., Kasai, S., Yamada, M., Nishi, N., Morioka, H., et al. (2003b). Syndecan binding sites in the laminin α1 chain G domain. *Biochemistry* 42, 12625–12633. doi: 10.1021/bi030014s
- Tashiro, K., Sephel, G. C., Weeks, B., Sasaki, M., Martin, G. R., Kleinman, H. K., et al. (1989). A synthetic peptide containing the IKVAV sequence from the α chain of laminin mediates cell attachment, migration, and neurite outgrowth. *J. Biol. Chem.* 264, 16174–16182.
- Thomas, P. K. (1964). The deposition of collagen in relation to schwann cell basement membrane during peripheral nerve regeneration. *J. Cell Biol.* 23, 375–382. doi: 10.1083/jcb.23.2.375
- Toyota, B., Carbonetto, S., and David, S. (1990). A dual laminin/collagen receptor acts in peripheral nerve regeneration. *Proc. Natl. Acad. Sci. U.S.A.* 87, 1319–1322. doi: 10.1073/pnas.87.4.1319
- Wang, K.-K., Nemeth, I. R., Seckel, B. R., Chakalis-Haley, D. P., Swann, D. A., Kuo, J.-W., et al. (1998). Hyaluronic acid enhances peripheral nerve regeneration *in vivo*. *Microsurgery* 18, 270–275.
- Yoshitani, M., Fukuda, S., Itoi, S., Morino, S., Tao, H., Nakada, A., et al. (2007). Experimental repair of phrenic nerve using a polyglycolic acid and collagen tube. *J. Thorac. Cardiovasc. Surg.* 133, 726–732. doi: 10.1016/j.jtcvs.2006.08.089

Conflict of Interest Statement: The authors declare that the research was conducted in the absence of any commercial or financial relationships that could be construed as a potential conflict of interest.

Received: 19 May 2014; accepted: 26 June 2014; published online: 18 July 2014.

Citation: Kakinoki S, Nakayama M, Moritan T and Yamaoka T (2014) Three-layer microfibrous peripheral nerve guide conduit composed of elastin-laminin mimetic artificial protein and poly(L-lactic acid). *Front. Chem.* 2:52. doi: 10.3389/fchem.2014.00052

This article was submitted to *Chemical Biology*, a section of the journal *Frontiers in Chemistry*.

Copyright © 2014 Kakinoki, Nakayama, Moritan and Yamaoka. This is an open-access article distributed under the terms of the Creative Commons Attribution License (CC BY). The use, distribution or reproduction in other forums is permitted, provided the original author(s) or licensor are credited and that the original publication in this journal is cited, in accordance with accepted academic practice. No use, distribution or reproduction is permitted which does not comply with these terms.



RGD-conjugated rod-like viral nanoparticles on 2D scaffold improve bone differentiation of mesenchymal stem cells

Pongkwan Sitasuwan^{1,2}, L. Andrew Lee^{1,2}, Kai Li^{1,3}, Huong Giang Nguyen^{1,4} and Qian Wang^{1*}

¹ Department of Chemistry and Biochemistry, University of South Carolina, Columbia, SC, USA

² Integrated Micro-Chromatography Systems, Columbia, SC, USA

³ Weifang Entry-Exit Inspection and Quarantine Bureau, Weifang, Shandong, China

⁴ Department of Chemistry, The Institute of Catalysis for Energy Processes, Northwestern University, Evanston, IL, USA

Edited by:

Carissa M. Soto, Naval Research Laboratory, USA

Reviewed by:

Shelli Renee McAlpine, University of New South Wales, Australia
Remigiusz Adam Serwa, Imperial College London, UK

***Correspondence:**

Qian Wang, Department of Chemistry and Biochemistry, University of South Carolina, 631 Sumter Street, Columbia, SC 29208, USA
e-mail: wang263@mailbox.sc.edu

Viral nanoparticles have uniform and well-defined nano-structures and can be produced in large quantities. Several plant viral nanoparticles have been tested in biomedical applications due to the lack of mammalian cell infectivity. We are particularly interested in using *Tobacco mosaic virus* (TMV), which has been demonstrated to enhance bone tissue regeneration, as a tunable nanoscale building block for biomaterials development. Unmodified TMV particles have been shown to accelerate osteogenic differentiation of adult stem cells by synergistically upregulating bone morphogenetic protein 2 (BMP2) and integrin-binding bone sialoprotein (IBSP) expression with dexamethasone. However, their lack of affinity to mammalian cell surface resulted in low initial cell adhesion. In this study, to increase cell binding capacity of TMV based material the chemical functionalization of TMV with arginine-glycine-aspartic acid (RGD) peptide was explored. An azide-derivatized RGD peptide was “clicked” to tyrosine residues on TMV outer surface via an efficient copper(I) catalyzed azide-alkyne cycloaddition (CuAAC) reaction. The ligand spacing is calculated to be 2–4 nm, which could offer a polyvalent ligand clustering effect for enhanced cell receptor signaling, further promoting the proliferation and osteogenic differentiation of bone marrow-derived mesenchymal stem cells (BMSCs).

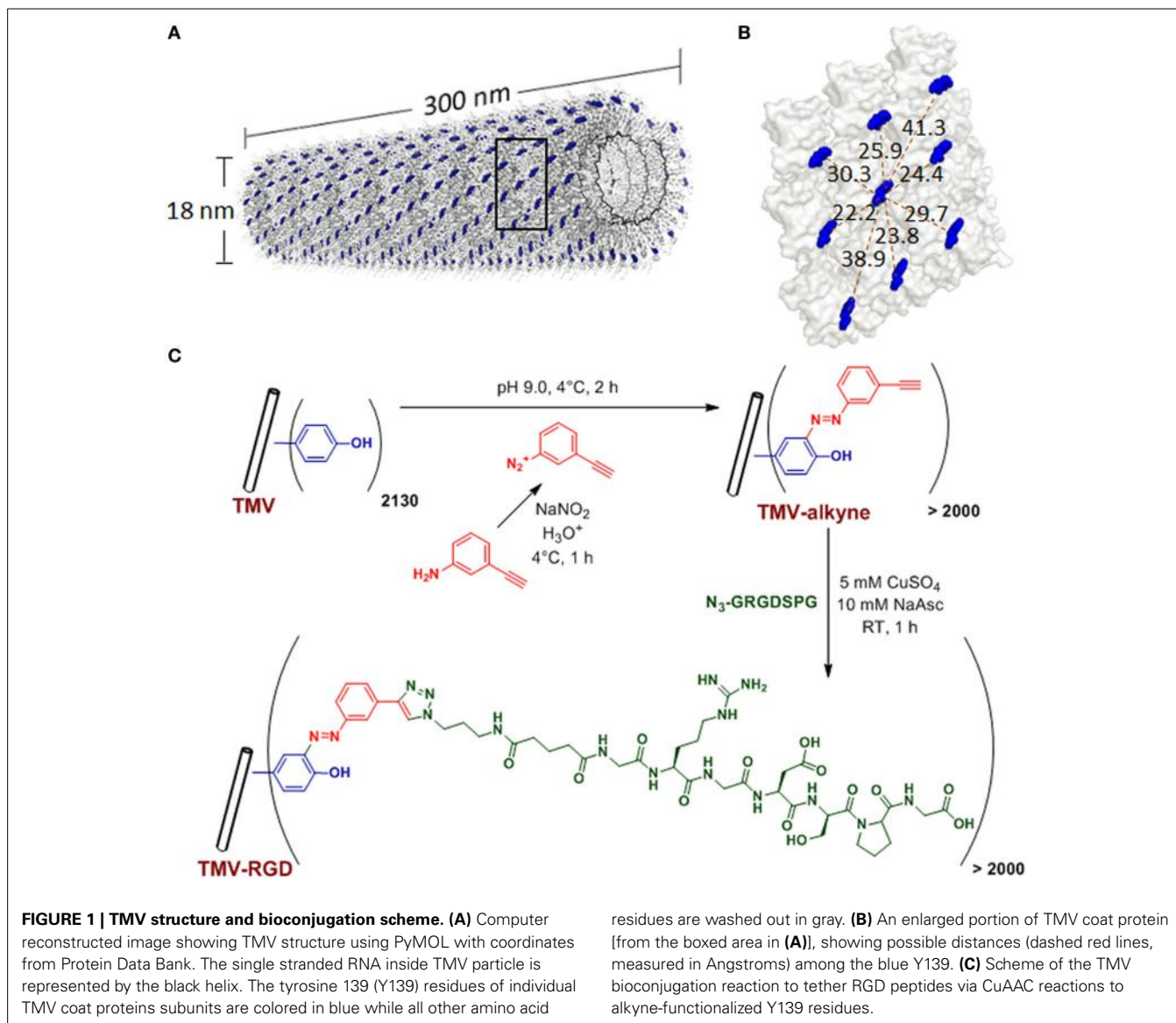
Keywords: viral nanoparticles, RGD peptide, click chemistry, osteogenesis, bone mesenchymal stem cells

INTRODUCTION

Plant viral nanoparticles are meta-stable, readily available, monodisperse, and structurally uniform bionanoparticles. Such plant-derived viral particles have gained great interest in nano- and biomedical applications. *Tobacco mosaic virus* (TMV) is among the most commonly used plant viruses, having a rod-shape measuring 300 nm in length and 18 nm in diameter (Figure 1A). The viral capsid consists of 2130 identical coat protein subunits assembled in a helical structure around the single stranded genomic RNA. The production of TMV is cost effective and the resulting viral particles are highly uniform in size. TMV nanoparticles have been demonstrated as powerful building blocks that can be efficiently functionalized via both genetic (Jiang et al., 2006; McCormick et al., 2006; Lee et al., 2012b) and chemical (Schlick et al., 2005; Bruckman et al., 2008) modifications. Due to its identical subunits and regular structure, the same modification occurs on each individual subunit to yield a polyvalent and monodisperse display of ligands within a single TMV particle.

The tripeptide arginine-glycine-aspartic acid (RGD) present in many adhesive proteins in the extracellular matrix (ECM) is a well-known general cell recognition motif via the cell surface integrin receptors (Ruoslahti and Pierschbacher, 1987). These proteins include fibronectin, vitronectin, osteopontin, collagen, thrombospondin, fibrinogen, and von Willebrand factor (Ruoslahti and Pierschbacher, 1987). Generally, the incorporation of RGD sequence into artificial scaffolds increases initial cell

adhesion to the scaffold and cell spreading, thus improving tissue regeneration process. It has been suggested that the spacing between RGD motifs needs to be less than 440 nm to mediate fibroblast adhesion and spreading and less than 140 nm to mediate focal adhesion assembly (Massia and Hubbell, 1991). Later, it was discovered that the RGD cluster spacings have a threshold less than 60 nm in order for NR6 fibroblasts to form focal adhesion and stress fiber (Maheshwari et al., 2000). Moreover, the threshold spacings are lower (closer) if there is less RGD clustering. In other words, at the same surface RGD density, the surface with RGD clusters present would provide greater cell adhesion strength (Maheshwari et al., 2000). Another study illustrated that integrin-mediated signaling requires RGD spacing of less than 58 nm (Cavalcanti-Adam et al., 2006). A more recent study showed that focal adhesion complexes between cell-membrane integrins and cytoskeleton, responsible for signal transduction from external stimuli to the cell, were formed when RGD spacing is less than 44 nm in endothelial cells (Le Saux et al., 2011). Specifically in the case of osteogenesis, there are several studies illustrating that the incorporation of RGD sequence into biomaterials improved bone differentiation and regeneration (Shin et al., 2004, 2005; Anderson et al., 2010; Peng et al., 2011; Qu et al., 2011). Especially, it was recently emphasized that a local clustering of RGD ligands is more essential than global RGD density (Deeg et al., 2011; Wang et al., 2013b). This clustering effect is believed to occur at an integrin-binding spacing less than an integrin itself, which has a size of 8–12 nm.



Many viral nanoparticles have been employed to achieve RGD-displaying clustering, such as M13 bacteriophage (Souza et al., 2006; Rong et al., 2008; Merzlyak et al., 2009; Chung et al., 2010; Wang et al., 2013a), *Cowpea mosaic virus* (Hovlid et al., 2012), *Turnip yellow mosaic virus* (Zeng et al., 2011; Zan et al., 2012), including genetically modified TMV with RGD peptides (Luckanagul et al., 2012; Lee et al., 2012a,b). However, to guarantee a successful assembly of final mutant TMV particles, TMV can only tolerate limited sequence diversity and length of the genetic peptide insertion (Lee et al., 2012b). Therefore, we explore the feasibility of TMV functionalization with the copper catalyzed alkyne-azide cycloaddition (CuAAC) reaction to display RGD peptides. In addition, the influence of RGD-presenting TMV, where RGD clustering is present (RGD spacing of 2–4 nm) (**Figure 1B**), on the osteogenic potential of bone marrow derived mesenchymal stem cells (BMSCs) is investigated.

MATERIALS AND METHODS

TMV ISOLATION, BIOCONJUGATION, AND CHARACTERIZATION

TMV was isolated and purified according to a protocol previously reported (Kaur et al., 2010a,b). The schematic representation of TMV bioconjugation is shown in **Figure 1C**. The RGD-azide peptide was synthesized using solid-phase peptide synthesis. The peptides were purified with FPLC and characterized by LC/ESI mass spectrometry. The CuAAC reaction to modify tyrosine residues on the exterior surface of TMV is performed according to protocols established by Schlick et al. (2005) and Bruckman et al. (2008) with slight modifications. Briefly, diazonium salt was synthesized by mixing 16 parts of 0.3 M *p*-toluenesulfonic acid, three parts of 0.67 M 3-aminophenylacetylene, and one part of 3 M sodium nitrite as published previously (Schlick et al., 2005). TMV was treated with 25 molar excess of the diazonium salt generated *in situ* from 3-aminophenylacetylene at 4°C in a pH 9.0 buffer solution to form alkyne grafted TMV particle. CuAAC reaction

was used to conjugate RGD-azide peptide to TMV particle (Wang et al., 2003). The CuAAC reaction was done with concentration of TMV-alkyne at 3 mg/mL and peptide-azide at 4 mg/mL in Tris HCl buffer (10 mM, pH 7.8), in the presence of 5 mM copper (II) sulfate and 10 mM sodium acetate. After 1 h incubation at room temperature, TMV-RGD was purified via a 10–50% sucrose gradient from which the light scattering region was collected. The modified virus was then pelleted using ultracentrifugation at 160,000 g for 2.5 h at 4°C. The pellet was dissolved in potassium phosphate buffer (10 mM, pH 7.4). MALDI-TOF mass spectrometry was used to confirm the modifications. The integrity of modified TMV particles was confirmed by AFM and TEM. The virus solutions were dialyzed against water prior to substrate coating.

PREPARATION OF VIRUS COATED SUBSTRATES

For cell culture experiments, 3-aminopropyltriethoxysilane (APTES) coated slides (Lab Scientific Inc.) were cut into 1.5 cm² wafers. The wafers were washed with ethanol before use. For virus coating, each wafer was coated with 0.2 mL of 0.2 mg/mL TMV or TMV-RGD solution diluted in water and the coated substrates were dried overnight in a sterile biosafety cabinet. The virus coverage on the wafers was characterized using tapping-mode AFM images using a NanoScope IIIA MultiMode AFM (Veeco). Si tips with a resonance frequency of approximately 300 kHz, a spring constant of about 40 N m⁻¹ and a scan rate of 1.0 Hz were used.

BMSC ISOLATION AND EXPANSION

Primary BMSCs were isolated from the bone marrow of young adult 80 g male Wister rats (Harlan Sprague Dawley, Inc.). The procedures were performed in accordance with the guidelines for animal experimentation by the Institutional Animal Care and Use Committee, School of Medicine, University of South Carolina. Cells were maintained in growth medium [DMEM supplemented with 10% fetal bovine serum (FBS), penicillin (100 U/mL), streptomycin (100 µg/mL), and amphotericin B (250 ng/mL)] and passaged no more than four times after isolation. To induce osteogenesis, growth media was replaced with osteogenic media consisting of DMEM supplemented with 10% FBS, penicillin (100 U/mL), streptomycin (100 µg/mL), amphotericin B (250 ng/mL), 10 mM sodium β-glycerophosphate, L-ascorbic acid 2-phosphate (50 µg/mL), and 10⁻⁸ M dexamethasone. Media was replenished every 3–4 days.

CELL PROLIFERATION

Substrates coated with TMV and TMV-RGD were seeded with 4 × 10⁴ cells per substrate and cells were allowed to attach overnight in growth media. The media was then replaced with osteogenic media and cultured for 22 days. CellTiter Blue® assay (Promega) was used to determine number of cells at 0, 2, 4, 9, 12, 16, and 22 days after osteogenic induction. Cell proliferation was determined by normalizing CellTiter Blue fluorescence intensities against initial signal intensity on day 0, which is the day of osteogenic induction.

QUANTITATIVE REAL-TIME RT-PCR ANALYSIS (RT-qPCR)

Virus coated wafers were seeded with 4 × 10⁴ cells per wafer and cells were allowed to attach overnight in growth media. The

unseeded cells were used as a control to normalize the change in gene expression. The media was replaced with osteogenic media and cultured for 7, 14, and 21 days. The cell cultures were terminated at these time points and total RNA was extracted using RNeasy mini purification kit (Qiagen). The quality and quantity of the extracted RNA was analyzed using Bio-Rad Experion (Bio-Rad Laboratories) and was reverse transcribed by using qScript™ cDNA Supermix (Quanta Biosciences). RT-qPCR (iQ5 real-time PCR detection system Bio-Rad Laboratories) was done by the method described as: 60 cycles of PCR (95°C for 20 s, 58°C for 15 s, and 72°C for 15 s), after initial denaturation step of 5 min at 95°C, by using 12.5 µL of iQ5 SYBR Green I Supermix, 2 pmol/µL of each forward and reverse primers and 0.5 µL cDNA templates in a final reaction volume of 25 µL. Glyceraldehyde 3-phosphate dehydrogenase (GAPDH) was used as the house-keeping gene. Data collection was enabled at 72°C in each cycle and C_T (threshold cycle) values were calculated using the iQ5 optical system software version 2.1. The expression levels of differentiated genes and undifferentiated genes were calculated using Pfaffl's method (M. W. Pfaffl, G. W. Horgan, and L. Dempfle, Relative expression software tool) for group-wise comparison and statistical analysis of relative expression results in real-time PCR, using GAPDH as the reference gene. Quantification of gene expression was based on the C_T value for each sample which was calculated as the average of three replicate measurements for each sample analyzed. “Pair Wise Fixed Reallocation Randomization Test” was performed on each sample and a value of *p* < 0.05 was regarded as significant. The primers used for RT-qPCR are shown in Figure S1.

ALKALINE PHOSPHATASE ACTIVITY

After 14 days in osteogenic cultures, CellTiter Blue® assay (Promega) was used to determine number of cells in each sample 1 h prior to cell fixation. BMSCs seeded on TMV and TMV-RGD were fixed with 4% paraformaldehyde for 15 min at room temperature. To determine alkaline phosphatase (ALP) activity, each fixed samples were incubated in 500 µL of 1-Step *p*-nitrophenyl phosphate solution (Thermo Scientific) for 15 min at room temperature. Then the solution was transferred to a new microfuge tube with 250 µL of 2 N NaOH and the absorbance at 405 nm was measured. The measured ALP activity from each sample was normalized to the corresponding cell number.

ALIZARIN RED STAINING

To visualize calcium deposition and to confirm osteogenic differentiation, fixed samples at day 14 were stained with 0.1% Alizarin red solution (Sigma-Aldrich) pH 4.1–4.5 for 30 min in the dark. The samples were washed with water (18.2 MΩ) prior to imaging.

RESULTS

The tyrosine residues (Y139) of TMV are viable for chemical ligation using electrophilic substitution reaction at the *ortho*-position of the phenol ring with diazonium salts (Schlick et al., 2005). TMV subunits are assembled in a highly regular helical structure, which resulted in uniform spacing between two subunits down to a nanometer scale. From coordinates provided by Protein Data Bank, the distance between neighboring Y139

residues of TMV coat proteins is calculated to be 2–4 nm apart as shown in **Figure 1B**. The CuAAC reaction has been confirmed to be a very efficient way to display functional groups on TMV in a controllable manner (Bruckman et al., 2008). Following the reported protocol (Schlick et al., 2005; Bruckman et al., 2008). We first prepared the alkyne derived TMV particles (**Figure 1C**). As shown in the MALDI-TOF MS analysis (**Figure 2A**), the peak of the coat protein (m/z 17534) disappeared after the diazonium coupling resulting in the TMV-alkyne product (m/z 17664), consistent with a previous report (Lee et al., 2012b). Similarly, the MALDI-TOF MS analysis indicated the correct mass shift for TMV-RGD confirmed the completion of the sequential CuAAC reaction (**Figure 2A**). The integrity of TMV-RGD was confirmed by AFM and TEM (**Figure 2B**). AFM images illustrated that the majority of TMV-RGD remained rod-shaped particles after the bioconjugation. The diameter observed under TEM ranged from 15–20 nm with lengths measuring approximately 300 nm, indicating the particles are intact after the two-step CuAAC reaction to Y139 (**Figure 2B**).

The effect of RGD-displaying TMV, as a polyvalent scaffold, on bone differentiation was explored. It has been demonstrated that unmodified TMV substrate accelerated osteogenesis by 7 days compared to standard tissue culture polystyrene (TCPS) control (Kaur et al., 2010a). The chemical incorporation of phosphate functional groups to TMV further enhanced bone differentiation of BMSCs (Kaur et al., 2010b). However, the interaction between BMSCs and TMV substrates were weak since the focal adhesion

complexes were found to be significantly smaller than the control (Sitasuwan et al., 2012). Since RGD ligand is known to promote cell attachment, the incorporation of RGD motifs into TMV based substrate is expected to increase the initial cell adhesion.

Prior to cell culture experiments, TMV and TMV-RGD were dialyzed several times against ultrapure water, due to concerns that residual Cu^I from the CuAAC reaction will affect cell viability. Optical images after 24 h of cell seeding in **Figure 3A** revealed that BMSCs can adhere and spread on both TMV and TMV-RGD substrates. There were slightly more cells visualized on TMV-RGD compared to TMV coated surface. The numbers of adherent cells were calculated to elucidate the result in a quantitative manner (**Figure 3B**). As expected, the average cell numbers on TMV-RGD was higher than that of TMV. To verify that TMV-RGD does not have cytotoxicity from residual Cu^I, the proliferation of BMSCs on both virus scaffolds was examined over 22 days in osteogenic conditions (**Figure 3C**). The proliferation percentage of each sample was calculated based on the initial cell attachment as a 100%. BMSCs proliferated comparably well on both virus substrates, thus TMV-RGD did not exhibit any cytotoxicity to the *in vitro* cell culture.

The differentiation potential of BMSCs was studied in order to substantiate the effect of RGD incorporation on osteogenesis. First, osteo-specific gene expression levels were quantified by RT-qPCR (**Figure 4A**). The expression levels are presented as fold change compared to BMSCs at day 0. There was no significant difference in the gene expression levels of alkaline phosphatase (*ALPL*), osteonectin (*SPARC*), and osteopontin (*SPP1*) over the 3 weeks. Another osteo-specific gene examined is osteocalcin (*BGLAP*), the most common marker of mature osteoblast, as this protein is only synthesized by fully differentiated osteoblasts (Fujisawa and Tamura, 2012), which are eventually accumulated in mineralized bone matrix by binding specifically to hydroxyapatite crystals (Owen et al., 1990). It has been documented that *BGLAP*, which is normally peaked at day 21 on standard tissue culture plate substrate, is peaked at day 14 when BMSCs are grown on TMV scaffold suggesting that TMV substrates accelerate the bone differentiation process by 7 days (Kaur et al., 2010a). The gene expression analysis of BMSCs on unmodified TMV scaffolds in **Figure 4A** was in agreement with the previous report (Kaur et al., 2010a), where *BGLAP* gene expression level was peaked at day 14 indicating a complete mineralization of mature osteoblasts. As a comparison, the incorporation of RGD peptide into TMV subunits also significantly increased *BGLAP* gene expression level at day 14 (**Figure 4A**). The gene expression level of integrin-binding bone sialoprotein (*IBSP*), a secreted ECM protein required for hydroxyapatite formation as well as collagen binding in mineralized tissues (Ogata, 2008), was also evaluated. *IBSP* is synthesized just before calcification (Fujisawa and Tamura, 2012) and real time PCR results from the previous study indicated that BMSCs on TMV substrates had significantly higher *IBSP* mRNA expression within 24 h while there was no change in *IBSP* mRNA expression levels in BMSCs on TCPS control (Sitasuwan et al., 2012). In this experiment, *IBSP* expression levels in cells on both TMV and TMV-RGD were highly upregulated during the

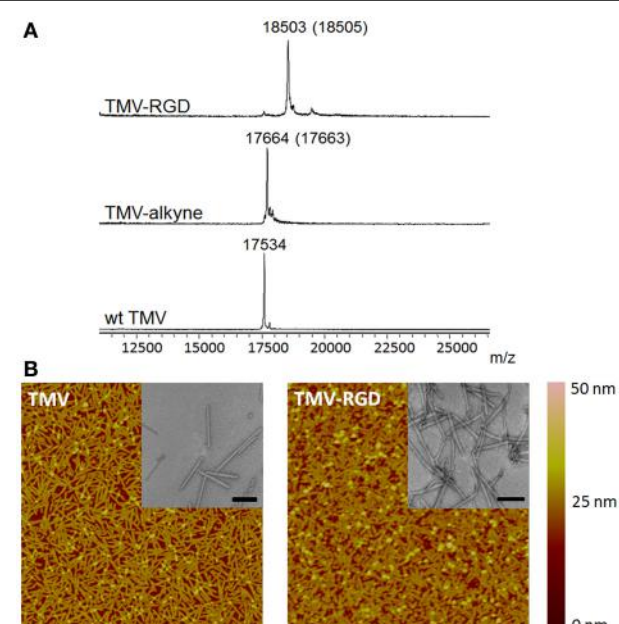


FIGURE 2 | Characterization of TMV particles. (A) MALDI-TOF MS spectra of the subunit protein of wild type TMV (17534 m/z), TMV-alkyne (17664 m/z), and the CuAAC reaction product TMV-RGD (18503 m/z). The numbers in parentheses refer to the theoretical masses. **(B)** The morphology of TMV particles before (TMV) and after (TMV-RGD) bioconjugation visualized by AFM and TEM (insets). Scan areas of AFM are 5 \times 5 μ m; and scale bars of TEM are 200 nm.

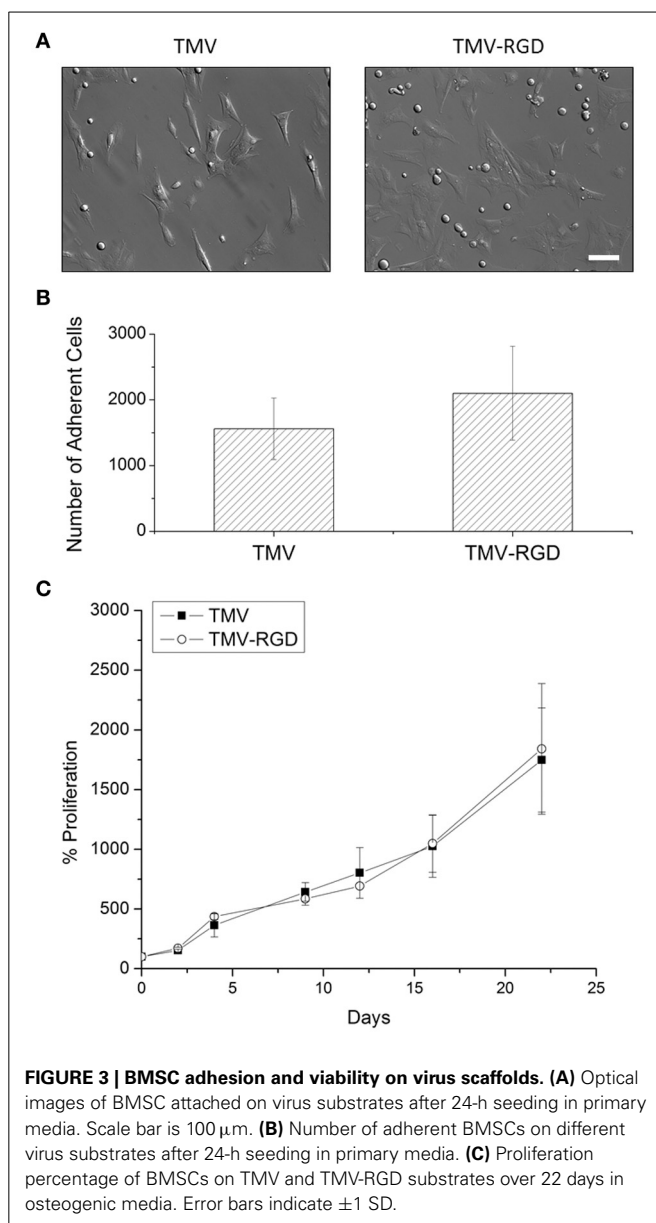


FIGURE 3 | BMSC adhesion and viability on virus scaffolds. **(A)** Optical images of BMSC attached on virus substrates after 24-h seeding in primary media. Scale bar is 100 μ m. **(B)** Number of adherent BMSCs on different virus substrates after 24-h seeding in primary media. **(C)** Proliferation percentage of BMSCs on TMV and TMV-RGD substrates over 22 days in osteogenic media. Error bars indicate ± 1 SD.

culture period (**Figure 4A**). However, BMSCs grown on TMV-RGD scaffolds expressed remarkably higher level of *IBSP* mRNA at day 21 when compared to those on native TMV scaffolds at the same time (**Figure 4A**).

In addition to the analysis of osteo-specific gene expressions, ALP activity was assessed. ALP is an early marker of osteogenesis and its activity mediates matrix mineralization. Although there was no difference in *ALPL* mRNA expressions at day 14 for cells grown on TMV compared to those on TMV-RGD as shown in **Figure 4A**, ALP enzyme activity assay showed a slight increase in BMSCs grown on TMV-RGD (**Figure 4B**). The staining for calcium deposition was also performed at day 14. A stronger staining was observed on TMV-RGD samples suggesting higher mineralization level (**Figure 4C**). This observation could be supported by previously mentioned increases in both *BGLAP* and *IBSP* mRNA expression levels (**Figure 4A**), possibly facilitating

the formation of hydroxyapatite crystals leading to mineralized matrix.

DISCUSSION

TMV has previously been shown to be an effective scaffold that accelerates bone differentiation of stem cells when coated on a 2D substrate and provides support for cell differentiation in 3D alginate hydrogels (Kaur et al., 2010a,b; Luckanagul et al., 2012; Sitasuwan et al., 2012). While the underlying mechanism is still unclear, the level of the potent osteogenic induction protein, bone morphogenetic protein 2 (BMP2), was significantly increased within 24 h for cells cultured on substrates with TMV coating compared to cells cultured on uncoated substrates or cells supplemented with TMV in suspension (Sitasuwan et al., 2012). One possible interpretation of this observation is that the topographical features created by TMV coating, compared to TMV in solution, plays a major role in the accelerated osteogenic differentiation.

Cells are capable of sensing the surrounding microenvironment, which provides both biochemical and biophysical cues, leading to downstream signaling cascades responsible for diverse cellular processes, such as adhesion, migration, proliferation, and apoptosis (Curtis and Wilkinson, 1997). For example, the nanoscale roughness of titanium surface implant can positively affect implant integration and bone differentiation (Lossdörfer et al., 2004; Mozumder et al., 2012; Olivares-Navarrete et al., 2012; Zhuang et al., 2012). In addition, the incorporation of growth factors (Crouzier et al., 2011; Wang et al., 2011; Kopf et al., 2012; Lee et al., 2013), adhesion ligands (Shin et al., 2005; Duggal et al., 2009; Qu et al., 2011), and osteoinductive compounds (Shu et al., 2003; Verma et al., 2010; Hao et al., 2011; Cameron et al., 2013) into biomaterial surface can further accelerate the bone formation process. Given the lack of affinity of native TMV viral particles to mammalian cell surface, which resulted in low initial cell adhesion (Sitasuwan et al., 2012), we hypothesized that combining the topological features offered by TMV with cellular adhesion molecules could synergistically enhance the bone formation process of stem cells.

In our previous study, we reported the genetic incorporation of RGD peptides on the coat protein of TMV particles and the resulting mutant virus could enhance the adhesion of BMSCs (Lee et al., 2012b) and accelerate the stem cell differentiation in serum free, chemically defined osteogenic media (Lee et al., 2012a). However, the genetic insertion suffers from the limited length and sequence diversity of the fusion peptides. To guarantee a successful assembly of final mutant TMV particles, TMV can only tolerate limited sequence diversity and length of the genetic peptide insertion. In this work, we demonstrate the feasibility of modulating mesenchymal stem cell differentiation on TMV-based scaffolds modified by CuAAC reaction. TMV was successfully modified with more than 95% conversion and the integrity of the virus particles was preserved. Scaffolds coated with TMV-RGD slightly improved initial BMSC adhesion, while maintaining the same cell proliferation rate with those coated with native TMV. The osteogenic differentiation of BMSCs was enhanced on TMV-RGD substrates since an increase in *BGLAP* and *IBSP* gene expression levels as well as mineralization level

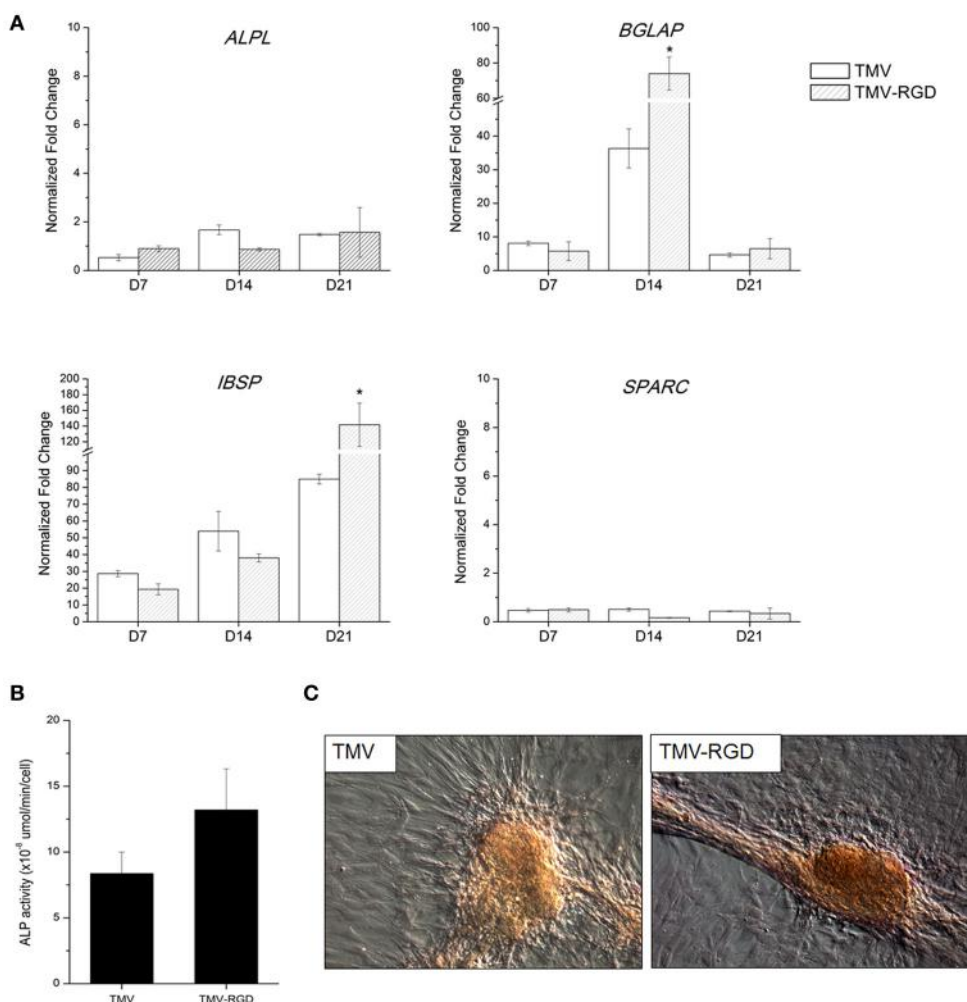


FIGURE 4 | Osteogenic differentiation of BMSCs on TMV and TMV-RGD substrates. **(A)** Osteo-specific gene expression profiles of BMSCs on TMV and TMV-RGD under osteogenic conditions over 21 days. For each sample, the profiles show 3 time points at 7, 14, and 21 days. BMSCs on TMV-RGD substrates have significantly higher *BGLAP* at day 14 and *IBSP* at day 21 when compared with unmodified TMV substrates. Error bars indicate ± 1 SD.

* $p < 0.05$. **(B)** Alkaline phosphatase activity of cells on TMV and TMV-RGD at day 14. BMSCs on TMV-RGD substrates have a slight increase in enzyme activity compared to cells on TMV. However, the difference is not statistically significant. **(C)** Optical images of Alizarin red S staining of cells cultured for 14 days on TMV or TMV-RGD substrate showing calcium deposition in red colour.

was observed, similar as TMV-RGD genetic mutant. However, the chemically tailored TMV particles have shown greater stability than TMV-RGD mutant particles.

It was expected that the displayed RGD peptides on TMV particles could lead to significantly greater cell attachment. However, it only facilitated a slight increase in the initial BMSC adhesion. A possible explanation is that TMV-RGD tends to aggregate leading to hindered ligand display. A precipitate was observed after the CuAAC reaction to functionalize TMV-alkyne with RGD peptide. Similarly, the rapid decomposition and aggregation of an icosahedral plant virus was previously observed when the virus is decorated with triazole with the presence of free copper ions in solution (Wang et al., 2003). Future studies will focus on controlling ligand density and using a variety of ligands including small molecules and other peptides on viral scaffold to study structure-property

relationship and modulate cell behavior. It is also important that a recent development of copper-free Click reaction (Lallana et al., 2011) may provide an alternative approach to chemically modify TMV without a concern about Cu^I contamination.

ACKNOWLEDGMENTS

This work was supported by the US NSF (CHE-0748690), the USC ASPIRE Award, the USC Science Undergraduate Research Fellowship Program (to Huong Giang Nguyen) and the Camille Dreyfus Teacher Scholar Award.

SUPPLEMENTARY MATERIAL

The Supplementary Material for this article can be found online at: <http://www.frontiersin.org/journal/10.3389/fchem.2014.00031/abstract>

Figure S1 | Primers used for RT-qPCR to measure gene expression levels.

ALPL, alkaline phosphatase; BGLAP, osteocalcin; IBSP, integrin-binding sialoprotein; SPARC, osteonectin; SPP1, osteopontin.

REFERENCES

- Anderson, J. M., Vines, J. B., Patterson, J. L., Chen, H., Javed, A., and Jun, H.-W. (2010). Osteogenic differentiation of human mesenchymal stem cells synergistically enhanced by biomimetic peptide amphiphiles combined with conditioned medium. *Acta Biomater.* 7, 675–682. doi: 10.1016/j.actbio.2010.08.016
- Bruckman, M. A., Kaur, G., Lee, L. A., Xie, F., Sepulveda, J., Breitenkamp, R., et al. (2008). Surface modification of tobacco mosaic virus with “Click” chemistry. *Chembiochem.* 9, 519–523. doi: 10.1002/cbic.200700559
- Cameron, K., Travers, P., Chander, C., Buckland, T., Campion, C., and Noble, B. (2013). Directed osteogenic differentiation of human mesenchymal stem/precursor cells on silicate substituted calcium phosphate. *J. Biomed. Mater. Res. A.* 101A, 13–22. doi: 10.1002/jbma.a.34261
- Cavalcanti-Adam, E. A., Micoulet, A., Blümmel, J., Auernheimer, J., Kessler, H., and Spatz, J. P. (2006). Lateral spacing of integrin ligands influences cell spreading and focal adhesion assembly. *Eur. J. Cell Biol.* 85, 219–224. doi: 10.1016/j.ejcb.2005.09.011
- Chung, W.-J., Merzlyak, A., Yoo, S. Y., and Lee, S.-W. (2010). Genetically engineered liquid-crystalline viral films for directing neural cell growth. *Langmuir* 26, 9885–9890. doi: 10.1021/la100226u
- Crouzier, T., Sailhan, F. D. R., Bequart, P., Guillot, R., Logeart-Avramoglou, D., and Picart, C. (2011). The performance of BMP-2 loaded TCP/HAP porous ceramics with a polyelectrolyte multilayer film coating. *Biomaterials* 32, 7543–7554. doi: 10.1016/j.biomaterials.2011.06.062
- Curtis, A., and Wilkinson, C. (1997). Topographical control of cells. *Biomaterials* 18, 1573–1583. doi: 10.1016/s0142-9612(97)00144-0
- Deeg, J. A., Louban, I., Aydin, D., Selhuber-Unkel, C., Kessler, H., and Spatz, J. P. (2011). Impact of local versus global ligand density on cellular adhesion. *Nano Lett.* 11, 1469–1476. doi: 10.1021/nl104079r
- Duggal, S., Fronsdal, K. B., Szoke, K., Shahdadfar, A., Melvik, J. E., and Brinchmann, J. E. (2009). Phenotype and gene expression of human mesenchymal stem cells in alginate scaffolds. *Tissue Eng. A.* 15, 1763–1773. doi: 10.1089/ten.tea.2008.0306
- Fujisawa, R., and Tamura, M. (2012). Acidic bone matrix proteins and their roles in calcification. *Front. Biosci.* 17, 1891–1903. doi: 10.2741/4026
- Hao, J., Kuroda, S., Ohya, K., Bartakova, S., Aoki, H., and Kasugai, S. (2011). Enhanced osteoblast and osteoclast responses to a thin film sputtered hydroxyapatite coating. *J. Mater. Sci. Mater. Med.* 22, 1489–1499. doi: 10.1007/s10856-011-4329-0
- Hovlid, M. L., Steinmetz, N. F., Laufer, B., Lau, J. L., Kuzelka, J., Wang, Q., et al. (2012). Guiding plant virus particles to integrin-displaying cells. *Nanoscale* 4, 3698–3705. doi: 10.1039/c2nr30571b
- Jiang, L., Li, Q., Li, M., Zhou, Z., Wu, L., Fan, J., et al. (2006). A modified TMV-based vector facilitates the expression of longer foreign epitopes in tobacco. *Vaccine* 24, 109–115. doi: 10.1016/j.vaccine.2005.09.060
- Kaur, G., Valarmathi, M. T., Potts, J. D., Jabbari, E., Sabo-Attwood, T., and Wang, Q. (2010a). Regulation of osteogenic differentiation of rat bone marrow stromal cells on 2D nanorod substrates. *Biomaterials* 31, 1732–1741. doi: 10.1016/j.biomaterials.2009.11.041
- Kaur, G., Wang, C., Sun, J., and Wang, Q. (2010b). The synergistic effects of multivalent ligand display and nanotopography on osteogenic differentiation of rat bone marrow stem cells. *Biomaterials* 31, 5813–5824. doi: 10.1016/j.biomaterials.2010.04.017
- Kopf, J., Petersen, A., Duda, G. N., and Knaus, P. (2012). BMP2 and mechanical loading cooperatively regulate immediate early signalling events in the BMP pathway. *BMC Biol.* 10:37. doi: 10.1186/1741-7007-10-37
- Lallana, E., Riguera, R., and Fernandez-Megia, E. (2011). Reliable and efficient procedures for the conjugation of biomolecules through huisgen azide-alkyne cycloadditions. *Angew. Chem. Int. Edn. Engl.* 50, 8794–8804. doi: 10.1002/anie.201101019
- Lee, L. A., Muhammad, S. M., Nguyen, Q. L., Sitasuwan, P., Horvath, G., and Wang, Q. (2012a). Multivalent ligand displayed on plant virus induces rapid onset of bone differentiation. *Mol. Pharm.* 9, 2121–2125. doi: 10.1021/mp300042t
- Lee, L. A., Nguyen, Q. L., Wu, L., Horvath, G., Nelson, R. S., and Wang, Q. (2012b). Mutant plant viruses with cell binding motifs provide differential adhesion strengths and morphologies. *Biomacromolecules* 13, 422–431. doi: 10.1021/bm2014558
- Lee, S. S., Huang, B. J., Kaltz, S. R., Sur, S., Newcomb, C. J., Stock, S. R., et al. (2013). Bone regeneration with low dose BMP-2 amplified by biomimetic supramolecular nanofibers within collagen scaffolds. *Biomaterials* 34, 452–459. doi: 10.1016/j.biomaterials.2012.10.005
- Le Saux, G., Magenau, A., Böcking, T., Gaus, K., and Gooding, J. J. (2011). The relative importance of topography and RGD ligand density for endothelial cell adhesion. *PLoS ONE* 6:e21869. doi: 10.1371/journal.pone.0021869
- Lossdörfer, S., Schwartz, Z., Wang, L., Lohmann, C. H., Turner, J. D., Wieland, M., et al. (2004). Microrough implant surface topographies increase osteogenesis by reducing osteoclast formation and activity. *J. Biomed. Mater. Res. A.* 70A, 361–369. doi: 10.1002/jbma.a.30025
- Lukanagul, J., Lee, L. A., Nguyen, Q. L., Sitasuwan, P., Yang, X., Shazly, T., et al. (2012). Porous alginate hydrogel functionalized with virus as three-dimensional scaffolds for bone differentiation. *Biomacromolecules* 13, 3949–3958. doi: 10.1021/bm301180c
- Maheshwari, G., Brown, G., Lauffenburger, D. A., Wells, A., and Griffith, L. G. (2000). Cell adhesion and motility depend on nanoscale RGD clustering. *J. Cell Sci.* 113, 1677–1686.
- Massia, S. P., and Hubbell, J. A. (1991). An RGD spacing of 440 nm is sufficient for integrin alpha V beta 3-mediated fibroblast spreading and 140 nm for focal contact and stress fiber formation. *J. Cell Biol.* 114, 1089–1100. doi: 10.1083/jcb.114.5.1089
- McCormick, A. A., Corbo, T. A., Wykoff-Clary, S., Nguyen, L. V., Smith, M. L., Palmer, K. E., et al. (2006). TMV-peptide fusion vaccines induce cell-mediated immune responses and tumor protection in two murine models. *Vaccine* 24, 6414–6423. doi: 10.1016/j.vaccine.2006.06.003
- Merzlyak, A., Indrakanti, S., and Lee, S.-W. (2009). Genetically engineered nanofiber-like viruses for tissue regenerating materials. *Nano Lett.* 9, 846–852. doi: 10.1021/nl8036728
- Mozumder, M. S., Zhu, J., and Perinpanayagam, H. (2012). Titania-polymeric powder coatings with nano-topography support enhanced human mesenchymal cell responses. *J. Biomed. Mater. Res. A.* 100A, 2695–2709. doi: 10.1002/jbma.a.34199
- Ogata, Y. (2008). Bone sialoprotein and its transcriptional regulatory mechanism. *J. Periodont. Res.* 43, 127–135. doi: 10.1111/j.1600-0765.2007.01014.x
- Olivares-Navarrete, R., Gittens, R. A., Schneider, J. M., Hyzy, S. L., Haithcock, D. A., Ullrich, P. F., et al. (2012). Osteoblasts exhibit a more differentiated phenotype and increased bone morphogenetic protein production on titanium alloy substrates than on poly-ether-ether-ketone. *Spine J.* 12, 265–272. doi: 10.1016/j.spinee.2012.02.002
- Owen, T. A., Aronow, M., Shalhoub, V., Barone, L. M., Wilming, L., Tassinari, M. S., et al. (1990). Progressive development of the rat osteoblast phenotype *in vitro*: Reciprocal relationships in expression of genes associated with osteoblast proliferation and differentiation during formation of the bone extracellular matrix. *J. Cell. Physiol.* 143, 420–430. doi: 10.1002/jcp.1041430304
- Peng, R., Yao, X., and Ding, J. (2011). Effect of cell anisotropy on differentiation of stem cells on micropatterned surfaces through the controlled single cell adhesion. *Biomaterials* 32, 8048–8057. doi: 10.1016/j.biomaterials.2011.07.035
- Qu, Z., Yan, J., Li, B., Zhuang, J., and Huang, Y. (2011). Improving bone marrow stromal cell attachment on chitosan/hydroxyapatite scaffolds by an immobilized RGD peptide. *Biomed. Mater.* 5:065001. doi: 10.1088/1748-6041/5/6/065001
- Rong, J., Lee, L. A., Li, K., Harp, B., Mello, C. M., Niu, Z., et al. (2008). Oriented cell growth on self-assembled bacteriophage M13 thin films. *Chem. Commun. (Camb.)* 5185–5187. doi: 10.1039/b811039e
- Ruoslahti, E., and Pierschbacher, M. D. (1987). New perspectives in cell adhesion: RGD and integrins. *Science* 238, 491–497.
- Schlück, T. L., Ding, Z., Kovacs, E. W., and Francis, M. B. (2005). Dual-surface modification of the tobacco mosaic virus. *J. Am. Chem. Soc.* 127, 3718–3723. doi: 10.1021/ja046239n
- Shin, H., Temenoff, J. S., Bowden, G. C., Zygourakis, K., Farach-Carson, M. C., Yaszemski, M. J., et al. (2005). Osteogenic differentiation of rat bone marrow stromal cells cultured on Arg-Gly-Asp modified hydrogels without dexamethasone and β-glycerol phosphate. *Biomaterials* 26, 3645–3654. doi: 10.1016/j.biomaterials.2004.09.050
- Shin, H., Zygourakis, K., Farach-Carson, M. C., Yaszemski, M. J., and Mikos, A. G. (2004). Modulation of differentiation and mineralization of marrow stromal cells cultured on biomimetic hydrogels modified with Arg-Gly-Asp containing peptides. *J. Biomed. Mater. Res. A.* 69A, 535–543. doi: 10.1002/jbma.a.30027

- Shu, R., McMullen, R., Baumann, M. J., and McCabe, L. R. (2003). Hydroxyapatite accelerates differentiation and suppresses growth of MC3T3-E1 osteoblasts. *J. Biomed. Mater. Res. A.* 67A, 1196–1204. doi: 10.1002/jbm.A.20021
- Sitasuwan, P., Andrew Lee, L., Bo, P., Davis, E. N., Lin, Y., and Wang, Q. (2012). A plant virus substrate induces early upregulation of BMP2 for rapid bone formation. *Integr. Biol.* 4, 651–660. doi: 10.1039/c2ib20041d
- Souza, G. R., Christianson, D. R., Staquicini, F. I., Ozawa, M. G., Snyder, E. Y., Sidman, R. L., et al. (2006). Networks of gold nanoparticles and bacteriophage as biological sensors and cell-targeting agents. *Proc. Natl. Acad. Sci. U.S.A.* 103, 1215–1220. doi: 10.1073/pnas.0509739103
- Verma, D., Katti, K. S., and Katti, D. R. (2010). Osteoblast adhesion, proliferation and growth on polyelectrolyte complex-hydroxyapatite nanocomposites. *Philos. Trans. A Math. Phys. Eng. Sci.* 368, 2083–2097. doi: 10.1098/rsta.2010.0013
- Wang, J., Wang, L., Li, X., and Mao, C. (2013a). Virus activated artificial ECM induces the osteoblastic differentiation of mesenchymal stem cells without osteogenic supplements. *Sci. Rep.* 3:1242. doi: 10.1038/srep01242
- Wang, Q., Chan, T. R., Hilgraf, R., Fokin, V. V., Sharpless, K. B., and Finn, M. G. (2003). Bioconjugation by copper(I)-catalyzed azide-alkyne [3 + 2] cycloaddition. *J. Am. Chem. Soc.* 125, 3192–3193. doi: 10.1021/ja021381e
- Wang, X., Oyane, A., Tsurushima, H., Sogo, Y., Li, X., and Ito, A. (2011). BMP-2 and ALP gene expression induced by a BMP-2 gene-fibronectin-apatite composite layer. *Biomed. Mater.* 6:045004. doi: 10.1088/1748-6041/6/4/045004
- Wang, X., Yan, C., Ye, K., He, Y., Li, Z., and Ding, J. (2013b). Effect of RGD nanospacing on differentiation of stem cells. *Biomaterials* 34, 2865–2874. doi: 10.1016/j.biomaterials.2013.01.021
- Zan, X., Sitasuwan, P., Powell, J., Dreher, T. W., and Wang, Q. (2012). Polyvalent display of RGD motifs on turnip yellow mosaic virus for enhanced stem cell adhesion and spreading. *Acta. Biomater.* 8, 2978–2985. doi: 10.1016/j.actbio.2012.04.027
- Zeng, Q., Saha, S., Lee, L. A., Barnhill, H., Oxsher, J., Dreher, T., et al. (2011). Chemosselective modification of turnip yellow mosaic virus by Cu(I) Catalyzed azide-alkyne 1,3-dipolar cycloaddition reaction and its application in cell binding. *Bioconjug. Chem.* 22, 58–66. doi: 10.1021/bc100351n
- Zhuang, L. F., Jiang, H. H., Qiao, S. C., Appert, C., Si, M. S., Gu, Y. X., et al. (2012). The roles of extracellular signal-regulated kinase 1/2 pathway in regulating osteogenic differentiation of murine preosteoblasts MC3T3-E1 cells on roughened titanium surfaces. *J. Biomed. Mater. Res. A.* 100A, 125–133. doi: 10.1002/jbm.a.33247

Conflict of Interest Statement: The authors declare that the research was conducted in the absence of any commercial or financial relationships that could be construed as a potential conflict of interest.

Received: 24 January 2014; accepted: 07 May 2014; published online: 27 May 2014.

Citation: Sitasuwan P, Lee LA, Li K, Nguyen HG and Wang Q (2014) RGD-conjugated rod-like viral nanoparticles on 2D scaffold improve bone differentiation of mesenchymal stem cells. *Front. Chem.* 2:31. doi: 10.3389/fchem.2014.00031

This article was submitted to Chemical Biology, a section of the journal *Frontiers in Chemistry*.

Copyright © 2014 Sitasuwan, Lee, Li, Nguyen and Wang. This is an open-access article distributed under the terms of the Creative Commons Attribution License (CC BY). The use, distribution or reproduction in other forums is permitted, provided the original author(s) or licensor are credited and that the original publication in this journal is cited, in accordance with accepted academic practice. No use, distribution or reproduction is permitted which does not comply with these terms.



Covalent modification of a ten-residue cationic antimicrobial peptide with levofloxacin

Carlos A. Rodriguez, Emilius A. Papanastasiou, Melanie Juba and Barney Bishop *

Department of Chemistry and Biochemistry, George Mason University, Fairfax, VA, USA

Edited by:

Carissa M. Soto, Naval Research Laboratory, USA

Reviewed by:

Paola Laurienzo, Italian Research Council (CNR), Italy

Huiwang Ai, University of California, Riverside, USA

***Correspondence:**

Barney Bishop, Department of Chemistry and Biochemistry, George Mason University, 4400 University Drive, 3E2, Fairfax, VA 22030, USA

e-mail: bbishop1@gmu.edu

The rampant spread of antibiotic resistant bacteria has spurred interest in alternative strategies for developing next-generation antibacterial therapies. As such, there has been growing interest in cationic antimicrobial peptides (CAMPs) and their therapeutic applications. Modification of CAMPs via conjugation to auxiliary compounds, including small molecule drugs, is a new approach to developing effective, broad-spectrum antibacterial agents with novel physicochemical properties and versatile antibacterial mechanisms. Here, we've explored design parameters for engineering CAMPs conjugated to small molecules with favorable physicochemical and antibacterial properties by covalently affixing a fluoroquinolone antibiotic, levofloxacin, to the ten-residue CAMP Pep-4. Relative to the unmodified Pep-4, the conjugate was found to demonstrate substantially increased antibacterial potency under high salt concentrations. Historically, it has been observed that most CAMPs lose antibacterial effectiveness in such high ionic strength environments, a fact that has presented a challenge to their development as therapeutics. Physicochemical studies revealed that P4LC was more hydrophobic than Pep-4, while mechanistic findings indicated that the conjugate was more effective at disrupting bacterial membrane integrity. Although the inherent antibacterial effect of the incorporated levofloxacin molecules did not appear to be substantially realized in this conjugate, these findings nevertheless suggest that covalent attachment of small molecule antibiotics with favorable physicochemical properties to CAMPs could be a promising strategy for enhancing peptide performance and overall therapeutic potential. These results have broader applicability to the development of future CAMP-antibiotic conjugates for potential therapeutic applications.

Keywords: cationic antimicrobial peptide, peptide conjugate, antibiotics, peptide modification, levofloxacin

INTRODUCTION

The emergence and spread of bacterial resistance to conventional antibiotics has resulted in interest in cationic antimicrobial peptides (CAMPs) as a potential therapeutic alternative (Gordon et al., 2005; Seo et al., 2012). These peptides demonstrate broad-spectrum antimicrobial activity and are essential elements of innate immunity in higher organisms. Yet, despite their extensive use in nature, bacteria have failed to develop wide-spread resistance to CAMPs, which has not been the case for conventional antibiotics (Zasloff, 2002). While CAMPs demonstrate extensive sequence and structural diversity, they are generally rich in cationic amino acids and adopt amphipathic structures that result in spatial partitioning of basic and hydrophobic residues. These peptides are thought to exert their antibacterial effect *via* mechanisms that at some level involve the targeting of anionic bacterial membranes through non-specific electrostatic and hydrophobic interactions. Many CAMPs are thought to also bind bacterial receptors and enzymes, or otherwise interfere with essential cellular processes (Epand and Vogel, 1999; Brogden, 2005; Jenssen et al., 2006).

While CAMPs represent a promising class of prospective therapeutics, their development as viable treatments has proven

challenging, with one major factor being that the effectiveness of many CAMPs are diminished or even abolished under salt concentrations consistent with physiologically relevant environments (Park et al., 2004; Yu et al., 2011; Chu et al., 2013). Researchers have investigated various strategies, including conjugation to auxiliary compounds, in order to enhance CAMP antibacterial performance and potential therapeutic utility (Arnusch et al., 2012; Devocelle, 2012). Conjugation is an appealing strategy because it provides a means for introducing new functionalities and directly enhancing CAMP antibacterial activity. For example, CAMPs have been conjugated to fatty acids (Li et al., 2013), sugars (Pal et al., 2011), pheromones, antibodies, synthetic polymers, and small molecule drugs to yield peptide constructs with improved antibacterial activity relative to their respective unmodified parent peptide variants (Devocelle, 2012). However, while conjugation can improve the performance of CAMPs, it has also been shown in some instances to abrogate antibacterial effectiveness (Chu-Kung et al., 2004; Radzishevsky et al., 2005). Therefore, the effect that conjugation may have on CAMP structure and physicochemical properties (e.g., charge, hydrophathy, and sterics, etc.) must be considered when engineering constructs. Conjugation of CAMPs to small molecules with favorable physicochemical

properties (such as hydrophobic and/or cationic functionalities) would provide a highly controlled means for augmenting peptide antibacterial performance. The incorporation of small molecule antibiotics in CAMP-based conjugates presents a particularly intriguing strategy, as these compounds could influence peptide effectiveness not only *via* alteration of physicochemical properties, but also through their intrinsic antibacterial activities. In this regard, fluoroquinolone antibiotics, which present both hydrophobic (e.g., aromatic and aliphatic moieties) and cationic functionalities, represent attractive candidates. Additionally, from a synthetic perspective, the carboxylate moieties that fluoroquinolones contain lend themselves to ready conjugation with CAMP primary amino groups.

In our previous studies, we found that Pep-4, a highly cationic peptide with a sequence (RGRRSSRRKK-NH₂) based on the C-terminal portion of human beta defensin-3 (hBD-3), retained significant antibacterial activity following acetylation of its N-terminal and side chain amino groups, despite the associated reduction in charge from +8 to +5 (Papanastasiou et al., 2009). These results suggest that this peptide is amenable to chemical modification and may be a good candidate for incorporation in CAMP-conjugates. Additionally, the sequence of Pep-4 provides a limited number of reactive functionalities, allowing convenient chemical modification with small molecules while reducing the potential for deleterious side reactions and byproducts. These qualities also facilitate isolation and characterization. Moreover, the small size of Pep-4 makes it especially appealing for use in CAMP-conjugates, as it lends itself to cost effective synthesis (Seo et al., 2012).

In order to explore design parameters for engineering antibacterial CAMP-conjugates and the incorporation of small molecules, such as antibiotics, we have synthesized a CAMP-conjugate consisting of a fluoroquinolone, levofloxacin (LVFX), covalently attached to the scaffold peptide Pep-4 *via* the primary amino groups present in the peptide. These studies have focused on evaluating the antibacterial performance of the Pep-4-LVFX Conjugate, P4LC, against the model gram-negative bacterium *E. coli* and gram-positive bacterium *B. cereus*. Our studies reveal that incorporation of LVFX significantly enhances the effectiveness of the conjugate under physiologically relevant environmental salt concentrations relative to the unmodified scaffold peptide Pep-4. These findings suggest that conjugation of CAMPs to auxiliary compounds, such as small molecule antibiotics with favorable physicochemical properties, to generate hybrid constructs could be a promising strategy for enhancing peptide therapeutic potential.

MATERIALS AND METHODS

Levofloxacin (LVFX), N-methylmorpholine (NMM) and resazurin were purchased from Sigma-Aldrich, Co. LLC (St. Louis, MO, USA). Bicinchoninic acid (BCA) and SYTOX Green were purchased from ThermoFisher Scientific, Inc. (Waltham, MA, USA). Fluoro-N,N,N',N'-tetramethylformamidinium hexafluorophosphate (TFFH) was purchased from EMD Millipore (a division of Merck KGaA; Darmstadt, Germany), Fmoc-Gly-Wang resin from Peptides International, Inc. (Louisville, KY, USA), and DiSC(3)5 from Anaspec, Inc. (Fremont, CA, USA). Deionized

water (dH₂O) was prepared using a Milli-Q Synthesis A10 system (Millipore). The bacterial strains *E. coli* (#25922) and *B. cereus* (#11778) were purchased from American Type Culture Collection (ATCC, Manassas, VA, USA). Pep-4 ($\geq 95\%$ purity) was custom synthesized by Genscript USA, Inc. (Piscataway, NJ, USA). Melittin ($\geq 95\%$) was purchased from Anaspec, Inc., and indolicidin was synthesized ($\geq 95\%$ purity) by AAPPTec, LLC (Louisville, KY, USA). Peptide identities were verified *via* matrix assisted laser desorption ionization time-of-flight (MALDI-TOF) mass spectrometry using a Shimadzu AXIMA Performance. Additionally, Pep-4 and the conjugate were submitted for amino acid analysis (UC Davis Genome Center Proteomics Core Facility) in order to establish molar concentrations.

P4LC SYNTHESIS AND PURIFICATION

The carboxyl group of LVFX allowed for conjugation to Pep-4 *via* direct acylation of the peptide's N-terminal and lysine side chain amino groups. LVFX was preactivated by converting its carboxyl moiety into an acyl fluoride in order to facilitate nucleophilic attack by peptide amino groups. Equimolar amounts of LVFX (6.7 mg, 18.6 mmol) and TFFH (4.90 mg, 18.6 mmol) were dissolved in 500 μ L of anhydrous DMF, and 20 μ L of NMM was then added to the solution. This reaction was allowed to stir at room temperature (rt), under N₂ in the dark. After 1 h, Pep-4 (2.4 mg, 1.86 mmol) dissolved in 200 μ L of anhydrous DMF was added to the reaction and allowed to continue stirring at rt, under N₂ in the dark. While the coupling reaction was stirring, Fmoc-Glycine-Wang resin (200 mg, 0.63 mmol/g amine loading) was suspended in 8 mL of DMF with agitation for 30 min to swell the resin, and the solvent was then removed *via* vacuum filtration. The suspension and filtration process was repeated. The swelled resin was then suspended in 8 mL of 50% piperidine in DMF for 30 min in order to remove the Fmoc protecting group. The reaction mixture was vacuum filtered and the resin resuspended in 8 mL of DMF and agitated for 15 min. The resin suspension was then vacuum filtered, and the deprotected particles were transferred to the reaction vessel. Following addition of the resin, the reaction was left stirring in the dark under N₂, overnight. Thereafter, the contents of the reaction vessel were filtered through a course frit directly into cold diethyl ether, and the resulting suspension was centrifuged so as to pellet the precipitated material. The pelleted precipitate was then dried under vacuum in order to remove residual ether. Crude conjugate was subsequently dissolved in 10 mL of 10 mM NaCl and dialyzed (0.5–1 kD M_w cutoff) in 10 mL 10 mM NaCl against 2 L dH₂O, which was replaced every 8 h (3x). The dialyzed solution was then lyophilized to yield 3.1 mg of purified P4LC ($\sim 87\%$ yield).

MASS SPECTROMETRY

Samples dissolved in dH₂O (1 pmol/ μ L) were mixed with α -cyano-4-hydroxycinnamic acid (CHCA) matrix solution (10 mg/ml in 50:50 water/acetonitrile with 0.1% TFA) and deposited onto a stainless steel target plate (Shimadzu Kratos Analytical) in 1 μ L aliquots. Mass spectra were collected using a Shimadzu AXIMA Performance MALDI-TOF mass spectrometer equipped with a 337 nm N₂ laser in reflectron mode and represent the average of at least 50 accumulated profiles. The

laser repetition rate was set to 50 Hz, and laser power was set to between 50 and 70%. The instrument was externally calibrated using angiotensin II, angiotensin I, and Adrenocorticotropin hormone (fragment 18–39). Lower molecular weight regions of spectra were assessed with the ion gate turned off, and control spectra were generated for matrix alone. CHCA peaks were used for internal calibration of the lower molecular weight regions of sample spectra. Matrix m/z values were verified using MassBank Mass Spectral Database (Accession: MCH00005).

ANTIBACTERIAL PERFORMANCE ASSAYS

The antibacterial activities of P4LC, Pep-4, LVFX, and free Pep-4 in combination with free LVFX (Pep-4/LVFX) were determined in a microplate-based assay using resazurin as an indicator for cell viability. Metabolically active cells convert resazurin, which is not fluorescent, to the highly fluorescent resorufin (530/590 nm_{em}), and the rate of this conversion provides a means for quantifying the concentration of viable bacteria (Shiloh et al., 1997; Lemos and Carareto-Alves, 1998; Okuda et al., 2006; Mariscal et al., 2009). In order to assess the effect environmental ionic strength had on antibacterial effectiveness, assays were conducted in buffers with the following ionic strengths: 26 mM, 111 mM, and 167 mM.

Frozen enumerated aliquots of bacteria were thawed and diluted into sterile buffer to a bacterial concentration of 2×10^6 CFU/mL. Wells of a 96-well polypropylene microtiter plate (Greiner Bio-One) were charged with 50 μL aliquots of buffer solutions containing serially diluted peptide, conjugate, or drug followed by 50 μL aliquots of diluted bacterial cells. Assays for each compound were prepared in triplicate. Control wells were prepared where the peptide/conjugate/drug solution was replaced with an equal volume of buffer alone. Following addition of bacteria, the microtiter plates were incubated for 3 h at either 37°C (*E. coli*) or 30°C (*B. cereus*). Aliquots of PBS solution (100 μL) containing resazurin and MHB were then added to each well to afford final concentrations of 100 μM resazurin and 0.2% MHB (wt/vol) for *E. coli* and 12.5 μM resazurin and 0.05% MHB (wt/vol) for *B. cereus*. Plates were then immediately placed in a SpectraMax Gemini EM plate-reading fluorometer for overnight monitoring of fluorescence (530 nm_{ex}/590 nm_{em}) at either 37°C (*E. coli*) or 30°C (*B. cereus*) with intermittent shaking. Onset

time of half maximal fluorescence ($T_{0.5}$) observed for each well was computed using the microplate data analysis software. In order to determine bacterial survival, it was necessary to establish correlations between bacterial concentration (CFU/mL) and $T_{0.5}$ values. Therefore, standard curve equations were generated in preliminary experiments using bacterial suspensions serially diluted ($\sim 10^6$ CFU/mL– 10^3 CFU/mL) in each of the three buffers used in the antibacterial assays. Plotting initial bacterial concentrations (determined via dilution plating onto MHB Agar plates) against observed $T_{0.5}$ values afforded equations 1 (*E. coli*) and 2 (*B. cereus*), which were used to interpolate viable bacterial concentration (CFU/mL) following incubation with peptide, conjugate or drug. The Y-intercept (Y_{int}) values for equations generated for the varied ionic strength buffer conditions were 9.41 (26 mM), 9.19 (111 mM), and 9.24 (167 mM) for *E. coli*, and 5.91 (26 mM), 6.20 (111 mM), and 6.36 (167 mM) for *B. cereus*.

$$\log(\text{CFU/mL}_{E.\text{coli}}) = -2.00 \times 10^{-4}(T_{0.5}) + Y_{\text{int}} \quad (1)$$

$$\log(\text{CFU/mL}_{B.\text{cereus}}) = -1.00 \times 10^{-4}(T_{0.5}) + Y_{\text{int}} \quad (2)$$

Antibacterial effectiveness against each microbe was determined by plotting bacterial survival as a function of the log of the concentration of P4LC, Pep-4, LVFX, or Pep-4/LVFX, and fitting the resulting data to a variable-slope sigmoidal regression model (equation 3) using Graphpad Prism 5 (GraphPad Software, Inc.). In this equation, $\log(\text{EC}_{50})$ represents the log of the concentration of P4LC, Pep-4, LVFX, or Pep-4/LVFX required to kill half of the bacterial population, where S_{min} and S_{max} correspond to the minimal and maximal bacterial survival values (respectively), and HS is the parameter defining the steepness of the transition slopes of sigmoidal survival curves.

$$\text{Bacterial Survival} = S_{\text{min}} + (S_{\text{max}} - S_{\text{min}}) / (1 + 10^{\log(\text{EC}_{50}) - \log(\text{PC}) * \text{HS}}) \quad (3)$$

Best-fit $\log(\text{EC}_{50})$ values generated for each compound were used to compare the antibacterial effectiveness of P4LC, Pep-4, LVFX, and Pep-4/LVFX against each bacterium. Antilogs of the $\log(\text{EC}_{50})$ values, the EC_{50} values, are tabulated in Table 1 along with their respective 95% confidence intervals.

Table 1 | Antibacterial effectiveness.

	P4LC	Pep-4	Pep-4/LVFX	LVFX
<i>E. COLI</i>				
μ_1	0.0167 (0.0132–0.0230)	0.0168 (0.0123–0.0234)	0.00375 (0.00314–0.00447)	0.00281 (0.00228–0.00344)
μ_2	1.71 (1.60–1.81)	28.3 (17.2–46.7)	0.00487 (0.00387–0.00617)	0.00223 (0.00164–0.00303)
μ_3	1.51 (1.41–1.82)	29.4* (21.9–35.4)*	0.00404 (0.00294–0.00556)	0.00277 (0.00200–0.00385)
<i>B. CEREUS</i>				
μ_1	0.0218 (0.0156–0.0287)	0.0271 (0.0217–0.0343)	0.112 (0.0794–0.165)	0.212 (0.104–0.450)
μ_2	2.17 (2.01–2.25)	178*(142–223)*	0.941 (0.645–1.27)	0.591 (0.381–0.918)
μ_3	40.0 (27.3–72.0)	404* (155–462)*	1.37 (0.801–2.32)	0.981 (0.57–1.67)

Antibacterial potencies for P4LC, Pep-4, Pep-4/LVFX and LVFX expressed in terms of EC_{50} values (μM) and corresponding 95% confidence interval ranges. Ionic strengths of assay media correspond to: $\mu_1 = 26$ mM, $\mu_2 = 111$ mM, and $\mu_3 = 167$ mM.

*Estimated values are given for Pep-4 under conditions where it failed to achieve sufficient killing (within the tested peptide concentration range) to define the lower survival boundary for fitting to Equation 3.

DiSC(3)5 MEMBRANE DEPOLARIZATION ASSAY

Enumerated frozen aliquots of *E. coli* and *B. cereus* cells were thawed and washed 3x with buffer (10 mM NaPO₄, pH 7.4). The washed cells were diluted in 10 mM NaPO₄ buffer containing 10 µg/mL DiSC(3)5 to afford a concentration of 4 × 10⁷ CFU/mL. Bacterial suspension was added to the wells of a black polypropylene microtiter plate (Greiner Bio-One) in 100 µL aliquots, and fluorescence was monitored (rt, with lid on) using a SpectraMax Gemini EM plate-reading fluorometer (622 nm_{ex} / 670 nm_{em}) until fluorescence quenching stabilized and maximal DiSC(3)5 uptake was achieved. Aliquots (100 µL) of P4LC, Pep-4, LVFX, or Pep-4/LVFX were added to the bacteria and changes in fluorescence were monitored for 30 min with the lid off. The final concentrations of each assessed compound in the wells were 33 µM (P4LC and Pep-4), 126 µM (Pep-4/LVFX), and 93 µM (LVFX), while final bacterial concentrations were 2 × 10⁷ CFU/mL. Assays were performed in triplicate for each compound assessed. Depolarization assays based on DiSC(3)5 are extremely time-sensitive; therefore, triplicate sets for each compound were prepared simultaneously using a multichannel pipettor. Prior experiments verified that each tested compound was able to exert full killing under the assay conditions. A negative control containing only bacteria and DiSC(3)5 was used to establish background fluorescence, while maximal membrane depolarization was established using melittin (33 µM), a known pore-forming CAMP (Lee et al., 2013b); these controls provided references for establishing relative effectiveness of P4LC, Pep-4, LVFX, and Pep-4/LVFX. The fluorescence kinetics data sets were normalized by setting emitted fluorescence to 0 at *t* = 0 s and presenting fluorescence intensity values as a fraction of maximal fluorescence observed for melittin.

SYTOX GREEN MEMBRANE PERTURBATION ASSAY

Enumerated frozen aliquots of *E. coli* and *B. cereus* cells were thawed and washed 3x with buffer (10 mM NaPO₄, pH 7.4). The washed cells were diluted to a concentration of 4 × 10⁷ CFU/mL in 10 mM NaPO₄ (pH 7.4) buffer containing 5 µM SYTOX Green, and the resulting suspension then stored in the dark for ~20 min. The bacterial suspension was then distributed in 100 µL aliquots to wells of a black polypropylene microtiter plate (Greiner Bio-One). Aliquots (100 µL) of buffer containing P4LC, Pep-4, LVFX, or Pep-4/LVFX were then added to wells containing cell suspension and gently mixed. The fluorescence of each well was immediately monitored (without the lid) using a SpectraMax Gemini EM plate-reading fluorometer (485/520 nm_{em}). As SYTOX Green assays can be time-sensitive, assays were prepared in triplicate using a multichannel pipettor. The reported SYTOX Green data reflects observations from biological triplicates. Antibacterial assays confirmed that each compound was able to exert full killing under these conditions and at the concentrations used in the DiSC(3)5 assay (33 µM P4LC, 33 µM Pep-4, 126 µM Pep-4/LVFX, and 93 µM LVFX). A negative control containing only bacteria and SYTOX Green was used to determine background fluorescence, and maximal perturbation of the bacterial cell membranes was established using melittin. The fluorescence

kinetics data sets were normalized by setting emitted fluorescence to 0 at *t* = 0 s and presenting fluorescence intensity values as a fraction of maximal fluorescence observed for melittin.

STATISTICAL ANALYSIS

An F test was used for determining whether log (EC₅₀) values generated for the assessed compounds were significantly different from each other (computed using GraphPad Prism). For membrane depolarization and perturbation experiments, fluorescence data was analyzed by comparing best-fit curves (GraphPad Prism). Fluorescence kinetic curves were fit to a polynomial regression model (equation 4) to allow for statistical comparison of the fluorescence data via an F test, with all four best-fit parameters used as criteria.

$$\text{RFU} = A_0 + A_1(t) + A_2(t)^2 + A_3(t)^3 + A_4(t)^4 \quad (4)$$

DISTRIBUTION COEFFICIENT

The relative hydrophobicities of P4LC, Pep-4, and LVFX were established using a biphasic system consisting of immiscible 1-octanol and 10 mM NaPO₄ (pH 7.4) to determine their respective distribution coefficients (D_{7.4}), with D_{7.4} corresponding to the concentration ratio of each compound between the octanol and aqueous phases (Brillault et al., 2010; Cheng et al., 2012; Chyan et al., 2014). In these experiments, P4LC, Pep-4 or free LVFX dissolved in 100 µL of 10 mM NaPO₄ (pH 7.4) buffer was combined with 100 µL of 1-Octanol in a 1.5 mL low binding polypropylene microcentrifuge tube (Corning). Each tube was vortexed for 10 min and the contained solvent allowed to settle. Once the aqueous and octanol layers had reestablished and fully separated, 25 µL aliquots were removed from the aqueous phase using a micropipette, and the peptide or conjugate concentration determined using an absorbance-based BCA kit (Wrolstad et al., 2004). Aqueous phase Pep-4 and P4LC concentrations were determined via interpolation based on standard curves that had been generated using two-fold serially diluted peptide or conjugate dissolved in 10 mM NaPO₄ (pH 7.4). The maximal concentrations of Pep-4 and P4LC in the calibration curves were also established using amino acid analysis (UC Davis Genome Center Proteomics Core Facility). The results from amino acid analysis were in agreement with those obtained using the BCA kit. The concentration of LVFX in the aqueous layer was interpolated from calibration curves established using absorbance at 298 nm (LVFX absorbs strongly at this wavelength). Indolicidin and melittin were used as reference peptides in these studies. The sequence of indolicidin suggests that it is highly hydrophobic, while that of melittin indicates that it should be moderately hydrophobic. Computational verification of the hydrophobicity of these reference peptides was performed using the Hopp and Woods scale (Hopp and Woods, 1981). The D_{7.4} values generated for P4LC, Pep-4, LVFX, indolicidin, and melittin were calculated (equation 5) based on their respective concentrations in the aqueous phase ([peptide]_{PO4buffer}) of the water/octanol biphasic system and their concentrations in the initial stock solution ([peptide]_{total}). Values

are averaged from six replicates.

$$\log D_{7.4} = \log \left(\frac{([\text{peptide}]_{\text{total}} - [\text{peptide}]_{\text{PO4buffer}})}{[\text{peptide}]_{\text{PO4buffer}}} \right) \\ = \log \left(\frac{[\text{peptide}]_{\text{octanol}}}{[\text{peptide}]_{\text{PO4buffer}}} \right) \quad (5)$$

RESULTS

SYNTHESIS AND PURIFICATION OF Pep-4-LVFX CONJUGATE

The carboxyl moiety of LVFX allowed for conjugation to Pep-4 via direct acylation of N-terminal and lysine side chain amino groups on the peptide (Figure 1). LVFX was preactivated with TFFH to convert the carboxyl moiety to an acyl fluoride prior to introduction of Pep-4. Excess activated LVFX was captured using a glycine-Wang resin. The resulting particle suspension was filtered through a medium glass frit into cold ether in order to remove the resin and precipitate the desired conjugate. The precipitated product

was dissolved in 10 mM NaCl and dialyzed against deionized water to remove water soluble, low molecular weight impurities and byproducts. This approach was employed because removal of intermediates and byproducts by chromatography and extraction proved challenging and resulted in significant loss of product. The isolated material was analyzed by MALDI-TOF mass spectrometry (Figure 2), which indicated the degree of drug loading to be 3:1 LVFX/peptide, with no free peptide detected. Moreover, no intermediate conjugate species were observed. Lower molecular weight regions of spectra from conjugate spectra were compared to the corresponding regions in reference spectra collected for free LVFX and matrix alone (Figure 3) in order to verify the absence of free drug and other low molecular weight impurities.

ANTIBACTERIAL EFFECTIVENESS

The antibacterial potencies of P4LC, Pep-4, and LVFX, as well as unmodified Pep-4 assayed in combination with free LVFX

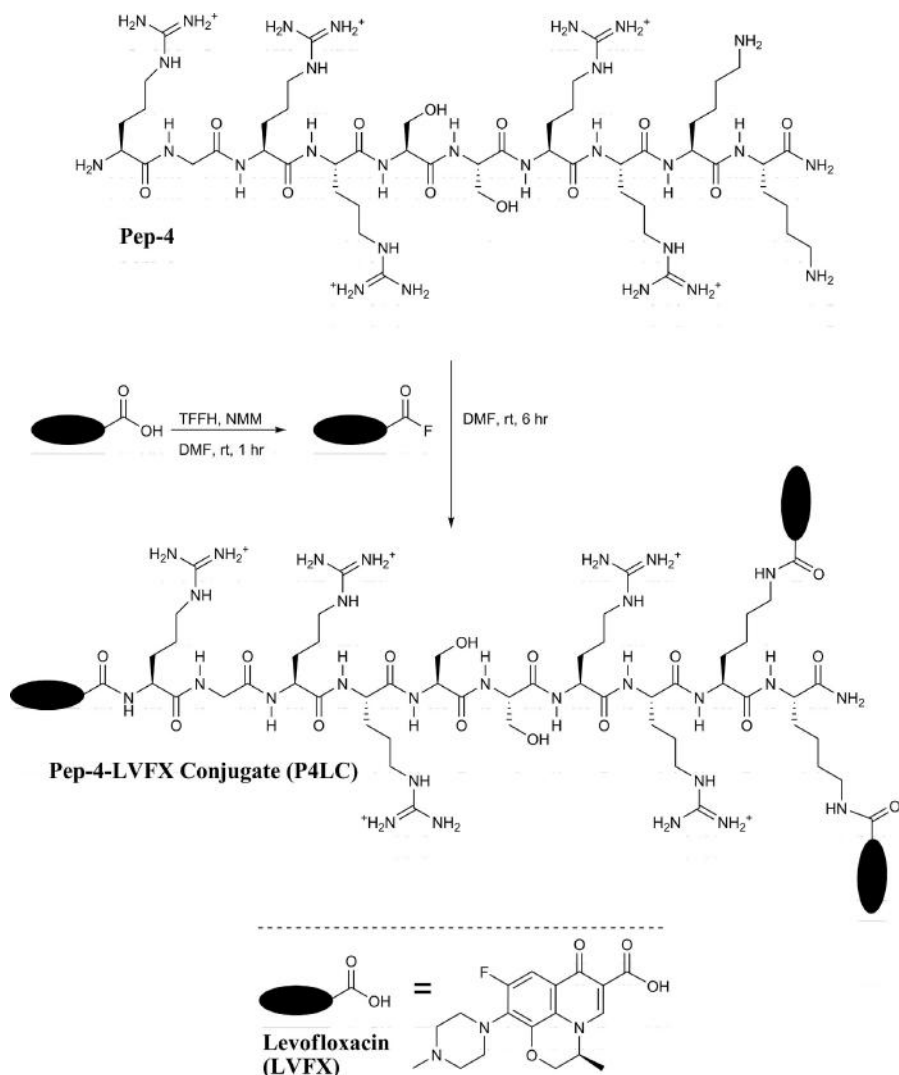


FIGURE 1 | Pep-4 was coupled to LVFX in a two-step, one-pot synthesis. The carboxyl moiety of LVFX was preactivated using TFFH to afford the acyl fluoride. Pep-4 was then added to the activated LVFX reaction mixture to yield P4LC.

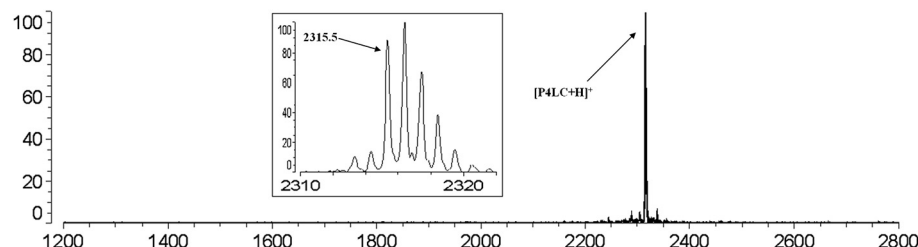


FIGURE 2 | MALDI-TOF mass spectrum of P4LC (m/z : 2315.5) obtained after purification indicates a 3:1 LVFX/Pep-4 loading stoichiometry. No peaks assignable to Pep-4 or intermediately

acylated conjugate species were observed. The baseline isotopic distribution for P4LC is shown in the inset with labeling of the monoisotopic peak.

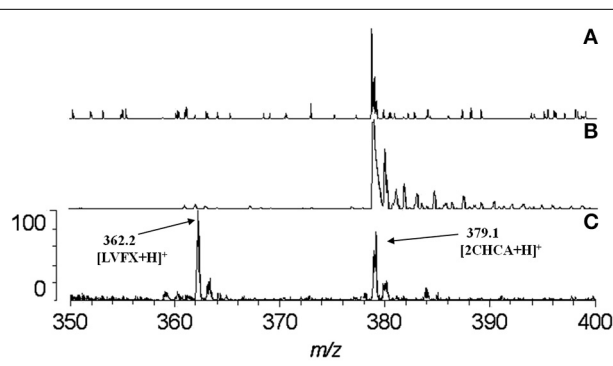


FIGURE 3 | Comparison of spectra at the region where LVFX m/z should appear. The absence of any discernible peak near 362.2 in the spectrum for P4LC (A) indicates that no LVFX contamination was present in isolated conjugate product. Spectra for matrix alone (B) and LVFX alone (C) are shown for comparison. As evidenced in the spectra, matrix-related peaks did not interfere with detection of the peak assigned to LVFX.

(Pep-4/LVFX), were evaluated against the model gram-negative and gram-positive bacteria *E. coli* and *B. cereus*, respectively. Assays were conducted under three different ionic strength (μ) buffer conditions in order to assess the effect salt concentration had on antibacterial effectiveness. The lowest ionic strength buffer used was 10 mM NaPO₄, pH 7.4, which corresponded to 26 mM total ionic strength. The intermediate ionic strength buffer consisted of 10 mM NaPO₄ combined with cation-adjusted PBS in a one to one volume ratio, which afforded a 111 mM ionic strength buffer with a pH of 7.4. Undiluted cation-adjusted PBS (pH = 7.4), with an ionic strength of 167 mM, was used as the high ionic strength buffer. Bacterial survival results were plotted against the log of the concentration of conjugate, peptide, or free drug. EC₅₀ values for each assessed compound were calculated by fitting the survival data to equation 3, which models typical sigmoidal dose-response behavior using a variable Hill slope. An F test was used to assess statistical significance, with the alpha level set to 0.05. EC₅₀ values and their respective 95% confidence intervals are shown in Table 1, and generated survival curves are shown in Figure 4.

In low ionic strength conditions (μ = 26 mM), P4LC demonstrated similar antibacterial activity to Pep-4 against both bacteria. Against *E. coli*, the conjugate demonstrated an EC₅₀ of 0.0167 μ M, which was not found to be significantly different

than that of the free peptide, which displayed an EC₅₀ value of 0.0168 μ M (p = 0.91). Against *B. cereus*, P4LC demonstrated an EC₅₀ value of 0.0218 μ M, while Pep-4 displayed an EC₅₀ of 0.0271 μ M, values which were also determined not to be significantly different (p = 0.21). The combination of free LVFX and Pep-4 (Pep-4/LVFX) demonstrated an EC₅₀ of 0.00375 μ M against *E. coli*, while that of free LVFX was 0.00281 μ M, values which were not significantly different from each other (p = 0.20). Against *B. cereus*, Pep-4/LVFX had an EC₅₀ of 0.112 μ M and free LVFX an EC₅₀ of 0.212 μ M, values which were approximately five-fold and ten-fold greater, respectively, than those determined for P4LC and Pep-4. The EC₅₀ value of Pep-4/LVFX was not significantly different than that of free LVFX alone (p = 0.36) against *B. cereus*.

P4LC demonstrated EC₅₀ values of 1.71 μ M and 2.17 μ M against *E. coli* and *B. cereus*, respectively, in intermediate ionic strength conditions (μ = 111 mM). These values are approximately 17-fold and 82-fold lower than those of Pep-4, 28.3 μ M (*E. coli*) and 178 μ M (*B. cereus*), under the same conditions. Against *B. cereus*, Pep-4 displayed antibacterial activity only at high peptide concentrations, killing a maximum of 69% of bacteria at the highest assessed peptide concentration (491 μ M). In order to fit the data to Equation 3 and estimate the potency of Pep-4, it was necessary to set the lower boundary to 0%, a constraint not typically imposed. Therefore, the EC₅₀ value given for Pep-4 against *B. cereus* under these conditions represents an estimated value. P4LC, LVFX, and Pep-4/LVFX provided sufficient data points in the lower survival ranges to fit the data by setting the lower survival boundary to $\geq 0\%$. Overall, the potencies of P4LC and Pep-4 decreased significantly compared to their respective performances against both bacteria under low salt conditions. Meanwhile, the potencies of Pep-4/LVFX (0.00487 μ M) and free LVFX (0.00223 μ M) against *E. coli* were not significantly affected by the increased ionic strength. However, in the case of *B. cereus*, the EC₅₀ values for Pep-4/LVFX (0.941 μ M) and free LVFX (0.591 μ M) were significantly higher than those observed under low ionic strength conditions. The potencies of Pep-4/LVFX and LVFX were not found to be significantly different from each other for either *E. coli* (p = 0.071) or *B. cereus* (p = 0.11) under these conditions.

Under high ionic strength conditions (μ = 167 mM), the conjugate demonstrated EC₅₀ values of 1.51 μ M and 40.0 μ M against *E. coli* and *B. cereus*, respectively. By comparison, the EC₅₀

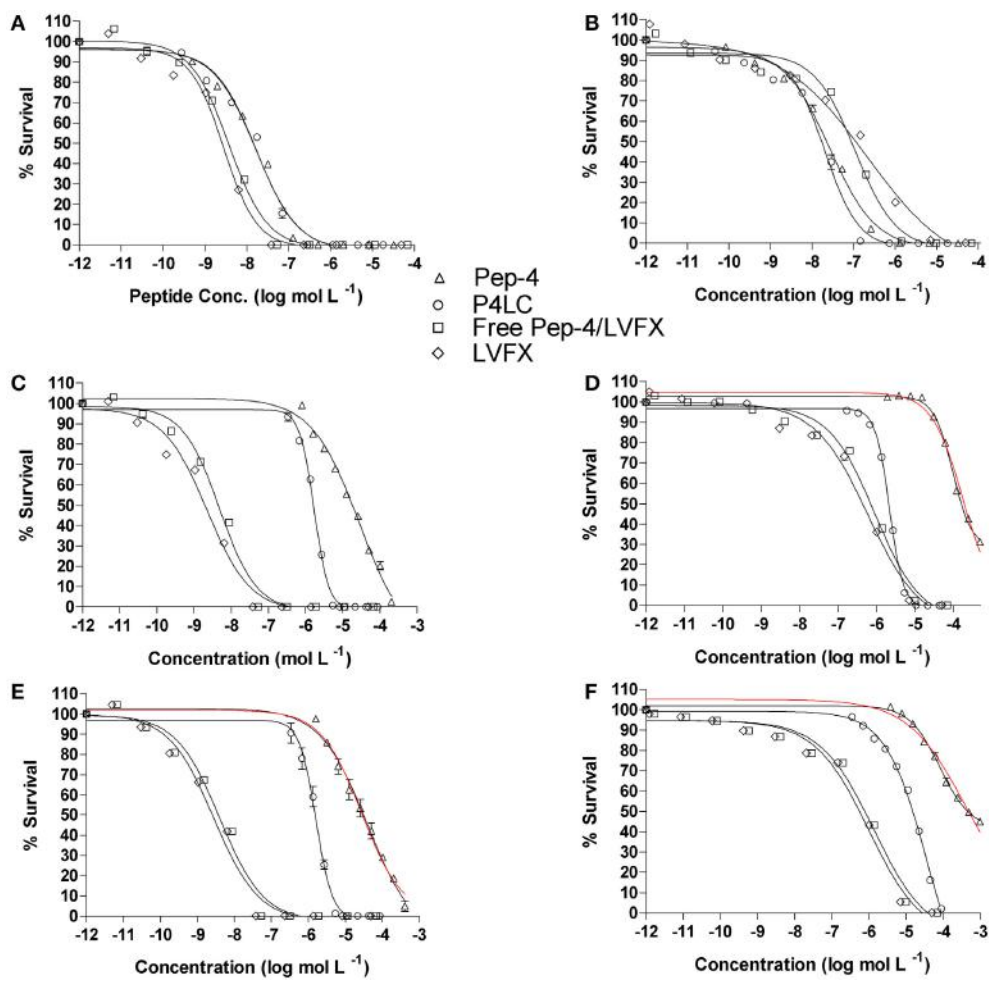


FIGURE 4 | Antibacterial effectiveness of P4LC, Pep-4, Pep-4/LVFX and LVFX against *E. coli* (A,C,E) and *B. cereus* (B,D,F). The top row (**A,B**) were generated for assays performed in low total ionic strength (26 mM), the middle row (**C,D**) for intermediate total ionic strength (111 mM), and the bottom row (**E,F**) for high total ionic strength (167 mM) conditions. Data were fit to equation 3, a standard variable

slope dose-response equation, in order to obtain EC₅₀ values. Pep-4 failed to achieve sufficient killing (within the tested peptide concentration range) to define the lower survival boundary for fitting to Equation 3 under higher ionic strength conditions (**D–F**), and it was necessary to set the lower boundary to 0%. Curves based on the data constraints are shown in red.

values achieved under high salt conditions with free peptide were 29.4 μM against *E. coli* and 404 μM against *B. cereus*. Thus, as was the case in the intermediate ionic strength environment, P4LC proved significantly more effective than Pep-4 (approximately 20-fold and 10-fold more potent against *E. coli* and *B. cereus*, respectively). Pep-4 failed to exert full killing activity under high ionic strengths within the range of concentrations evaluated, killing a maximum of 90% of *E. coli* (highest tested peptide concentration was 410 μM) and 56% of *B. cereus* (highest peptide concentration tested was 983 μM). Therefore, it was necessary to set the lower survival boundary to 0% against both bacteria for Pep-4. The conjugate's EC₅₀ against *E. coli* did not change significantly as a result of the ionic strength increase from 111 to 167 mM, while its effectiveness against *B. cereus* decreased by approximately an order of magnitude as a result of the change in environment. This trend was similar to that observed with Pep-4, where the peptide exhibited a substantial increase in its EC₅₀ value

against *B. cereus*, though not against *E. coli*, as a result of the assay ionic strength increase from 111 to 167 mM. Under high ionic strength conditions, the Pep-4/LVFX combination demonstrated an EC₅₀ of 0.00404 μM against *E. coli* and free LVFX exhibited an EC₅₀ of 0.00277 μM. The values were not found to be significantly different from each other ($p = 0.51$). Moreover, their high salt EC₅₀ values were not significantly different from the EC₅₀ values that they demonstrated under intermediate ionic strength conditions. Meanwhile, Pep-4/LVFX exhibited an EC₅₀ of 1.37 μM against *B. cereus*, and free LVFX showed an EC₅₀ of 0.981 μM, values that were determined to not be significantly different from each other or the corresponding values observed under intermediate ionic strength conditions.

MEMBRANE DISRUPTION

CAMPs have been shown to directly perturb bacterial membrane integrity, with the degree of inflicted disruption varying

depending on both the peptide and the bacteria being targeted. CAMP-induced membrane disruption can range from the formation of minor transient gaps that result in depolarization of the membrane to the formation of larger perturbations and pores (Kaplan et al., 2011). The degree of disruption in bacterial cell membranes can be probed using fluorometric reporter molecules such as DiSC(3)5 (for depolarization) (Síp et al., 1990; Zhu and Shin, 2009) and SYTOX Green (for more substantial membrane disruption) (Luque-Ortega et al., 2008).

The ability of P4LC, Pep-4, LVFX, and Pep-4/LVFX to depolarize bacterial membranes was examined using the carbocyanin dye DiSC(3)5. When exposed to live cells, DiSC(3)5 concentrates in hyperpolarized membranes (Síp et al., 1990; Kaplan et al., 2011), which results in quenching of its fluorescence (622/670 nm_{em}). Dissipation of membrane potential gradients resulting from even minor transient disruptions in lipid bilayer integrity inflicted by antibacterial agents such as CAMPs results in the release of trapped DiSC(3)5, which can be detected by monitoring DiSC(3)5 fluorescence (Rathinakumar et al., 2009; Zhu and Shin, 2009). In this study, fluorescence induction curves were generated for conjugate, peptide, or drug in the presence of *E. coli* and *B. cereus* cells that had been charged with DiSC(3)5. The data sets for P4LC, Pep-4, LVFX, and Pep-4/LVFX were compared to that obtained for melittin (Lee et al., 2013b), a known pore-forming CAMP that was used as a positive control to establish maximal depolarization. Data for DiSC(3)5 release was fit

to a polynomial regression model (equation 4, see Materials and Methods) and these data were then subjected to an F test, with the alpha level set to 0.01, in order to allow comparison of curves and establish statistical significance of any observed similarities or differences. Fitted curves are shown in **Figures 5A,B**.

Addition of P4LC to wells containing *E. coli* and *B. cereus* led to a rapid increase in fluorescence in both cases. Compared to the results obtained for melittin, P4LC was able to cause 53.6 and 33.5% mean maximal fluorescence against *E. coli* and *B. cereus*, respectively. In contrast, Pep-4 caused 26.6% maximal fluorescence against *E. coli* and 7% against *B. cereus*. Similarly, Pep-4/LVFX induced 25% maximal fluorescence against *E. coli* and 7.4% against *B. cereus*. Finally, free LVFX was only able to cause 8.4% and 2.5% of maximal fluorescence against *E. coli* and *B. cereus*, respectively. The best-fit curves generated for P4LC and free LVFX were found to be significantly different from those of Pep-4 and Pep-4/LVFX, as well as from each other. Meanwhile, the curves generated for Pep-4 and for Pep-4/LVFX were found to not be significantly different from each other ($p = 0.32$ for *E. coli*; $p = 0.071$ for *B. cereus*).

The membrane impermeable reporter SYTOX green was used as a probe to gain further insight into the effects of P4LC, Pep-4, LVFX, and Pep-4/LVFX on *E. coli* and *B. cereus* cell membrane integrity. SYTOX Green has been shown to bind DNA, which results in a >500-fold increase in fluorescence intensity. The DNA found in intact bacteria is inaccessible to SYTOX Green binding,

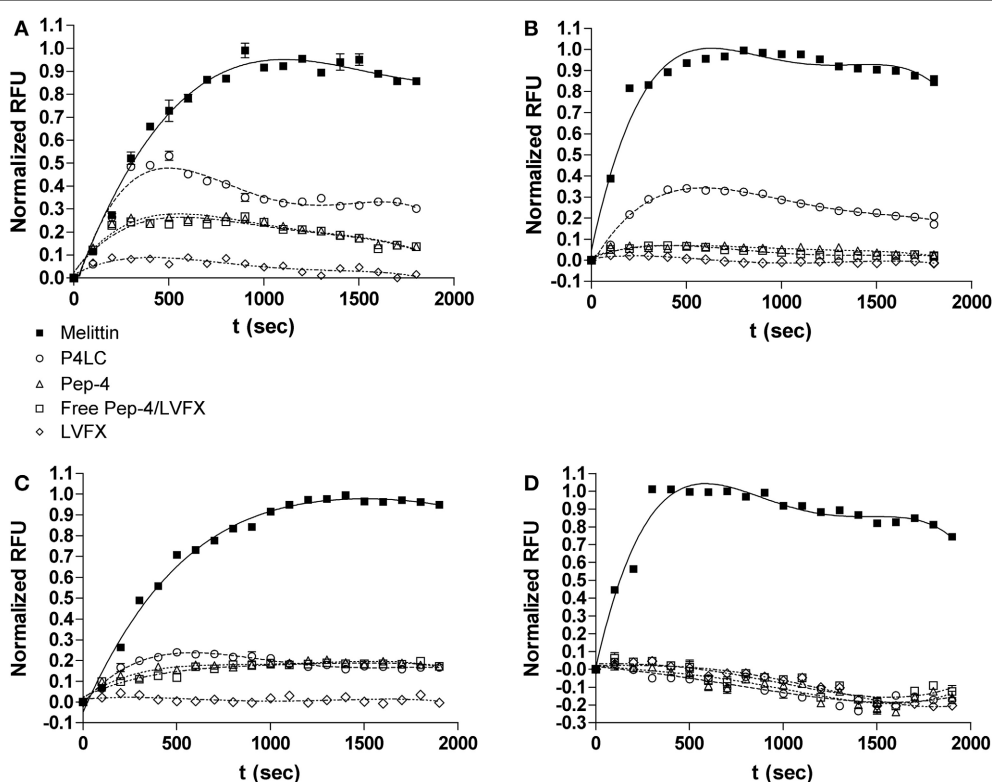


FIGURE 5 | Depolarization (top row) and perturbation (bottom row) of *E. coli* membranes (A,C) and *B. cereus* membranes (B,D) induced by P4LC, Pep-4, Pep-4/LVFX, LVFX and melittin.

Fluorescence values are presented as a percentage of the maximal fluorescence signal intensities observed for the pore-forming CAMP, melittin.

with fluorescence occurring only after the integrity of the bacterial membrane has been sufficiently compromised (Roth et al., 1997). Whereas DiSC(3)5 requires only minor and transient disruption in membrane integrity for its release from membranes, SYTOX Green requires more substantial perturbation to enter the bacterial cytoplasm and bind DNA. Accordingly, incubation of bacteria with CAMPs that perturb membrane integrity sufficiently for SYTOX green to enter the cytoplasm results in an increase in fluorescence (Lee et al., 2013b). As with the membrane depolarization studies described above, fluorescence curves were generated for P4LC, Pep-4, LVFX, and Pep-4/LVFX, and the data sets compared to those generated for melittin, which was used as the positive reference to establish maximal SYTOX Green fluorescence. Fluorescence induction curves were fit to equation 4 for statistical assessment (**Figures 5C,D**).

Addition of P4LC to wells containing *E. coli* led to a moderate increase in fluorescence; however, no noticeable increase in fluorescence was noted for *B. cereus*. In the case of *E. coli*, incubation with P4LC resulted in 21.4% mean maximal fluorescence relative to the results obtained for melittin. Pep-4 afforded 19.1% maximal fluorescence against *E. coli* and, similar to P4LC, yielded no noticeable fluorescence increase with *B. cereus*. The best-fit curve for P4LC when incubated with *E. coli* was found to be significantly different than that of Pep-4 ($p < 0.0001$), while the curves for Pep-4 and P4LC against *B. cereus* were not found to be significantly different ($p = 0.44$). Similar to P4LC and Pep-4, Pep-4/LVFX provided approximately one fifth of the maximal fluorescence increase when incubated with *E. coli* and no noticeable increase with *B. cereus*. The best-fit curves for Pep-4/LVFX were found to be significantly different than those of P4LC ($p < 0.0001$) for both bacteria. However, the best-fit curves for Pep-4/LVFX were determined to not be significantly different from those of Pep-4 ($p = 0.012$ for *E. coli*; $p = 0.062$ for *B. cereus*). No increase in fluorescence was noted when either bacterium was incubated with LVFX.

DISTRIBUTION COEFFICIENT

Hydrophobic moment is known to be a crucial factor influencing CAMP membrane dynamics and overall antibacterial activity (Liu and Deber, 1998; Stark et al., 2002; Chen et al., 2007; Yin et al., 2012; Lee et al., 2013a). In order to gain insight into the relative hydrophobicities of P4LC, Pep-4, and LVFX, their partitioning between aqueous 10 mM NaPO₄ (pH 7.4) and 1-octanol, a non-polar solvent that is immiscible with water, was assessed. The concentration ratios of each compound between the two liquid phases were used to establish distribution coefficients ($D_{7.4}$). Indolicidin and melittin were used as reference peptides in these studies. Indolicidin is a short tryptophan and proline-rich CAMP with a high overall hydrophobicity (Podorjeszach and Huttunen-Hennelly, 2010), while melittin is a well-studied peptide with an intermediately hydrophobic sequence (Li et al., 2013). LogD_{7.4} values for Pep-4, P4LC, LVFX, melittin, and indolicidin are shown in **Figure 6**. Based on the results of these partitioning studies, Pep-4 was found to be the least hydrophobic of the CAMPs tested, demonstrating a logD_{7.4} of -2.57. By comparison, the logD_{7.4} of P4LC was found to be -1.65 ($D_{7.4} = 0.0210$), approximately an order of magnitude greater than that of

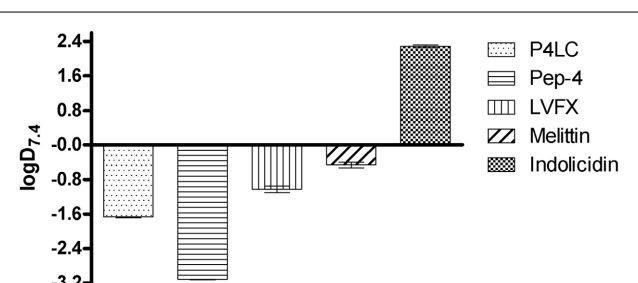


FIGURE 6 | Experimentally determined logD_{7.4} values for P4LC, Pep-4, LVFX, melittin, and indolicidin.

Pep-4. Meanwhile, LVFX demonstrated a logD_{7.4} value of -1.05 ($D_{7.4} = 0.094$), which was about 4.5-fold greater than P4LC in terms of D_{7.4}. The reference peptide indolicidin was found to have a logD_{7.4} value of 2.30, which was substantially higher than that observed for any other compound tested. The logD_{7.4} value for melittin, which was predicted to exhibit intermediate hydrophobicity, was determined to be -0.46, approximately an order of magnitude greater than that of the conjugate.

DISCUSSION

These studies have focused on the antibacterial performance of a peptide conjugate comprised of the fluoroquinolone LVFX covalently affixed to Pep-4, a ten-residue CAMP based on the c-terminal sequence of hBD-3. The conjugate, P4LC, was synthesized via acylation of primary amino groups in Pep-4 using the carboxyl moiety of LVFX. Our findings reveal that attachment of LVFX to Pep-4 yields a conjugate with significantly enhanced potency relative to the scaffold peptide in physiologically relevant ionic strength conditions. The results observed for unmodified Pep-4 coadministered with free LVFX suggests that the conjugate's antibacterial potency is not due to extracellular release of free drug.

The antibacterial effectiveness of P4LC, Pep-4, LVFX, and free peptide in combination with free drug (Pep-4/LVFX) were assessed against the model gram-negative and gram-positive bacteria, *E. coli* and *B. cereus*, respectively. Assays were conducted in various ionic strength environments, including physiologically relevant conditions, in order to evaluate the effect that salt concentration had on their antibacterial potencies. While P4LC and Pep-4 did not demonstrate significantly different EC₅₀ values against either bacterium in the lowest ionic strength conditions tested ($\mu = 26$ mM), the conjugate was found to be substantially more effective than the free peptide at higher ionic strengths. At an ionic strength of 111 mM, P4LC was found to be 17-fold more effective than Pep-4 against *E. coli* and 82-fold more effective against *B. cereus*. In the highest salt concentrations tested ($\mu = 167$ mM), P4LC was 20-fold more effective than free peptide against *E. coli* and 10-fold more effective against *B. cereus*. Meanwhile, EC₅₀ values determined for Pep-4/LVFX were significantly lower than those of the conjugate in all conditions, with the exception being the lowest ionic strength environment, where the conjugate was significantly more effective against *B. cereus*. These findings suggest that the enhanced activity of the conjugate

relative to the free peptide is likely not due to the activity of extracellular LVFX release. Our findings also suggest that there was no synergistic enhancement of LVFX activity conferred by coadministration of unmodified Pep-4 with free LVFX, as EC₅₀ values for Pep-4/LVFX were in most cases not found to be significantly lower than those of LVFX.

In order to gain insights into the antibacterial mechanisms of P4LC and Pep-4, experiments were performed to investigate their interactions with bacterial membranes. The fluorescent potentiometric probe DiSC(3)5 was used to assess the extent to which P4LC, Pep-4, LVFX, and Pep-4/LVFX were able to induce bacterial membrane depolarization. Compared to melittin, a known pore-forming CAMP, P4LC induced moderate levels of depolarization against both *E. coli* and *B. cereus*. Whereas, the depolarization affected by Pep-4 in *E. coli* and *B. cereus* was found to be approximately a half and a third, respectively, of that caused by the conjugate. Similar to Pep-4, the Pep-4/LVFX combination afforded minimal depolarization, with fluorescence curves found not to be significantly different than those achieved using the free peptide alone. Meanwhile, LVFX induced almost no detectable depolarization. These results suggest that the covalently bound fluoroquinolone enhanced the peptide's ability to depolarize the membranes of both *E. coli* and *B. cereus* relative to the free peptide.

The membrane impermeable DNA-binding dye SYTOX Green was used to further probe the interactions of P4LC and Pep-4 with bacterial membranes. In the case of *E. coli*, P4LC and Pep-4 were observed to induce a moderate increase in fluorescence, equivalent to approximately one fifth of that observed for the positive reference melittin. Yet, the conjugate induced a more rapid increase in fluorescence than did the free peptide, a difference that was verified through statistical analysis of regression curves fit to the observed fluorescence kinetics data sets. In the case of *B. cereus*, almost no detectable fluorescence increase was observed for either P4LC or Pep-4. Meanwhile, the data sets acquired for Pep-4/LVFX against both bacteria more closely resembled those of Pep-4 than those of P4LC, an observation that was statistically verified. Treatment with free LVFX was not found to produce an increase in fluorescence against either bacterium. Taken together, these results suggest that P4LC and Pep-4 both induce a moderate degree of membrane perturbation against *E. coli*, but little, if any, perturbation of *B. cereus* membranes. However, this data also suggests that differences may exist in the membrane disruption mechanisms employed by P4LC and Pep-4 against *E. coli*.

It has been shown that alteration of peptide hydrophobicity can influence CAMP interaction with membranes (Dathe and Wieprecht, 1999; Podorieszach and Huttunen-Hennelly, 2010; Lee et al., 2013a). Introduction of the moderately lipophilic LVFX would be expected to effectively increase the hydrophobic character of the conjugate relative to the unmodified parent peptide. Using a biphasic 1-octanol/phosphate partitioning system, we found that the conjugate was approximately one order of magnitude more hydrophobic than Pep-4 based on their respective dissociation constants, D_{7.4} (Pep-4 logD_{7.4} = -2.57 vs. P4LC logD_{7.4} = -1.65). This finding was consistent with the observation that the hydrophobicity of the free drug was approximately

one and a half orders of magnitude greater than that of free Pep-4 (LVFX logD_{7.4} = -1.05). The logD_{7.4} determined for LVFX that is reported here is in agreement with previously reported values (Brillault et al., 2010; Lemaire et al., 2011). Interestingly, it has been shown previously that increasing the hydrophobicity of ten-residue peptides with similar sequences to Pep-4 resulted in enhanced membrane interactions and reduced sensitivity to environmental salt concentration (Bai et al., 2009). The enhanced hydrophobicity conferred by the attached LVFX groups noted here is likely a factor contributing to the more substantial membrane interactions and increased salt resistance observed for the conjugate relative to the free peptide.

CONCLUSION

In an effort to explore design parameters for engineering CAMP conjugates with enhanced properties, a novel antimicrobial peptide conjugate, P4LC, was generated by attaching multiple units of the fluoroquinolone antibiotic LVFX to Pep-4, a ten residue CAMP that presents multiple primary amino groups suitable for drug attachment via acylation. Our studies revealed that while P4LC displayed similar antibacterial effectiveness as the unmodified parent peptide Pep-4 under low salt conditions, it was substantially more potent under physiologically relevant high salt conditions. This finding is significant because most CAMPs have historically been found to lose antibacterial effectiveness in physiological ionic strength environments, a fact which has presented a challenge to the development of these peptides for therapeutic applications. Our studies also suggest that the conjugate's antibacterial potency is not due to extracellular release of free drug, as evidenced by the results observed for unmodified Pep-4 coadministered with free LVFX. Partitioning studies revealed that P4LC was more hydrophobic than Pep-4, while depolarization studies indicated that the conjugate was able to disrupt membrane integrity to a greater degree than the free peptide. We propose that the conjugate's observed increased hydrophobicity plays a role both in its enhanced salt resistance and ability to depolarize bacterial membranes. However, the influence that the LVFX groups have on the performance of the conjugate may not solely be attributable to the increased hydrophobicity. In our prior studies with Pep-4, acetylation of its amino groups was found to decrease the effective positive charge character of the peptide, which resulted in a significant reduction in potency under low salt conditions. In contrast, acylation of Pep-4 with LVFX did not result in a loss of potency under similar conditions. The superior performance of P4LC, relative to acetylated Pep-4, could reflect contributions from multiple factors. Unlike acetyl groups, LVFX contains protonatable nitrogens that could contribute to the overall cationic character of the conjugate. Additionally, the affixed LVFX groups may contribute some aspects of their inherent antimicrobial activity to that of the conjugate. Future efforts will focus on further investigating factors contributing to the antibacterial properties of P4LC and related conjugates. Parameters contributing to more effectively capturing the inherent antibacterial potency of LVFX will be of particular interest. Insights gained from studying the performance and physicochemical properties of P4LC will provide valuable information that can be used in the design of new conjugates incorporating different peptide scaffolds and a

broader lexicon of auxiliary molecules, including antibiotics or chemotherapeutics.

ACKNOWLEDGMENTS

This work was supported by funds provided by the College of Science and the Department of Chemistry and Biochemistry at George Mason University. Publication of this article was funded in part by the George Mason University Libraries Open Access Publishing Fund.

REFERENCES

- Arnusch, C. J., Pieters, R. J., and Breukink, E. (2012). Enhanced membrane pore formation through high-affinity targeted antimicrobial peptides. *PLoS ONE* 7:e39768. doi: 10.1371/journal.pone.0039768
- Bai, Y., Liu, S., Jiang, P., Zhou, L., Li, J., Tang, C., et al. (2009). Structure-dependent charge density as a determinant of antimicrobial activity of peptide analogues of defensin. *Biochemistry* 48, 7229–7239. doi: 10.1021/bi900670d
- Brillault, J., De Castro, W. V., and Couet, W. (2010). Relative contributions of active mediated transport and passive diffusion of fluoroquinolones with various lipophilicities in a Calu-3 lung epithelial cell model. *Antimicrob. Agents Chemother.* 54, 543–545. doi: 10.1128/AAC.00733-09
- Brogden, K. A. (2005). Antimicrobial peptides: pore formers or metabolic inhibitors in bacteria? *Nat. Rev. Microbiol.* 3, 238–250. doi: 10.1038/nrmicro1098
- Chen, Y., Guarneri, M. T., Vasil, A. I., Vasil, M. L., Mant, C. T., and Hodges, R. S. (2007). Role of peptide hydrophobicity in the mechanism of action of alpha-helical antimicrobial peptides. *Antimicrob. Agents Chemother.* 51, 1398–1406. doi: 10.1128/AAC.00925-06
- Cheng, T. J., Weinheimer, S., Tarbet, E. B., Jan, J. T., Cheng, Y. S., Shie, J. J., et al. (2012). Development of oseltamivir phosphonate congeners as anti-influenza agents. *J. Med. Chem.* 55, 8657–8670. doi: 10.1021/jm3008486
- Chu, H. L., Yu, H. Y., Yip, B. S., Chih, Y. H., Liang, C. W., Cheng, H. T., et al. (2013). Boosting salt resistance of short antimicrobial peptides. *Antimicrob. Agents Chemother.* 57, 4050–4052. doi: 10.1128/AAC.00252-13
- Chu-Kung, A. F., Bozzelli, K. N., Lockwood, N. A., Haseman, J. R., Mayo, K. H., and Tirrell, M. V. (2004). Promotion of peptide antimicrobial activity by fatty acid conjugation. *Bioconjug. Chem.* 15, 530–535. doi: 10.1021/bc0341573
- Chyan, W., Zhang, D. Y., Lippard, S. J., and Radford, R. J. (2014). Reaction-based fluorescent sensor for investigating mobile Zn²⁺ in mitochondria of healthy versus cancerous prostate cells. *Proc. Natl. Acad. Sci. U.S.A.* 111, 143–148. doi: 10.1073/pnas.1310583110
- Dathe, M., and Wieprecht, T. (1999). Structural features of helical antimicrobial peptides: their potential to modulate activity on model membranes and biological cells. *Biochim. Biophys. Acta* 1462, 71–87. doi: 10.1016/S0005-2736(99)00201-1
- Devocelle, M. (2012). Targeted antimicrobial peptides. *Front. Immunol.* 3:309. doi: 10.3389/fimmu.2012.00309
- Epanid, R. M., and Vogel, H. J. (1999). Diversity of antimicrobial peptides and their mechanisms of action. *Biochim. Biophys. Acta* 1462, 11–28. doi: 10.1016/S0005-2736(99)00198-4
- Gordon, Y. J., Romanowski, E. G., and McDermott, A. M. (2005). A review of antimicrobial peptides and their therapeutic potential as anti-infective drugs. *Curr. Eye Res.* 30, 505–515. doi: 10.1080/02713680590968637
- Hopp, T. P., and Woods, K. R. (1981). Prediction of protein antigenic determinants from amino acid sequences. *Proc. Natl. Acad. Sci. U.S.A.* 78, 3824–3828. doi: 10.1073/pnas.78.6.3824
- Jensen, H., Hamill, P., and Hancock, R. E. (2006). Peptide antimicrobial agents. *Clin. Microbiol. Rev.* 19, 491–511. doi: 10.1128/CMR.00056-05
- Kaplan, C. W., Sim, J. H., Shah, K. R., Kolesnikova-Kaplan, A., Shi, W., and Eckert, R. (2011). Selective membrane disruption: mode of action of C16G2, a specifically targeted antimicrobial peptide. *Antimicrob. Agents Chemother.* 55, 3446–3452. doi: 10.1128/AAC.00342-11
- Lee, J. K., Park, S. C., Hahm, K. S., and Park, Y. (2013a). Antimicrobial HPA3NT3 peptide analogs: placement of aromatic rings and positive charges are key determinants for cell selectivity and mechanism of action. *Biochim. Biophys. Acta* 1828, 443–454. doi: 10.1016/j.bbamem.2012.09.005
- Lee, M. T., Sun, T. L., Hung, W. C., and Huang, H. W. (2013b). Process of inducing pores in membranes by Melittin. *Proc. Natl. Acad. Sci. U.S.A.* 110, 14243–14248. doi: 10.1073/pnas.1307010110
- Lemaire, S., Tulkens, P. M., and Van Bambeke, F. (2011). Contrasting effects of acidic pH on the extracellular and intracellular activities of the anti-gram-positive fluoroquinolones moxifloxacin and delafloxacin against *Staphylococcus aureus*. *Antimicrob. Agents Chemother.* 55, 649–658. doi: 10.1128/AAC.01201-10
- Lemos, E. G. M., and Carareto-Alves, L. M. (1998). Short communication: resazurin reducing time as an indicator of bradyrhizobium viable cell count. *World J. Microbiol. Biotechnol.* 14, 139–141. doi: 10.1023/A:1008849206064
- Li, Z., Yuan, P., Xing, M., He, Z., Dong, C., Cao, Y., et al. (2013). Fatty acid conjugation enhances the activities of antimicrobial peptides. *Recent Pat. Food Nutr. Agric.* 5, 52–56. doi: 10.2174/2212798411305010008
- Liu, L. P., and Deber, C. M. (1998). Guidelines for membrane protein engineering derived from *de novo* designed model peptides. *Biopolymers* 47, 41–62.
- Luque-Ortega, J. R., van't Hof, W., Veerman, E. C., Saugar, J. M., and Rivas, L. (2008). Human antimicrobial peptide histatin 5 is a cell-penetrating peptide targetin mitochondrial ATP synthesis in Leishmania. *FASEB J.* 22, 1817–1828. doi: 10.1096/fj.07-096081
- Mariscal, A., Lopez-Gigosos, R. M., Carnero-Varo, M., and Fernandez-Crehuet, J. (2009). Fluorescent assay based on resazurin for detection of activity of disinfectants against bacterial biofilm. *Appl. Microbiol. Biotechnol.* 82, 773–783. doi: 10.1007/s00253-009-1879-x
- Okuda, D., Yomogida, S., Tamura, H., and Nagaoaka, I. (2006). Determination of the antibacterial and lipopolysaccharide-neutralizing regions of guinea pig neutrophil cathelicidin peptide CAP11. *Antimicrob. Agents Chemother.* 50, 2602–2607. doi: 10.1128/AAC.00331-06
- Pal, S., Mitra, K., Azmi, S., Ghosh, J. K., and Chakraborty, T. K. (2011). Towards the synthesis of sugar amino acid containing antimicrobial non-cytotoxic CAP conjugates with gold nanoparticles and a mechanistic study of cell disruption. *Org. Biomol. Chem.* 9, 4806–4810. doi: 10.1039/c1ob05338h
- Papanastasiou, E. A., Hua, Q., Sandouk, A., Son, U. H., Christenson, A. J., Van Hoek, M. L., et al. (2009). Role of acetylation and charge in antimicrobial peptides based on human beta-defensin-3. *APMIS* 117, 492–499. doi: 10.1111/j.1600-0463.2009.02460.x
- Park, I. Y., Cho, J. H., Kim, K. S., Kim, Y. B., Kim, M. S., and Kim, S. C. (2004). Helix stability confers salt resistance upon helical antimicrobial peptides. *J. Biol. Chem.* 279, 13896–13901. doi: 10.1074/jbc.M311418200
- Podorjeszach, A. P., and Huttunen-Hennelly, H. E. (2010). The effects of tryptophan and hydrophobicity on the structure and bioactivity of novel indolicidin derivatives with promising pharmaceutical potential. *Org. Biomol. Chem.* 8, 1679–1687. doi: 10.1039/b921248e
- Radzishevsky, I. S., Rotem, S., Zaknoon, F., Gaidukov, L., Dagan, A., and Mor, A. (2005). Effects of acyl versus aminoacyl conjugation on the properties of antimicrobial peptides. *Antimicrob. Agents Chemother.* 49, 2412–2420. doi: 10.1128/AAC.49.6.2412-2420.2005
- Rathinakumar, R., Walkenhorst, W. F., and Wimley, W. C. (2009). Broad-spectrum antimicrobial peptides by rational combinatorial design and high-throughput screening: the importance of interfacial activity. *J. Am. Chem. Soc.* 131, 7609–7617. doi: 10.1021/ja8093247
- Roth, B. L., Poot, M., Yue, S. T., and Millard, P. J. (1997). Bacterial viability and antibiotic susceptibility testing with SYTOX green nucleic acid stain. *Appl. Environ. Microbiol.* 63, 2421–2431.
- Seo, M. D., Won, H. S., Kim, J. H., Mishig-Ochir, T., and Lee, B. J. (2012). Antimicrobial peptides for therapeutic applications: a review. *Molecules* 17, 12276–12286. doi: 10.3390/molecules17102276
- Shiloh, M. U., Ruan, J., and Nathan, C. (1997). Evaluation of bacterial survival and phagocyte function with a fluorescence-based microplate assay. *Infect. Immun.* 65, 3193–3198.
- Sip, M., Herman, P., Plásek, J., and Hrouda, V. (1990). Transmembrane potential measurement with carbocyanine dye diS-C3-(5): fast fluorescence decay studies. *J. Photochem. Photobiol. B Biol.* 4, 321–328. doi: 10.1016/1011-1344(90)85037-W
- Stark, M., Liu, L. P., and Deber, C. M. (2002). Cationic hydrophobic peptides with antimicrobial activity. *Antimicrob. Agents Chemother.* 46, 3585–3590. doi: 10.1128/AAC.46.11.3585-3590.2002

- Wrolstad, R. E., Decker, E. A., Schatz, S. J., and Sporns, P. (2004). *Handbook of Food Analytical Chemistry, Water, Proteins, Enzymes, Lipids, and Carbohydrates, 1st Edn.* Hoboken, NJ: Wiley & Sons, Inc
- Yin, L. M., Edwards, M. A., Li, J., Yip, C. M., and Deber, C. M. (2012). Roles of hydrophobicity and charge distribution of cationic antimicrobial peptides in peptide-membrane interactions. *J. Biol. Chem.* 287, 7738–7745. doi: 10.1074/jbc.M111.303602
- Yu, H. Y., Tu, C. H., Yip, B. S., Chen, H. L., Cheng, H. T., Huang, K. C., et al. (2011). Easy strategy to increase salt resistance of antimicrobial peptides. *Antimicrob. Agents Chemother.* 55, 4918–4921. doi: 10.1128/AAC.00202-11
- Zasloff, M. (2002). Antimicrobial peptides of multicellular organisms. *Nature* 415, 389–395. doi: 10.1038/415389a
- Zhu, W. L., and Shin, S. Y. (2009). Effects of dimerization of the cell-penetrating peptide Tat analog on antimicrobial activity and mechanism of bactericidal action. *J. Pept. Sci.* 15, 345–352. doi: 10.1002/psc.1120

Conflict of Interest Statement: The authors declare that the research was conducted in the absence of any commercial or financial relationships that could be construed as a potential conflict of interest.

Received: 31 May 2014; accepted: 07 August 2014; published online: 18 September 2014.

*Citation: Rodriguez CA, Papanastasiou EA, Juba M and Bishop B (2014) Covalent modification of a ten-residue cationic antimicrobial peptide with levofloxacin. *Front. Chem.* 2:71. doi: 10.3389/fchem.2014.00071*

This article was submitted to Chemical Biology, a section of the journal Frontiers in Chemistry.

Copyright © 2014 Rodriguez, Papanastasiou, Juba and Bishop. This is an open-access article distributed under the terms of the Creative Commons Attribution License (CC BY). The use, distribution or reproduction in other forums is permitted, provided the original author(s) or licensor are credited and that the original publication in this journal is cited, in accordance with accepted academic practice. No use, distribution or reproduction is permitted which does not comply with these terms.



Magnetic biocatalysts and their uses to obtain biodiesel and biosurfactants

Carmen López^{1,2}, Álvaro Cruz-Izquierdo¹, Enrique A. Picó¹, Teresa García-Bárcena¹, Noelia Villarroel¹, María J. Llama¹ and Juan L. Serra^{1*}

¹ Enzyme and Cell Technology Group, Department of Biochemistry and Molecular Biology, Faculty of Science and Technology, University of the Basque Country (UPV/EHU), Bilbao, Spain

² IKERBASQUE, Basque Foundation for Science, Bilbao, Spain

Edited by:

Carissa M. Soto, Naval Research Laboratory, USA

Reviewed by:

Jin Montclare, New York University Polytechnic School of Engineering, USA

Terence Schull, Naval Surface Warfare Center IHEODTD, USA

***Correspondence:**

Juan L. Serra, Enzyme and Cell Technology Group, Department of Biochemistry and Molecular Biology, Faculty of Science and Technology, University of the Basque Country (UPV/EHU), PO Box 644, 48080 Bilbao, Spain
e-mail: juanl.serra@ehu.es

Nanobiocatalysis, as the synergistic combination of nanotechnology and biocatalysis, is rapidly emerging as a new frontier of biotechnology. The use of immobilized enzymes in industrial applications often presents advantages over their soluble counterparts, mainly in view of stability, reusability and simpler operational processing. Because of their singular properties, such as biocompatibility, large and modifiable surface and easy recovery, iron oxide magnetic nanoparticles (MNPs) are attractive superparamagnetic materials that serve as a support for enzyme immobilization and facilitate separations by applying an external magnetic field. Cross-linked enzyme aggregates (CLEAs) have several benefits in the context of industrial applications since they can be cheaply and easily prepared from unpurified enzyme extracts and show improved storage and operational stability against denaturation by heat and organic solvents. In this work, by using the aforementioned advantages of MNPs of magnetite and CLEAs, we prepared two robust magnetically-separable types of nanobiocatalysts by binding either soluble enzyme onto the surface of MNPs functionalized with amino groups or by cross-linking aggregates of enzyme among them and to MNPs to obtain magnetic CLEAs. For this purpose the lipase B of *Candida antarctica* (CALB) was used. The hydrolytic and biosynthetic activities of the resulting magnetic nanobiocatalysts were assessed in aqueous and organic media. Thus, the hydrolysis of triglycerides and the transesterification reactions to synthesize biodiesel and biosurfactants were studied using magnetic CLEAs of CALB. The efficiency and easy performance of this magnetic biocatalysis validates this proof of concept and sets the basis for the application of magnetic CLEAs at industrial scale.

Keywords: magnetic nanoparticles (MNPs), magnetic cross-linked enzyme aggregates (mCLEAs), biodiesel, biosurfactants, sucrose monopalmitate

INTRODUCTION

The use of nanobiocatalysts, with the combination of nanotechnology and biocatalysis, is considered as an exciting and rapidly emerging area. Thus, nanobiocatalysis, as a new frontier of biotechnology, is a new innovative sub-field of biocatalysis which explores more advanced materials as enzyme carriers as well as provides robust nanostructured materials with properties tailored to their applications as enzyme scaffolds (Xin et al., 2010).

One of the great challenges that the industries face nowadays is the transition to greener and more sustainable manufacturing processes that minimize, or preferably avoid, the generation of waste and the use of toxic and/or hazardous materials. Biocatalysis has many benefits to offer in this respect, since enzymatic processes generate less waste than conventional synthetic routes, are more energy efficient, and provide products in higher purity (Sheldon, 2011).

Enzymes are versatile nanoscale biocatalysts which can be used in many areas of application, including industrial biocatalysis and bioremediation. However, the use of enzymes in soluble form is often hampered by their price, instability and the difficulty in

its recovery and reutilization. These drawbacks can generally be overcome by immobilizing the enzyme to solid supports, since the immobilized biocatalyst shows improved storage and operational stability (e.g., toward denaturation by heat or organic solvents or by autolysis) and it can be easily separated from the products in the reaction mixture and reused. Moreover, reutilization of enzyme in consecutive catalytic cycles significantly decreases the costs of the biocatalyst which otherwise would not have been economically viable using the free enzyme (Sheldon, 2011; Sheldon and van Pelt, 2013).

Recent advances in nanotechnology provide a range of more diverse nanomaterials and the approach to immobilize enzymes on these nanosupports has grown in popularity in recent years. At the present time, the use of iron oxide magnetic nanoparticles (MNPs) as enzyme immobilization carriers, has drawn great attention because of their unique properties, such as controllable particle size, large surface area, modifiable surface, and easy recovery by applying a magnetic field which allows its reuse for successive catalytic cycles (Johnson et al., 2011; Liese and Hilterhaus, 2013; Verma et al., 2013; Kopp et al., 2014).

Enzyme immobilization on magnetic supports was first reported by Matsunaga and Kamiya (1987) who used magnetic particles isolated from magnetotactic bacteria. Later Dyal et al. (2003) reported magnetic (maghemite) nanoparticles for the immobilization of *Candida rugosa* lipase. Further progress in the use of magnetic materials for enzyme immobilization has been dependent on developments in MNP synthesis/handling and control over magnetic properties (Yiu and Keane, 2012).

Magnetic nanomaterials greatly facilitate separation, allowing the use of a magnet to quickly and efficiently remove the immobilized enzyme from the product (Safarik and Safarikova, 2009; Ren et al., 2011). This allows greater reusability and preservation of stability of the attached enzyme as compared to conventional matrices, where centrifugation/filtration is the only option to separate the enzyme from the product. Such operations might lead to enzyme leaching/instability due to mechanical shear while mixing the pellet with the appropriate buffer to begin a new reaction (Yiu and Keane, 2012). The low process costs of magnetic nanocarriers have therefore shown them to be an interesting and economic option (Verma et al., 2013).

In the past couple of decades, cross-linked enzyme aggregates (CLEAs) have emerged as a novel and versatile carrier-free immobilization technique (Cao et al., 2000; Sheldon, 2011). Moreover, the use of CLEAs presents several advantages compared to the free enzyme, since they are more stable with temperature and show good reusability, retaining a high percentage of their initial activity after several cycles. The preparation of CLEAs involves the precipitation of the enzyme (that does not need to be pure) and subsequent chemical cross-linking of the resulting protein aggregates with glutaraldehyde. This bi-functional reagent is generally the cross-linker of choice as it is inexpensive and readily available in commercial quantities (Sheldon and van Pelt, 2013).

Despite the advantages of CLEAs, the number of enzymes immobilized by this technology is limited, mainly due to the low Lys residue contents in the external surface of some enzymes (Sheldon, 2007), and the increased size (clumping) of CLEAs clusters due to separation of CLEAs from reaction mixture by centrifugation or filtration (Montoro-García et al., 2010; Wang et al., 2011). The latter limitation can be overcome if the CLEAs are magnetically-separable and their recovery can be easily achieved using a magnet instead of using centrifugation or filtration methods which inevitably lead to clumping of CLEAs. mCLEAs of α -amylase from *Bacillus* sp. (Talekar et al., 2012) and lipase from *Aspergillus niger* (Tudorache et al., 2013) were successfully prepared and used to hydrolyze starch and to obtain glycerol carbonate, respectively.

Biodiesel is as a mixture of fatty acid alkyl esters (FAAEs) which can be produced by transesterification of oils or by esterification of free fatty acids (FFAs) catalyzed either chemically or enzymatically using a lipase. Chemically-catalyzed production of biodiesel is industrially acceptable for its high conversion and reaction rates. However, downstream processing costs, environmental issues associated with biodiesel production and byproducts recovery have led to the search for alternative more eco-friendly production methods (Bisen et al., 2010). Thus, lipase-mediated biodiesel production presents more advantages

over the chemical method since it is eco-friendly, chemically selective and requires lower temperatures (Verma et al., 2013).

Sugar fatty acid esters (SFAEs), synthesized from renewable resources, have broad applications in detergent, food and cosmetic industries (van Kempen et al., 2013). Moreover, these biodegradable biosurfactants present antitumor, antimicrobial and insecticidal properties. SFAEs can be synthesized by chemical methods, although these reactions must be performed at high temperature and pressure in alkaline media and result in poor selectivity and colored side-products (Huang et al., 2010; Gumel et al., 2011; van den Broeck and Boeriu, 2013). SFAEs were also enzymatically synthesized using immobilized lipase and obtaining high production yields (Ferrer et al., 2002), with recovery of the granulated enzyme by decantation.

In this work, by using the aforementioned advantages of MNPs of magnetite and those of CLEAs, we prepared two robust magnetically-separable types of nanobiocatalysts by binding either the soluble lipase B of *Candida antarctica* (CALB) onto the surface of MNPs functionalized with $-\text{NH}_2$ groups (MNP-CALB) or by cross-linking with glutaraldehyde aggregates of enzymes among themselves and to MNPs to obtain magnetic CLEAs (mCLEA-CALB). Both biocatalysts were used to obtain: (i) fatty acid ethyl and propyl esters (biodiesel) by esterification of FFAs and transesterification of non-edible vegetable oils; (ii) sucrose monopalmitate (biosurfactant) from sucrose and vinyl, ethyl and methyl palmitate. The rapid magnetic recovery of the biocatalysts, their stability and the simple reaction media are exploited to establish an enzymatic process which could be easily transferable to industrial scale.

MATERIALS AND METHODS

MATERIALS

3-Aminopropyltriethoxysilane (APTS), NaBH_4 , FeCl_2 , FeCl_3 , dimethylsulfoxide (DMSO), 2-methyl-2-propanol (2M2P), *p*-nitrophenyl acetate (*p*NPA), 4 Å molecular sieves and Triton X-100 were purchased from Sigma-Aldrich (St. Luis, MO, USA). Coomassie Blue (PhastGel™ Blue R) was obtained from GE Healthcare (Uppsala, Sweden). Vinyl, methyl and ethyl palmitate and FFAs were purchased from TCI Chemicals (Portland, OR, USA). Non-edible vegetable oils (unrefined soybean, jatropha and camelina) were obtained from Bunge Ibérica, S.A. (Zierbena, Spain), Jatropha Hispania, S.L. (Toledo, Spain), and Camelina Company (Madrid, Spain), respectively. Olive oil used as a control was purchased from Carbonell (Madrid, Spain). All other chemicals were supplied by Merck (Darmstadt, Germany).

ENZYME

Lipozyme® CALB L, lipase B of *C. antarctica* (CALB, EC 3.1.1.3, 19.1 U/mg protein; 7.50 mg protein/ml) was kindly provided by Novozymes (Bagsvaerd, Denmark).

SYNTHESIS AND FUNCTIONALIZATION OF MAGNETIC NANOPARTICLES (MNPs)

MNPs of magnetite (Fe_3O_4) were synthesized by coprecipitation of iron salts in alkaline medium following the method described by Cruz-Izquierdo et al. (2012). Briefly, an aqueous solution

containing 0.36 M FeCl₂ and 0.72 M FeCl₃ was pumped to 1 M NH₄OH solution under continuous mechanic stirring at room temperature. The obtained black precipitate was separated from the liquid phase using a magnetic field, and then magnetically washed with water and PBS buffer (100 mM sodium phosphate, 150 mM NaCl, pH 7.4). In order to functionalize the resulting MNPs with -NH₂ groups, MNPs were incubated with APTS, washed with PBS and maintained at 4°C until use.

PREPARATION OF IMMOBILIZED ENZYMES ON MNPs

MNP-NH₂ (20 mg dry weight) was functionalized with aldehyde groups by incubation with 250 mM glutaraldehyde for 4 h in a final volume of 10 ml (phosphate buffer solution 100 mM, pH 7.4). The protein (50 µg/mg MNPs) was added to the mixture, which was maintained overnight at 4°C. After the immobilization, the MNP-enzyme was washed with 2 M NaCl and 1% Triton X-100 (v/v) in order to remove ionic and hydrophobic interactions, respectively. Finally, the enzyme was washed with buffer and maintained at 4°C.

PREPARATION OF MAGNETIC CLEAS

mCLEAs of CALB (mCLEA-CALB) were prepared following the methodology proposed by Cruz-Izquierdo et al. (2012). MNP-NH₂ was incubated with the corresponding enzyme to obtain 25–100 µg CALB/mg MNP-NH₂ in the presence of 100 mmol ammonium sulfate/mg protein. After 10 min, a solution of glutaraldehyde was added to reach a final concentration of 12.5 mM and the suspension was maintained for 5 h in agitation. mCLEAs were then washed with 2 M NaCl, 1% (v/v) Triton X-100 and 200 mM bicarbonate buffer, pH 9.0.

CHARACTERIZATION OF MNPs AND IMMOBILIZED ENZYMES

Elemental analysis was performed using a Euro EA Elemental Analyzer CHNS (EuroVector, Milan, Italy) with quantification limit of 0.1%. The particle size and morphology of MNPs was determined by transmission electron microscopy (TEM, JEOL 1010, Peabody, MA, USA). The magnetic characteristics were measured using different devices: for the calculation of magnetic saturation (M_s) 2 K hysteresis loops were performed using a vibrating sample magnetometer (VSM) in a superconducting magnet (14 T) cooled by a closed circuit of He (CFMS, Cryogenic Ltd., London, UK). To calculate coercivity (H_c) and remanence (M_r) an electromagnet was used at room temperature and moderate fields (0.9 T). The size distribution of magnetic particles was calculated from the magnetization data according to Langevin's equations adjusted for non-interacting superparamagnetic model. MNPs dry weight and concentration were analyzed using a vacuum concentrator (Savant SpeedVac concentrator, Thermo Scientific, Waltham, MA, USA).

ENZYMATIC ACTIVITY MEASUREMENTS

Esterase activity of CALB

The activity of soluble and immobilized CALB was assayed with pNPA as substrate according to Gao et al. (2004) with minor modifications. Specifically, soluble or immobilized lipase (1–2 µg protein) was added to a reaction mixture which contained 10 µl of pNPA (100 mM in DMSO) in 980 µl of PBS. The reaction mixture was maintained for 15 min at room temperature with rotational

mixing at 30 rpm (Intelli-Mixer RM-2, Elmi Ltd., Riga, Latvia). Samples were withdrawn every 5 min (in the case of immobilized lipase the magnetic biocatalysts were separated from the liquid phase using a magnet) and the appearance of *p*-nitrophenol (*p*NP) was measured spectrophotometrically (Beckman Coulter DU 800, Brea, CA, USA) at 405 nm ($\epsilon_{pNP} = 9.43 \text{ mM}^{-1} \cdot \text{cm}^{-1}$). One unit (*U*) of esterase activity was defined as the amount of enzyme that catalyzes the appearance of 1 µmol *p*NP per min under the assay conditions.

Hydrolytic activity of CALB

The hydrolytic activity of CALB was analyzed by the hydrolysis of tributyrin, and the release of butyric acid was volumetrically measured using a pH-stat (Metrohm 842 pH-Stat Autotitrator, Herisau, Switzerland) with 10 mM NaOH as alkaline solution. CALB (0.01 mg of free enzyme, 1 mg of MNP-CALB or 0.25 mg of mCLEA-CALB) was incubated in 9 ml of 5 mM phosphate buffer, pH 7.3, at 30°C. Tributyrin was then added (0.5 ml) and the increase of pH was registered. One unit (*U*) of activity was defined as the amount of enzyme that catalyzes the release of 1 µmol butyric acid per min under the assay conditions.

Transesterification activity of CALB

Olive oil (0.2 g) and 2-propanol (1:6 molar ratio oil:alcohol) were incubated with 1% (w/w of oil) of magnetic catalyst. The reaction was maintained at 40°C and 30 rpm with rotational mixing. The initial reaction rate for biodiesel production was assessed by withdrawing aliquots (5 µl) of the liquid phase at defined intervals which were analyzed by high-performance liquid chromatography (HPLC) as indicated below. Transesterification activity was defined as mg of oil transformed to biodiesel (fatty acid propyl esters, FAPEs) per mg of MNP-NH₂ and time (h) considering the initial reaction rate of transesterification.

SYNTHESIS OF BIOPRODUCTS

Synthesis of biodiesel

Biodiesel (Fatty Acid Ethyl Esters, FAEEs) was obtained by esterification of FFAs. For that, a mixture of FFAs which simulates the composition of FFAs coming from microalgae (*Scenedesmus* sp.) was applied: 4.1% stearic acid, 23.6% palmitic acid, 52.1% oleic acid, 12.4% linoleic acid, and 7.8% linolenic acid. Ethanol (10:1 alcohol:FFA, mol:mol) was added to FFAs mixture (500 µmol) and 2 mg mCLEA-CALB. FAEEs were also obtained by transesterification of a mixture (0.2 g) of vegetable oils, composed of 80% palm oil, 10% soybean oil and 10% olive oil, with ethanol as alkyl donor in molar ratio of 30:1 (alcohol:oil) and 1% (w/w of oil) of magnetic biocatalyst. FAPEs were produced by transesterification of vegetable oil (0.2 g) using 2-propanol as alkyl donor (6:1 molar ratio alcohol:oil) and 1% (w/w of oil) of magnetic catalyst. In all the cases, the reactions were carried out in a solvent-free medium at 25°C with rotational mixing (Intelli-Mixer RM-2, Elmi Ltd., Riga, Latvia). The reactions were followed by withdrawing aliquots (10 µl) of the liquid phase. Semi-quantitative analyses of samples were performed by thin layer chromatography (TLC) and the quantitative analysis using control FFAs and olive oil was performed by HPLC, as described above.

Synthesis of biosurfactant

Sucrose 6'-monopalmitate (SMP) was synthesized by transesterification of sucrose and vinyl, methyl or ethyl palmitate catalyzed by mCLEA-CALB. Sucrose (100 mg/ml) was added to DMSO and stirred for 10 min at 70°C, or to 2M2P and stirred for 24 h at 70°C, in order to obtain a homogeneous mixture. Molecular sieves (4 Å) were added to solid sucrose, DMSO and 2M2P stocks in order to absorb their water content. Vinyl, methyl or ethyl palmitate was then added in a molar sucrose:alkyl palmitate ratio of 1:1, 1:2, or 1:3. mCLEA-CALB were washed with the corresponding solvent and used as catalysts in a concentration of 4 mg/ml. The reactions (5 ml) were incubated at 60°C and stirred using magnetic agitation (Carousel 12 Plus, Radleys, UK). Samples (100 µl) were withdrawn and the liquid phase was separated from the solid biocatalyst using a magnetic field. When using DMSO, the same volume of ethanol was added to the aliquots in order to overcome the immiscibility between palmitate esters and DMSO. Semi-quantitative and quantitative analyses of samples were performed by TLC and HPLC-MS, respectively, as described above.

ANALYTICAL METHODS

HPLC analysis of biodiesel

Five microliter of samples withdrawn from the reaction mixture were diluted in 250 µl of *n*-hexane and analyzed by HPLC (Waters™ Corporation, Milford, MA, USA) using a diode array detector according to Holčapek et al. (1999). The C₁₈ column (5 µm, 4.6 × 250 mm, Tracer Lichrosorb RP18) was eluted at a flow rate of 1 ml/min using a mixture of acetonitrile:H₂O (1:1 v/v) (phase A) and 100% pure methanol (phase B) as mobile eluting phase and a gradient from 75 to 100% phase B in 15 min. The injection volume was 10 µl and peaks were detected at 205 nm.

HPLC-MS analysis of biosurfactants

Analysis of SMP was carried out by HPLC (Alliance e2695, Waters™ Corporation, Milford, MA, USA) coupled with a triple quadrupole masses spectrometer (QqQ) (Quattro micro Api, Waters™ Corporation, Milford, MA, USA). The column (2.6 µm, 2.10 × 50 mm, Kinetex C18, Phenomenex) was eluted at 30°C and 0.2 ml/min flow-rate. 0.1% (v/v) formic acid in H₂O (phase A) and 0.1% (v/v) formic acid in methanol (phase B) were employed as mobile phase, with a gradient from 50 to 100% phase B in 9 min. The injection volume was 10 µl. For the ionization of the SMP, a positive electrospray was used with 3200 V capillary voltage at 120°C. Nitrogen was used as desolvation gas at 300°C and 450 l/h flow-rate. SMP was monitorized using MRM (multiple reaction monitoring) with a lineal calibration (10–500 ng/ml) following the next transition: 603.2 to 441.3 nm (for quantification) and 603.2 to 203.1 nm.

Thin layer chromatography (TLC) analysis

A semi-quantitative analysis of biodiesel and biosurfactant was also assessed using TLC. Silica gel 60 coated plates (Merck, Darmstadt, Germany) were activated for 30 min at 100°C and 0.5 µl samples were applied. For biodiesel analysis, the ternary mixture *n*-hexane:ethyl acetate:acetic acid (90:10:1, v/v/v)

was used as eluting phase (Samakawa et al., 2000). After chromatography development (about 40 min), plates were air dried at room temperature, and then immersed for 1 min with gentle orbital shaking in a 0.02% (w/v) solution of Coomassie Blue R-350 (Nakamura and Handa, 1984), prepared in acetic acid:methanol:H₂O (1:3:6, v/v/v) as indicated by the manufacturer. Finally, the plates were air-dried at room temperature. Spots corresponding to substrates and products of the transesterification reaction were identified by using appropriate reference external standards run in parallel. For biosurfactant analysis, the eluting phase was composed of a mixture of toluene:ethyl acetate:ethanol (2:1:1, v/v/v). Spots corresponding to sucrose and SMP were detected by spraying the plates with a solution of urea (1 g urea, 4.05 ml phosphoric acid and 48 ml water-saturated 1-butanol) and heating them at 100°C for 15 min.

RESULTS AND DISCUSSION

CHARACTERIZATION OF MNPs AND IMMOBILIZED ENZYMES

MNPs were synthesized in our laboratory and analyzed by X-ray diffractography, which confirmed the presence of magnetite (data not shown). The increase of N content in MNPs with –NH₂ groups was confirmed by comparing the content of N, C, and H in naked MNPs and MNP-NH₂ using elemental analysis (see Figure 1). Percentage of N was negligible in non-functionalized nanoparticles, and increased up to 1% in particles whose surfaces were coated with groups. The increase was consistent with the presence of amine groups in the MNP-NH₂. The increment of C content in functionalized nanoparticles was also noticeable, and could correspond to the C content of the functionalizing agent (APTS) used.

The functionalized MNP-NH₂ were then employed for the immobilization of CALB by two different procedures: (i) covalent immobilization by cross-linking of the protein on the surface of MNP-NH₂ (MNP-CALB, see Figure 2A); (ii) covalent immobilization of cross-linked enzyme aggregates (mCLEA-CALB, see Figure 2B). In both cases glutaraldehyde was used as a bifunctional cross-linking reagent. Both types of immobilized enzymes of CALB were selected as model biocatalysts for characterization purposes.

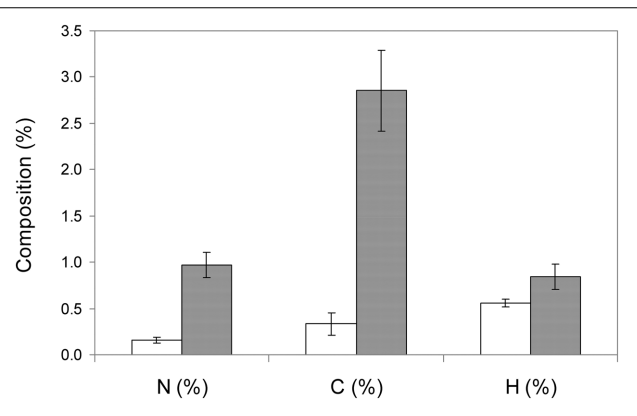


FIGURE 1 | Elemental analysis of naked MNPs (white bars) and MNP-NH₂ (gray bars).

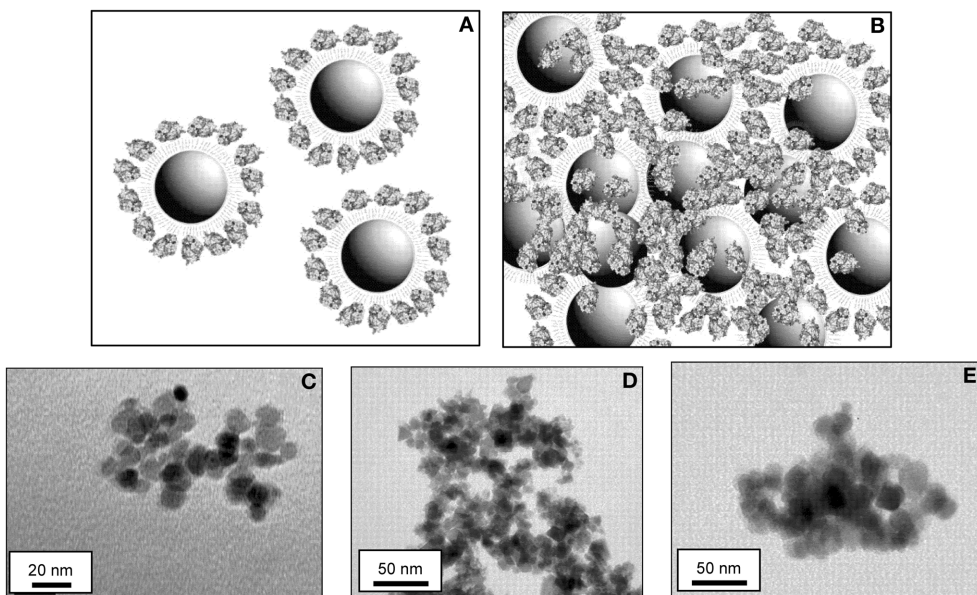


FIGURE 2 | Scheme of a scale representation of the magnetic biocatalysts obtained with CALB and TEM micrographs of the magnetic biocatalysts of CALB used in this work. Artwork is a hypothetical model of (A) MNP-CALB and (B) mCLEA-CALB complexes. Both models simulate a cross-section of a three-dimensional structure. The

MNPs are 10 nm in diameter, the APTs/glutaraldehyde bridge provides a spacer arm of 2.5 nm (Dauphas et al., 2009) and the size of CALB is $3 \times 4 \times 5$ nm (Uppenberg et al., 1994). TEM images of naked MNPs (C), MNP-CALB (D) and mCLEA-CALB (E). Bars represent 20 nm in C, and 50 nm in D,E.

The shape and size of MNPs and resulting immobilized enzymes were analyzed by TEM. Naked MNPs appeared as spherical particles with a uniform and defined size (see Figure 2C). Because the protein is not as opaque to electrons as MNPs, the presence of CALB bound directly to the surface of MNPs (Figure 2D) or forming mCLEA-CALB (Figure 2E) resulted in MNPs showing more fuzzy and diffuse edges than the naked counterparts.

Trying to determine if the binding of the protein could modify the magnetic properties of the particles, magnetic behavior of both protein-free MNP-NH₂ and immobilized enzymes (MNP-CALB and mCLEA-CALB) was analyzed at different magnetic fields and at 300 K (see Figure 3). At this temperature, the shape of the magnetization curve vs. magnetic field was similar for the three biocatalysts. In the three cases, when the external magnetic field was removed the particles lost the magnetization. Also, once saturation reached, magnetization only disappeared when magnetic field was reduced to zero. These two properties are represented by the concepts of magnetic remanence (M_r) and coercivity (H_c), which were very close to zero, being a characteristic of superparamagnetic nanoparticles. The saturation magnetization (M_s) of MNP-NH₂ was 82.5 emu/g (Table 1), similar to the value corresponding to bulk magnetite (89 emu/g, Ramírez and Landfester, 2003). The presence of cross-linked enzyme lowered the value of M_s , and that reduction increased at higher protein concentration, because the saturation magnetization value was referred to the total mass of biocatalyst instead of the mass of the magnetic support. Fitting magnetic results to the Langevin's function, particle size distribution of naked MNPs was obtained.

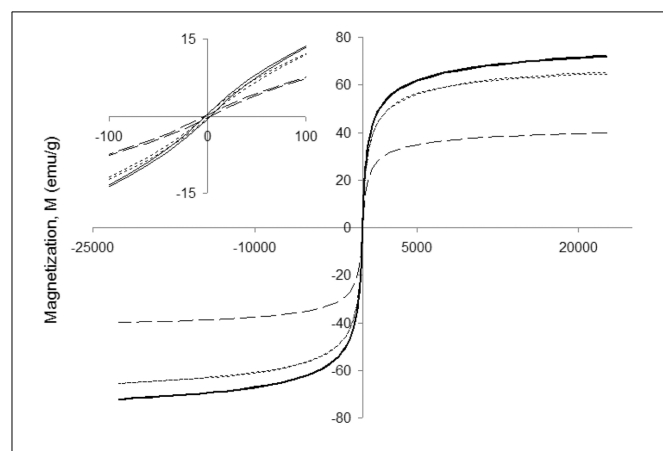


FIGURE 3 | Magnetization analysis at 300 K of the magnetic biocatalysts obtained with CALB. MNP-CALB (solid lines), mCLEA-CALB with 25 µg protein/mg MNPs (dotted lines with short strokes) and mCLEA-CALB with 100 µg protein/mg MNPs (dotted lines with long strokes). Inlet shows a detail of magnetization for values of magnetic field near to 0 Oe.

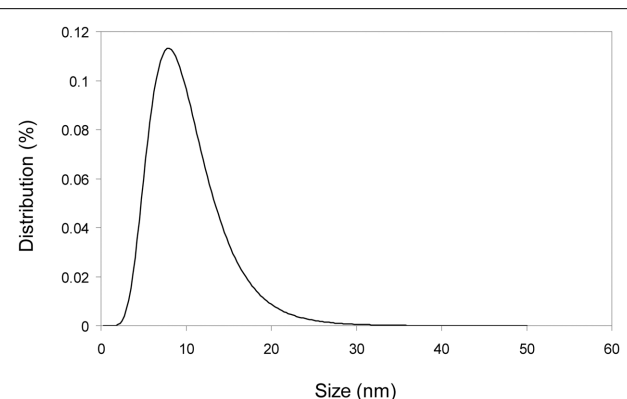
Figure 4 shows a mean nanoparticle diameter of 9.5 nm with a dispersion of ± 6 nm.

CATALYTIC PROPERTIES OF FREE AND IMMOBILIZED CALB

The use of magnetic supports for immobilization of enzymes provides well-known facilities for the recovery and reuse of

Table 1 | Magnetic parameters of MNP-NH₂ and biocatalysts obtained of CALB.

Support or biocatalyst	Immobilized CALB ($\mu\text{g}/\text{mg}$ MNPs)	M_s (emu/g)	M_r (emu/g)
MNP-NH ₂	–	82.5	1.0
MNP-CALB	25	65.3	0.5
mCLEA-CALB	25	72.1	0.5
	100	40.0	0.3

**FIGURE 4 | Particle size distribution of MNPs.** The distribution was fitted to the Langevin's function yielding a mean particle size of 9.5 nm and dispersion of ± 6 nm.

the catalysts. The benefits in terms of catalytic properties were checked using CALB as model enzyme and three types of immobilization: MNP-CALB (50 μg protein/mg MNPs), mCLEA-CALB with low load of protein (25 μg protein/mg MNPs), and mCLEA-CALB with high load of protein (100 μg protein/mg MNPs) (Table 2). Using non-aggregated enzyme, 50% of the protein was measured in the liquid phase, indicating that only 25 μg protein/mg MNPs was firmly attached to the support. However, using covalent CLEAs the immobilization efficiency reached 100%.

The effect of immobilization was assessed by the measurement of three enzymatic activities using preparations of the free and immobilized biocatalysts: (i) esterase activity using pNPA which is converted to pNP, (ii) hydrolysis of tributyrin to butyric acid, and (iii) the transesterification of olive oil with propanol to obtain FAPEs.

Having in mind the concentration of immobilized CALB (μg protein/mg MNPs), esterase activities of free and immobilized biocatalysts can be compared in terms of specific activities (U/mg protein): 20, 15.2, 10.8, and 10 U/mg protein for free enzyme, MNP-CALB and mCLEA-CALB of low and high load, respectively. The decrease in specific activity of immobilized enzymes compared to free enzymes could be associated to diffusional limitations which usually occur in immobilized biocatalysts due to steric hindrance. In that case, the rate of diffusion of substrates and/or products to and from the active site of the enzyme is lower than the enzymatic reaction rate (Pésic et al., 2012). These

Table 2 | Main properties of magnetic biocatalysts obtained of CALB.

Property	Free lipase	MNP-CALB	mCLEA-CALB	
			Immobilized CALB ($\mu\text{g}/\text{mg}$ MNPs)	Activity ^a
Activity ^a	20	0.38	0.27	1.0
Hydrolytic (U/mg catalyst)	1416.2	0.2	7.2	28.8
Transesterification (U/mg catalyst)	–	2.0	2.6	6.5
Biodiesel conversion (%)	–	20.5	30.3	66.7
Stability ^b	–	9.4	13.7	59.3
Biodiesel conversion after 10 cycles (%)	–	10	10	10

^aActivities were assayed as detailed in Materials and Methods.

^bStability was assessed as a measure of the biodiesel (FAPEs) conversion after 10 consecutive catalytic cycles of 24 h at 40°C.

diffusional problems were higher when using CLEAs than for non-aggregated enzyme, which indicates that enzyme aggregation could hinder the diffusion of compounds. The difference between free and immobilized enzyme activities was even more evident when analyzing the hydrolysis of tributyrin, due to the very fast enzymatic reaction.

mCLEA-CALB containing 100 μg protein/mg MNPs resulted to be the most appropriate biocatalyst in terms of enzymatic activities (U/mg MNPs), including the transesterification of olive oil to biodiesel, where a very high conversion was obtained after 24 h (Table 2). Moreover, the biocatalyst was much more stable than the other immobilized enzymes tested, maintaining practically the same conversion to biodiesel after 10 reaction cycles. Thermal stability was also considerably higher, as the biocatalyst only lost 10% of the initial activity when heated at 60°C for 30 min, while MNP-CALB and mCLEA-CALB (25 μg protein/mg MNPs) lost 70 and 50%, respectively. In any case, the immobilized biocatalysts were much more stable than the free enzyme, which lost 95% of the initial activity when heated at 60°C for 30 min. MNPs attached to previously aggregated and cross-linked enzymes (mCLEAs) represent the best option for the synthesis of magnetic biocatalysts, as high concentrations of protein can be attached to the enzyme, and this is more protected against destabilizing agents.

SYNTHESIS OF BIODIESEL

The ability of the prepared magnetic biocatalysts to synthesize biodiesel was tested using preparations of both FFAs and vegetable oils in a solvent-free system (see Figure 5).

The esterification of FFAs was performed using a mixture of them which mimics the composition of reserve lipids present in the microalga *Scenedesmus* sp., which mainly consisted of C14 and C16 saturated and unsaturated fatty acids. Ethanol was selected as alkyl donor in a molar ratio of 10:1 (alcohol:FFA), acting also as solvent of FFAs. The reaction (Figure 5A) was followed by both TLC and HPLC, and results are shown in Figures 6, 7, respectively. TLC plates stained with Coomassie Blue is a useful tool to identify and semi-quantify not only FAEEs but also FFAs. Figure 6 reveals that the esterification of FFAs was noticeable at 30 min,

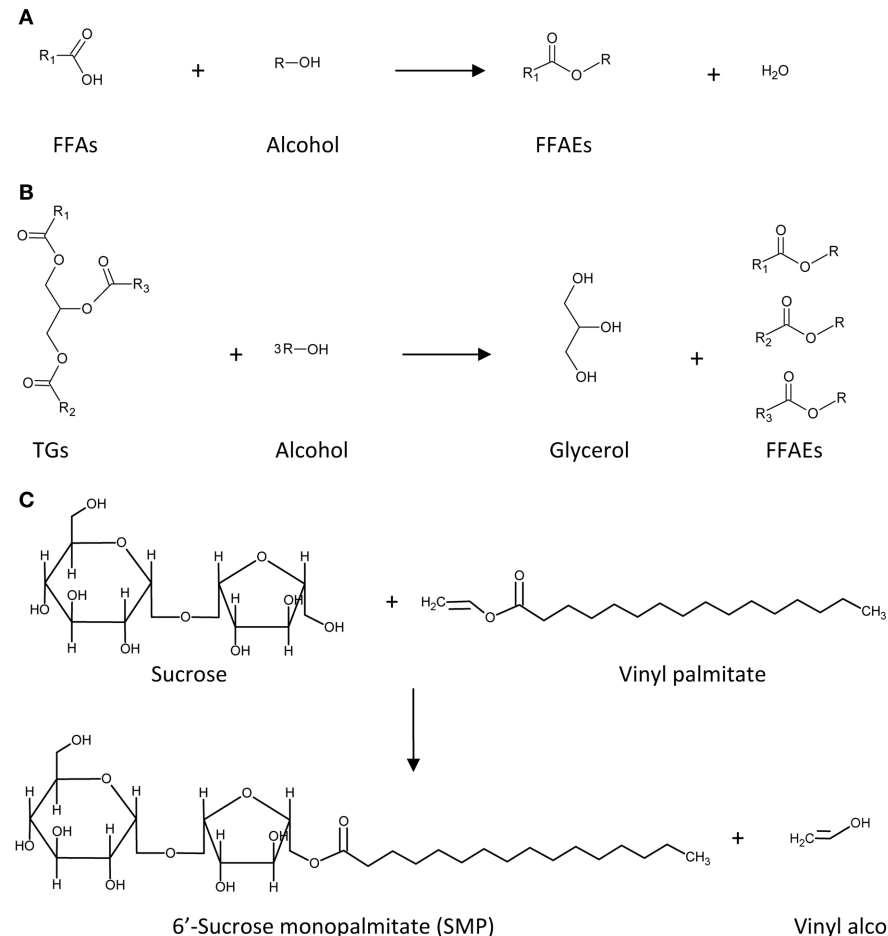


FIGURE 5 | Reactions of (trans)esterification catalyzed by CALB. Synthesis of biodiesel from (A) free fatty acids (FFAs) and (B) triglycerides (TGs). Synthesis of biosurfactant (C).

and was practically completed after 5 h of reaction. These values were confirmed by HPLC-quantification of FFAEs (data not shown) and unsaturated FFAs (**Figure 7**), which indicated conversions of 60% for C16:2 and C16:3 at 30 min and 90% after 5 h of reaction.

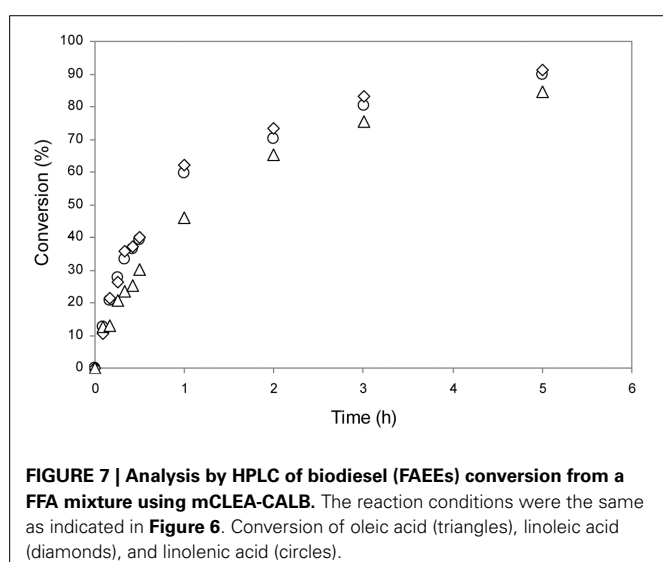
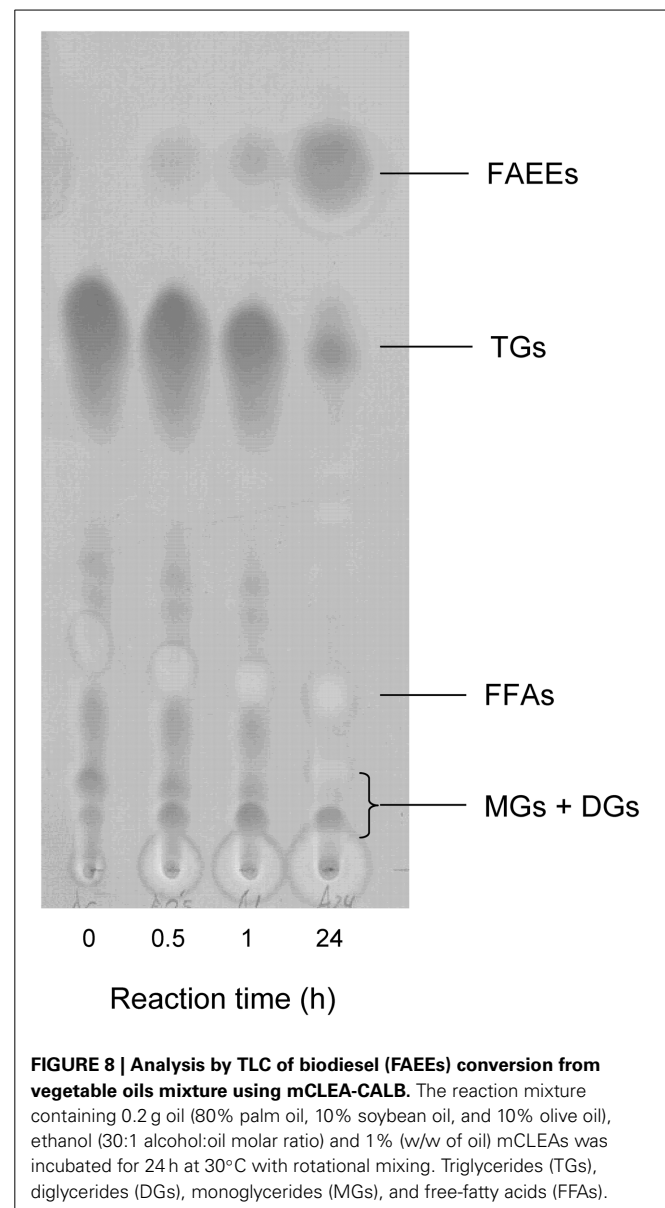
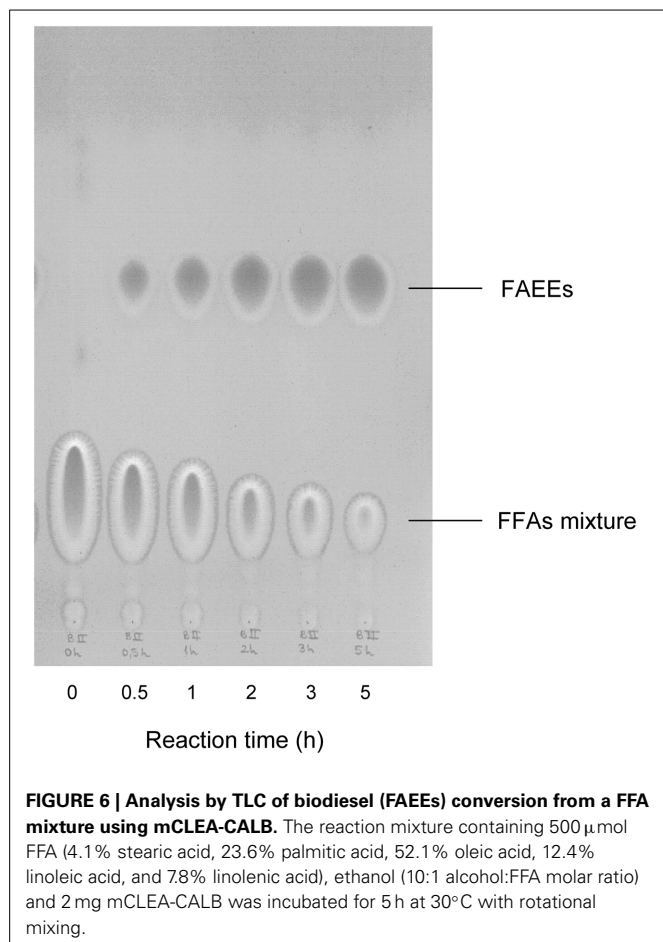
Trying to improve the simulation of microalgae oil, a mixture of vegetable oils (80% palm oil, 10% soybean oil and 10% olive oil) was prepared and used as substrate for the transesterification reaction. Taking into account the stoichiometry of the reaction (3:1, **Figure 5B**) and the molar excess of ethanol considered for FFAs, a molar ratio of 30:1 (alcohol:oil) was selected for the transesterification of this oil mixture. TLC analysis of the initial sample (**Figure 8**, lane 1) indicates the presence of triglycerides, but also the perceptible presence of FFAs, monoglycerides and diglycerides. After 1 h, the spot corresponding to triglycerides decreased, and after 24 h a high amount of triglycerides was converted to FFAEs. The presence of FFAs not only did not interfere in the transesterification of the oil but also they were converted to FFAEs in the reaction catalyzed by CALB. This point is remarkable because, as it is well-known, the presence of FFAs drastically reduces the yield and quality of the product obtained by some

of the usual chemical processes applied for the synthesis of biodiesel (Leung et al., 2010). On the other hand, the diversity and complexity of the oil mixture made the transesterification rate significantly lower than the rate of FFAs esterification (**Figure 6**).

Finally, the benefits of mCLEA-CALB as biocatalyst for the transesterification of vegetable oils were pointed out by comparing the three synthesized magnetic CALB catalysts for the synthesis of biodiesel from olive (used as a control), unrefined soybean, jatropha and camelina oils (**Figure 9**). The behavior of the biocatalysts seemed to be independent of the non-edible oil selected. The comparison of MNP-CALB with mCLEA-CALB of the same protein concentration revealed that the formation of CLEAs before immobilization contributes to the stabilization of the enzyme, and consequently, its maximal exploitation during the enzymatic reaction. Even so, the best conversion results were obtained when the highest concentration of protein was immobilized, reaching biodiesel conversion over 90% in 24 h at 30°C.

SYNTHESIS OF BIOSURFACTANTS

The enzymatic synthesis of SFAEs is usually limited by its low productivity, as the reaction only occurs in a medium where polar



sugar and non-polar fatty acid donor could be soluble. Some attempts were performed to find an adequate medium, which must fulfill solubilization requirements and preserve biocatalyst activity. Commercial immobilized CALB (Novozyme 435) was

applied for this purpose with low productivities (Ferrer et al., 1999).

Taking advantage of the high stability showed by mCLEA-CALB for the synthesis of biodiesel, the utility of this magnetic separable biocatalyst was tested for the transesterification of sucrose with different alkyl palmitate esters (vinyl, methyl and ethyl palmitate) as shown in **Figure 5C**. DMSO was selected as solvent due to its polar aprotic characteristic, dissolving both polar and non-polar compounds. The palmitate ester was added to 292 mM sucrose dissolved in DMSO in molar ratios sucrose:palmitate of 1:1, 1:2, and 1:3, and the enzymatic reaction using mCLEA-CALB was performed at 60°C for 24 h. **Figure 10** shows the results obtained by TLC analysis of the samples. After staining the plates with urea solution, the spots corresponding to sucrose and SMP became visible. Spots corresponding to SMP appeared only when vinyl palmitate was used as fatty acid

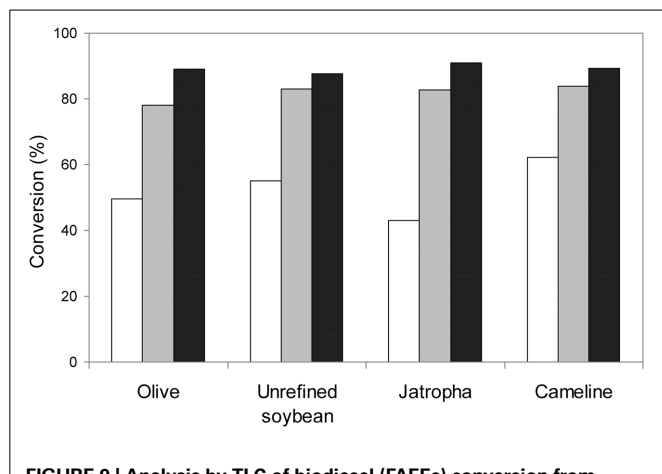


FIGURE 9 | Analysis by TLC of biodiesel (FAEEs) conversion from different non-edible vegetable oils catalyzed by magnetic biocatalysts of CALB. The reaction mixture containing 0.2 g oil, 2-propanol (6:1 alcohol:oil molar ratio) and 1% (w/w of oil) of catalyst was incubated for 72 h at 30°C with rotational mixing. MNP-CALB (white bars), mCLEA-CALB with 25 µg protein/mg MNP (gray bars), and mCLEA-CALB with 100 µg protein/mg MNP (black bars). Olive oil was used as a control.

donor, and the highest concentration corresponded to a molar ratio of 1:3. This result is consistent with previous studies, which point out that the vinyl alcohol formed during the process could tautomerize to the low-boiling-point acetaldehyde, shifting the equilibrium toward the ester formation. However, by employing alkyl fatty acid esters the transesterification reactions became reversible, resulting in low yields (Cruces et al., 2001).

Studies of soluble CALB and mCLEA-CALB stabilities in different polar and non-polar solvents revealed that the magnetic biocatalyst is much more stable than the free enzyme, although the stability in DMSO is still low (the half life of the magnetic enzyme is below 3 h, data not shown). Other solvents were tried in order to enhance enzyme stability, and the solubility losses were overcome with intense magnetic agitation. Results of reaction performed in 2M2P were compared to those obtained using DMSO in Table 3. The presence of DMSO inactivated the enzyme, resulting in a low conversion, which occurred in the first 5 h of reaction. However, taking advantage of stability improvement, mCLEA-CALB catalyzed the production of 40 mM SMP (23 g/l) using 2M2P as solvent.

CONCLUSIONS

In this paper we report that robust magnetically-separable biocatalysts of lipase show higher stability and better performance than the soluble enzymes. Moreover, they can be reused after easily recovery by a magnetic field avoiding the use of filtration or centrifugation which inevitably led to enzyme clumping. We have demonstrated the utility of these biocatalysts to catalyze reactions in both aqueous and non-aqueous media to obtain bioproducts of interest such as biodiesel or biosurfactants from sustainable and renewable sources. These results indicate that synergism of using properly functionalized magnetic nanosupports combined with suitable selection of the adequate enzyme can lead to the development of novel robust magnetic nanobiocatalysts of interest for

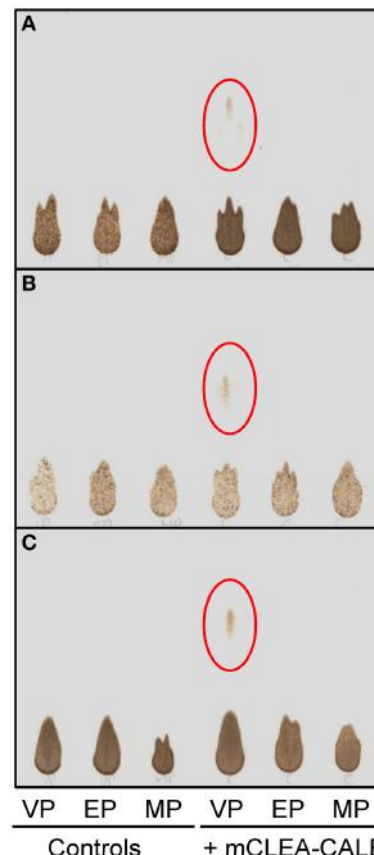


FIGURE 10 | Analysis by TLC of the SMP conversion from sucrose and different alkyl palmitates catalyzed mCLEA-CALB. The reaction mixture containing 100 mg/ml sucrose (292 mM), alkyl palmitate and 4 mg/ml mCLEA-CALB in 1 ml DMSO was incubated for 24 h at 60°C. Vinyl palmitate (VP), methyl palmitate (MP), and ethyl palmitate (EP) were used. Sucrose:alkyl palmitate molar rates were 1:1 in (A), 1:2 in (B), and 1:3 in (C).

Table 3 | Effect of the solvent used on the production of sucrose 6'-monopalmitate (SMP)^a.

Time (h)	SMP (mM)	
	Dimethylsulfoxide	2-Methyl-2-propanol
0	0	0
5	0.39	1.59
72	0.40	24.1
168	0.40	39.6

^aThe reaction mixture (5 ml) contained sucrose (292 mM) and vinyl palmitate (876 mM) in the presence of the solvents DMSO or 2M2P. mCLEA-CALB (20 mg) was used to catalyze the reaction at 60°C with magnetic stirring. At the indicated times samples were withdrawn and analyzed by HPLC-MS.

industry. Enzyme inactivation by solvents or byproducts during bioproducts obtainment can be minimized or avoided by searching for a robust enzyme. The combination of nanotechnology and biocatalysis represents a promising opportunity to develop novel

stable and efficient magnetic biocatalysts which can be easily recovered from the reaction mixture and reused in new catalytic cycles thus greatly improving the economic viability for its use to obtain bioproducts at industrial scale.

ACKNOWLEDGMENTS

This work was supported by grants from the University of the Basque Country (UPV/EHU, GIU11/25), the Spanish Ministry of Economy and Competitiveness (CTQ2011-25052), the Basque Government (SAIOTEK S-PE12UN041), and European Union (Energreen, POCTEFA EFA217/11). We are grateful to Mr. Ramiro Martínez (Novozymes A/S, Spain) for providing us with CALB samples. Álvaro Cruz-Izquierdo and Noelia Villarroel were the recipients of scholarships from the UPV/EHU.

REFERENCES

- Bisen, P. S., Sanodiya, B. S., Thakur, G. S., Baghel, R. K., and Prasad, G. B. (2010). Biodiesel production with special emphasis on lipase-catalyzed transesterification. *Biotechnol. Lett.* 32, 1019–1030. doi: 10.1007/s10529-010-0275-z
- Cao, L., van Rantwijk, F., and Sheldon, R. A. (2000). Cross-linked enzyme aggregates: a simple and effective method for the immobilization of penicillin acylase. *Org. Lett.* 2, 1361–1364. doi: 10.1021/o1005593x
- Cruces, M. A., Plou, F. J., Ferrer, M., Bernabé, M., and Ballesteros, A. (2001). Improved synthesis of sucrose fatty acid monoesters. *J. Am. Oil Chem. Soc.* 78, 541–546. doi: 10.1007/s11746-001-0300-5
- Cruz-Izquierdo, Á., Picó, E. A., Anton-Helas, Z., Boeriu, C. G., Llama, M. J., and Serra, J. L. (2012). Lipase immobilization to magnetic nanoparticles: methods, properties and applications for biobased products. *New Biotechnol.* 29S, S100–S101. doi: 10.1016/j.nbt.2012.08.283
- Dauphas, S., Ababou-Girard, S., Girard, A., Bihan, F. L., Mohammed-Brahim, T., Vié, V., et al. (2009). Stepwise functionalization of SiN_x surfaces for covariant immobilization of antibodies. *Thin Solid Films* 517, 6016–6022. doi: 10.1016/j.tsf.2009.05.014
- Dyal, A., Loos, K., Noto, M., Chang, S. W., Spagnoli, C., Shafi, K. V. P. M., et al. (2003). Activity of *Candida rugosa* lipase immobilized on $\gamma\text{-Fe}_2\text{O}_3$ magnetic nanoparticles. *J. Am. Chem. Soc.* 125, 1684–1685. doi: 10.1021/ja021223n
- Ferrer, M., Cruces, M. A., Bernabé, M., Ballesteros, A., and Plou, F. J. (1999). Lipase-catalyzed regioselective acylation of sucrose in two-solvent mixtures. *Biotechnol. Bioeng.* 65, 10–16.
- Ferrer, M., Plou, F. J., Fuentes, G., Cruces, M. A., Andersen, L., Kirk, O., et al. (2002). Effect of the immobilization method of lipase from *Thermomyces lanuginosus* on sucrose acylation. *Biocatal. Biotransform.* 20, 63–71. doi: 10.1080/10242420210153
- Gao, L., Xu, J.-H., Li, X.-J., and Liu, Z.-Z. (2004). Optimization of *Serratia marcescens* lipase production for enantioselective hydrolysis of 3-phenylglycidic acid ester. *J. Ind. Microbiol. Biotechnol.* 31, 525–530. doi: 10.1007/s10295-004-0182-1
- Gumel, A. M., Annuar, M. S. M., Heidelberg, T., and Chisti, T. (2011). Lipase mediated synthesis of sugar fatty acid esters. *Proc. Biochem.* 46, 2079–2090. doi: 10.1016/j.procbio.2011.07.021
- Holčapek, M., Jandera, P., Fischer, J., and Prokeš, B. (1999). Analytical monitoring of the production of biodiesel by high-performance liquid chromatography with various detection methods. *J. Chrom. A* 858, 13–31. doi: 10.1016/S0021-9673(99)00790-6
- Huang, D., Jiang, X., Zhu, H., Fu, X., Zhong, K., and Gao, W. (2010). Improved synthesis of sucrose fatty acid monoesters under ultrasonic irradiation. *Ultrasound Sonochim.* 17, 352–355. doi: 10.1016/j.ultsonch.2009.08.009
- Johnson, P. A., Park, H. J., and Driscoll, A. J. (2011). Enzyme nanoparticle fabrication: magnetic nanoparticle synthesis and enzyme immobilization. *Methods Mol. Biol.* 679, 183–191. doi: 10.1007/978-1-60761-895-9_15
- Kopp, W., da Costa, T. P., Pereira, S. C., Jafelicci, M. Jr., Giordano, R. C., Marques, R. F. C., et al. (2014). Easily handling penicillin G acylase magnetic cross-linked enzymes aggregates: catalytic and morphological studies. *Proc. Biochem.* 49, 38–46. doi: 10.1016/j.procbio.2013.09.024
- Leung, D. Y. C., Wu, X., and Leung, M. K. H. (2010). A review on biodiesel production using catalyzed transesterification. *Appl. Energy* 87, 1083–1095. doi: 10.1016/j.apenergy.2009.10.006
- Liese, A., and Hilterhaus, L. (2013). Evaluation of immobilized enzymes for industrial applications. *Chem. Soc. Rev.* 42, 6236–6249. doi: 10.1039/c3cs35511j
- Matsunaga, T., and Kamiya, S. (1987). Use of magnetic particles isolated from magnetotactic bacteria for enzyme immobilization. *Appl. Microbiol. Biotechnol.* 26, 328–332. doi: 10.1007/BF00256663
- Montoro-García, S., Gil-Ortíz, F., Navarro-Fernández, J., Rubio, V., García-Carmona, F., and Sánchez-Ferrer, A. (2010). Improved cross-linked enzyme aggregates for the production of desacetyl β -lactam antibiotics intermediates. *Biores. Technol.* 101, 331–336. doi: 10.1016/j.biortech.2009.08.016
- Nakamura, K., and Handa, S. (1984). Coomassie brilliant blue staining of lipids on thin-layer plates. *Anal. Biochem.* 142, 406–410. doi: 10.1016/0003-2697(84)90484-6
- Pesić, M., López, C., Álvaro, G., and López-Santín, J. (2012). A novel immobilized chloroperoxidase biocatalyst with improved stability for the oxidation of amino alcohols to amino aldehydes. *J. Mol. Catal. B Enz.* 84, 144–151. doi: 10.1016/j.molcatb.2012.04.010
- Ramírez, L. P., and Landfester, K. (2003). Magnetic polystyrene nanoparticles with a high magnetic content obtained by miniemulsion processes. *Macromol. Chem. Phys.* 204, 22–31. doi: 10.1002/macp.200290052
- Ren, Y., Rivera, J. G., He, L., Kulkarni, H., Lee, D. K., and Messersmith, P. B. (2011). Facile, high efficiency immobilization of lipase enzyme on magnetic iron oxide nanoparticles via a biomimetic coating. *BMC Biotechnol.* 11:63. doi: 10.1186/1472-6750-11-63
- Safarik, I., and Safarikova, M. (2009). Magnetic nano- and microparticles in biotechnology. *Chem. Papers* 63, 497–505. doi: 10.2478/s11696-009-0054-2
- Samakawa, T., Kaieda, M., Matsumoto, T., Ban, K., Kondo, A., Shimada, Y., et al. (2000). Pretreatment of immobilized *Candida antarctica* lipase for biodiesel fuel production from plant oil. *J. Biosci. Bioeng.* 90, 180–183. doi: 10.1016/S1389-1723(00)80107-3
- Sheldon, R. A. (2007). Cross-linked enzyme aggregates (CLEAs): stable and recyclable biocatalysts. *Biochem. Soc. Trans.* 35, 1583–1587. doi: 10.1042/BST0351583
- Sheldon, R. A. (2011). Characteristic features and biotechnological applications of cross-linked enzyme aggregates (CLEAs). *Appl. Microbiol. Biotechnol.* 92, 467–477. doi: 10.1007/s00253-011-3554-2
- Sheldon, R. A., and van Pelt, S. (2013). Enzyme immobilization in biocatalysis: why, what and how. *Chem. Soc. Rev.* 42, 6223–6235. doi: 10.1039/c3cs60075k
- Talekar, S., Ghodake, V., Ghogte, T., Rathod, P., Deshmukh, P., Nadar, S., et al. (2012). Novel magnetic cross-linked enzyme aggregates (magnetic CLEAs) of α -amylase. *Biores. Technol.* 123, 542–547. doi: 10.1016/j.biortech.2012.07.044
- Tudorache, M., Nae, A., Coman, S., and Parvulescu, V. (2013). Strategy of cross-linked enzyme aggregates onto magnetic particles adapted to the green design of biocatalytic synthesis of glycerol carbonate. *RSC Adv.* 3, 4052–4058. doi: 10.1039/c3ra23222k
- Uppenberg, J., Hansen, M. T., Patkar, S., and Jones, T. A. (1994). The sequence, crystal structure determination and refinement of two crystal forms of lipase B from *Candida antarctica*. *Structure* 2, 293–308. doi: 10.1016/S0969-2126(00)00031-9
- van den Broeck, L. A. M., and Boeriu, C. G. (2013). Enzymatic synthesis of oligo- and polycarbohydrate fatty acid esters. *Carbohydr. Polym.* 93, 65–72. doi: 10.1016/j.carbpol.2012.05.051
- van Kempen, S. E. H. J., Boeriu, C. G., Schols, H. A., de Waard, P., van der Linden, E., and Sagis, L. M. C. (2013). Novel surface-active oligofructose fatty acid mono-esters by enzymatic esterification. *Food Chem.* 138, 1884–1891. doi: 10.1016/j.foodchem.2012.09.133
- Verma, M. L., Barrow, C. J., and Puri, M. (2013). Nanobiotechnology as a novel paradigm for enzyme immobilisation and stabilisation with potential applications in biodiesel production. *Appl. Microbiol. Biotechnol.* 97, 23–39. doi: 10.1007/s00253-012-4535-9
- Wang, M., Jia, C., Qi, W., Yu, Q., Peng, X., Su, R., et al. (2011). Porous-CLEAs of papain: application to enzymatic hydrolysis of macromolecules. *Biores. Technol.* 102, 3541–3545. doi: 10.1016/j.biortech.2010.08.120

- Xin, B. J., Si, S. F., and Xing, G. W. (2010). Protease immobilization on γ -Fe₂O₃/Fe₃O₄ magnetic nanoparticles for the synthesis of oligopeptides in organic solvents. *Chem. Asian J.* 5, 1389–1394. doi: 10.1002/asia.200900696
- Yiu, H. H. P., and Keane, M. A. (2012). Enzyme-magnetic nanoparticle hybrids: new effective catalysts for the production of high value chemicals. *J. Chem. Technol. Biotechnol.* 87, 583–594. doi: 10.1002/jctb.3735

Conflict of Interest Statement: The authors declare that the research was conducted in the absence of any commercial or financial relationships that could be construed as a potential conflict of interest.

Received: 30 April 2014; accepted: 08 August 2014; published online: 26 August 2014.

Citation: López C, Cruz-Izquierdo Á, Picó EA, García-Bárcena T, Villarroel N, Llama MJ and Serra JL (2014) Magnetic biocatalysts and their uses to obtain biodiesel and biosurfactants. *Front. Chem.* 2:72. doi: 10.3389/fchem.2014.00072
This article was submitted to Chemical Biology, a section of the journal *Frontiers in Chemistry*.

Copyright © 2014 López, Cruz-Izquierdo, Picó, García-Bárcena, Villarroel, Llama and Serra. This is an open-access article distributed under the terms of the Creative Commons Attribution License (CC BY). The use, distribution or reproduction in other forums is permitted, provided the original author(s) or licensor are credited and that the original publication in this journal is cited, in accordance with accepted academic practice. No use, distribution or reproduction is permitted which does not comply with these terms.



Development of organophosphate hydrolase activity in a bacterial homolog of human cholinesterase

Patricia M. Legler^{1*}, Susanne M. Boisvert², Jaimee R. Compton³ and Charles B. Millard⁴

¹ Naval Research Laboratory, Center for Bio/Molecular Science and Engineering, Washington, DC, USA

² Department of Chemistry, Texas State University, San Marcos, TX, USA

³ Nova Research Inc., Alexandria, VA, USA

⁴ United States Army Medical Research and Materiel Command, Fort Detrick, MD, USA

Edited by:

Carissa M. Soto, Naval Research Laboratory, USA

Reviewed by:

Jiaoyang Jiang, University of Wisconsin-Madison, USA
Christian W. Gruber, Medical University of Vienna, Austria
Markus Kaiser, University of Duisburg-Essen, Germany

***Correspondence:**

Patricia M. Legler, Naval Research Laboratory, Center for Bio/Molecular Science and Engineering, 4555 Overlook Ave., Washington, DC 20375, USA
e-mail: patricia.legler@nrl.navy.mil

We applied a combination of rational design and directed evolution (DE) to *Bacillus subtilis* p-nitrobenzyl esterase (pNBE) with the goal of enhancing organophosphorus acid anhydride hydrolase (OPAAH) activity. DE started with a designed variant, pNBE A107H, carrying a histidine homologous with human butyrylcholinesterase G117H to find complementary mutations that further enhance its OPAAH activity. Five sites were selected (G105, G106, A107, A190, and A400) within a 6.7 Å radius of the nucleophilic serine O_y. All 95 variants were screened for esterase activity with a set of five substrates: pNP-acetate, pNP-butyrate, acetylthiocholine, butyrylthiocholine, or benzoylthiocholine. A microscale assay for OPAAH activity was developed for screening DE libraries. Reductions in esterase activity were generally concomitant with enhancements in OPAAH activity. One variant, A107K, showed an unexpected 7-fold increase in its k_{cat}/K_m for benzoylthiocholine, demonstrating that it is also possible to enhance the cholinesterase activity of pNBE. Moreover, DE resulted in at least three variants with modestly enhanced OPAAH activity compared to wild type pNBE. A107H/A190C showed a 50-fold increase in paraoxonase activity and underwent a slow time- and temperature-dependent change affecting the hydrolysis of OPAA and ester substrates. Structural analysis suggests that pNBE may represent a precursor leading to human cholinesterase and carboxylesterase 1 through extension of two vestigial specificity loops; a preliminary attempt to transfer the Ω-loop of BChE into pNBE is described. Unlike butyrylcholinesterase and pNBE, introducing a G143H mutation (equivalent to G117H) did not confer detectable OP hydrolase activity on human carboxylesterase 1 (hCE1). We discuss the use of pNBE as a surrogate scaffold for the mammalian esterases, and the importance of the oxyanion-hole residues for enhancing the OPAAH activity of selected serine hydrolases.

Keywords: organophosphate, cholinesterase, directed evolution, catalytic bioscavenger, nerve agent, hysteresis

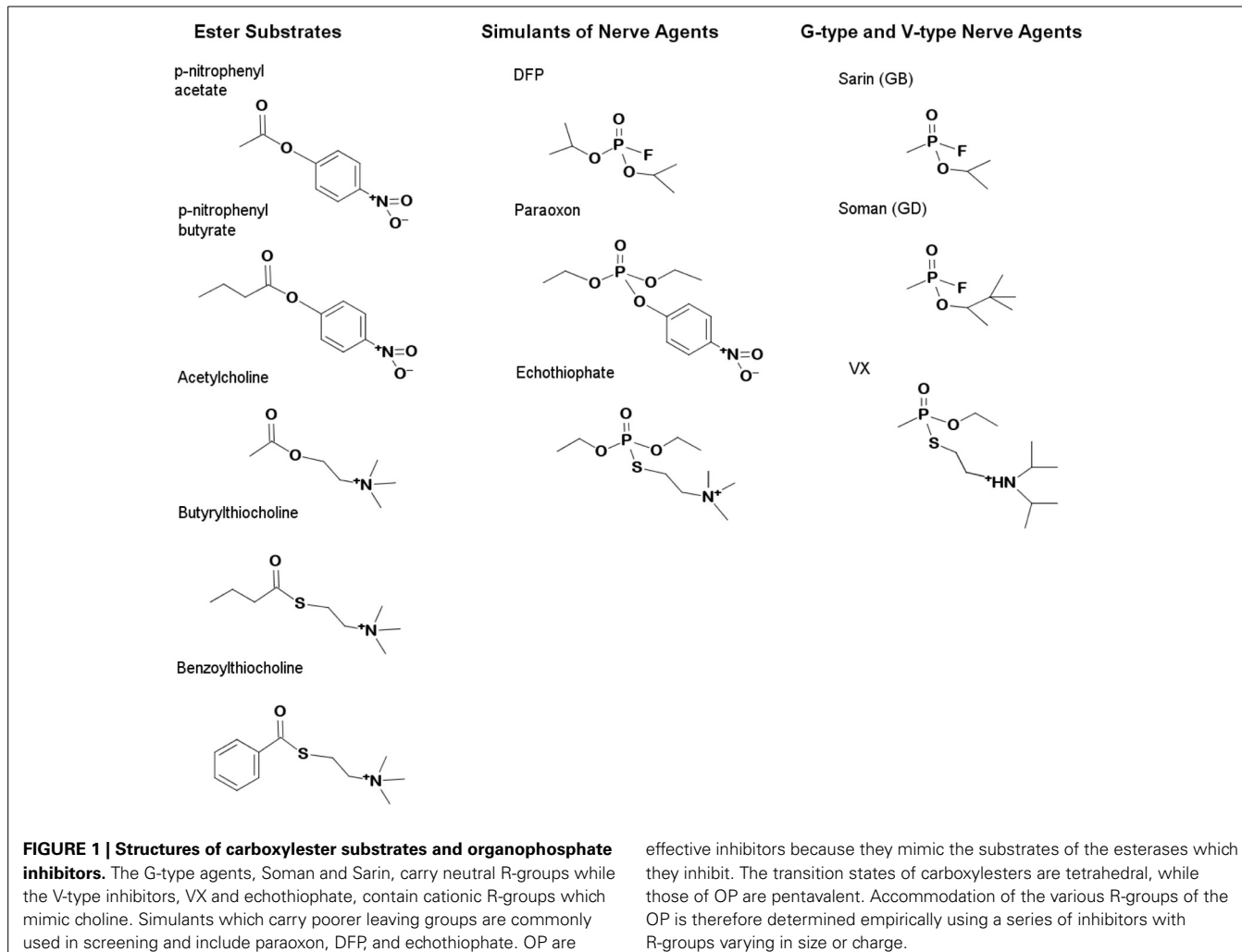
INTRODUCTION

Butyrylcholinesterase (BChE; EC 3.1.1.8) and its genetically engineered variants are being developed as therapeutic enzyme “bioscavengers” of organophosphorus acid anhydrides (OPAA) to prevent or treat OPAA poisoning (Millard et al., 1995a; Doctor and Saxena, 2005; Saxena et al., 2006) and also have been investigated to reverse cocaine addiction (Xie et al., 1999; Zheng and Zhan, 2008; Masson and Rochu, 2009). OPAA compounds (**Figure 1**) are highly toxic or lethal primarily because they

rapidly, completely, and irreversibly inhibit essential biological stores of synaptic acetylcholinesterase (AChE; EC 3.1.1.7) leading to rigid paralysis, asphyxiation, and seizures (Shih et al., 2003). OPAA are archetypical irreversible inhibitors of serine hydrolases (**Scheme S1**), but in some cases the inhibition is slowly reversed (half-time of hours or days) because the phosphorylated esterase undergoes spontaneous hydrolysis of the covalent adduct to yield reactivated enzyme (Main, 1979). Human BChE has been proposed as a prophylactic antidote because it is able to react rapidly with essentially all toxic pesticides and military “nerve agents” in the blood stream to prevent inhibition of AChE (reviewed in Ashani, 2000; Doctor and Saxena, 2005; Nachon et al., 2013).

The primary limitation to employing natural human BChE as a therapeutic is that each enzyme molecule can react only once with an OPAA inhibitor molecule and therefore will require an estimated dose of 200–1820 mg/70 kg of BChE to confer protection against 2 × LD₅₀ of most nerve agents (Ashani, 2000; Geyer et al., 2010). For therapeutic enzyme bioscavengers, catalyzed

Abbreviations: AtCh, acetylthiocholine; BME, beta-mercaptopethanol; BtCh, butyrylthiocholine; BzCh, benzoylthiocholine; CD, circular dichroism; CE, carboxylesterase; DMSO, dimethylsulfoxide; DTNB, dithiobis(2-nitrobenzoic acid); DTT, dithiothreitol; EB, equilibration buffer; hCE1, human carboxylesterase 1; IPTG, isopropyl-β-thiogalactoside; Ω-loop, residues between Cys-67-Cys-94 (TcAChE numbering); OPAA, organophosphorus acid anhydride inhibitors; OPAAH, organophosphorus acid anhydride hydrolase; paraoxon, diethyl p-nitrophenylphosphate; pNBE, p-nitrobenzylesterase; pNPA, p-nitrophenyl acetate; pNPB, p-nitrophenyl butyrate; SDS-PAGE, sodium dodecyl sulfate polyacrylamide gel electrophoresis; WT, wild type.



turnover could significantly enhance the rate of OPAA hydrolysis and reduce the amount of enzyme needed for protection. Using rational protein design, Millard and colleagues introduced a single histidine residue (G117H) into the oxyanion hole of human BChE to increase the rate of spontaneous reactivation and thereby convert OPAs from inhibitors into xenobiotic substrates which could be hydrolyzed by the mutant enzyme (Millard et al., 1995a; Lockridge et al., 1997). G117H enhanced the hydrolysis of paraoxon or echothiophate by 100,000-fold (Lockridge et al., 1997), and a second mutation (G117H/E197Q) permitted hydrolysis of even the most toxic nerve agents known (soman, sarin, or VX) by increasing the rate of spontaneous reactivation and simultaneously decreasing an unwanted side reaction known as “aging” (**Scheme S1**) (Shafferman et al., 1996; Millard et al., 1998).

Cholinesterase “aging” is an irreversible dealkylation of the phosphorylated serine that proceeds through enzyme-catalyzed formation of a carbocation leaving group (**Scheme S1**) (Michel et al., 1967; Li et al., 2007; Masson et al., 2010). Dealkylation results in an anionic phosphoester adduct that is resistant to nucleophilic attack. Aging involves the same cholinesterase residues that stabilize the binding of positively charged leaving groups of choline esters or V-type nerve agents (VX and VR),

including, Glu-197, and Trp-82 within the Ω -loop of BChE (**Figure S1**, **Figure 2**) (Hosea et al., 1996; Masson et al., 1997a; Kua et al., 2003). Cholinesterases are predominantly found in higher eukaryotes and the Ω -loop may have arisen specifically to bind and hydrolyze choline esters (**Figure 2**) because very few esterases react efficiently with cationic ligands (Cousin et al., 1996). Structurally related esterases [such as human carboxylesterase (hCE)] that lack the homologous Trp do not exhibit significant cholinesterase activity and do not undergo comparable aging after OPAA inhibition (Hemmert et al., 2010).

Human BChE and its variants offer several important advantages as therapeutic enzymes (Doctor and Saxena, 2005), and transgenic animals bearing the G117H BChE variant have shown limited resistance to OPAA poisoning (Wang et al., 2004). A pegylated WT BChE enzyme (Protezia[®]) has also shown protection *in vivo* against soman and VX (Lenz et al., 2007; Mumford and Troyer, 2011). In addition to BChE, other enzymes such as AChE, hCE, or the metalloenzyme paraoxonase (PON1) have shown promise as bioscavengers. Both BChE (Saxena et al., 2006; Lenz et al., 2007; Mumford and Troyer, 2011) and PON1 (Costa et al., 1990; Li et al., 1995; Valiyaveettil et al., 2011) have shown limited protection against nerve agent and OP-pesticide intoxication in

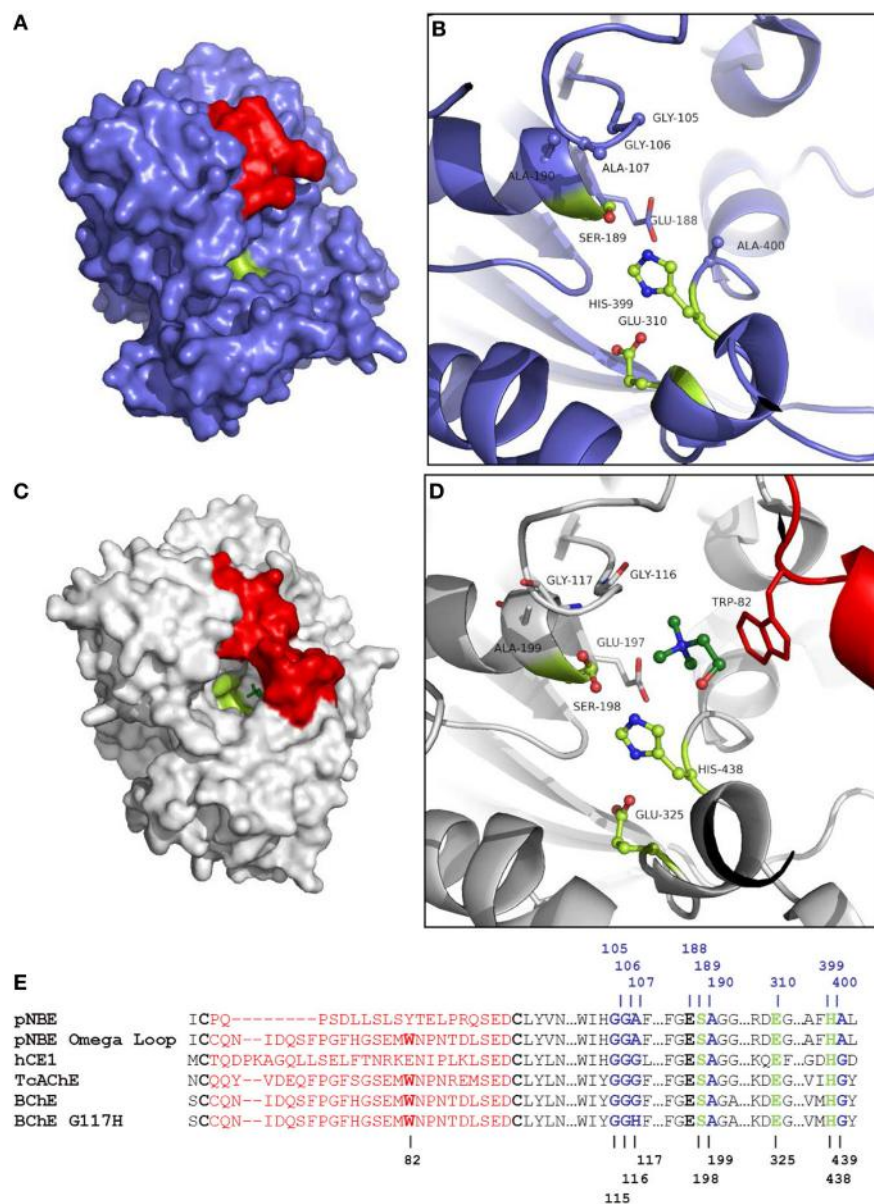


FIGURE 2 | Comparison of pNBE and BChE. **(A)** Structure of pNBE (PDB 1QE3) (Spiller et al., 1999). **(B)** Active site of WT pNBE. The catalytic triad, Glu-310, His-399, Ser-189, is shown in lime. The residues selected for DE (G105, G106, A107, A190, and A400) are shown in blue ball and stick representation. The A107 residue is equivalent to G117 in butyrylcholinesterase. Structured residues between Cys-61 and Cys-82 corresponding to the Ω -loop of BChE are shown in red. pNBE and BChE are structurally similar and two structures can be superposed with an rmsd = 2.1 Å over 350 C_{α} . **(C)** Structure of BChE (PDB 1P0M) (Nicolet et al., 2003). The Ω -loop of BChE is shown in red, choline is shown in dark green. The narrow gorge of BChE is partially formed by the Ω -loop. The catalytic triad is found at the bottom of the gorge. **(D)** The Ω -loop forms

part of the choline binding site and carries Trp-82; this residue forms an energetically significant cation-pi interaction with cationic choline substrates (Ordentlich et al., 1993, 1995). Glu-197 also plays an important role in choline binding (Ordentlich et al., 1995; Masson et al., 1997b), and a residue equivalent to Glu-197 is present in pNBE. **(E)** Partial sequence alignment of pNBE, the pNBE Ω -loop variant, hCE1, TcAChE, BChE, and BChE G117H variant. The Ω -loop residues between Cys-65 and Cys-92 are shown in red and are unstructured in pNBE [PDB 1QE3 (Spiller et al., 1999)]. The Ω -loop of BChE was transferred to pNBE to form the chimeric variant. The Ω -loop is well formed in hCE1, AChE, and BChE. The Trp residue of the choline binding site is notably absent from pNBE and hCE1. The roles of these residues in catalysis are shown in **Figure S1**.

animal models. PON1 has been mutated to hydrolyze both G-type (soman and sarin) and V-type (VX) nerve agents (Cherny et al., 2013; Kirby et al., 2013). While PON1 is able to hydrolyze selected OP nerve agents at much faster rates *in vitro* than G117H or hCE, the K_m values for WT PON1 and its variants are in

the millimolar range (Otto et al., 2010). High turnover numbers can be achieved by PON1 at saturating concentrations of OPAA (Kirby et al., 2013) but these concentrations are well above the levels of nerve agent that can be tolerated in living systems ($LD_{50}^{\text{soman}} = 113 \mu\text{g/kg} = 0.00062 \text{ mmol/kg}$ in mice; Maxwell and

Koplovitz, 1990) and the IC₅₀ of AChE (IC₅₀^{soman} = 0.88–2.53 nM, IC₅₀^{sarin} = 3.27–6.15 nM; Fawcett et al., 2009). Consequently, each class of enzyme bioscavenger has advantages and disadvantages (Trovaslet-Leroy et al., 2011), and efforts to improve binding and expand the substrate specificities of several candidates is ongoing (Otto et al., 2010; Trovaslet-Leroy et al., 2011; Kirby et al., 2013; Mata et al., 2014).

Unfortunately, the modest OPAA rate enhancements conferred on BChE by the G117H mutation have not been improved upon for the past two decades (Millard et al., 1995a, 1998; Lockridge et al., 1997). Emerging technologies for protein engineering, especially directed evolution (DE) or biological incorporation of unnatural amino acids into the active site to improve OPAAH rates, have not been applied to cholinesterases largely because these eukaryotic enzymes have complex tertiary structures with extensive post-/co-translational modifications (e.g., glycosylation, GPI-anchor, disulfides) and, therefore, are not amenable to facile manipulation and expression in prokaryotic systems (Masson et al., 1992; Ilyushin et al., 2013). In contrast, DE has been successfully applied to paraoxonase using variants of human PON1 which produce soluble and active enzyme in *E. coli* (Aharoni et al., 2004).

To explore a combination of rational design and DE methods on a bacterial enzyme that shares the cholinesterase fold, we selected *Bacillus subtilis* p-nitrobenzyl esterase (pNBE, EC 3.1.1.-; Spiller et al., 1999). We chose pNBE as a surrogate scaffold because: (i) the X-ray structures suggest that pNBE may represent a prokaryotic structural precursor to the cholinesterases (AChE or BChE) (Spiller et al., 1999), as well as to the related family of hCE (Figure S1); (ii) pNBE appears to have a more open active site (Figure 2) and was shown previously to permit DE modifications of substrate specificity loops without compromising protein folding (Giver et al., 1998; Spiller et al., 1999); and (iii) pNBE, like the family of hCE (Fleming et al., 2007), lacks the amino acid present in BChE and AChE that is known to promote the deleterious aging reaction (e.g., W82 of BChE) (Masson et al., 1997a). We created and screened a library of 162 pNBE variants to identify mutations which could enhance OPAAH activity and expand the substrate and inhibitor specificities of this enzyme. The mutations were then transferred to hCE1 to determine if pNBE could be used as a surrogate scaffold. We identified one pNBE variant with a three-order of magnitude enhancement in somanase activity compared with WT. Unexpectedly, the variant with the largest enhancement in OPAA activity also underwent a slow time- and temperature-dependent change in activity. We correlate our results with the solved X-ray structures of pNBE to understand possible mechanisms for engineered OPAAH activity, and discuss complications posed by hysteretic forms in the kinetic and structural analysis of mutant pNBE, AChE and BChE (Masson et al., 2005; Badiou et al., 2008; Lushchekina et al., 2014).

MATERIALS AND METHODS

MATERIALS

BugBuster™ and the pTriEx-3 vector were from Novagen (San Diego, CA). Chelating Sepharose, Q-Sepharose, and PD-10 columns were from GE Healthcare Life Sciences (Piscataway, NJ). QuikChange™ kits were purchased from Stratagene (La

Jolla, CA). Benzoylthiocholine (BzCh) was purchased from TCI America (Portland, OR). The 96-well, clear polystyrene HIS-Select® High Capacity Nickel Coated Plates were purchased from Sigma. All other chemicals were purchased from Sigma. Echothiophate was from Wyeth Pharmaceuticals Inc. (Philadelphia, PA).

CONSTRUCTION OF THE DE LIBRARY

Five sites in pNBE were selected for the directed-evolution library: G105, G106, A107, A190, and A400. The C_α of each of the five residues was between 5.0 and 6.7 Å from the Ser-189-Oγ. The A107H mutation was also present in each starting variant with the exception of the twenty variants of A107. The plasmids of the DE library were synthesized by GeneArt, Inc. (Regensburg, Germany). The pNBE expression vector (pTriEx-3, Novagen Inc.) contained an N-terminal PreScission™ Protease cleavage site and a hexa-histidine tag preceding the pNBE sequence.

CONSTRUCTION OF THE CHIMERIC BChE/pNBE Ω-LOOP VARIANT

The megaprimer method (Sarkar and Sommer, 1990) was used to construct the chimeric BChE-pNBE variant. A megaprimer containing a sequence from one of the known cholinesterase substrate specificity loops, in this case the “Ω-loop” of BChE, was used to replace the homologous sequence in pNBE. The variant was sequenced to confirm the substitution. Protein sequences are included in the **Supplemental Information**.

SMALL SCALE PROTEIN EXPRESSION AND PURIFICATION

All 95 constructs in the DE library expressed soluble protein under these conditions. Four milliliter cultures of LB containing 100 µg/mL Ampicillin were inoculated with frozen glycerol stocks and grown for 3 h at 37°C with shaking (200 rpm). Cultures were induced with 1 µL of 1.0 M IPTG overnight at 17°C. Bacteria were pelleted and then lysed in 0.5 mL Lysis Buffer (87.5% BugBuster™, 2 mM BME, 50 mM Tris pH 7.6, 375 mM NaCl) at room temperature (17–22°C) for at least 1 h. Lysed bacteria were centrifuged at 4800 × g for 10 min. Clarified lysates were then loaded onto nickel-charged Chelating Sepharose columns (0.5 mL slurry per disposable column) equilibrated with three column volumes of equilibration buffer (EB; 50 mM Tris pH 7.6, 500 mM NaCl, 2 mM BME). After the supernatant was loaded, the columns were washed again with three column volumes of EB. To elute contaminants, the columns were washed with three column volumes of EB containing 60 mM Imidazole. Proteins were isocratically eluted with EB containing 300 mM Imidazole. Imidazole readily reacts with the carboxyl ester substrates used to assay the enzyme; thus, it was necessary to buffer exchange the enzymes with BioMax (10,000 NMWL) ultrafiltration units three times with 50 mM HEPES pH 7.0, 150 mM NaCl to remove the imidazole. Purified enzymes ran as single bands in SDS-PAGE gels and were judged to be ≥90% pure.

LARGE SCALE PROTEIN EXPRESSION AND PURIFICATION

Large scale preps of selected variants were used for kinetic analysis. LB (1–3 L) containing 100 µg/mL Ampicillin was grown with shaking at 37°C and induced overnight with 0.2 mM IPTG at 17°C. Bacterial pellets were lysed in 40 mL of lysis buffer containing ~30 mg lysozyme and then sonicated for 1 min in an ice bath.

Lysates were clarified by centrifugation (30 min at 20,500 × g). Supernatants were loaded onto a 20 mL nickel-charged Chelating Sepharose column. After loading, the column was washed with EB containing 60 mM imidazole until the A_{280} returned to a level baseline. Protein was eluted with EB containing 300 mM imidazole. Fractions containing pNBE were combined and dialyzed against 50 mM Tris pH 7.6, 150 mM NaCl, 2 mM BME. Protein was loaded onto a 30 mL Q-Sepharose column and eluted between 260 and 400 mM NaCl during the gradient.

CARBOXYLESTERASE ASSAYS

Steady state kinetic parameters for the enzyme catalyzed hydrolysis of p-nitrophenyl acetate (pNPA) and p-nitrophenyl butyrate (pNPB) were measured in triplicate at room temperature in 50 mM HEPES 7.0, 150 mM NaCl (405 nm). Substrate and inhibitors were dissolved in DMSO and accounted for less than 1% of the reaction volume.

Acetylthiocholine (AtCh), butyrylthiocholine (BtCh), or benzoylthiocholine (BzCh) hydrolysis was measured in triplicate at 412 nm in cuvettes or a plate reader using Ellman's reagent (0.5 mM DTNB) (Ellman et al., 1961). All assays were done in 1× Sorensen's buffer (53.4 mM Na_2HPO_4 , 13.4 mM KH_2PO_4) pH 7.4 at room temperature ($22 \pm 2^\circ\text{C}$). An extinction coefficient of $13.6 \text{ mM}^{-1}\text{cm}^{-1}$ was used for calculations. One Unit of activity (U) was defined as 1 μmol product produced per min, and specific activity (S.A.) was defined as Units per milligram of enzyme (U/mg).

PRIMARY ASSAY FOR SCREENING

HIS-Select® plates were washed once with 200 μL of binding buffer (50 mM Hepes pH 7.0, 150 mM NaCl). Each his-tagged protein ($\sim 25 \text{ mU}$) in the same buffer (100 μL) was added to two wells and allowed to bind for 1 h at 37°C . All wells contained enzyme after each plate setup. The OPAA inhibitor was added (0.5–5 μL) to one of the two wells and incubated for 10 min at room temperature. Cautionary note: the OPAA compounds used in this study are highly toxic and must only be handled with adequate legal authority, training, and safety precautions. Liquid was removed by a multichannel pipettor, and plates were washed four times with 200 μL of appropriate reaction buffer. Buffer (90 or 95 μL) and 0.5 M EDTA (10 or 5 μL) were then added to each well to elute the protein. Plates were left at room temperature or at 37°C , and aliquots of enzyme (10 μL) were removed over time and assayed in separate 96-well plates using 5 mM pNPButyrate in binding buffer. Activity was measured at 4–6 time points to confirm reactivation of a single clone. For the clones which reactivated in the 96-well assay, large scale preps were then used to more accurately quantitate the enhancements in the rates of reactivation.

LARGE SCALE DISCONTINUOUS SPONTANEOUS REACTIVATION ASSAYS

Spontaneous reactivation was measured essentially as previously described (Millard et al., 1995a; Lockridge et al., 1997). Briefly, an aliquot of uninhibited enzyme or the OPAA-inhibited (>95% inhibited) enzyme was loaded onto PD-10 gel filtration columns equilibrated with 50 mM Tris pH 7.6, 150 mM NaCl, 2 mM BME. At time $t = 0$, the columns were loaded, and the protein was

rapidly eluted; fractions were incubated at 37°C , activity was measured for the uninhibited enzyme, and inhibited enzyme and percentages of reactivated enzyme were calculated. The pseudo first order rate constant for spontaneous reactivation due to the hydrolysis of the serinyl-phosphate adduct, k_r , was determined by fitting the data to the following equation (Wang and Braid, 1967; Main, 1979):

$$A_t = A_{\max} \left(1 - e^{-k_r t} \right)$$

where A_t is the percent reactivated at time t and A_{\max} is the maximal percent reactivated at final observation time $>> t_0$. For the A107H/A190C variant, which exhibited a form of hysteresis (Hanozet et al., 1981; Uto and Brewer, 2008), the enzyme was incubated at 37°C for at least 2 h after exchanging the buffer using a PD-10 column equilibrated with 50 mM Tris pH 7.6, 150 mM NaCl, 2 mM BME. The enzyme was then inhibited, and rates of reactivation were measured.

ORGANOPHOSPHATE INACTIVATION

Aliquots of enzyme were inhibited with different concentrations of inhibitor, and the activity was measured discontinuously using pNPButyrate at different time points. Data were plotted and fit to a single exponential decay equation to obtain k_{obs} , the observed first order rate constant. A secondary plot was used to determine the maximal rate constant for inactivation, k_2 , at infinite inhibitor concentration. The rate constant was determined by plotting k_{obs} vs. [I] concentration and fitting the data to the following equation (or by extrapolation using the double-reciprocal form of the equation) from Kitz and Wilson (1962):

$$k_{obs} = \frac{k_2}{1 + K_p/[I]}$$

The apparent bimolecular rate constant, k_i , for formation of the covalent E-I complex from free enzyme and free inhibitor was calculated according to the following:

$$k_i = k_2/K_p$$

where K_p is a Michaelis-type constant for the inhibitor.

RESULTS

SELECTION OF RESIDUES FOR DIRECTED EVOLUTION (DE)

Prior to the creation of the DE library, we produced the A107H pNBE variant by analogy with BChE G117H (Millard et al., 1995a; Lockridge et al., 1997) and demonstrated that it possesses increased OPAAH activity (Table 1). The OPAAH activity of the pNBE A107H variant was found to be acid-catalyzed and 4-fold higher at pH 7.0 than at pH 7.6 (Table 1). At pH 7.0 the reactivation rate of the A107H variant was 46-fold higher when compared with WT and 18-fold higher at pH 7.6.

To identify mutations which could further enhance the OPAAH activity of A107H, we constructed a DE library of double mutants at five different sites: A107H/G105X, A107H/G106X, A107H/A190X, and A107H/A400X (where X stands for any amino acid). We also examined the A107X single mutation variants of pNBE. Each residue selected for DE (G105, G106, A107,

Table 1 | pH dependence of reactivation rates after inhibition with ethyl paraoxon.

Enzyme	Inhibitor	pH	% Reactivation	$k_{\text{reactivation}}$ (1/h)
WT	Paraoxon	7.6	110 ± 10%	0.03 ± 0.01
	Paraoxon	7.0	91 ± 8	0.05 ± 0.01
	Paraoxon	6.5	88 ± 6	0.035 ± 0.007
	Paraoxon	6.0	52 ± 2	0.042 ± 0.005
A107H	Paraoxon	7.6	102 ± 5	0.53 ± 0.09
	Paraoxon	7.0	90 ± 10	2.3 ± 0.3
BChE Ω Loop Mutant with A107H	Paraoxon	7.6	86 ± 4	1.0 ± 0.1

Rates were measured in 50 mM Tris pH 7.6, 150 mM NaCl, 2 mM BME; 50 mM Hepes 7.0, 150 mM NaCl, 2 mM BME; 50 mM MES pH 6.5, 150 mM NaCl, 2 mM BME; or 50 mM MES pH 6.0, 150 mM NaCl, 2 mM BME at 37°C.

A190, or A400) was within 6.7 Å of the Oγ of the nucleophilic Ser-189 in pNBE and was conserved in BChE and hCE1 (**Figure 2**). Based upon the X-ray structure of pNBE, we concluded that the backbone NH groups of G106, A107, and A190 form a 3-point oxyanion hole (**Figure S1**). Gly-105 is situated near the oxyanion hole, but is not part of the oxyanion hole. The corresponding G105A variant in human AChE affected the turnover number of the substrate, but not the K_m ; this substitution was suggested to affect the conformational mobility of the adjacent residues of the oxyanion hole (Ordentlich et al., 1998). The side-chain of Alanine-190 was hypothesized to exert an effect on the polarity and/or orientation of the backbone NH groups of A107 and G106 and thereby affect TS stabilization. The oxyanion hole is the primary source of transition state stabilization in serine hydrolases (Bryan et al., 1986). The A190 side-chain is situated directly behind the loop carrying A107 and G106. The Cβ of A190 is 3.6–3.7 Å away from the backbone NH of A107 and G106 (**Figures S1B,D**). The A400 residue is located on a loop of pNBE. The A400T mutation in pNBE was shown previously to project into the active site (6.7 Å from the Ser-189-Oγ) and enhance the thermostability of pNBE in DE experiments by Spiller et al. (1999). Spiller et al. proposed that the Thr side-chain of residue-400 may stabilize His-399 of the catalytic triad. A400 was also near the choline leaving group in overlays of pNBE with a BChE-choline co-crystal structure (1P0M) (Nicolet et al., 2003) (**Figure S1C**). We selected it here to find variants which might stabilize a particular conformer of His-399 or stabilize the alkyl groups of the soman pinacolyl group, the DFP *iso*-propyl groups, or, alternatively, the cationic choline-like leaving groups of V-type nerve agents and simulants (e.g., echothiophate).

SUBSTRATE SPECIFICITY

Five substrates were tested with single point assays and the DE library of variants to determine if the mutations altered substrate specificities: pNPA, pNPB, AtCh, BtCh, and BzCh (**Figure S2**). WT pNBE had the highest substrate specificity for pNP-butrate as judged by the bimolecular rate constant, $k_{\text{cat}}/K_m = 14,000 \pm 2000 \text{ min}^{-1} \text{ mM}^{-1}$. A detectable level of CE activity is needed to measure reactivation rates by the discontinuous method.

All 95 of the variants had detectable levels of CE activity when pNP-butrate was used as the substrate. This allowed the use of a common substrate for activity measurements at different time points during reactivation experiments. No significant enhancement in the substrate specificities of the DE library variants for pNPA or pNPB was observed.

CHARACTERIZATION OF VARIANTS WITH ENHANCED CHOLINESTERASE ACTIVITY

Ideally, universal OP bioscavenging enzymes should scavenge both G-type and V-type agents (**Figure 1**). V-type agents, such as VX and VR, and V-type simulants like echothiophate mimic positively charged choline esters (**Scheme S1**) and readily inhibit AChE and BChE. Echothiophate and VX are slowly turned over by the BChE G117H variant (Millard et al., 1995a). Cholinesterase activity can only be found in a subset of esterases, typically those of eukaryotes (Cousin et al., 1996). The cationic choline esters are accommodated by two key residues at the bottom of the gorge of BChE and AChE, Trp-84/82, and Glu-199/197 (TcAChE/BChE numbering) (Ordentlich et al., 1995). These residues also play a role in the binding specificity of tetrahedral cationic V-type agents in AChE (Hosea et al., 1996), as well as in the unfavorable “aging” process (Shafferman et al., 1996). A residue within the peripheral anionic site (PAS) at the top of the gorge, Asp-72/70, also plays a role in V-type agent binding (Hosea et al., 1996), but is relatively distant from the choline binding pocket (~7 Å); hCE1 and pNBE lack a homologous Asp residue (**Figure 2E**). Since hCE1 and pNBE are structurally similar to AChE and BChE (**Figure S1A**) but are not known to hydrolyze choline esters or become inhibited by V-type agents, we also examined the DE library for the development of cholinesterase activity and susceptibility to inhibition by echothiophate (last section).

Cholinesterases contain an omega-shaped loop between the disulfide bonded cysteines, Cys-67 and Cys-94 (TcAChE numbering) (**Figure 2**, **Figure S1**). The Ω-loop carries Asp-72/70 and Trp-84/82 of the choline binding site. To determine if a cholinesterase Ω-loop could be inserted, we substituted the Ω-loop sequence of BChE into the pNBE A107H variant. The chimeric variant folded as a functional esterase (**Table 2**). The K_m and k_{cat} values for pNPA were similar to those of the WT enzyme. However, the loop insertion alone did not confer cholinesterase activity, and the k_{cat} and K_m for BzCh and BtCh were similar to those of the A107H pNBE variant (**Table 3**). Thus, the DE library was made with the A107H pNBE variant, rather than the loop-insertion variant.

All 95 variants were initially examined for cholinesterase activity using single point assays (**Figure S2**). To determine if the pNB-esterase variants could bind and turnover cationic OPAA like echothiophate, we first looked for cholinesterase activity. AChE, BChE, hCE1, and pNB-esterase all share the same fold (**Figure S1A**). Steady state kinetic parameters for the variants which showed significant increases in cholinesterase activity are shown in **Table 3**. Unexpectedly, the variant which showed the largest increase in cholinesterase activity was a single mutant with a positively charged lysine residue, A107K. This variant showed a 7-fold increase in the k_{cat}/K_m and an 8-fold increase in the k_{cat} of benzoylthiocholine, while the K_m was similar to WT. Substitution of Arg (A107R) in place of Lys did not significantly enhance

benzoylthiocholinesterase activity, but resulted in a 3-fold higher K_m suggesting that the larger Arg side-chain may interfere with substrate binding. Substitution of A107 by the neutral residue, Gln, and by hydrophobic residues yielded similar K_m values and no enhancement of k_{cat} . Substitution of A107 by His also did not confer significant cholinesterase activity.

Butyrylthiocholinesterase activity was the highest in the A107S, A107T, A107H/A190R, and A107H/A400D variants

(Table 3). A400 was predicted to be near the choline group from structural overlays. The A107H/A400D variant had a 2-fold increase in the k_{cat}/K_m for benzoylthiocholine and 9-fold increase for butyrylthiocholine when compared to A107H; however, the K_m values for all of the variants were >1 mM, indicating that the pNBE variants could only weakly bind cationic substrates.

OPTIMIZATION OF THE PRIMARY ASSAY USED FOR SCREENING THE DE LIBRARY

To develop a micro-scale assay for reactivation, (His)₆-tagged enzymes were bound to nickel-coated 96-well plates. To maintain near physiological conditions, the pH was kept at 7.6; measurement at a sub-optimal pH also allowed for a longer time period to carry out the subsequent steps. Two wells were coated with enzyme (≤ 0.025 U per well) for each variant to measure the activity of the uninhibited and inhibited enzyme. The enzyme was inhibited on the plate, and excess enzyme and inhibitor were removed. The plates were then washed with buffer. Rates of reactivation were comparable after one, two, or four washes. For the plate assay, four washes were done to ensure removal of the OPAA. After washing away excess inhibitor and unbound enzyme, the enzyme was eluted from the plate with 50 mM EDTA. Imidazole was avoided because it readily reacted with the ester substrates (Bruice and Schmir, 1956). Aliquots were removed and assayed over time. The rate constant for reactivation for A107H using the microscale assay ($k_r^{2\text{washes}} = 0.22 \pm 0.08 \text{ h}^{-1}$; $k_r^{4\text{washes}} = 0.3 \pm 0.2 \text{ h}^{-1}$) was comparable with that determined using a gel

Table 2 | Substrate specificities of pNBE and selected variants.

Enzyme	Substrate	k_{cat} (1/min)	K_m (mM)	k_{cat}/K_m (1/min*mM)
WT	pNPA	370 ± 30	1.2 ± 0.3	300 ± 80
	pNPB	1100 ± 40	0.08 ± 0.01	14000 ± 2000
A107H	pNPA	130 ± 10	5.6 ± 0.7	23 ± 3
	pNPB	520 ± 20	0.12 ± 0.02	4300 ± 700
A107H/A190C	pNPA	70 ± 10	0.9 ± 0.4	70 ± 30
	pNPB	7 ± 1	0.3 ± 0.1	20 ± 10
A107H/A400T	pNPB	460 ± 10	0.12 ± 0.02	3800 ± 600
A107H/A400V	pNPB	510 ± 30	0.17 ± 0.03	3000 ± 600
BChE Ω Loop	pNPA	185 ± 6	1.6 ± 0.1	116 ± 8
Mutant with A107H				

pNPA (pNP-acetate) and pNPB (pNP-butyrat)e assays were run in 50 mM HEPES pH 7.0, 150 mM NaCl, 22 ± 3°C. All enzymes had the N-terminal His-tag.

Table 3 | Steady state kinetic parameters for selected pNBE variants of the DE library.

Substrate	Benzoylthiocholine ^a			Butyrylthiocholine ^b			
	Enzyme	k_{cat} (1/min)	K_m (mM)	k_{cat}/K_m (1/min*mM)	k_{cat} (1/min)	K_m (mM)	k_{cat}/K_m (1/min*mM)
WT		70 ± 9	1.2 ± 0.3	58 ± 16	130 ± 10	5.4 ± 0.8	24 ± 4
A107H		13 ± 1	0.6 ± 0.2	22 ± 7	35 ± 8	17 ± 5	2.0 ± 0.9
A107H ΩLoop		8 ± 1	0.9 ± 0.3	9 ± 3	10.4 ± 0.9	8.0 ± 0.7	1.3 ± 0.2
A107K		570 ± 50	1.4 ± 0.2	410 ± 70	>20	>8 ^c	–
A107Q		40 ± 4	1.0 ± 0.2	39 ± 9	40 ± 10	19 ± 7	2 ± 1
A107R		90 ± 20	5 ± 1	20 ± 6	>50	>8 ^c	–
A107S		39 ± 9	1.4 ± 0.6	30 ± 10	780 ± 30	14.4 ± 0.7	54 ± 3
A107T		36 ± 3	0.6 ± 0.2	60 ± 20	240 ± 30	11 ± 2	22 ± 5
A107V		38 ± 4	0.5 ± 0.2	80 ± 30	56 ± 8	8 ± 2	7 ± 2
A107Y		21 ± 2	0.6 ± 0.1	35 ± 8	45 ± 5	6.0 ± 0.9	7 ± 1
A107H/A190G		29 ± 4	0.9 ± 0.3	30 ± 10	50 ± 30	11 ± 7	5 ± 4
A107H/A190R		12 ± 1	0.6 ± 0.2	20 ± 7	200 ± 30	13 ± 2	15 ± 3
A107S/A190G		23 ± 4	2.2 ± 0.6	10 ± 3	90 ± 30	11 ± 4	9 ± 4
A107V/A190G		21 ± 2	0.6 ± 0.1	35 ± 7	45 ± 5	6.0 ± 0.9	8 ± 1
A107H/A400D		80 ± 10	2.1 ± 0.6	40 ± 10	190 ± 60	11 ± 5	18 ± 9
A107H/A190S/A400S		6.4 ± 0.9	0.8 ± 0.2	9 ± 3	115 ± 14	9 ± 1	13 ± 3

Benzoylthiocholine and butyrylthiocholine were used as substrates. Specific activities of the other variants are shown graphically in the **Supplemental Information**.

^aBenzoylthiocholine has limited solubility in DMSO, the highest substrate concentration tested was 2.5 mM.

^bButyrylthiocholine was also a poor substrate of pNBE, and K_m values were in the mid-millimolar range. Saturation was not achieved at the highest substrate concentration tested (8 mM). K_m values were extrapolated from double reciprocal plots.

^cSaturation was not achieved at $[S] = 8$ mM, and the plot of velocity vs. $[S]$ was linear. Extrapolated K_m 's exceeded 40 mM.

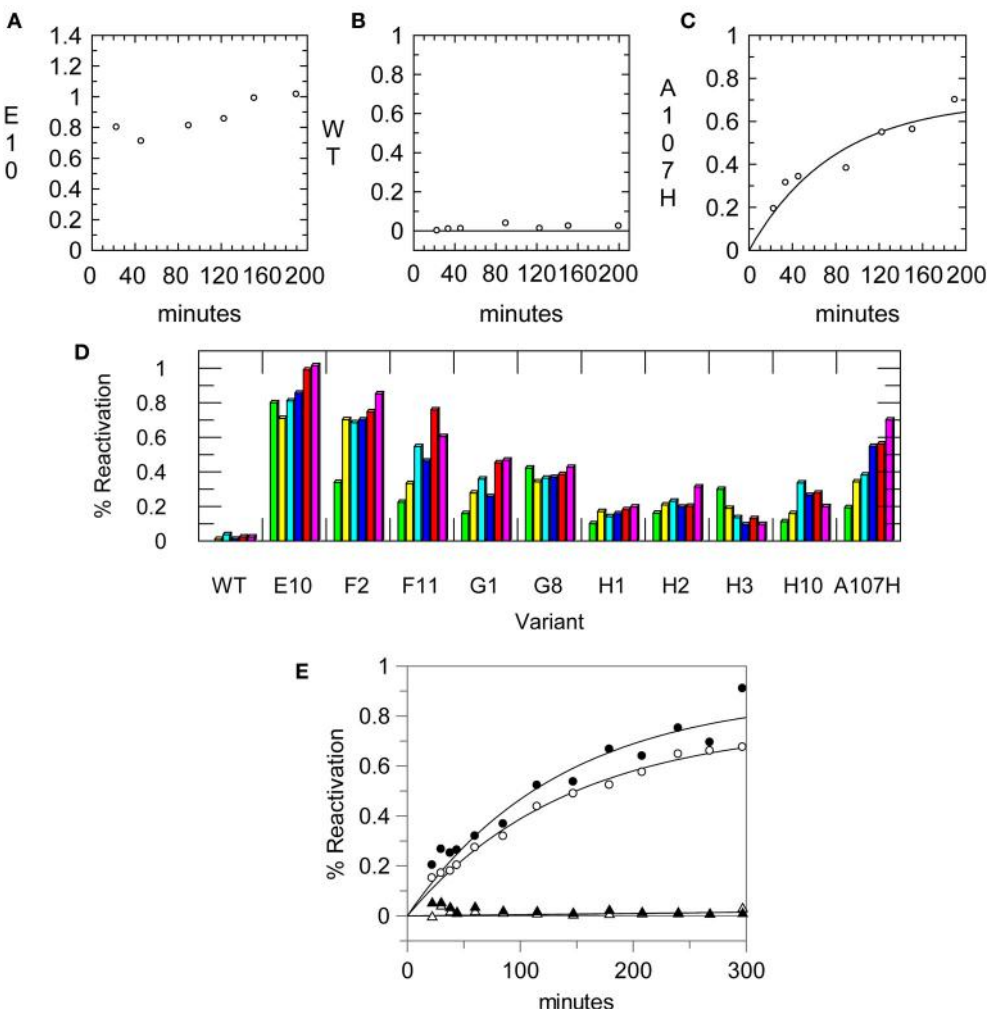


FIGURE 3 | Reactivation data from the primary assay using a 96-well

His-Select® plate. Aliquots of enzyme were removed once at each time point and assayed for CE activity using pNP-butyrate. Enzymes were reactivated in 50 mM Tris pH 7.6, 150 mM NaCl. Reactivation rates measured using the assay for **(A)** the A107H/A190C (E10) variant, **(B)** the WT pNBE, and **(C)** the A107H variant. **(D)** Example of reactivation rates using single point measurements for selected variants at different time points using the 96-well

plate assay. Some variants showed full reactivation by the first time point while others progressively reactivated over longer time periods. **(E)** Reactivation rates measured for the A107H variant using the 96-well plate assay after one (○) or two (●) washes to remove the inhibitor, Paraoxon. The reactivation of the WT enzyme is also shown after one (▲) or two (△) washes for comparison. Rates were measured in 50 mM Tris pH 7.6, 150 mM NaCl at 37°C.

filtration column ($k_r = 0.53 \pm 0.09 \text{ h}^{-1}$) at the same pH and temperature. Data collected using the microscale assay and 2 washes are shown in **Figure 3**. The DE library was screened one to two times with the various OP. From the first round, 26 of the 95 variants were more carefully examined with large scale preps and kinetic experiments. Error in the values of k_r was higher using data collected from the microscale assay, suggesting that it is better suited for large-scale screening than for precise determination of kinetic parameters.

For slow and moderate rates of reactivation the microscale assay was useful as a primary assay for the exploration of OP inhibitors and reaction conditions (**Figure 3D**). The microscale assay helped identify the variants which could reactivate faster than the single variant, A107H. The vast majority of the variants did not show significant enhancements in OPAAH activity

using either the discontinuous assay or a continuous assay with paraoxon; these results are consistent with other applications of DE (Dalby, 2003; Goldsmith and Tawfik, 2013). Using the OPAA activity of A107H as a screening threshold, approximately 3% of the library was advanced for further testing.

The half time of reactivation for pNBE A107H was $t_{1/2} = 78 \text{ min}$. Thus, observation of full reactivation at $\sim 20 \text{ min}$ indicated that the k_r was $\geq 1.9 \text{ h}^{-1}$ or ≥ 4 -fold faster than the A107H variant. Reactivation rates for the top hits were more accurately measured using large scale preps of the enzymes and gel filtration columns.

It should be noted that the measurement of reactivation rates alone cannot identify a mechanism of OP resistance. Resistance to OP inhibition can arise from reduced binding of OP, poor stabilization of the TS, poor accommodation of the R-groups

as the pentavalent TS forms, or increased OPAAH activity. These possibilities can only be distinguished by additional kinetic experiments. These methods are routinely used to characterize pesticide resistance mechanisms in insecticide-insensitive AChE variants (Newcomb et al., 1997; Temeyer et al., 2012; Zhang et al., 2012).

VARIANTS WITH ENHANCED OPAAH ACTIVITY

After screening the library of 95 variants for reactivation after paraoxon inhibition, three variants were found to reactivate faster than the A107H variant: A107H/A400M (H2), A107H/A190G (F2), and A107H/A190C (E10). The A107H/A190C double variant was found to have the greatest rate enhancement. Relative to the WT pNBE ($k_r^{\text{Paraoxon}} = 0.03 \pm 0.01 \text{ h}^{-1}$), the rate constant for reactivation following paraoxon inhibition was 18-fold higher for the A107H variant ($k_r^{\text{Paraoxon}} = 0.53 \pm 0.09 \text{ h}^{-1}$), and 50-fold higher for the A107H/A190C double variant ($k_r = 1.5 \pm 0.2 \text{ h}^{-1}$) (Table 4). Consistent with the aliesterase hypothesis (Oppenorth and van Asperen, 1960), the turnover number for pNBE-catalyzed

hydrolysis of the ester substrates, pNPA or pNPB, progressively decreased as OP-hydrolase activity increased (Table 2). Thus, as OP-hydrolase activity is evolved to accommodate a pentavalent TS of an OP, the carboxylesterase activity and stabilization of a tetrahedral transition state is lost (Oppenorth and van Asperen, 1960). For soman, the largest rate enhancements were observed (Table 5). Somanase activity was not observed in the G117H BChE single mutant (Millard et al., 1998) until a second mutation was added (G117H/E197Q). In pNBE, the A107H mutation (equivalent to G117H in BChE) enhanced the rate of spontaneous reactivation after soman inhibition, but an additional rate enhancement was achieved with the A107H/A190C variant. The k_r for A107H ($k_r^{\text{Soman}} = 0.7 \pm 0.1 \text{ h}^{-1}$) was 700-fold above WT ($k_r^{\text{Soman}} = 0.001 \pm 0.004 \text{ h}^{-1}$) and 4000-fold higher for the A107H/A190C variant ($k_r^{\text{Soman}} = 4 \pm 1 \text{ h}^{-1}$). The trends were similar to those observed with paraoxon (Table 4). A190 in pNBE is also at a different location than E197 in BChE, and rate enhancements in OP-hydrolase activity have not been reported from mutations at this site (Figure S1D).

The variant which displayed the greatest rate enhancements in OP-hydrolase activity, A107H/A190C, exhibited unexpected kinetic complexity consistent with a slow conformational change in the enzyme. Pre-incubation of the purified A107H/A190C enzyme at 37°C in the absence of any substrate or inhibitor caused a subsequent time-dependent increase in V_{\max} for CE activity and the reactivation rate constants for selected OPAA (Figure S3). Maximal CE activity could be achieved by pre-incubating the enzyme at 37°C in 50 mM Tris pH 7.6, 150 mM NaCl, 2 mM BME for ≥2 h. Likewise, pre-equilibrating A107H/A190C to 37°C for ≥2 h doubled the apparent dephosphorylation rate constant following paraoxon or soman inhibition (Tables 4, 5). The dephosphorylation rate constant following DFP inhibition was not similarly affected. The DFP-inhibited A107H/A190C variant reactivated 5-fold more slowly than did A107H (Table 6), and no further increases could be gained by heating the enzyme. We also tested the triple mutant, A107H/A190C/A400M, for temperature-dependent hysteresis but found no significant effect on reactivation (Table 5).

Several mutations at the A190 and A400 positions were compatible with A107H. The backbone NH groups of A107 and A190 form part of the oxyanion hole. Changes in the polarity of these NH groups have been proposed to enhance OPAAH activity

Table 4 | Rates of reactivation after ethyl paraoxon inhibition measured for the DE variants at 37°C in 50 mM Tris pH 7.6, 150 mM NaCl, 2 mM BME.

Enzyme	CLONE	$k_{\text{reactivation}}$ (1/h)	% Reactivation
A107	D3	0.03 ± 0.01	110 ± 10
A107C	D4	0.15 ± 0.03	40 ± 3
A107D	D5	0.31 ± 0.02	90 ± 2
A107E	D6	0.048 ± 0.006	46 ± 4
A107F	D7	0.023 ± 0.004	130 ± 10
A107G	D8	0.0114 ± 0.0009	70 ± 4
A107H	–	0.53 ± 0.09	102 ± 5
A107I	D9	0.013 ± 0.004	70 ± 4
A107K	D10	0.04 ± 0.02	25 ± 6
A107L	D11	0.030 ± 0.005	25 ± 2
A107M	D12	0.06 ± 0.03	90 ± 10
A107N	E1	0.04 ± 0.01	60 ± 10
A107Q	E3	0.05 ± 0.02	110 ± 10
A107R	E4	0.14 ± 0.03	27 ± 2
A107S	E5	0.03 ± 0.01	100 ± 10
A107T	E6	0.034 ± 0.006	40 ± 5
A107V	E7	0.22 ± 0.03	28 ± 1
A107Y	E9	0.012 ± 0.003	7 ± 1
A107H/A190C	E10	1.5 ± 0.2 ^a	62 ± 3
A107H/A190V	G2	0.4 ± 0.1	73 ± 9
A107H/A190G	F2	0.7 ± 0.3	90 ± 10
A107H/A190H	F3	0.10 ± 0.02	66 ± 8
A107H/A190M	F7	0.3 ± 0.2	17 ± 5
A107H/A400W	H10	0.4 ± 0.2	130 ± 50
A107H/A400M	H2	1.0 ± 0.2	97 ± 7
A107H/A400V	H9	0.6 ± 0.1	130 ± 20
A107H/A190C/A400T	A8	0.43 ± 0.07	92 ± 7
A107H/A190C/A400T	A8	1.0 ± 0.1 ^a	75 ± 5
A107H/A190C/A400M	C4	1.0 ± 0.1 ^a	75 ± 5

^aEnzymes were heated at 37°C prior to reactivation.

Table 5 | Rates of reactivation after inhibition with soman.

Enzyme	$k_{\text{reactivation}}$ (1/h)	% Reactivated	Fold increase
WT	0.001 ± 0.004	<4% after 5.5 h	–
A107H	0.7 ± 0.1	106 ± 8	700
A107H/A190C ^a	1.8 ± 0.2	44 ± 5	1800
A107H/A190C ^b	4 ± 1	43 ± 6	4000
A107H/A190C/A400M ^a	0.7 ± 0.2	20 ± 2	700
A107H/A190C/A400M ^b	1.2 ± 0.5	17 ± 2	1200

^aWithout heating prior to inhibition.

^bWith 2 h of heating at 37°C prior to reactivation at 37°C.

(Yao et al., 2012). Hydrophobic mutations A400M and A400V within the loop slightly enhanced the rate of reactivation. The A107H/A400M (H2) and A107H/A190G (F2) double mutants showed the second largest enhancements, but additive effects were not observed in the A107H/A190C/A400M variant or any other triple mutant.

Having constructed a DE library with all 20 amino acids at position A107, we also determined if other residues at this position were more effective than histidine in catalyzing reactivation. In addition to A107H, the variants A107C, A107D, and A107V showed apparent reactivation rate enhancements for selected OPAA compared with WT pNBE. Of this group, however, only A107H and A107D fully reactivated after inhibition by paraoxon (Table 4). This result is similar to what was reported by Schopfer et al. (2004). Schopfer observed OP hydrolase activity in G117D, G117E, and L286H variants of BChE.

TRANSFER OF MUTATIONS ONTO hCE1

The spontaneous reactivation rate constant for WT hCE1 inhibited with paraoxon was low (Table 7). This is consistent with reports that WT hCE1 can be irreversibly inhibited by stereoisomers of soman or cyclosarin (Hemmert et al., 2010). The mutation equivalent to G117H in BChE was made in hCE1 (G143H), but did not enhance or confer OPAAH activity (Table 7). The hCE1 loop residues 302–320 (equivalent to 276–290 in BChE) that form the acyl pocket differ significantly among hCE1, pNBE, and BChE. In snake AChE, the single G122H mutation (homologous to BChE G117H) did not increase OPAAH activity; only introduction of two additional mutations (G122H/Y124Q/S125T) permitted engineering of limited spontaneous reactivation following slow inhibition with selected OPAA (Poyot et al., 2006). Thus, while pNBE is more similar to hCE1

in terms of substrate specificity, the utility of pNBE as a surrogate scaffold still remains to be explored.

INHIBITION BY PARAOXON

Reliable measurement of IC_{50} or K_i values requires enzyme concentrations below the K_i . For enzymes with IC_{50} values in the nM range, only upper limits can typically be measured. The minimum amount of enzyme needed to obtain a signal/noise ratio >2 was 0.5 nM of enzyme. The observed IC_{50} (0.37 nM) for paraoxon was almost equal with the enzyme concentration (0.5 nM), suggesting that the $IC_{50} \leq 0.5$ nM. Thus, pNBE is an effective scavenger of paraoxon at low nM concentrations. Similar values have been reported for AChE with soman and sarin [$IC_{50}^{\text{soman}} = 0.88\text{--}2.53$ nM, $IC_{50}^{\text{sarin}} = 3.27\text{--}6.15$ nM (Fawcett et al., 2009)].

INHIBITION BY ECHOTHIOPHATE

pNBE and hCE1 share the cholinesterase fold, but lack cholinesterase activity. To determine if V-type inhibitors with choline-like leaving groups could be accommodated by variants, we screened the library with echothiophate and looked for irreversible inhibition. Through one mutation, A107S, we were able to achieve a 50-fold increase in the rate of inhibition. However, for the pNBE variants tested, the K_p values remained high (millimolar range) compared with those of natural cholinesterases (Table 8).

DISCUSSION

Arnold and colleagues have shown that *B. subtilis* pNBE can be modified to achieve increased thermostability, broadened substrate specificity, or improved reactivity in organic solvents using DE (Giver et al., 1998; Spiller et al., 1999; Brustad and Arnold, 2011). DE is a large scale site-directed mutagenesis experiment where selected residues are mutated to all 20 amino acids, or random mutations are introduced to alter catalytic activity and/or substrate specificity (Brustad and Arnold, 2011). This process generates 20 different enzymes for each selected site or thousands of variants with mutations at random sites (reviewed by Goldsmith and Tawfik, 2013); screening thousands of mutants is typically impractical. Several approaches are available for

Table 6 | Rates of reactivation at pH 7.6 after inhibition with DFP.

Enzyme	$k_{\text{reactivation}}$ (1/h)	% Reactivated
A107H	0.6 ± 0.1	110 ± 10
A107H/A190C	0.13 ± 0.08	150 ± 40
A107H/A190C ^a	0.17 ± 0.01	69 ± 2
A107H/A190G	0.63 ± 0.06	108 ± 3

^aHeated for 3 h at 37°C prior to reactivation.

Table 7 | Rates of reactivation of hCE1 after inhibition with paraoxon.

Enzyme	pH	$k_{\text{reactivation}}$ (1/h)	% Reactivated
hCE1 WT	7.0	0.078 ± 0.006	92 ± 3
	7.6	0.102 ± 0.006	98 ± 3
hCE1 G143H	7.0	0.025 ± 0.008	45 ± 8
	7.6	0.03 ± 0.03	15 ± 2
hCE1 G143H/A222C	7.0	0.007 ± 0.003	120 ± 60
	7.6	0.009 ± 0.007	11 ± 8

Table 8 | Inhibition by echothiophate.

Enzyme	k_2 (1/min)	K_p (mM)	k_2/K_p (1/min*mM)
A107H	0.013 ± 0.005	9 ± 4	0.0014 ± 0.0008
A107K	0.014 ± 0.005	10 ± 4	0.0014 ± 0.0008
A107S	0.7 ± 0.4	10 ± 7	0.07 ± 0.06
A107T	0.06 ± 0.05	11 ± 8	0.006 ± 0.006
A107R	0.02 ± 0.04	>5	0.00045 ± 0.00009 ^a
A107Q	0.079 ± 0.008	3 ± 1	0.026 ± 0.009
A107V	0.10 ± 0.02	20 ± 4	0.005 ± 0.001
A107Y	0.06 ± 0.04	20 ± 1	0.004 ± 0.004

Rates were measured using 1× Sorensen's buffer pH 7.4 at room temperature (22 ± 2°C).

^aInhibition was observed; however, the intercept could not be determined accurately from a distant extrapolation (very weak binding).

generating large libraries of mutants, but there are far fewer validated methods for selecting mutants with the desired activity. Here we constructed a “focused” DE library, utilized a bacterial homolog as a surrogate scaffold, and restricted the mutations to residues within a 7 Å radius of the nucleophilic serine. While pNBE, AChE, BChE, and hCE1 share a common fold (**Figure S1**), it is known that the single mutation analogous to G117H in BChE does not confer OP-hydrolase activity in AChE (Ordentlich et al., 1998; Poyot et al., 2006). Based upon substrate specificities, we show that pNBE and hCE1 are similar (this paper). However, when we examined the A107H variant of pNBE and the G123H variant of hCE1, we found that the histidine substitution only conferred OP-hydrolase activity in pNBE. Our preliminary results demonstrate that pNBE is a suitable prokaryotic scaffold for engineering improved reactivity with a range of OPAA inhibitors including soman, but that it is sufficiently different from hCE1 that additional mutations would be required.

While a significant enhancement in the rate of reactivation after soman inhibition was achieved (10^3 -fold increase, **Table 5**) the pNBE A107H variant did not achieve the same rates of reactivation as the BChE G117H variant [$k_r^{\text{BChE-Soman}} = 6000 \pm 600$ 1/min (Millard et al., 1998) vs. $k_r^{\text{pNBE-E10-Soman}} = 0.07 \pm 0.02$ 1/min]. This may in part be due to the more open active site of pNBE (**Figure 2A**) vs. the tunnel-like gorge of AChE and BChE.

One other complication was a slow time- and temperature-dependent change in activity in the variant which had the largest enhancement (10^3 -fold) in OP-hydrolase activity. Various forms of hysteresis in AChE and BChE have been observed kinetically (Masson et al., 2005; Badiou et al., 2008; Masson and Lockridge, 2010; Lushchekina et al., 2014), and possibly structurally (Nachon et al., 2011). Non-linear kinetic curves for BChE G117H also were observed with selected substrates (Millard et al., 1995b). Hysteresis affecting CE activity of both BChE and AChE (Masson et al., 2005; Badiou et al., 2008; Masson and Lockridge, 2010; Lushchekina et al., 2014) and OP-hydrolase activity (Masson, 2012) has been reported and has been attributed to the flipping of the His of the catalytic triad. A pronounced lag phase (3 min) was observed in the BChE A328C mutant at 25°C (Masson, 2012); the side chain of this residue is near His-438 of the triad (~4.5 Å). In pNBE the mechanism of hysteresis may or may not be the same since the A190 side chain is behind the oxyanion hole residues and is relatively distant from His-399 (>7 Å) (**Figure S1**). If the His of the catalytic triad is involved, however, the methionine residue in the A107H/A190C/A400M variant which did not display hysteresis may stabilize a particular rotamer of His-399. This mutant displayed a lower percentage of reactivated enzyme after soman inhibition when compared with A107H/A190C (**Table 5**) suggesting that conformational changes may be important in the mechanism of reactivation.

Hysteresis is rarely considered during DE screening, but can limit achievable rates of hydrolysis. It also complicates the interpretation of site-directed mutagenesis and structural studies since the crystallized structure may (or may not) represent the catalytically competent state. We observed kinetic complexity in the A107H/A190C pNBE variant that affected both esterase and OP-hydrolase activity. This suggests the involvement of a residue(s) which plays a role in both esterase and OP-hydrolase activity.

INTRODUCTION OF OPAAH ACTIVITY TO pNBE

The overarching goal of developing a nerve agent bioscavenger is to find or engineer a biocompatible enzyme that rapidly binds and hydrolyzes a broad range of neutral (G-type agents) and positively charged (V-type) OPAA under physiological conditions where the inhibitor is present at sub-micromolar concentrations. Cholinesterases react rapidly with all known OPAA nerve agents, but effectively remain inhibited irreversibly due to the stability of the OPAA-enzyme complex.

Introducing a single His (G117H) into human BChE converts the enzyme into a modest OPAAH by increasing the spontaneous reactivation rate constant while retaining reactivity with a broad range of inhibitors (Millard et al., 1995a; Lockridge et al., 1997). Follow-on attempts to incorporate His-117 into human or *Bungarus fasciatus* AChE were relatively unsuccessful (Poyot et al., 2006). pNBE is the second esterase to show an enhancement in OPAAH activity by introduction of a single His (A107H corresponds to G117H) and is significantly more amenable to *E. coli* expression.

Lockridge and colleagues rationally designed and tested more than 60 double or triple mutants of human BChE based upon the initial success with His-117, but none of these variants improved upon the OPAAH activity of G117H (Lockridge et al., 1997; Schopfer et al., 2004). We find a similar result using DE with pNBE. Although enhancements of spontaneous reactivation compared to WT were measured following paraoxon inhibition for pNBE A107D, A107V or A107C, the histidine mutant (A107H) showed the fastest and most complete dephosphorylation (**Table 4**). pNBE A107D is homologous with the blowfly CE G137D mutant that was isolated by screening OP-resistant populations of *Lucilia cuprina* for naturally occurring variants of G117H (Newcomb et al., 1997). A107D showed enhanced spontaneous reactivation compared with WT, but the turnover rates with paraoxon were slower than those of either pNBE A107H or the blowfly CE G137D (cf. **Table 4** and Kirby et al., 2013).

Cholinesterases and carboxylesterases must stabilize a tetrahedral transition state to catalyze carboxyl ester hydrolysis, whereas the transition state of an organophosphate is generally a pentavalent trigonal bipyramidal. Consequently, all attempts to engineer OPAAH activity into these enzymes must accept a significant risk of concomitant loss of natural esterase activity. Oppenorth’s “aliesterase hypothesis” was based upon this observed interchange in substrate specificities (Oppenorth and van Asperen, 1960). Our results with pNBE generally confirmed this hypothesis with the trend showing that mutations increasing OPAAH activity also showed decreasing carboxylesterase activity (**Tables 1–7**).

The pNBE A107H/A190C variant showed a slow time- and temperature-dependent increase in CE activity and the rate of spontaneous reactivation following inhibition with paraoxon or soman (**Figure S3; Tables 4, 5**), but not with DFP (**Table 6**). DFP, unlike soman or paraoxon, has two bulky R-groups (**Figure 1**) which may restrict the pNBE active site from reaching the temperature-induced conformational change required for the higher level of activity. It has been shown that the DFP reaction significantly alters the conformation of the acyl pocket loop of AChE (Millard et al., 1999; Hornberg et al., 2007). The corresponding loop of pNBE is predicted to be nearby His-107

(**Figure 2**). Thus, the catalytically competent conformer of the histidine or hydrolytic water molecule may be affected by conformational changes in the loop. The simultaneous mutation of two residues (A107/A190) may permit subtle, local movements of the NH groups of the oxyanion hole that are sufficient to enhance catalysis (Yao et al., 2012). Alternatively, the double mutant may have more distal effects to structure the disordered loops of WT pNBE. It was shown previously that mutations which thermally stabilize the enzyme also increase the optimal temperature for pNBE carboxylesterase activity (Giver et al., 1998); the omega loop of the thermal stable pNBE variant (PDB 1C7I) is structured (Spiller et al., 1999).

IMPORTANCE OF THE OXYANION HOLE

Much of the catalytic power of serine hydrolases derives from the oxyanion hole (Bryan et al., 1986; Zhang et al., 2002; Warshel, 2003; Bobofchak et al., 2005), and we hypothesize that the same is true for engineered OPAAH activity. Millard and colleagues originally proposed the spontaneous reactivation of G117H was acid catalyzed and might involve a direct H-bond from the imidazolium to the phosphonyl (double bond) oxygen to stabilize the dephosphylation transition state, or an indirect steric effect that distorts the preformed electrostatic environment of the oxyanion hole and thereby permits the catalytic triad His-438 to catalyze reactivation (Millard et al., 1995a, 1998). Related and alternative mechanisms subsequently have been proposed (Lockridge et al., 1997; Newcomb et al., 1997; Albaret et al., 1998; Schopfer et al., 2004; Poyot et al., 2006; Nachon et al., 2011; Yao et al., 2012), supported, or refuted based upon analogy with follow-on His-117 mutations to related enzymes, molecular modeling studies (Amitay and Shurki, 2009; Yao et al., 2012) or static, medium resolution X-ray crystal structures (Masson et al., 2007); however, the actual enzyme mechanism of G117H remains unresolved.

Our studies on the structurally homologous pNBE mutants may provide useful data for ongoing efforts to elucidate the G117H mechanism. First, like G117H, placing a histidine residue at the homologous A107H position in the oxyanion hole enhanced OPAAH activity with a range of inhibitors (**Tables 4, 5**). Second, OPAAH activity increased as the pH decreased from 7.6 to 7.0, consistent with a mechanism that is acid-catalyzed. Third, the A190C mutation further enhanced the rate of reactivation of the A107H mutation. The NH group of A190 forms part of the 3-point oxyanion hole, and the side chain would be expected to point away from the oxyanion. Finally, we observed a slow time- and temperature-dependent change in carboxylesterase and OPAAH activity of the A107H/A190C variant that may be consistent with a conformational change or some other reversible modification in the free enzyme which enhances the role of these residues in catalysis. Additional work is required to determine if these observations can be translated to improve human BChE G117H activity.

INTRODUCTION OF LIMITED CHOLINESTERASE ACTIVITY

One objective of this work was to determine if cholinesterase activity could be introduced into pNBE. The active site cavity of pNBE is formed by four loops that are largely disordered in

the WT enzyme crystal structure, viz. residues 64–71 (unstructured) and 413–417 (unstructured) on one side of the active site, and 316–320 (unstructured) and 260–268 (structured) on the other side (Spiller et al., 1999). It appears that these flexible loops become longer, more differentiated and ordered through evolution to form the substrate specificity loops observed in the X-ray structures of AChE and BChE. One side becomes the cholinesterase “acyl pocket loop,” which we have shown previously to have reversible conformational flexibility in *Torpedo californica* (*Tc*) AChE when binding selected OPAA (Millard et al., 1999; Hornberg et al., 2007). The other side develops the so-called Ω-loop carrying Trp-84 (*Tc*AChE numbering; Trp-82 in BChE), a residue that complements trimethyl or choline-like substrate leaving groups.

Residues corresponding to the cholinesterase Ω-loop are disordered in the structure of WT pNBE [PDB 1QE3 (Spiller et al., 1999)]. Both pNBE and hCE1 lack the critical Trp-84 side chain (**Figure 2E**) (Satoh and Hosokawa, 1995; Imai et al., 2006), and this probably explains why these enzymes are relatively poor at binding cationic substrates (e.g., ATCh and BTCh; **Table 3**) or echothiophate (**Table 8**). Our initial experiment to insert the entire Ω-loop into pNBE is a first step in evolving the bacterial enzyme toward a cholinesterase. The loop was accepted by the pNBE fold and had little or no effect on the reactivity of the enzyme with neutral substrates or inhibitor; however it also did not result in detectable activity with positively charged substrates (**Table 3**). While this rational design attempt with the Ω-loop failed to increase cholinesterase activity, the focused DE exploration succeeded in finding A107K which demonstrated an almost 10-fold increase in its specificity constant for benzylthiocholine compared with WT.

COMPARISON OF pNBE AND hCE1

Human carboxylesterase has been proposed as an alternative or adjunct bioscavenger to the cholinesterases because hCE1 is abundant in human liver, binds and hydrolyzes some neutral OPAA nerve agents, and does not undergo significant aging after inhibition with the most deadly OPAA nerve agent, soman (Hemmert et al., 2010). However, the primary limitation to using hCE as a nerve agent bioscavenger is the slow reaction rates with positively charged OPAA. In our study, cholinesterase activity could be introduced into pNBE by the A107K mutation, but the amount was still several orders of magnitude below that of cholinesterases and the mutation had no effect on the bimolecular rate constant for inhibition by a cationic OPAA (echothiophate; **Table 8**). More importantly, the G143H mutation did not confer OPAAH activity in hCE1 (**Table 7**).

In summary, along with its primary sequence and structural homology to the cholinesterases and the shared use of a rare Glu residue instead of Asp in the catalytic triad, we have shown that *B. subtilis* pNBE can accommodate the cholinesterase Ω-loop without detriment to protein folding or endogenous esterase activity. We have also identified an unexpected point mutation (A107K) that significantly increases turnover of a positively charged substrate. Moreover, like BChE but not AChE or hCE1, the pNBE structure accepts substitutions (A107H or A107H/A190C) corresponding with G117H that confer

significant OPAAH activity, thereby expanding the enzyme's natural substrate specificity to include phosphoric and phosphonic acid esters. Taken together, these results suggest to us that pNBE is an excellent prokaryotic scaffold for follow-on DE studies, as well as other methods like incorporation of unnatural amino acids, that can inform new pathways for continued engineering of useful cholinesterase and/or OPAAH activity within the α/β -hydrolase superfamily.

ACKNOWLEDGMENTS

We thank SSG Derrick Robinson for assistance with steady state kinetic assays and Dr. Michael S. Lee for helpful discussions. Dr. Phillip Potter of St. Jude Children's Research Hospital kindly provided us with the clone for WT pNBE. This work was funded by the U.S. Defense Threat Reduction Agency JSTO award 1.D0006_08_WR_C (Charles B. Millard). The opinions or assertions contained herein belong to the authors and are not necessarily the official views of the U.S. Army, U.S. Navy, or the U.S. Department of Defense.

SUPPLEMENTARY MATERIAL

The Supplementary Material for this article can be found online at: <http://www.frontiersin.org/journal/10.3389/fchem.2014.00046/abstract>

A graph of the esterase activities of the individual mutants in the DE library, evidence of reversible hysteresis, and sequence alignments of the enzymes discussed in this study are included in the **Supplemental Information**.

Scheme S1 | Organophosphate inhibition, spontaneous reactivation, and aging.

Figure S1 | Acylation-the first step in the catalytic cycle. (A) The serine hydrolases AChE (2ACE), BChE (1P0M), hCE1 (2HRR), and pNBE-esterase (1QE3) all share a common fold, but have very different substrate specificities. This is in part due to residues within the Ω -loop (colored red) which form part of the choline binding pocket in AChE and BChE. The equivalent loop in pNBE is disordered in the crystal structure 1QE3. (B) The acylation step and active site of pNBE. Residues of the catalytic triad are boxed. (C) The acylation step and active site of BChE. The cationic choline ester is accommodated by Glu-197 and Trp-82. Trp-82 of the Ω -loop makes an important cation-pi interaction with the choline ester and V-type agents (VX and VR) which mimic choline esters. (D) Alternate views of the Ala-190 side chain. A190 is behind the loop of the oxyanion hole residues G106 and A107.

Figure S2 | Specific activities (S.A., U/mg) for all 95 variants in the DE library using five substrates: pNPA, pNPB, benzoylthiocholine, butyrylthiocholine, and acetylthiocholine.

S.A. from single point assays were measured using 5, 1, 2.5, 2.5, and 2.5 mM of the substrates, respectively. In well D3 is the WT pNBEsterase enzyme (where A107 is an alanine). For all other mutants the A107H mutation is present in combination with the denoted mutation. For the A107X mutants (where X = any amino acid), only the single mutation is present. Note, the y-scale has been adjusted for some graphs. For variants with no visible bars, values near the spontaneous rate of hydrolysis were measured and plotted. One substrate, pNPB, was hydrolyzed at detectable levels for all of the mutants. The S.A. were needed to determine the number of Units per well to use in the microscale reactivation rate experiments described.

Steady state kinetic parameters were measured for selected variants which showed enhancements in esterase activity and are described in **Tables 2, 3**. Reductions in carboxylesterase activity were expected for variants which had acquired OP-hydrolase activity [Aliesterase Hypothesis (Oppenoorth and van Asperen, 1960)]. SDS-PAGE gel showing the purity of 10 variants purified using small scale preps and single columns.

Figure S3 | Effect of hysteresis on carboxylester hydrolysis. The E10 A107H/A190C double variant showed a 6-fold increase in its carboxylesterase activity after elution from a PD-10 column during 37°C incubation periods. For assays, 10 μ L of the enzyme was added to a 1 mL reaction volume, and rates were measured at R.T. This dramatic increase in activity was not observed for any other variant.

Supplemental Information | Sequence alignment of the constructs discussed. The pNBE sequence corresponds to P37967; it contains strain-specific differences from the sequence of PDB 1QE3.

REFERENCES

- Aharoni, A., Gaidukov, L., Yagur, S., Toker, L., Silman, I., and Tawfik, D. S. (2004). Directed evolution of mammalian paraoxonases PON1 and PON3 for bacterial expression and catalytic specialization. *Proc. Natl. Acad. Sci. U.S.A.* 101, 482–487. doi: 10.1073/pnas.2536901100
- Albarete, C., Masson, P., Broomfield, C. A., El Kaim, L., and Fortier, P. L. (1998). “Mechanical aspects of the phosphotriesterase activity of human butyryl-cholinesterase G117H mutant,” in *Structure and Function of Cholinesterases and Related Proteins*, ed B. P. Doctor (New York, NY: Plenum Press), 399–405. doi: 10.1007/978-1-4899-1540-5_117
- Amitay, M., and Shurki, A. (2009). The structure of G117H mutant of butyrylcholinesterase: nerve agents scavenger. *Proteins* 77, 370–377. doi: 10.1002/prot.22442
- Ashani, Y. (2000). Prospective of human butyrylcholinesterase as a detoxifying anti-dote and potential regulator of controlled-release. *Drugs Dev. Res.* 50, 298–308. doi: 10.1002/1098-2299(200007/08)50:3/4<298::AID-DDR13>3.0.CO;2-X
- Badiou, A., Froment, M. T., Fournier, D., Masson, P., and Belzunges, L. P. (2008). Hysteresis of insect acetylcholinesterase. *Chem. Biol. Interact.* 175, 410–412. doi: 10.1016/j.cbi.2008.05.039
- Bobofchak, K. M., Pineda, A. O., Mathews, F. S., and Di, C. E. (2005). Energetic and structural consequences of perturbing Gly-193 in the oxyanion hole of serine proteases. *J. Biol. Chem.* 280, 25644–25650. doi: 10.1074/jbc.M503499200
- Bruce, T. C., and Schmir, G. L. (1956). The catalysis of the hydrolysis of p-nitrophenyl acetate by imidazole and its derivatives. *Arch. Biochem. Biophys.* 63, 484–486. doi: 10.1016/0003-9861(56)90068-6
- Brustad, E. M., and Arnold, F. H. (2011). Optimizing non-natural protein function with directed evolution. *Curr. Opin. Chem. Biol.* 15, 201–210. doi: 10.1016/j.cbpa.2010.11.020
- Bryan, P., Pantoliano, M. W., Quill, S. G., Hsiao, H. Y., and Poulos, T. (1986). Site-directed mutagenesis and the role of the oxyanion hole in subtilisin. *Proc. Natl. Acad. Sci. U.S.A.* 83, 3743–3745. doi: 10.1073/pnas.83.11.3743
- Cherny, I., Greisen, P., Ashani, Y., Khare, S. D., Oberdorfer, G., Leader, H., et al. (2013). Engineering V-type nerve agents detoxifying enzymes using computationally focused libraries. *ACS Chem. Biol.* 8, 2394–2403. doi: 10.1021/cb4004892
- Costa, L. G., McDonald, B. E., Murphy, S. D., Omenn, G. S., Richter, R. J., Motulsky, A. G., et al. (1990). Serum paraoxonase and its influence on paraoxon and chlorpyrifos-oxon toxicity in rats. *Toxicol. Appl. Pharmacol.* 103, 66–76. doi: 10.1016/0041-008X(90)90263-T
- Cousin, X., Hotelier, T., Lievin, P., Toutant, J. P., and Chatonnet, A. (1996). A cholinesterase genes server (ESTHER): a database of cholinesterase-related sequences for multiple alignments, phylogenetic relationships, mutations and structural data retrieval. *Nucleic Acids Res.* 24, 132–136. doi: 10.1093/nar/24.1.132
- Dalby, P. A. (2003). Optimising enzyme function by directed evolution. *Curr. Opin. Struct. Biol.* 13, 500–505. doi: 10.1016/S0959-440X(03)00101-5
- Doctor, B. P., and Saxena, A. (2005). Bioscavengers for the protection of humans against organophosphate toxicity. *Chem. Biol. Interact.* 157–158, 167–171. doi: 10.1016/j.cbi.2005.10.024

- Ellman, G. L., Courtney, K. D., Andres, V. Jr., and Feather-Stone, R. M. (1961). A new and rapid colorimetric determination of acetylcholinesterase activity. *Biochem. Pharmacol.* 7, 88–95. doi: 10.1016/0006-2952(61)90145-9
- Fawcett, W. P., Aracava, Y., Adler, M., Pereira, E. F., and Albuquerque, E. X. (2009). Acute toxicity of organophosphorus compounds in guinea pigs is sex- and age-dependent and cannot be solely accounted for by acetylcholinesterase inhibition. *J. Pharmacol. Exp. Ther.* 328, 516–524. doi: 10.1124/jpet.108.146639
- Fleming, C. D., Edwards, C. C., Kirby, S. D., Maxwell, D. M., Potter, P. M., Cerasoli, D. M., et al. (2007). Crystal structures of human carboxylesterase 1 in covalent complexes with the chemical warfare agents soman and tabun. *Biochemistry* 46, 5063–5071. doi: 10.1021/bi700246n
- Geyer, B. C., Kannan, L., Garnaud, P. E., Broomfield, C. A., Cadieux, C. L., Cherni, I., et al. (2010). Plant-derived human butyrylcholinesterase, but not an organophosphorous-compound hydrolyzing variant thereof, protects rodents against nerve agents. *Proc. Natl. Acad. Sci. U.S.A.* 107, 20251–20256. doi: 10.1073/pnas.1009021107
- Giver, L., Gershenson, A., Freskgard, P. O., and Arnold, F. H. (1998). Directed evolution of a thermostable esterase. *Proc. Natl. Acad. Sci. U.S.A.* 95, 12809–12813. doi: 10.1073/pnas.95.22.12809
- Goldsmith, M., and Tawfik, D. S. (2013). “Methods in protein design,” in *Enzyme Engineering by Targeted Libraries, Chapter 12, 1st Edn.*, ed Amy E. Keating (Amsterdam: Academic Press/Elsevier), 257–283.
- Hanozet, G., Pircher, H. P., Vanni, P., Oesch, B., and Semenza, G. (1981). An example of enzyme hysteresis. The slow and tight interaction of some fully competitive inhibitors with small intestinal sucrase. *J. Biol. Chem.* 256, 3703–3711.
- Hemmert, A. C., Otto, T. C., Wierdl, M., Edwards, C. C., Fleming, C. D., MacDonald, M., et al. (2010). Human carboxylesterase 1 stereoselectively binds the nerve agent cyclosarin and spontaneously hydrolyzes the nerve agent sarin. *Mol. Pharmacol.* 77, 508–516. doi: 10.1124/mol.109.062356
- Hornberg, A., Tunemalm, A. K., and Ekstrom, F. (2007). Crystal structures of acetylcholinesterase in complex with organophosphorus compounds suggest that the acyl pocket modulates the aging reaction by precluding the formation of the trigonal bipyramidal transition state. *Biochemistry* 46, 4815–4825. doi: 10.1021/bi0621361
- Hosea, N. A., Radic, Z., Tsigelny, I., Berman, H. A., Quinn, D. M., and Taylor, P. (1996). Aspartate 74 as a primary determinant in acetylcholinesterase governing specificity to cationic organophosphonates. *Biochemistry* 35, 10995–11004. doi: 10.1021/bi9611220
- Ilyushin, D. G., Haertley, O. M., Bobik, T. V., Shamborant, O. G., Surina, E. A., Knorre, V. D., et al. (2013). Recombinant human butyrylcholinesterase as a new-age bioscavenger drug: development of the expression system. *Acta Naturae* 5, 73–84.
- Imai, T., Taketani, M., Shii, M., Hosokawa, M., and Chiba, K. (2006). Substrate specificity of carboxylesterase isozymes and their contribution to hydrolase activity in human liver and small intestine. *Drug Metab. Dispos.* 34, 1734–1741. doi: 10.1124/dmd.106.009381
- Kirby, S. D., Norris, J. R., Richard, S. J., Bahnsen, B. J., and Cerasoli, D. M. (2013). Human paraoxonase double mutants hydrolyze V and G class organophosphorus nerve agents. *Chem. Biol. Interact.* 203, 181–185. doi: 10.1016/j.cbi.2012.10.023
- Kitz, R., and Wilson, I. B. (1962). Esters of methanesulfonic acid as irreversible inhibitors of acetylcholinesterase. *J. Biol. Chem.* 237, 3245–3249.
- Kua, J., Zhang, Y., Eslami, A. C., Butler, J. R., and McCammon, J. A. (2003). Studying the roles of W86, E202, and Y337 in binding of acetylcholine to acetylcholinesterase using a combined molecular dynamics and multiple docking approach. *Protein Sci.* 12, 2675–2684. doi: 10.1110/ps.03318603
- Lenz, D. E., Yeung, D., Smith, J. R., Sweeney, R. E., Lumley, L. A., and Cerasoli, D. M. (2007). Stoichiometric and catalytic scavengers as protection against nerve agent toxicity: a mini review. *Toxicology* 233, 31–39. doi: 10.1016/j.tox.2006.11.066
- Li, H., Schopfer, L. M., Nachon, F., Froment, M. T., Masson, P., and Lockridge, O. (2007). Aging pathways for organophosphate-inhibited human butyrylcholinesterase, including novel pathways for isomalathion, resolved by mass spectrometry. *Toxicol. Sci.* 100, 136–145. doi: 10.1093/toxsci/kfm215
- Li, W. F., Furlong, C. E., and Costa, L. G. (1995). Paraoxonase protects against chlorpyrifos toxicity in mice. *Toxicol. Lett.* 76, 219–226. doi: 10.1016/0378-4274(95)80006-Y
- Lockridge, O., Blong, R. M., Masson, P., Froment, M. T., Millard, C. B., and Broomfield, C. A. (1997). A single amino acid substitution, Gly117His, confers phosphotriesterase (organophosphorus acid anhydride hydrolase) activity on human butyrylcholinesterase. *Biochemistry* 36, 786–795. doi: 10.1021/bi961412g
- Lushchekina, S. V., Nemukhin, A. V., Varfolomeev, S. D., and Masson, P. (2014). Molecular modeling evidence for His438 flip in the mechanism of butyrylcholinesterase hysteretic behavior. *J. Mol. Neurosci.* 52, 434–445. doi: 10.1007/s12031-013-0178-2
- Main, A. R. (1979). Mode of action of anticholinesterases. *Pharmac. Ther.* 6, 579–628. doi: 10.1016/0163-7258(79)90066-4
- Masson, P. (2012). Time-dependent kinetic complexities in cholinesterase-catalyzed reactions. *Biochemistry (Mosc.)* 77, 1147–1161. doi: 10.1134/S0006297912100070
- Masson, P., Adkins, S., Pham-Trong, P., and Lockridge, O. (1992). “Expression and refolding of functional human butyrylcholinesterase from *E. Coli*,” in *Multidisciplinary Approaches to Cholinesterase Functions*, eds A. Shafferman and B. Velan (New York, NY: Springer), 49–52. doi: 10.1007/978-1-4615-3046-6_6
- Masson, P., Fortier, P. L., Albaret, C., Froment, M. T., Bartels, C. F., and Lockridge, O. (1997a). Aging of di-isopropyl-phosphorylated human butyrylcholinesterase. *Biochem. J.* 327(Pt 2), 601–607.
- Masson, P., Froment, M. T., Gillon, E., Nachon, F., Lockridge, O., and Schopfer, L. M. (2007). Hydrolysis of oxo- and thio-esters by human butyrylcholinesterase. *Biochim. Biophys. Acta* 1774, 16–34. doi: 10.1016/j.bbapap.2006.10.012
- Masson, P., Legrand, P., Bartels, C. F., Froment, M. T., Schopfer, L. M., and Lockridge, O. (1997b). Role of aspartate 70 and tryptophan 82 in binding of succinylthiobacine to human butyrylcholinesterase. *Biochemistry* 36, 2266–2277. doi: 10.1021/bi962484a
- Masson, P., and Lockridge, O. (2010). Butyrylcholinesterase for protection from organophosphorus poisons: catalytic complexities and hysteretic behavior. *Arch. Biochem. Biophys.* 494, 107–120. doi: 10.1016/j.abb.2009.12.005
- Masson, P., Nachon, F., and Lockridge, O. (2010). Structural approach to the aging of phosphorylated cholinesterases. *Chem. Biol. Interact.* 187, 157–162. doi: 10.1016/j.cbi.2010.03.027
- Masson, P., and Rochu, D. (2009). Catalytic bioscavengers against toxic esters, an alternative approach for prophylaxis and treatments of poisonings. *Acta Naturae* 1, 68–79.
- Masson, P., Schopfer, L. M., Froment, M. T., Debouzy, J. C., Nachon, F., Gillon, E., et al. (2005). Hysteresis of butyrylcholinesterase in the approach to steady-state kinetics. *Chem. Biol. Interact.* 157–158, 143–152. doi: 10.1016/j.cbi.2005.10.019
- Mata, D. G., Rezk, P., Sabnekar, P., Cerasoli, D. M., and Chilukuri, N. (2014). Investigation of evolved paraoxonase-1 variants for prevention of organophosphorous pesticide compound intoxication. *J. Pharmacol. Exp. Ther.* 349, 549–558. doi: 10.1124/jpet.114.213645
- Maxwell, D. M., and Koplovitz, I. (1990). Effect of endogenous carboxylesterase on HI-6 protection against soman toxicity. *J. Pharmacol. Exp. Ther.* 254, 440–444.
- Michel, H. O., Hackley, B. E. Jr., Berkowitz, L., List, G., Hackley, E. B., Gillilan, W., et al. (1967). Ageing and dealkylation of Soman (pinacolylmethylphosphonofluoride)-inactivated eel cholinesterase. *Arch. Biochem. Biophys.* 121, 29–34. doi: 10.1016/0003-9861(67)90006-9
- Millard, C. B., Kryger, G., Ordentlich, A., Greenblatt, H. M., Harel, M., Raves, M. L., et al. (1999). Crystal structures of aged phosphorylated acetylcholinesterase: nerve agent reaction products at the atomic level. *Biochemistry* 38, 7032–7039. doi: 10.1021/bi982678j
- Millard, C. B., Lockridge, O., and Broomfield, C. A. (1995a). Design and expression of organophosphorus acid anhydride hydrolase activity in human butyrylcholinesterase. *Biochemistry* 34, 15925–15933. doi: 10.1021/bi00049a007
- Millard, C. B., Lockridge, O., and Broomfield, C. A. (1995b). *Presentation at Structure and Function of Regulatory Proteins* Bethesda: MD, NIH, Fogarty International Center.
- Millard, C. B., Lockridge, O., and Broomfield, C. A. (1998). Organophosphorus acid anhydride hydrolase activity in human butyrylcholinesterase: synergy results in a somanase. *Biochemistry* 37, 237–247. doi: 10.1021/bi972057c
- Mumford, H., and Troyer, J. K. (2011). Post-exposure therapy with recombinant human BuChE following percutaneous VX challenge in guinea-pigs. *Toxicol. Lett.* 206, 29–34. doi: 10.1016/j.toxlet.2011.05.1016
- Nachon, F., Brazzolotto, X., Trovaslet, M., and Masson, P. (2013). Progress in the development of enzyme-based nerve agent bioscavengers. *Chem. Biol. Interact.* 206, 536–544. doi: 10.1016/j.cbi.2013.06.012

- Nachon, F., Carletti, E., Wandhammer, M., Nicolet, Y., Schopfer, L. M., Masson, P., et al. (2011). X-ray crystallographic snapshots of reaction intermediates in the G117H mutant of human butyrylcholinesterase, a nerve agent target engineered into a catalytic bioscavenger. *Biochem. J.* 434, 73–82. doi: 10.1042/BJ20101648
- Newcomb, R. D., Campbell, P. M., Ollis, D. L., Cheah, E., Russell, R. J., and Oakeshott, J. G. (1997). A single amino acid substitution converts a carboxylesterase to an organophosphorus hydrolase and confers insecticide resistance on a blowfly. *Proc. Natl. Acad. Sci. U.S.A.* 94, 7464–7468. doi: 10.1073/pnas.94.14.7464
- Nicolet, Y., Lockridge, O., Masson, P., Fontecilla-Camps, J. C., and Nachon, F. (2003). Crystal structure of human butyrylcholinesterase and of its complexes with substrate and products. *J. Biol. Chem.* 278, 41141–41147. doi: 10.1074/jbc.M210241200
- Oppenorth, F. J., and van Asperen. (1960). Allelic genes in the housefly producing modified enzymes that cause organophosphate resistance. *Science* 132, 298–299. doi: 10.1126/science.132.3422.298
- Ordentlich, A., Barak, D., Kronman, C., Ariel, N., Segall, Y., Velan, B., et al. (1995). Contribution of aromatic moieties of tyrosine 133 and of the anionic subsite tryptophan 86 to catalytic efficiency and allosteric modulation of acetylcholinesterase. *J. Biol. Chem.* 270, 2082–2091. doi: 10.1074/jbc.270.5.2082
- Ordentlich, A., Barak, D., Kronman, C., Ariel, N., Segall, Y., Velan, B., et al. (1998). Functional characteristics of the oxyanion hole in human acetylcholinesterase. *J. Biol. Chem.* 273, 19509–19517. doi: 10.1074/jbc.273.31.19509
- Ordentlich, A., Barak, D., Kronman, C., Flashner, Y., Leitner, M., Segall, Y., et al. (1993). Dissection of the human acetylcholinesterase active center determinants of substrate specificity. Identification of residues constituting the anionic site, the hydrophobic site, and the acyl pocket. *J. Biol. Chem.* 268, 17083–17095.
- Otto, T. C., Kasten, S. A., Kovaleva, E., Liu, Z., Buchman, G., Tolosa, M., et al. (2010). Purification and characterization of functional human paraoxonase-1 expressed in Trichoplusia ni larvae. *Chem. Biol. Interact.* 187, 388–392. doi: 10.1016/j.cbi.2010.02.022
- Poyot, T., Nachon, F., Froment, M. T., Loiodice, M., Wieseler, S., Schopfer, L. M., et al. (2006). Mutant of *Bungarus fasciatus* acetylcholinesterase with low affinity and low hydrolase activity toward organophosphorus esters. *Biochim. Biophys. Acta* 1764, 1470–1478. doi: 10.1016/j.bbapap.2006.07.008
- Sarkar, G., and Sommer, S. S. (1990). The “megaprimer” method of site-directed mutagenesis. *Biotechniques* 8, 404–407.
- Satoh, T., and Hosokawa, M. (1995). Molecular aspects of carboxylesterase isoforms in comparison with other esterases. *Toxicol. Lett.* 82–83, 439–445. doi: 10.1016/0378-4274(95)03493-5
- Saxena, A., Sun, W., Luo, C., Myers, T. M., Koplovitz, I., Lenz, D. E., et al. (2006). Bioscavenger for protection from toxicity of organophosphorus compounds. *J. Mol. Neurosci.* 30, 145–148. doi: 10.1385/JMN:30:1:145
- Schopfer, L. M., Boeck, A. T., Broomfield, C. A., and Lockridge, O. (2004). Mutants of human butyrylcholinesterase with organophosphate hydrolase activity; evidence that His117 is a general base catalyst for hydrolysis of echothiophate. *J. Med. Chem. Def.* 2, 1–21.
- Shafferman, A., Ordentlich, A., Barak, D., Stein, D., Ariel, N., and Velan, B. (1996). Aging of phosphorylated human acetylcholinesterase: catalytic processes mediated by aromatic and polar residues of the active centre. *Biochem. J.* 318(Pt 3), 833–840.
- Shih, T. M., Duniho, S. M., and McDonough, J. H. (2003). Control of nerve agent-induced seizures is critical for neuroprotection and survival. *Toxicol. Appl. Pharmacol.* 188, 69–80. doi: 10.1016/S0041-008X(03)00019-X
- Spiller, B., Gershenson, A., Arnold, F. H., and Stevens, R. C. (1999). A structural view of evolutionary divergence. *Proc. Natl. Acad. Sci. U.S.A.* 96, 12305–12310. doi: 10.1073/pnas.96.22.12305
- Temeyer, K. B., Brake, D. K., and Schlechte, K. G. (2012). Acetylcholinesterase of *Haematobia irritans* (Diptera: Muscidae): baculovirus expression, biochemical properties, and organophosphate insensitivity of the G262A mutant. *J. Med. Entomol.* 49, 589–594. doi: 10.1603/ME11211
- Trovaslet-Leroy, M., Musilova, L., Renault, F., Brazzolotto, X., Misik, J., Novotny, L., et al. (2011). Organophosphate hydrolases as catalytic bioscavengers of organophosphorus nerve agents. *Toxicol. Lett.* 206, 14–23. doi: 10.1016/j.toxlet.2011.05.1041
- Uto, I. S., and Brewer, J. M. (2008). Hysteresis on heating and cooling of *E. coli* alkaline phosphatase. *Protein Pept. Lett.* 15, 516–520. doi: 10.2174/092986608784567582
- Valiyaveettil, M., Alamneh, Y., Rezk, P., Biggemann, L., Perkins, M. W., Sciuto, A. M., et al. (2011). Protective efficacy of catalytic bioscavenger, paraoxonase 1 against sarin and soman exposure in guinea pigs. *Biochem. Pharmacol.* 81, 800–809. doi: 10.1016/j.bcp.2010.12.024
- Wang, E. I., and Braid, P. E. (1967). Oxime reactivation of diethylphosphoryl human serum cholinesterase. *J. Biol. Chem.* 242, 2683–2687.
- Wang, Y., Boeck, A. T., Duyse, E. G., Van, K. M., Saunders, T. L., and Lockridge, O. (2004). Resistance to organophosphorus agent toxicity in transgenic mice expressing the G117H mutant of human butyrylcholinesterase. *Toxicol. Appl. Pharmacol.* 196, 356–366. doi: 10.1016/j.taap.2003.12.018
- Warshel, A. (2003). Computer simulations of enzyme catalysis: methods, progress, and insights. *Annu. Rev. Biophys. Biomol. Struct.* 32, 425–443. doi: 10.1146/annurev.biophys.32.110601.141807
- Xie, W., Altamirano, C. V., Bartels, C. F., Speirs, R. J., Cashman, J. R., and Lockridge, O. (1999). An improved cocaine hydrolase: the A328Y mutant of human butyrylcholinesterase is 4-fold more efficient. *Mol. Pharmacol.* 55, 83–91.
- Yao, Y., Liu, J., and Zhan, C. G. (2012). Why does the G117H mutation considerably improve the activity of human butyrylcholinesterase against sarin? Insights from quantum mechanical/molecular mechanical free energy calculations. *Biochemistry* 51, 8980–8992. doi: 10.1021/bi3009246
- Zhang, N. N., Liu, C. F., Yang, F., Dong, S. L., and Han, Z. J. (2012). Resistance mechanisms to chlorpyrifos and F392W mutation frequencies in the acetylcholine esterase ace1 allele of field populations of the tobacco whitefly, *Bemisia tabaci* in China. *J. Insect Sci.* 12, 41. doi: 10.1673/031.012.4101
- Zhang, Y., Kua, J., and McCammon, J. A. (2002). Role of the catalytic triad and oxyanion hole in acetylcholinesterase catalysis: an *ab initio* QM/MM study. *J. Am. Chem. Soc.* 124, 10572–10577. doi: 10.1021/ja020243m
- Zheng, F., and Zhan, C. G. (2008). Structure-and-mechanism-based design and discovery of therapeutics for cocaine overdose and addiction. *Org. Biomol. Chem.* 6, 836–843. doi: 10.1039/b716268e

Conflict of Interest Statement: While the Guest Associate Editor Carissa M. Soto and the author Patricia M. Legler are affiliated to the same Institution, the review process was handled objectively as established by the journal guidelines. The authors declare that the research was conducted in the absence of any commercial or financial relationships that could be construed as a potential conflict of interest.

Received: 13 March 2014; accepted: 19 June 2014; published online: 16 July 2014.

Citation: Legler PM, Boisvert SM, Compton JR and Millard CB (2014) Development of organophosphate hydrolase activity in a bacterial homolog of human cholinesterase. *Front. Chem.* 2:46. doi: 10.3389/fchem.2014.00046

This article was submitted to Chemical Biology, a section of the journal *Frontiers in Chemistry*.

Copyright © 2014 Legler, Boisvert, Compton and Millard. This is an open-access article distributed under the terms of the Creative Commons Attribution License (CC BY). The use, distribution or reproduction in other forums is permitted, provided the original author(s) or licensor are credited and that the original publication in this journal is cited, in accordance with accepted academic practice. No use, distribution or reproduction is permitted which does not comply with these terms.



The emergence of *Clostridium thermocellum* as a high utility candidate for consolidated bioprocessing applications

Hannah Akinosh ^{1,2}, Kelsey Yee ^{2,3}, Dan Close ³ and Arthur Ragauskas ^{2,4*}

¹ School of Chemistry and Biochemistry, Institute of Paper Science and Technology, Georgia Institute of Technology, Atlanta, GA, USA

² Oak Ridge National Laboratory, BioEnergy Science Center, Oak Ridge, TN, USA

³ Biosciences Division, Oak Ridge National Laboratory, Oak Ridge, TN, USA

⁴ Department of Chemical and Biomolecular Engineering and Department of Forestry, Wildlife, and Fisheries, University of Tennessee, Knoxville, TN, USA

Edited by:

Carissa M. Soto, Naval Research Laboratory, USA

Reviewed by:

Tatiana A. Vishnivetskaya, University of Tennessee, USA

Stephen Fong, Virginia Commonwealth University, USA

***Correspondence:**

Arthur Ragauskas, Oak Ridge National Laboratory, Department of Chemical and Biomolecular Engineering and Department of Forestry, Wildlife, and Fisheries, BioEnergy Science Center, University of Tennessee, 419 Dougherty Engineering Building, 1512 Middle Drive, Knoxville, TN 37996-2200, USA
e-mail: aragausk@utk.edu

First isolated in 1926, *Clostridium thermocellum* has recently received increased attention as a high utility candidate for use in consolidated bioprocessing (CBP) applications. These applications, which seek to process lignocellulosic biomass directly into useful products such as ethanol, are gaining traction as economically feasible routes toward the production of fuel and other high value chemical compounds as the shortcomings of fossil fuels become evident. This review evaluates *C. thermocellum*'s role in this transitory process by highlighting recent discoveries relating to its genomic, transcriptomic, proteomic, and metabolomic responses to varying biomass sources, with a special emphasis placed on providing an overview of its unique, multivariate enzyme cellulosome complex and the role that this structure performs during biomass degradation. Both naturally evolved and genetically engineered strains are examined in light of their unique attributes and responses to various biomass treatment conditions, and the genetic tools that have been employed for their creation are presented. Several future routes for potential industrial usage are presented, and it is concluded that, although there have been many advances to significantly improve *C. thermocellum*'s amenability to industrial use, several hurdles still remain to be overcome as this unique organism enjoys increased attention within the scientific community.

Keywords: *Clostridium thermocellum*, cellulosic ethanol, consolidated bioprocessing, omics, cellulosome, biomass utilization

INTRODUCTION

The current, non-renewable fossil fuels that supply the vast majority of energy needed for transportation will inevitably increase in cost as their supplies are depleted, and already present significant concerns relating to their longevity and sustainability, energy security, and environmental impact. For these reasons, renewable energy sources are attracting considerable attention as alternatives to their non-renewable counterparts. However, in the search for an alternative replacement, any new fuel compound must first meet three primary considerations in order to be regarded as a viable candidate: it must have the potential to supply the world's energy demands, it must be able to reduce negative environmental effects relative to current fossil fuels, and it must be cost-competitive. With the current state of the art, ethanol derived from lignocellulosic biomass addresses two of these considerations, however, its production in a cost-effective manner is currently lacking due to the difficulties in breaking down and converting the sugars locked within the lignocellulosic feedstocks.

These feedstocks consist primarily of cellulose, hemicellulose, and lignin, collectively referred to as lignocellulose (**Figures 1A–C**), with smaller contributions consisting of pectin, extractives, and the remaining structural ash. The cellulose

component of these mixtures is a linear polymer composed of 7000–15,000 glucose units linked by β -(1-4) glycosidic linkages (Gibson, 2012) arranged into variable repeats of crystalline, paracrystalline, and amorphous regions. The hemicellulose components of lignocellulose, on the other hand, are \sim 200–400 unit branched or linear polymers comprised of five or six carbon sugars, linked together by glycosidic bonds. The final component, lignin, is a networked polymer composed of phenyl propane units (Zeng, 2013).

One of the major barriers to the microbial production of lignocellulosic ethanol is the conversion of the cellulose and hemicellulose components of biomass to fermentable carbohydrates (Viikari et al., 2012). To overcome this hurdle, several strategies have been proposed including thermal, chemical, biochemical, or microbial approaches, as well as their various combinations, to produce fermentable carbohydrates consisting of either monomeric or polymeric C₆ and C₅ sugars. In most process schemes, this conversion of biomass into sugars typically requires an initial pretreatment step to increase plant polysaccharide accessibility, followed by the hydrolytic production of glucose from cellulose, fermentation of the pentose and hexose monomeric sugar streams to ethanol, and distillation of the

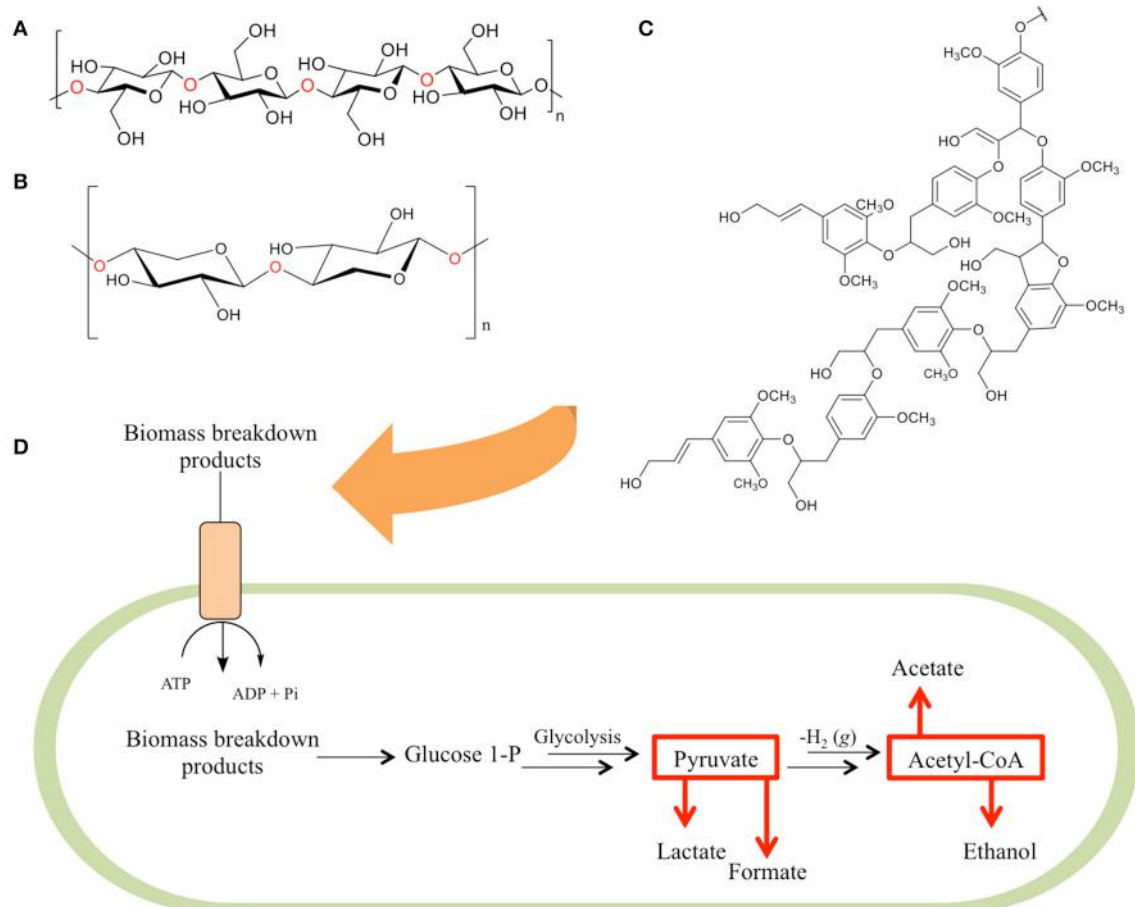


FIGURE 1 | The three primary constituents of biomass. Biomass is primarily composed of a combination of **(A)** cellulose—a homopolymer of glucose units, **(B)** hemicellulose (here depicted as xylan—a homopolymer of xylose units), and **(C)** lignin (here depicted as hardwood lignin)—a biopolymer composed of aromatic monomeric units. As these components are degraded

(D) their fermentable breakdown products are shuttled into bacterial cells via ATP binding cassette transporter proteins and internally converted to glucose-1-phosphate (G1P). G1P is utilized in a modified form of glycolysis that produces pyruvate, which is then broken down into lactate and formate, or converted to acetyl-CoA and further metabolized to acetate and ethanol.

ethanol from the fermentation mixture (Gupta and Demirbas, 2010). The pretreatment stage of this process is employed to modify the structure of the biomass, increasing accessibility and facilitating improved enzymatic hydrolysis of cellulose. During the hydrolysis stage, acids or hydrolytic enzymes degrade the cellulose into glucose monomers. These acidic treatments, which disrupt the glycosidic linkages in both cellulose (Orozco et al., 2007) and hemicellulose (Lavarack et al., 2002), can further be subdivided into distinct categories depending on the methods employed. In practice, however, most major approaches utilize the application of either concentrated or dilute, ionic-liquid-mediated or solid acids (Amarasekara, 2013).

While this acid-based approach offers lower costs, shorter processing times and greater resistance to product inhibition than hydrolytic enzyme-based approaches, cellulases remain the preferred tools for carrying out hydrolysis. This is because, unlike acid hydrolysis, cellulase-based enzymatic hydrolysis employs milder conditions, reduces capital costs, produces higher yields, and does not generate inhibitory byproducts that can disrupt

downstream fermentation by microorganisms (Taherzadeh and Karimi, 2007). In addition, the acid-catalyzed hydrolysis of cellulose generates carbohydrate-derived dehydration products, which are undesirable for the cellulase-based deconstruction of cellulose (Kumar et al., 2013). Recently, studies have been conducted to improve the efficiency and decrease the cost of the enzymatic hydrolysis process using recombinant technologies (Fang and Xia, 2013), ionic liquids (Engel et al., 2012), accessory enzymes (Hu et al., 2011), and alterations of plant cell wall structure focused on modification to their lignin content (Chen and Dixon, 2007; Hisano et al., 2009; Fu et al., 2011; Shen et al., 2013), however, this stage still remains as the main bottleneck preventing cost efficiency. Therefore, as an alternative, the direct saccharification of lignocellulosic biomass has similarly been investigated, but has been shown to negatively impact the efficiency of enzymatic hydrolysis when compared to the saccharification of pretreated substrates in a variety of biomass sources (Intanakul et al., 2003; Zhang et al., 2007a,b).

Currently, most industrial lignocellulosic bioprocessing applications utilize *Escherichia coli*, *Zymomonas mobilis*, *Saccharomyces cerevisiae*, or a handful of other yeast strains in conjunction with exogenous hydrolytic enzymes to release fermentable sugars from the biomass substrate. These organisms, however, are utilized primarily because of their thoroughly developed and studied genetic engineering toolkits, physiology, and metabolic pathways. As a possible exception, *S. cerevisiae* does have several advantageous traits such as its natural ethanol tolerance and ability to grow at acidic pH, however, it remains incapable of surviving at the optimal temperatures of exogenous hydrolytic enzymes and, in its wild type form, is unable to ferment pentose sugars (Vermerris, 2008; Tracy et al., 2012).

One promising approach to circumventing the cost and restriction of this conventional workflow is the use of consolidated bioprocessing (CBP). CBP technologies combine the enzyme production, hydrolysis, and fermentation stages into a single step, improving processing efficiencies, eliminating the need for added exogenous hydrolytic enzymes, and reducing the sugar inhibition of cellulases (Lynd et al., 2005; Xu et al., 2009b; Olson et al., 2012). This approach reduces the number of unit operations, and lowers the overall capital cost of the process (Olson et al., 2010, 2012).

However, for this approach to be economically feasible, an industrially relevant CBP microorganism is required that produces a hydrolytic enzyme system capable of solubilizing a realistic biomass substrate and fermenting both hexose and pentose sugars to ethanol at >90% of its theoretical yield, a titer of at least 40 g/L, and a fermentation rate of >1 g/L/h (Lynd, 1996; Dien et al., 2003). Unfortunately, no microorganisms with these characteristics have yet been discovered, and therefore genetic engineering strategies will be required to develop such a strain. In this regard, two strategies have been developed to engineer an appropriate organism. The first approach seeks to engineer a naturally highly efficient cellulolytic microbe to produce the desired product. The second approach applies a recombinant cellulolytic strategy, and strives to engineer a microbe with naturally high product titer, rate, and yield to express a hydrolytic enzyme system that efficiently solubilizes biomass substrates (Lynd et al., 2005; Alper and Stephanopoulos, 2009; Olson et al., 2012; Blumer-Schuette et al., 2013).

While there are myriad gene sets available that encode enzymes capable of degrading plant biomass, heterologously expressing these suites of enzymes in a non-natively cellulolytic host microorganism requires the transfer, optimization, expression, and coordination of many genes. This potentially represents a more difficult barrier to overcome than engineering a naturally cellulolytic microorganism to produce ethanol. Therefore, thermophilic cellulolytic microorganisms have become attractive targets for this approach, as their growth at high temperatures reduces the risk of contamination, integrates well with existing processing streams, and increases the solubility and digestibility of their required substrates (Demain et al., 2005; Egorova and Antranikian, 2005; Blumer-Schuette et al., 2013). However, regardless of which strategy is realized, each has the potential to unlock an efficient method for the production of ethanol from lignocellulosic biomass (Lynd et al., 2002, 2005; Dien et al.,

2003; Zhang, 2011; Olson et al., 2012). To date, a wide variety of microorganisms have been investigated for this process (Taylor et al., 2009; Hasunuma et al., 2013), however, *Clostridium thermocellum* has emerged as a particularly attractive high utility candidate because its use of a cellulosome has demonstrated remarkable enzymatic hydrolysis efficiency compared to free cellulases (Johnson et al., 1982; Lu et al., 2006). This review will therefore focus specifically on *C. thermocellum*'s role as a candidate for CBP and how it can be utilized to improve the suitability of this process toward the production of ethanol as a realistic replacement for existing liquid transportation fuel sources.

CLOSTRIDIUM THERMOCELLUM

ISOLATION AND INITIAL CHARACTERIZATION

C. thermocellum is an anaerobic, rod shaped, Gram positive thermophile that is capable of producing ethanol directly from cellulose. Despite its relatively recent rise to popularity in the literature, it was first isolated in 1926 by Viljoen et al. in an attempt to identify novel organisms capable of degrading cellulose. This initial characterization by Viljoen, while basic, provided the framework required for future investigators to work with and develop this unique organism, but proved unreliable due to potential contamination of the culture with additional organisms (Viljoen et al., 1926). The first robust description, therefore, was not available until almost 30 years later. This characterization was the first to report that *C. thermocellum* could grow at temperatures between 50 and 68°C, and demonstrated this growth on cellulose, cellobiose, xylose, and hemicelluloses. It also detailed the major fermentation products, consisting primarily of carbon dioxide and hydrogen gases, formic, acetic, lactic, and succinic acids, and ethanol (McBee, 1954). It is important to note, however, that significant discrepancies in the list of fermentable carbon sources have been shown to exist among alternate characterized *C. thermocellum* strains, so caution must be taken when comparing the growth conditions in the early literature (McBee, 1950).

Following these initial characterizations, there were still many setbacks in the initial attempts at culturing *C. thermocellum* and isolating pure stocks (McBee, 1948). Fortunately, these have largely been overcome with the development of defined media that allow for routine growth and maintenance of *C. thermocellum* cultures (Fleming and Quinn, 1971; Johnson et al., 1981), significantly improving the ease of subculturing and providing an ideal environment for defined selection and genetic modification. As these media were developed, they determined a requirement for several essential vitamins, including biotin, pyridoxamine, B₁₂, and *p*-aminobenzoic acid (Johnson et al., 1981) and demonstrated a requirement for pH maintenance between 6.2 and 7.7. It is now known, however, that the optimal pH for growth occurs between 6.7 and 7.0 (Freier et al., 1988) and that the optimal growth temperature is 55°C.

Employing these defined growth techniques, *C. thermocellum* can be cultured using either batch or continuous flow approaches, with growth rates of 0.10/h and 0.16/h, respectively (Lynd et al., 1989). However, in the presence of cellulosic material *C. thermocellum* has been observed to form biofilms, which may more closely resemble its growth under environmental conditions.

Upon biofilm formation, *C. thermocellum* will orient itself parallel to the carbon fibers of its substrate, forming a single monolayer of cells that will gradually spread outward from the initial site of colonization. These cells will closely mimic the topography of the substrate, with each cell maintaining direct contact if possible (Dumitache et al., 2013). This orientation may be maintained in order to facilitate the extracellular hydrolysis of the substrate, which is then incorporated into the cell directly as soluble oligosaccharides and used for fermentative catabolism (Zhang and Lynd, 2005). Throughout this process, cells are constantly attaching and detaching from the carbon source, with no apparent correlation to cellular life cycling, and relatively similar percentages of cells involved in division or sporulation in either their attached ($11 \pm 3\%$) or detached ($5 \pm 3\%$) states (Dumitache et al., 2013).

One of the main products of this fermentation activity, and indeed the reason that *C. thermocellum* has enjoyed increased attention in the recent past, is ethyl alcohol. However, despite the production of this fermentation end product, wild type *C. thermocellum* can only tolerate ethanol up to 5 g/L before it is significantly inhibited (Herrero and Gomez, 1980). A contributing factor toward this sensitivity has been determined to be the endogenous membrane structure. The predominant lipids that make up *C. thermocellum*'s cell wall are branched and straight chain 16 carbon fatty acids, and 16 carbon plasmalogens that, along with the other components, display a total lipid content of $\sim 82 \mu\text{g}/\text{mg}$ dry cell weight, with roughly 28% of that weight comprised of plasmoglycerols (Timmons et al., 2009). This membrane orientation leads to a high degree of fluidity that is compounded by the presence of moderate levels of ethanol. As the fluidity increases, the membrane begins to lose its integrity and the health of the cell is negatively impacted. Therefore, in order to tolerate increased levels of ethanol *C. thermocellum* must alter its membrane composition to decrease fluidity and compensate for the artificial fluidity imparted by its own fermentation products.

AMENABILITY TO CONSOLIDATED BIOPROCESSING

Despite its endogenous disadvantage of ethanol inhibition, *C. thermocellum* retains many qualities that position it well for use as a CBP organism, including its fast rate of digestion of cellulose from plant biomass and its ability to hydrolyze both hemicellulose and cellulose. In addition, it is capable of naturally producing ethanol, albeit at low concentrations ($< 3 \text{ g/L}$), and one strain, DSM 1313, has both a finished genome sequence and a developed genetic transformation system that allows for the construction of mutant strains (Tyurin et al., 2004; Tripathi et al., 2010; Feinberg et al., 2011; Olson and Lynd, 2012b; Mohr et al., 2013). Although it does suffer from a detriment in that it can only utilize C₆ sugars, it has been demonstrated to perform efficiently in co-culture with C₆ and C₅ utilizing thermophilic anaerobic bacteria, making it an excellent springboard for development into a CBP host.

STRUCTURE, FUNCTION, AND FERMENTATIVE CHARACTERISTICS OF THE *C. thermocellum* CELLULOSOME

The distinguishing feature of *C. thermocellum*, and indeed its most attractive feature as a platform for development into a CBP

host, is its cellulosome. The cellulosome is an extracellular multi-enzyme complex 18 nm in diameter with a molecular weight greater than $2 \times 10^6 \text{ Da}$ (Uversky and Kataeva, 2006) that is central to *C. thermocellum*'s ability to reduce lignocellulosic biomass recalcitrance (Figure 2) (Bayer et al., 2009). This multi-enzyme complex consists of over 20 distinct enzymes (Wertz and Bédué, 2013), housing cellulases, hemicellulases, pectinases, chitinases, glycosidases, and esterases for the breakdown of lignocellulose (Spinnler et al., 1986; Zverlov et al., 2005a).

Characterization of the cellulosome began in the 1980s, and since that time a stream of discoveries have elucidated its role in cellulose binding (Bayer et al., 1983; Lamed et al., 1983), its position on the bacterial cell wall surface (Bayer et al., 1985), its structure during cellulose degradation (Bayer and Lamed, 1986), and its diversity of associated cellulases (Garcia-Martinez et al., 1980). Central to the assembly of this complex is a macromolecular non-catalytic scaffoldin protein known as CipA. This CipA scaffoldin contains nine type I cohesin domains that bind to type I dockerin domains, which are in turn connected to the catalytic domains of their enzymes through a linker (Dror et al., 2003b) in a calcium-dependent fashion (Shimon et al., 1997). CipA is itself anchored to the bacterial cell surface by way of a type II dockerin and mediated by the LpB, Orf2p, and SdbA anchoring proteins (Dror et al., 2003b) and, in addition, also contains a carbohydrate binding module that attaches the cellulosome to its carbohydrate substrate (Gilbert, 2007).

Crystallographic interrogation has suggested that these integral cohesin-dockerin complexes are primarily mediated by hydrophobic interactions, (Carvalho et al., 2003), and these results have been supported via subsequent molecular dynamics simulations as well (Xu et al., 2009a). As such, it has been presumed that the cellulosome assembles in a non-selective or mildly selective manner due to the inability to assign each dockerin to a single cohesin and the relative similarities in affinity between several dockerins and cohesins (Shimon et al., 1997). However, evidence has recently surfaced that suggests some degree of selectivity. Sakka et al. observed the binding of the CelJ dockerin only to selected cohesin modules, indicating a degree of specificity during cohesin-dockerin recognition that was not previously detected (Sakka et al., 2009). Similarly, Borne et al. have studied the role of randomness during the binding of an alternative *Clostridium cellulolyticum* dockerin to a chimeric scaffoldin containing one *C. cellulolyticum* cohesin and one *C. thermocellum* cohesin. In this case, binding occurred successively in a manner dependent on linker length, reinforcing the notion of order during cellulosomal assembly (Borne et al., 2013).

Findings that support selectivity surrounding enzyme recruitment and/or synergistic effects present during the digestion of biomass point toward major advancements in the production of cellulosic ethanol via the optimization of enzyme combinations. For example, opportunities for synergy between cellulases in *C. thermocellum*'s cellulosome during the degradation of crystalline cellulose increase statistically as the number of cohesins present on the scaffoldin increases. In one study, the inclusion of two cohesins instead of one on the cellulosome increased synergism by a factor of 1.7 (Krauss et al., 2012).

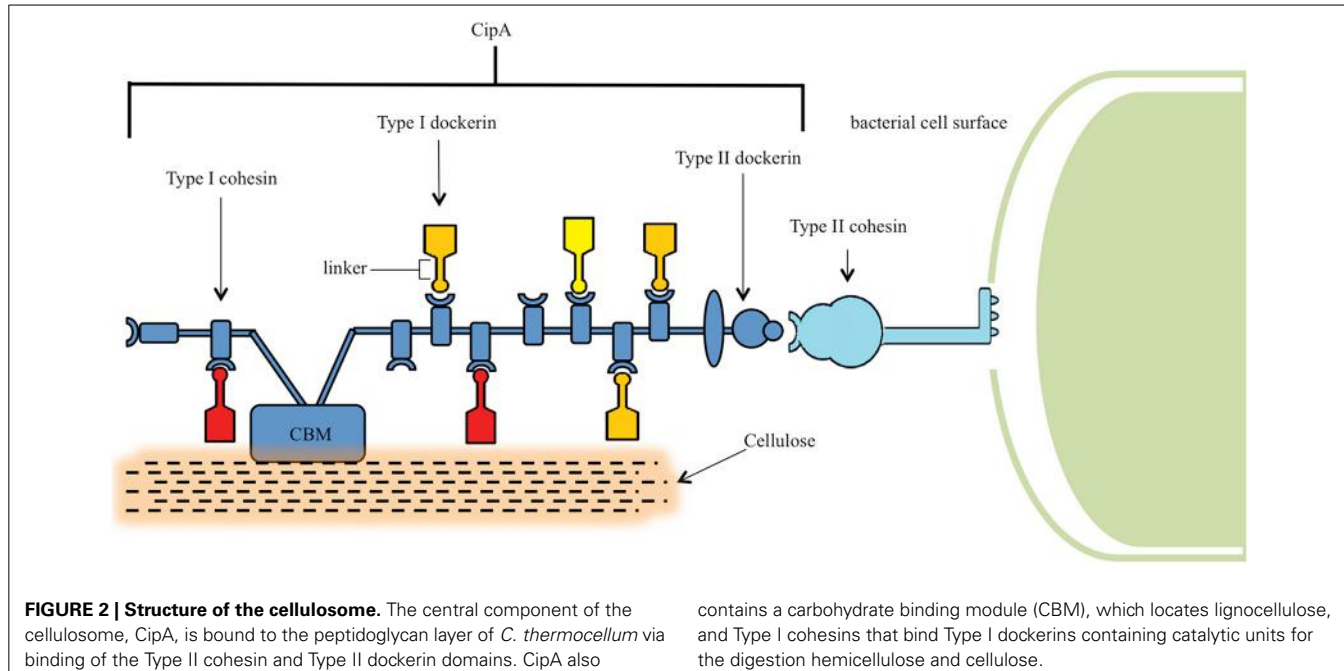


FIGURE 2 | Structure of the cellulosome. The central component of the cellulosome, CipA, is bound to the peptidoglycan layer of *C. thermocellum* via binding of the Type II cohesin and Type II dockerin domains. CipA also

contains a carbohydrate binding module (CBM), which locates lignocellulose, and Type I cohesins that bind Type I dockerins containing catalytic units for the digestion hemicellulose and cellulose.

To take advantage of this fact, and leverage the utility of the cellulosome itself, an artificial cellulosome, termed the rosettosome has been genetically engineered to incorporate the dockerin domains of cellulases from *C. thermocellum*. Just as with the native cellulosome, this rosettosome has demonstrated enhanced cellulolytic activities as additional cellulases have been attached (Mitsuzawa et al., 2009). Building upon these efforts, Gefen et al. have developed a chimeric cellulosome, BglA-CohII, that was designed to manage cellobiose inhibition by affixing a β -glucosidase (BGL) to one of the open binding domains. This attachment of BGL lessened cellobiose inhibition in the presence of Avicel and pretreated switchgrass relative to the native cellulosome with or without BGL present (Gefen et al., 2012).

These findings have led to the development of the plasticity theory, which rationalizes this synergistic behavior. This theory contends that the flexibility of a linker within the cellulosome directly leads to its enhanced adaptability toward utilization of different substrates. Coarse-grain models have investigated this theory by monitoring plasticity and uncovering the preferential scaffoldin binding of dockerins from CbhA, a large endoglucanase, over those from the smaller CelS exoglucanase and Cel5B endoglucanase, even though each had the potential to bind to any cohesin. In these models, the large structure of the CelS exoglucanase appeared to influence key parameters such as its extended scaffoldin residence time and its prolonged diffusion rate, both of which improved its likelihood of binding (Bomble et al., 2011).

Regardless of the components employed, the cellulosome breaks down its lignocellulosic substrate into celodextrins, which are brought into the cell via one of at least five identified ATP binding cassette transporter proteins (Nataf et al., 2009) in order to support a modified form of glycolysis (Gefen et al., 2012). Once within the cell, cellobiose phosphorylase or cellodextrin phosphorylase phosphorylates the cellobiose or cellodextrin, respectively,

to yield glucose-1-phosphate and glucose. These compounds are then shunted to the Embden-Meyerhof pathway, and glycolysis takes place to yield pyruvate, GTP, and ATP. Thereafter, a series of phosphorylation reactions follow, although the exact nature and flux of these reactions has not yet been fully elucidated (Zhou et al., 2013). Under our current understanding, both ATP and GTP-linked glucokinases have been identified in *C. thermocellum*, as well as phosphoenolpyruvate carboxykinase, which may be responsible for the conversion of phosphoenolpyruvate to oxaloacetic acid. This has led to the assumption that both of these compounds undergo glycolysis to produce ethanol during fermentation (Zhou et al., 2013). Pyruvate is similarly converted into several fermentation products depending on the enzyme that catalyzes the reaction, with lactate dehydrogenase forming lactate and pyruvate formate-lyase forming formate (Rydzak et al., 2011). These products are then available for use just as with traditional processing strategies, completing the CBP process.

The cellulosome is one of the fastest crystalline cellulose utilizers, however, there are many other hydrolytic enzymes associated with the cellulosome, including pectinases and hemicellulases, which are also essential for digestion of biomass feedstocks. While relatively fewer studies have been undertaken to explore these components, when *C. thermocellum*'s draft genome sequence was screened for open reading frames related to cellulosomal components, it was discovered that only one third of these were related to cellulases and the rest were related to hemicellulases, pectinases, chitinases, glycosidases, and esterases (Zverlov et al., 2005a). Of particular interest from these groups of enzymes are the hemicellulases, which can degrade the hemicellulose matrix through the random cleavage of carbohydrates. Zverlov et al. characterized the structure and activity of two hemicellulolytic cellulosome components consisting of xyloglucanase Xgh74A and endoxylanase Xyn10D, demonstrating that when their lysis events occurred

in close enough proximity, short oligosaccharides were formed that assisted in exposing the underlying cellulose (Zverlov et al., 2005b). Moreover, it has been demonstrated that *C. thermocellum* JW20 (ATCC 31549) preferentially digests high degree of polymerization xylan, a hemicellulose common to birch wood, with degradation becoming increasingly efficient as the number of monomer units in xylan exceeds six. In contrast, degradation of lower, 2–5 unit, degree of polymerization xylan did not occur until 240 h later and, after 300 h, only xylose remained, as these monomers are not imported by the cell (Wiegel et al., 1985). Taken together, these findings support the hypothesis that *C. thermocellum*'s hemicellulases preferentially degrade high degree of polymerization hemicellulose.

Current studies evaluating the interaction of the cellulosome relative to free cellulases for digestion of either crystalline cellulose or plant biomass have provided additional insights into their mechanisms of hydrolysis, potentially leading to improvements in the deconstruction step through enzyme engineering and optimization of biomass pretreatment conditions. For instance, the cell free cellulosome of *C. thermocellum* can process roughly 40% of high degree of polymerization cellulose (presented as Whatman filter paper) in 120 h, compared with free *Trichoderma reesei* cellulases that can only achieve less than 20% conversion in the same time frame (Resch et al., 2013). However, in contrast, the *T. reesei* free enzyme system was more active on plant biomass than the cell free cellulosome extract. Moreover, post enzymatic hydrolysis images of the crystalline cellulose substrate determined that the mechanisms were vastly different between the free enzyme cocktail, which used a fibril sharpening method, and the cellulosome, which splayed open and separated the individual microfibrils (Resch et al., 2013). Most importantly, however, has been the demonstration of synergistic effects when these two approaches are combined. Ding et al. revealed that this is likely due to a difference in mechanisms between the free enzyme systems and the cellulosome. Using real-time imaging, to show the production of solubilization pits in the surface of the delignified plant biomass treated with free enzyme systems and the splaying of individual microfibrils in cellulosome-treated biomass, they concluded that biomass pretreatments which remove the highest amount of lignin and leave the largest amount of carbohydrates will facilitate improved hydrolysis regardless of whether a free enzyme system or cellulosome is employed (Ding et al., 2012).

FERMENTATION OF BIOMASS BY *C. thermocellum*

The high degree of biomass recalcitrance is one of the major factors limiting the cost-effective production of lignocellulosic ethanol. Therefore, the ability of *C. thermocellum* to efficiently digest a range of biomass structures is an important consideration for its practicality as a CBP host. To investigate its fermentative abilities, Puls et al. compiled one of the earliest characterization studies relating to the solid residuals remaining after cellulosomal processing of steam pretreated, sodium chlorite delignified birch-wood by *C. thermocellum*. It was discovered that, following treatment, the solid residuals contained an unchanged crystallinity content (52%) that was attributed to the simultaneous hydrolysis of amorphous and crystalline cellulose. Cellulose experienced an increase in its weight-average degree of polymerization,

while the polydispersity remained the same following microbial treatment, indicating the preferential consumption of low degree of polymerization cellulose. These findings ran contrary to those obtained using free cellulases from *Neocallimastix frontalis*, *Trichoderma koningii*, and *Penicillium pinophilum*, providing one of the first indications that the organization and ultrastructure of *C. thermocellum*'s cellulosome contained unusual properties (Puls and Wood, 1991).

Since that time, many additional studies have been performed to elucidate the function of *C. thermocellum*'s cellulosome on a variety of substrates. One of the main focal points of these studies has been to determine how *C. thermocellum*'s cellulosome circumvents the inhibition of activity and adsorption that cellulose crystallinity has imparted on many previously characterized fungal cellulases (Hall et al., 2010; Zhao et al., 2012). In this regard, it has been determined that *C. thermocellum* approaches deconstruction atypically, in that it displays a remarkable propensity toward the hydrolysis of crystalline cellulose. For instance, *C. thermocellum* is capable of converting 100% of Avicel, which is 74% crystalline, in 100 h, compared to free cellulases isolated from *T. reesei*, which were only able to consume 50% of Avicel in the same time frame (Resch et al., 2013). While this is encouraging, it should be noted that, in general, Avicel demonstrates excellent conversion properties in comparison to pretreated biomass. Therefore, to expand the scope of this evaluation, Shao et al. further identified differences in *C. thermocellum*'s efficiency during the CBP of Avicel and ammonia fiber expansion pretreated (AFEX) corn stover. While Avicel displayed high conversion rates (>95%) after 24 h when treated with *C. thermocellum*, AFEX pretreated corn stover glucan experienced lower conversion rates (60–70%), even after extended incubation times of 4 days. While the reason for this discrepancy in efficiencies was not elucidated during this study, initial enzyme concentrations and restricted cell growth on AFEX pretreated corn stover were ruled out as possibilities (Shao et al., 2011a).

Along with differences in biomass structure, the employment of differing pretreatment methods have also been shown to influence *C. thermocellum*'s digestion and fermentation efficiency. Hörmeyer et al. investigated the treatment of Avicel, poplar (*Populus tremuloides*), and wheat straw (*Triticum vulgare*) with *C. thermocellum* strain NCIB 10682 using either unpretreated, organosolv (methanol/water), or hydrothermolysis pretreated biomass, and used pH to indicate the extent of cellulose metabolism via acetic acid production. Under this experimental design, hydrothermally-treated poplar produced lower pHs (~6.0–7.0) than unpretreated poplar (~7.4) after 150 min of processing, signifying an increased efficiency in the presence of the hydrothermal substrate (Hörmeyer et al., 1988). Likely, this increase in efficiency can be attributed to the structural changes incurred by the biomass during pretreatment, which led to an increased accessibility of the sugars during digestion while maintaining favorable conditions for growth and enzymatic function (Resch et al., 2013). Alternate strategies for overcoming the recalcitrance barrier, such as altering the plant cell wall structure to be more easily digested by reducing lignin content or altering lignin composition, have also been employed (Chen and Dixon, 2007; Hisano et al., 2009). Fu et al. and Yee et al. demonstrated the

feasibility of this approach, showing that a transgenic switchgrass with reduced lignin content and syringyl/guaiacyl (S/G) ratios had improved fermentation yield and required a lower severity pretreatment and less enzyme loading to obtain equivalent yields to their control switchgrass when employing a yeast-based fermentation with exogenous hydrolytic enzymes in a simultaneous saccharification and fermentation (SSF) format. More importantly, they observed that *C. thermocellum* exhibited equivalent or higher fermentation yields than the yeast-based SSF approach, which lead to the hypothesis that the cellulosome is more reactive in a CBP format than a cell-free extract configuration (Fu et al., 2011; Yee et al., 2012). In an alternate approach, Bothun et al. subjected *C. thermocellum* to elevated hydrostatic pressures (7.0 and 17.3 MPa) in a high pressure bioreactor, resulting in a ~100-fold rise in the ethanol:acetate ratio compared to batch cultures at atmospheric pressure. These results were attributed to the enhanced solubility of gaseous fermentation products under their reaction conditions (Bothun et al., 2004), further demonstrating the importance of pretreatment conditions on hydrolysis and fermentation efficiency.

GENOMIC, TRANSCRIPTOMIC, PROTEOMIC, AND METABOLIC RESPONSES TO ETHANOL PRODUCTION

Due to its high amenability toward use as a CBP organism, *C. thermocellum* has attracted significant interest in its genomic, transcriptomic, proteomic, and metabolomic profiles and their respective dynamics throughout the CBP process. These evaluations have been performed across a variety of different strains and, taken together, provide crucial insight into how it is able to perform the complex reactions necessary to break down and utilize cellulosic material.

At its most basic level, the genome of the type strain, *C. thermocellum* 27405, consists of 3.8 Mb of DNA arranged as a single chromosome. The average guanine/cytosine (GC) content of the genome is a moderate 38.9%, and 3173 candidate protein encoding genes have been identified via automated analysis (Hauser et al., 2010). In addition to the type strain, sequences for several additional strains have also been elucidated and yielded similar characteristics (Hemme et al., 2010; Feinberg et al., 2011; Brown et al., 2012). Genomic analysis following adaptation to increased ethanol tolerance has indicated several conserved genetic alterations, including changes to glucokinases, aminotransferases, transcriptional regulators, aldehyde/alcohol dehydrogenases, and aspartate carbamoyltransferases. In addition, non-conserved changes have been identified in a variety of membrane proteins as well. Taken together, these genetic changes significantly improved *C. thermocellum*'s ethanol tolerance from ~15 to 50 g/L and improved its utility as a CBP host (Shao et al., 2011b).

While relatively few genetic changes were discovered related to enhanced ethanol tolerance, significantly more transcriptomic alterations have been observed that can provide insight into how *C. thermocellum* responds to changes in substrate availability and ethanol production. Transcriptomic analysis revealed a set of 348 genes that displayed significant variation in their expression levels in response to utilization of either cellulose or cellobiose as a carbon source, or concurrent with changes in growth rate resulting

from nutrient availability and population density. Of these 348 genes, 78 demonstrated a significant decrease in expression when cellobiose was provided as a carbon source and 95 were up regulated. Of note is that the majority of these genes contained signal peptides, or were transcriptional regulators, indicating that they are likely involved in the extracellular recruitment and uptake of metabolites, demonstrating *C. thermocellum*'s ability to sense and respond to external cues regarding nutrient availability (Riederer et al., 2011). Similarly, switching from cellobiose to cellulose fermentation elicited changes in the expression of roughly 40% of all genes, with expression profiles generally indicating increased transcription levels for those genes related to energy production, translation, glycolysis, and amino acid, nucleotide, and coenzyme metabolism. Expression of these genes under cellulose utilization was shown to be growth stage dependent, with transcription decreasing as the available cellulose is consumed and transcription of genes encoding for cellular structure and motility, chemotaxis, signal transduction, transcription, and cellulosomal proteins becoming increased, presumably due to an increased necessity to discover alternative carbon sources in accordance with the classic feast-or-famine survival strategy (Raman et al., 2011). When pretreated biomass was supplied in place of cellulose or cellobiose, an even larger number of genes displayed differential regulation. Using pretreated yellow poplar as a model carbon source, 1211 genes were up regulated, and 314 were down regulated compared to growth on cellobiose. Of particular note is that 47 of the 81 recognized cellulose genes (58%) were up regulated upon yellow poplar-mediated biomass growth, compared with only 4 that showed lower expression levels relative to cellobiose fermentation. In addition to these cellulose genes, significant up regulation was also observed for genes involved in inorganic ion transport and metabolism, signal transduction, and amino acid transport (Wei et al., 2014). Similar regulation profiles were found, albeit with up regulation of phosphate transport and Resistance-Nodulation-Division (RND) transporters, when pretreated switchgrass was substituted for poplar (Wilson et al., 2013a). Together, these results demonstrate the significant differences that can be imparted when *C. thermocellum* transitions between prepared sugars and raw biomass as carbon sources.

In general, the results obtained from these transcriptomic studies are supported by similar proteomic studies that have directly interrogated protein levels under similar growth conditions. Expression of the core metabolic proteins, as predicted, reveals that they are primarily growth-phase dependent in order to position *C. thermocellum* for the most efficient use of the nutrients on hand under growth and stationary phases, leading to much more consistent expression levels relative to specialized proteins such as those found in the cellulosome. Approximately a quarter of the 144 core metabolic proteins demonstrate only a moderate change in expression as the cells transition from exponential to stationary phase, with several notable exceptions including decreases in the presence of pyruvate synthesis machinery and increases in the prevalence of glycogen metabolism, pyruvate catabolism, and end product synthesis pathway proteins (Rydzak et al., 2012). Much more expression variability has been detected, and indeed much more research has been focused, on the proteins comprising the cellulosome. Unlike the relatively

consistent expression of core metabolic proteins, cellulose proteins demonstrate expression variability in response to changes in carbon source availability. When presented with cellobiose, hemicellulases are the most abundant cellulose components, with XynA, XynC, XynZ, and XghA up regulated alongside of the endoglucanase CelA and GH5 endoglucanases CelB, CelE, and CelG. Conversely, when presented with cellulose as a carbon source, the GH9 cellulases represented the most abundant group, along with the cell surface anchor protein OlpB and the exoglucanases CelS and CelK (Gold and Martin, 2007). These same trends continue to manifest when pretreated switchgrass is used as a feedstock, with the exoglucanase CelK and the GH9 cellulases further increasing in abundance relative to cellulose fermentation. Notably, under switchgrass utilization the xylanases decrease in prevalence, possibly due to removal of the majority of hemicellulose and reduction of xylan content in the switchgrass following dilute acid pretreatment (Raman et al., 2009). Importantly, it has also been noted that expression of many of the cellulose proteins is decreased following adaption to increased ethanol tolerance. Indeed, while ethanol tolerant strains can still degrade cellulose, both the rate and extent of this degradation is impaired due to this down regulated expression (Williams et al., 2007).

Compared to the genetic, transcriptomic, and proteomic studies that have been performed, there have been relatively few investigations regarding *C. thermocellum*'s metabolomics under laboratory or natural growth conditions. It is known, however, that, relative to cellobiose, growth on cellulose results in diversion of carbon flow into a transhydrogenase-malate pathway, resulting in increases to available NADPH and GTP supplies. Assimilation of ammonia is also up regulated under these growth conditions, resulting from an increase in the production of glutamate dehydrogenase as *C. thermocellum* repositions itself to produce the biosynthetic intermediates necessary to respond to cellulose utilization (Burton and Martin, 2012). Additional evidence suggests that the end products of this fermentative process can similarly alter metabolic activity as well. As ethanol and lactate collect, H₂ and acetate yields coordinately increase, while ethanol yields themselves are shown to increase upon accumulation of H₂, acetate, and lactate (Rydzak et al., 2011). In an effort to improve our knowledge regarding *C. thermocellum* metabolism, and to aid in the development of engineered strains, a flux balance model of *C. thermocellum* metabolism has recently been developed (Roberts et al., 2010) that will hopefully aid in developing this nascent field.

EFFORTS TO ENHANCE ETHANOL PRODUCTION FROM *C. thermocellum*

DEVELOPMENT OF ENGINEERED STRAINS

In nature, *C. thermocellum*'s main ecological function is to degrade cellulose, and in this regard it is one of the fastest crystalline cellulose utilizers. This characteristic has led to a series of studies that have robustly characterized its function in regards to the digestion of plant biomass (Saddler and Chan, 1982; Lynd et al., 1989; Raman et al., 2009; Fu et al., 2011; Shao et al., 2011a; Yee et al., 2012; Wilson et al., 2013a), however, until recently there has been a deficit in our understanding of *C. thermocellum*'s

genetic and proteomic functions that have hindered its development as an ideal CBP host. The recent attainment of a finished, annotated genome sequence and an enhanced understanding of its gene and protein expression, in combination with metabolic pathway models, has filled this gap and become essential for the development of targeted genetic engineering strategies and optimization of fermentation conditions that are needed to move forward in strain development. In a wider sense, these aspects have also been crucial for improving the feasibility of CBP as a platform for production of biofuels as well (Stevenson and Weimer, 2005; Lu et al., 2006; Brown et al., 2007; Islam et al., 2009; Raman et al., 2009, 2011; Roberts et al., 2010; Rydzak et al., 2011, 2012; Shao et al., 2011b; Ellis et al., 2012; Li et al., 2012; Wilson et al., 2013a,b).

To this end, several engineered strains have been developed using adapted or directed evolution to improve ethanol or inhibitor tolerance, as these traits have been deemed the most important for industrial applications (Table 1). Linville et al. reported the development of a mutant strain through direct evolution of *C. thermocellum* ATCC 27405 that displayed an enhanced growth rate and tolerance up to 17.5% vol/vol dilute acid pretreated poplar hydrolysate (Linville et al., 2013). Resequencing of the wild type and mutant strains indicated that multiple mutations were responsible for this phenotype, including genes related to cell repair and energy metabolism. Similarly, a wild type *C. thermocellum* culture was adapted through sequential passaging to tolerate 8% wt/vol (80 g/L) ethanol and several analysis were performed to determine the basis of this increased tolerance in the mutant strain, which was designated strain *C. thermocellum* EA. Proteomic analysis of this strain by Williams et al. showed changes in membrane-associated proteins, leading them to hypothesize that the increased tolerance was the result of lower quantities and/or lower incorporation rates of proteins into the membrane, preventing increased fluidity upon ethanol exposure (Williams et al., 2007). Further analysis by Timmons et al. corroborated this hypothesis by observing changes in the fatty acid membrane composition that endowed the mutant strain with increased membrane rigidity, reducing the fluidizing effect of ethanol (Timmons et al., 2009). Recently, Brown et al. resequenced the genome of the mutant strain and, in comparison to the wild type, identified the genetic basis of this tolerance as a mutation in the bifunctional *adhE* gene. This was then confirmed by recreating the mutation in the more genetically tractable DSM 1313 strain (Brown et al., 2011).

Isolation of additional *C. thermocellum* strains is also ongoing, with the novel CS7, CS8, and S14 strains being isolated from compost and bagasse paper sludge, respectively (Tachaapaikoon et al., 2012; Lv and Yu, 2013). Interestingly, when the CS7 and CS8 strains were characterized for growth on crystalline cellulose and cellobiose, in contrast to the majority of *C. thermocellum* strains, neither exhibited any xylanase activity. However, both of these strains demonstrated increased ethanol:acetate ratios and enhanced cellulase activity in comparison to the wild type strain. Strain S14 also proved to be notable, as its cellulosomal glycoside hydrolases provided increased crystalline cellulose degradation rates relative to both the wild type and to strain JW20. In addition, strain S14 was found to tolerate both a higher temperature (70°C)

Table 1 | Natural and engineered *C. thermocellum* strains used for consolidated bioprocessing.

Strain	Growth conditions						Products				Efficiency			References
	Substrate	Medium	Temp (°C)	pH	Ethanol (g/L)	Acetate (g/L)	Lactate (g/L)	Propionate (g/L)	CO ₂ (g/L)	H ₂ (g/L)	Carbon Recovery	Yield	Economic feasibility	
27405	0.3 % wt/vol Milled Filter Paper	EM	60	7.0	0.80	0.54	ND	ND	ND	ND	ND	ND	Low	Lv and Yu, 2013
	Microcrystalline Cellulose (1 % wt/vol)	BM7	60	6.0–7.5	1.09	1.49	2.43	0.25	ND	ND	ND	ND	Low	Tachaapaikoon et al., 2012
	¹⁵ N Cellulose (5 g/L)	MTC	58	6.8	1.34	1.17	ND	ND	ND	ND	ND	ND	0.50 (g/g)	Low
	¹⁴ N Cellulose (5 g/L)				1.27	1.16							0.49 (g/g)	Raman et al., 2009
	Cellobiose (5 g/L)				1.02	1.43							0.49 (g/g)	
	Z-Trim® (5 g/L)				0.54	0.81							0.45 (g/g)	
	Cellulose-Xylan (5 g/L)				0.62	0.71							0.44 (g/g)	
	Cellulose-Pectin (5 g/L)				0.49	0.69							0.39 (g/g)	
	Cellulose-Pectin-Xylan (5 g/L)				0.54	0.60							0.38 (g/g)	
	Pretreated Switchgrass (5 g/L)				0.32	0.60							0.37 (g/g)	
DSM 1313	Pretreated Switchgrass (5 g/L)	MTC	58	6.8	0.20	0.50	ND	ND	ND	ND	ND	ND	Low	Wilson et al., 2013a
	Pretreated Populus(5 g/L)	MTC	58	7.0	0.83	0.83	ND	ND	ND	ND	ND	ND	Low	Low
	Avicel (5 g/L)				0.30	0.80							Low	Raman et al., 2011
	Cellulose	CM3	60	7.8	0.96	0.75	0.38	ND	1.20	0.04	0.88	ND	Low	Weimer and Zeikus, 1977
	Avicel (19.5 g/L)	MTC	55	7.0	1.32	2.74	2.49	ND	ND	ND	0.72	ND	Low	Agyros et al., 2011
CS7	Cellobiose (5 g/L)	Rich media	55	7.0	0.68	1.10	0.25	ND	ND	ND	ND	ND	Low	Tripathi et al., 2010
	Avicel (5 g/L)				0.70	1.10	0.05							
	0.3 % wt/vol Milled Filter Paper	EM	60	7.0	0.79	0.32	ND	ND	ND	ND	ND	ND	Low	Lv and Yu, 2013
CS8	0.3 % wt/vol Milled Filter Paper				0.83	0.43	ND	ND	ND	ND	ND	ND	Low	Lv and Yu, 2013
S14	Microcrystalline Cellulose (1 % wt/vol)	BM7	60	6.5–7.0	1.90	3.72	0.74	1.23	ND	ND	ND	ND	Low	Tachaapaikoon et al., 2012
YS	Cellulose Cellobiose	CM3	60	7.3	1.40	1.90	ND	ND	ND	0.10	ND	ND	Low	Lamed et al., 1988

(Continued)

Table 1 | Continued

Strain	Growth conditions				Products				Efficiency	References				
	Substrate	Medium	Temp (°C)	pH	Ethanol (g/L)	Acetate (g/L)	Lactate (g/L)	Propionate (g/L)	CO ₂ (g/L)	H ₂ (g/L)	Carbon Recovery			
LQRI	0.4% wt/vol Cellulose	GS	60	7.0	0.71	0.96	0.31	ND	1.33	0.05	≥0.80	ND	Low	Ng et al., 1981
	0.4% wt/vol Glucose				0.75	0.89	0.22		1.21	0.04				
	0.4% wt/vol Celllobiose				0.72	0.74	0.21		1.52	0.06				
	Cellulose	CM3	60	7.3	0.90	2.90	ND	ND	ND	0.20				
	Celllobiose				0.90	3.00				0.20				
JW20	1% (wt/vol) Cellulose	Minimal Media	58–61	6.1–7.5	0.61	1.21	0.43	ND	2.38	0.14	0.87	ND	Low	Freier et al., 1988
BC1	Cellulose, glucose, sorbitol	ND	67	ND	ND	ND	ND	ND	ND	ND	ND	ND	Low	Koeck et al., 2013
M1570	Avicel (19.5 g/L)	MTC	55	70	5.61	0.16	0.11	ND	ND	0.61	ND	ND	Low	Argyros et al., 2011

ND, Not defined in original publication.

and pH (9.0) than the wild type while consuming a broader range of substrates including sorbitol. However, as of yet, CS7, CS8, and S14 do not have draft genome sequences, which will be crucial for the development of genetic or metabolic engineering approaches in these strains.

Draft or finished genome sequences are, however, currently available for six *C. thermocellum* strains including the wild type (ATCC 27405), YS, LQRI, JW20, BC1, and DSM 1313 (Hemme et al., 2010; Feinberg et al., 2011; Brown et al., 2012; Wilson et al., 2013a). *C. thermocellum* YS was isolated from hot springs at Yellow Stone national park and has been characterized as a highly efficient cellulose utilizer. Notably, it is this strain, in tandem with the adherence-defective mutant *C. thermocellum* AD2 strain, that was used in the studies that reported the initial description of the adherence of *C. thermocellum* to insoluble cellulose substrate and paved the way for the discovery of the cellulosome (Bayer et al., 1983; Lamed et al., 1983). Strain YS has since been leveraged for multiple studies reporting on the digestion of lignocellulosic feedstocks, cell surface interactions, the structure and function of the cellulosome, and transcriptomic evaluations in response to plant biomass hydrolysis (Bayer et al., 1985; Lamed et al., 1988; Poole et al., 1992; Fernandes et al., 1999; Dror et al., 2003a, 2005). *C. thermocellum* JW20 was isolated from a cotton bale in Louisiana and LQRI was isolated from a contaminated culture of strain DSM 1313, which at the time was referred to as LQ8 (Ng and Zeikus, 1981; Ng et al., 1981; Hemme et al., 2010). The growth and physiological properties for each of these strains have since been characterized (Lamed and Zeikus, 1980; Ng et al., 1981), with strain JW20 demonstrating the ability to utilize a spectrum of growth substrates ranging from crystalline cellulose to lignocellulosic feedstocks, including pretreated hardwood, straw, and hay (Freier et al., 1988). Most recently, *C. thermocellum* BC1 was isolated from a compost treatment site in Germany, and a draft genome sequence has been established (Koeck et al., 2013). This strain has exhibited improved cellulose hydrolysis and utilization of a wider range of substrates, including glucose and sorbitol, at a higher temperature (67°C) than the wild type strain. The diversity of unique characteristics demonstrated by these strains, and the important contributions they have made toward improving *C. thermocellum*'s position as a relevant CBP host, highlight the importance of continuing to isolate, characterize, and compare new strains that may have advantageous characteristics for CBP applications.

C. thermocellum DSM 1313, previously known as *C. thermocellum* LQ8, represents arguably the most important of the strains discovered to date. First isolated in 1926 by Viljoen et al. from manure or soil (Viljoen et al., 1926), it has been widely studied for its cellulolytic and physiological properties, and has been characterized on celllobiose, crystalline cellulose, and lignocellulosic feedstocks (Weimer and Zeikus, 1977; Wiegel and Dykstra, 1984). However, DSM 1313's high utility comes from the establishment of its draft genome sequence in 2011 and the subsequent development of a genetic system for its transformation that has allowed for the construction of mutant strains (Tyurin et al., 2004; Tripathi et al., 2010; Feinberg et al., 2011; Olson and Lynd, 2012b; Mohr et al., 2013). This ability has allowed investigators to

target specific genetic changes within the DSM 1313 background, leading to an unparalleled ability to interrogate the genetic basis for observed phenotypes and to develop strains endowed with specific, engineered functions.

In one such study, comparisons were drawn to previous investigations focusing on the use of proteomic analysis and global gene expression data to enhance understanding of *C. thermocellum*'s highly efficient cellulosomal hydrolysis of cellulose and hemicellulose. These initial investigations demonstrated that the catalytic sub-units of the cellulosome were assembled based on their substrate and growth rate (Raman et al., 2009; Wilson et al., 2013a), allowing researchers to create mutant strains of DSM 1313 with knockouts of the *cel48S* gene, that encode an abundant and up regulated cellulase during growth on crystalline cellulose, in order to investigate its role in hydrolysis (Olson et al., 2010). Through the use of this targeted approach, they were able to determine that the deletion of *cel48S* reduced growth rate and specific activity by 2-fold, however, also discovered that it was still able to completely solubilize a 10 g/L loading of Avicel. Without the ability to establish this targeted mutation, it would be difficult, if not impossible, to hypothesize this retention of biomass utilization efficiently in light of such a deleterious mutation. Furthermore, these studies are also important in advancing the creation of designer multi-enzyme complexes for industrial applications (Gold and Martin, 2007; Raman et al., 2009; Fontes and Gilbert, 2010; Olson et al., 2010), as was highlighted by the recent improvement in hydrolysis performance achieved by Gefen et al. through targeted cellulosome engineering, resulting in a three-fold increase in crystalline cellulose hydrolysis and a two-fold improvement for switchgrass hydrolysis (Gefen et al., 2012).

Mutational strain development has also been leveraged to increase ethanol titer and tolerance toward the minimum value of 40 g/L that is required for the economic viability of cellulosic ethanol production (Lynd, 1996; Dien et al., 2003). While wild type *C. thermocellum* strains only produce <3 g/L and are tolerant to <16 g/L of ethanol (Rani et al., 1996; Blumer-Schuette et al., 2013), mutant strains constructed through adapted evolution have shown ethanol tolerance up to 80 g/L, albeit with inconsistent and slow growth, and up to 50 g/L with stable growth (Williams et al., 2007; Brown et al., 2011). To achieve these results, mutant strains of DSM 1313 were constructed with disrupted end product fermentation pathways that altered their natural carbon flow and, conversely, increased their ethanol yield (Argyros et al., 2011; Deng et al., 2013; Mohr et al., 2013; Van Der Veen et al., 2013). These strains were established through mutations in their acetate and lactate pathways ($\Delta hpt \Delta ldh \Delta pta$), however, once subsequently evolved, they produced contrasting results in their effect on ethanol yield. In one case, no increase in ethanol yield was observed following mutation (Van Der Veen et al., 2013), while in a separate report a 4-fold increase was detected (Argyros et al., 2011). However, in both cases it was hypothesized that the mutations led to a redox imbalance because of the secretion of pyruvate and amino acids into the fermentation broth, low product yields, unsubstantial increases in ethanol, and resulting open carbon balances. In an attempt to reconcile these reports, Mohr et al. used a thermotargetron approach to disrupt the acetate

and lactate pathways in place of the homologous recombination approach used by Argyros and van der Veen, resulting in a decrease to lactate and acetate production, a slight increase in ethanol production and a 6-fold increase in pyruvate production (Mohr et al., 2013).

Building upon these studies, Deng et al. noted that pyruvate kinase had not been annotated in the DSM 1313 genome sequence and did not register during enzymatic assays. This led them to the hypothesis that a malate shunt was being used to convert phosphoenol pyruvate to pyruvate (Deng et al., 2013). Leveraging the genetic tractability of DSM 1313, they were able to improve ethanol yield by expressing an exogenous pyruvate kinase and deleting the malic enzyme gene in the lactate and acetate pathway deficient strain. As a result, their novel mutant strain achieved a ~3-fold higher ethanol yield, increased carbon recovery, increased formate production, increased ethanol tolerance, and decreased amino acid secretion relative to the parent strain. The sheer number of mutations and genetic knowledge required to achieve this goal perfectly demonstrates the necessity of obtaining a fundamental understanding of gene expression, regulation, redox state, carbon catabolism, and metabolic modeling, and the prerequisite of establishing a functional genetic manipulation system that must be obtained prior to the development of mutant strains for use in CBP settings (Roberts et al., 2010; Blumer-Schuette et al., 2013).

CO-CULTURE OF *C. thermocellum* WITH OTHER ORGANISMS

In addition to the development and isolation of additional *C. thermocellum* strains, it is worth noting that there are naturally highly efficient cellulolytic consortia and mixed cultures of *C. thermocellum* that can be employed as well. However, significant difficulties exist in engineering these populations toward the production of their desired fermentation products at high yields for industrial applications. Nonetheless, these populations still pose a high value in that they can be mined for novel cellulolytic microorganisms (Haruta et al., 2002; Kato et al., 2004; Izquierdo et al., 2010; Sizova et al., 2011; Li et al., 2012; Zuroff and Curtis, 2012). While consortia and mixed-cultures will not be covered in depth in this review, defined co-cultures containing *C. thermocellum* have previously been studied for the digestion of lignocellulosic biomass (Ng et al., 1981; Le Ruyet et al., 1984; Mori, 1990; Geng et al., 2010; He et al., 2011; Li et al., 2012; Lü et al., 2013) and have recently been reviewed elsewhere (Blumer-Schuette et al., 2013). In general, these co-cultures are utilized due to *C. thermocellum*'s unique ability to hydrolyze hemicellulose and cellulose utilizing only the cellobextrin breakdown products and forgoing the consumption of C₅ sugars (Zhang and Lynd, 2005; Blumer-Schuette et al., 2008), making it amenable to co-culture with pentose utilizing thermophiles. Notably, the highest ethanol titer yet reported for the fermentation of crystalline cellulose has been obtained under these conditions, with the co-culture of a metabolically engineered *C. thermocellum* and *Thermoanaerobacterium saccharolyticum*. This fermentation achieved ~80% of theoretical ethanol yield at 38 g/L, and was able to keep organic acid concentrations below their detection limits (Argyros et al., 2011), demonstrating the utility of this type of approach.

TOOLS FOR GENETIC MANIPULATION

The evolution and selection of naturally occurring *C. thermocellum* strains has provided an initial springboard for development of more industrially relevant organisms, however, the full realization of this effort requires targeted development and optimization of specific characteristics that will enable *C. thermocellum* to function synergistically toward the production of fuels and chemicals from cellulosic biomass. While development of the tools required for the genetic manipulation of *C. thermocellum* is still in its infancy, significant strides have already been made to enable the introduction of exogenous DNA and selection of successfully modified strains. The utilization and expansion of these efforts will be key to achieving *C. thermocellum*'s full potential as a CBP host.

METHODS FOR INTRODUCING FOREIGN DNA

The primary method for introducing DNA into *C. thermocellum* has been through electroporation. This method, which transiently applies an electrical field to generate openings on the cell surface for the introduction of DNA, has been successfully demonstrated for several available strains (ATCC 27405, DSM 1313, and DSM 4150) and has been optimized specifically for strain DSM 1313 (Tyurin et al., 2004). Particularly of note for the application of this technique to *C. thermocellum* transformation is the relationship between current oscillation and transfection efficiency. Tyurin et al. have demonstrated a one-to-one correspondence between the presence of 24 MHz oscillations and successful transformations, noting that the proper oscillations can be achieved by using a >12 kV/cm field strength during transformation. This field strength was itself noted to contribute significantly to transformation optimization as well, with increasing field strengths up to 25 kV/cm producing higher efficiencies (Tyurin et al., 2005). Using this technique, it has been possible both to present exogenous genes for expression and to introduce genetic modification systems capable of altering the native *C. thermocellum* genome and knocking out endogenous loci (Olson and Lynd, 2012b).

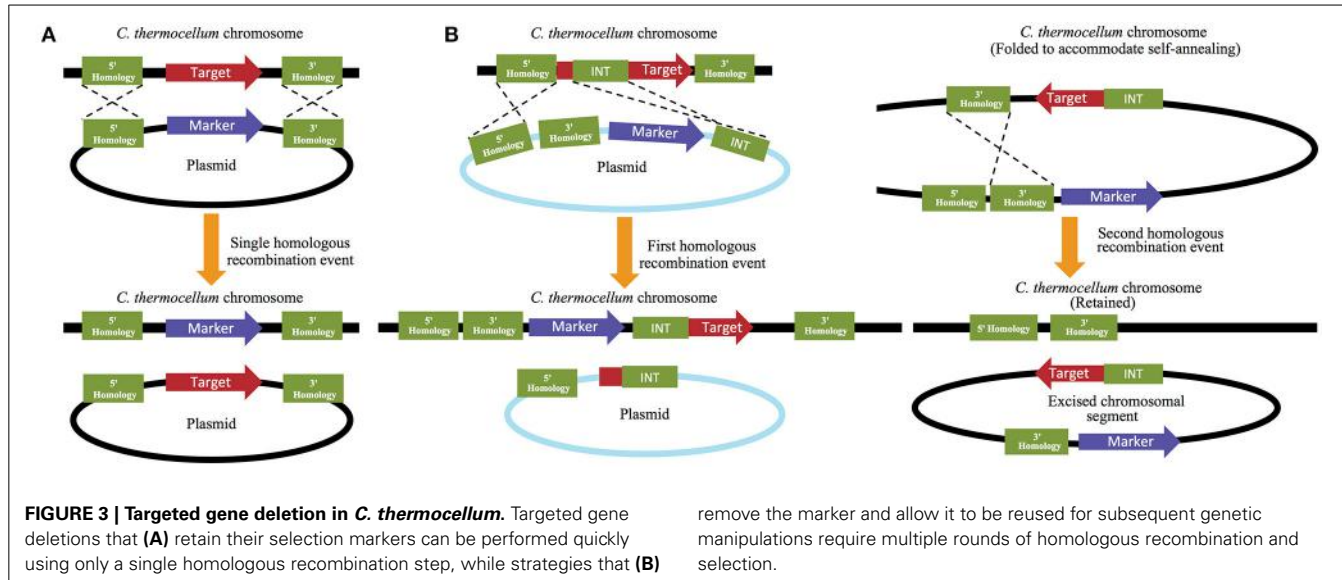
GENETIC DELIVERY SYSTEMS

Three basic strategies exist for the genetic modification of *C. thermocellum*. The first of these simply places additional genetic material into the organism for expression, ideally adding functionality or complimenting a deficiency in order to better prepare the organism for its intended task. Under this strategy, plasmid DNA is introduced using the electroporation approach discussed above. Depending upon the design of the introduced vector, the gene of interest is then either expressed directly from the plasmid or incorporated into the host genome and replicated along with the endogenous DNA during routine cell maintenance. For plasmid-based expression, in addition to the gene of interest, the plasmid must also contain an origin of replication and a selectable marker. There are several selection markers available (discussed below) but, in general, the thermophilic RepB origin of replication is the most prevalent for use in *C. thermocellum*. This origin, which works via rolling circle replication, has also been synthetically modified to generate a temperature sensitive variant that cannot function above 55°C. This provides

an additional layer of flexibility that can be utilized for controllable expression of the novel DNA sequence being added (Olson and Lynd, 2012a). It is also possible to integrate the target DNA sequence directly into the genome through the incorporation of homologous loci up- and downstream of the gene of interest. Under this design, once the construct is successfully introduced the homologous regions can permit recombination for the gene of interest into the *C. thermocellum* genome. This forgoes the need to maintain an additional plasmid within the host, but requires the remaining plasmid DNA to be cured following genetic introduction. Either of these two approaches is equally acceptable, and their utilization is usually made on a case-by-case basis following careful assessment of the experimental design.

The second system performs the opposite function by permitting the removal of endogenous genes from the *C. thermocellum* genome. This plasmid-based strategy can be performed either by replacing the targeted deletion gene with a selectable marker, or by a multi-step process that allows for gene removal followed by marker removal. While the former is a much quicker process, the latter allows for the recycling of selectable markers and therefore permits additional downstream modifications to occur (Figure 3). For retention of the selective marker, 5' and 3' flanking regions that match 500–100 bp of the 5' and 3' flanking regions of the deletion target are designed and placed up- and downstream of the marker. The 5' flanking region/selective marker/3' flanking region cassette is then introduced into the cell where the selective marker is homologously recombined in place of the target gene (Olson and Lynd, 2012b). For marker free gene removal, the 5' and 3' flanking regions are both placed upstream of the *cat* and *hpt* selection makers (described in detail below) and a third region, which is referred to as the "int region" and is homologous to a 500–1000 bp region of the gene of interest, is placed downstream of the selection markers. In this multi-step process, an initial selection is performed to isolate strains that have achieved homologous recombination at the 5' flanking and int regions, which successfully replaces a portion of the gene of interest with the remaining 3' flanking region and *cat* and *hpt* selection markers. A second selection is then made to remove these markers (and the remaining portion of the gene of interest) and isolate the subset of strains that have performed a second homologous recombination event between the two 3' flanking regions that are now present on the chromosome. This second recombination will successfully remove all exogenous material, leaving only the 5' and 3' flanking regions on the chromosome, with no genetic material between them (Argyros et al., 2011). Because this method allows the selective makers to be reused, it is often utilized over the alternative method, despite its additional investment in time and resources.

The third, and newest of the approaches, leverages the function of a mobile group II intron, often referred to as a "targetron," from *Thermosynechococcus elongatus* to knock out expression of an endogenous gene via the insertion of a non-coding intron into the native sequence. The advantage of this strategy is that the intron can be engineered by the researcher to insert at any desired location within the genome by including short, homologous sequences flanking the intron that will be used to direct it to its



intended location within the genome. In addition to these regions of homology, an intron encoded reverse transcriptase protein is required that aids in locally melting the target region of the chromosome and facilitating the insertion of the intron sequence. Fortunately, because of the thermophilic temperatures present during the culture of *C. thermocellum*, the function of this secondary protein product is minimized and the homology of the targeting regions becomes the most important factor regulating insertion efficiency. The plasmid containing these required sequences is incorporated into the organism using standard electroporation techniques, but then does not require any additional cofactors in order to function. When deployed in *C. thermocellum*, this approach was able to knock out six chromosomal genes with efficiencies ranging from 67 to 100%, resulting in the development of a lactate dehydrogenase deficient strain with increased ethanol production (Mohr et al., 2013). The development of this system to function in thermophilic bacteria, and *C. thermocellum* in particular, is a promising development that will hopefully significantly improve the ease with which mutant strains can be developed.

SELECTION OF MODIFIED STRAINS

A key component of any genetic modification strategy is the ability to select for the resulting altered strain at the conclusion of the procedure. Although not nearly as many markers are available as are for mesophilic bacteria such as *E. coli*, a host of selection markers are available and have been validated in *C. thermocellum*. For negative selection, expression of the Thymidine kinase (*tkd*) or Hygromycin phosphotransferase (*hpt*) markers may be used to provide resistance against 5-fluorodeoxyuridine and hygromycin, respectively. Of these, *tkd* is often preferred since *C. thermocellum* has an endogenous *hpt* homolog, and thus requires an *hpt* deficient genetic background for proper function (Olson and Lynd, 2012b). The chloramphenicol acetyltransferase (*cat*) and aminoglycoside phosphotransferase (*neo*) markers can be similarly employed for positive selection, however, the former is

preferred as the latter has been demonstrated to inhibit growth at the expression levels required for selection (Olson et al., 2010). An additional marker, orotidine 5-phosphate decarboxylase (*pyrF*) can also act as either a positive or negative selection marker. On the one hand, expressing the *pyrF* gene in a *pyrF* deficient host makes it possible to compliment a uracil auxotroph and select only for strains actively expressing the maker. On the other hand, treatment of *pyrF*-expressing strains with 5-fluoroorotic acid will lead to cellular death as those harboring the gene will incorporate it as a toxic uracil analog (Tripathi et al., 2010). Used together, these markers allow researchers to select and modify strains in efforts to further engineer *C. thermocellum* for the optimized production of high value products.

FUTURE DIRECTIONS

Although ethanol has been the focus of this review, *C. thermocellum* produces several additional fermentation products that may have value in a variety of industries. The production optimization of these pathways can serve to position *C. thermocellum* as a key industrial organism on par with existing models such as *S. cerevisiae*. One potential route for initial optimization is the production of hydrogen, which can serve as a potential energy source for combustion engines or fuel cells when produced in sufficient quantities. Five strains of *C. thermocellum* (1237, 1313, 2360, 4150, and 7072) have already been evaluated to assess their efficiencies in hydrogen production after using microcrystalline cellulose as a feedstock. Under these conditions, yields ranged between 0.7 and 1.2 mol of hydrogen per mol of glucose (Cheng and Liu, 2011). Acknowledging this potential for hydrogen generation, additional recent studies have investigated the steps involved in *C. thermocellum*'s hydrogen synthesis pathways (Carere et al., 2008) and evaluated inclusion of an electrohydrogenesis stage (Lalaurette et al., 2009) to boost hydrogen production.

In addition to hydrogen, lignocellulosic biomass remains an attractive starting material for the production of lactic acid,

formic acid, and acetic acid using *C. thermocellum*'s natural fermentation pathways. By mimicking the action of existing lactic acid bacteria or the fungus *Rhizopus oryzae*, which have previously been demonstrated to produce lactate using corn starch biomass (Hou and Shaw, 2008), it would be possible to assemble the basic units for a variety of high value bio-based polymers. Similarly, while methanol carbonylation is currently used to synthesize the majority of acetic acid (Acton, 2013), this process could also be offloaded to *C. thermocellum* under the appropriate CBP conditions. Regardless, the success of these processes will rely heavily on several factors, such as the existing limitation regarding lactic acid (Cheng and Liu, 2011) and formic acid (Sparling et al., 2006) yields, which are currently inversely related to hydrogen production.

Similarly, the production of butanol from lignocellulosic biomass using a CBP platform is another attractive option because butanol, which is more similar to gasoline than ethanol, has a higher energy density, and can be mixed with gasoline at higher ratios. Unfortunately, all *Clostridium* spp that naturally produce butanol are non-cellulolytic, and only two, *Clostridium acetobutylicum* and *Clostridium beijerinckii*, have been studied in detail (Gheshlaghi et al., 2009). Moving toward this goal of butanol production, there have been a series of studies utilizing co-cultures of *C. thermocellum*, and it has recently been reported that a co-culture of *C. thermocellum* and *Clostridium saccharoperbutylacetonicum* N1-4 can produce up to 7.9 g/L butanol in 9 days using crystalline cellulose as a carbon source (Nakayama et al., 2011). Moreover, the recent development of a transformation system for *C. thermocellum* has led to research efforts aimed at engineering *C. thermocellum* with new pathways to produce butanol as well (Kastelowitz et al., 2014). Through these, and other related pathway studies, it may one day be possible to shift all of *C. thermocellum*'s natural array of products toward industrial scale production.

ACKNOWLEDGMENTS

Funding for this review was provided by the Georgia Institute of Technology, Institute of Paper Science Paper Science and Technology Fellowship and an Oak Ridge National Laboratory Directed Research and Development grant. Additional funding was provided by the Bioenergy Science Center (BESC), which is a U.S. Department of Energy Bioenergy Research Center supported by the Office of Biological and Environmental Research in the DOE Office of Science. This manuscript has been authored by a contractor of the U.S. Government under contract DE-AC05-00OR22725.

REFERENCES

- Acton, Q. A. (2013). *Acetates—Advances in Research and Application: 2013 Edition*. Atlanta, GA: Scholarly Editions.
- Alper, H., and Stephanopoulos, G. (2009). Engineering for biofuels: exploiting innate microbial capacity or importing biosynthetic potential? *Nat. Rev. Microbiol.* 7, 715–723. doi: 10.1038/nrmicro2186
- Amarasekara, A. S. (2013). *Handbook of Cellulosic Ethanol*. Salem, MA: Wiley-Scrivener.
- Argyros, D. A., Tripathi, S. A., Barrett, T. F., Rogers, S. R., Feinberg, L. F., Olson, D. G., et al. (2011). High ethanol titers from cellulose by using metabolically engineered thermophilic, anaerobic microbes. *Appl. Environ. Microbiol.* 77, 8288–8294. doi: 10.1128/AEM.00646-11
- Bayer, E. A., Henrissat, B., and Lamed, R. (2009). "The cellulosome: a natural bacterial strategy to combat biomass recalcitrance," in *Biomass Recalcitrance* ed M. E. Himmel (Oxford, UK: Blackwell Publishing Ltd.), 407–435.
- Bayer, E. A., Kenig, R., and Lamed, R. (1983). Adherence of *Clostridium thermocellum* to cellulose. *J. Bacteriol.* 156, 818–827.
- Bayer, E. A., and Lamed, R. (1986). Ultrastructure of the cell surface cellulosome of *Clostridium thermocellum* and its interaction with cellulose. *J. Bacteriol.* 167, 828–836.
- Bayer, E., Setter, E., and Lamed, R. (1985). Organization and distribution of the cellulosome in *Clostridium thermocellum*. *J. Bacteriol.* 163, 552–559.
- Blumer-Schuette, S. E., Brown, S. D., Sander, K. B., Bayer, E. A., Kataeva, I., Zurawski, J. V., et al. (2013). Thermophilic lignocellulose deconstruction. *FEMS Microbiol. Rev.* 38, 393–448. doi: 10.1111/1574-6976.12044
- Blumer-Schuette, S. E., Kataeva, I., Westpheling, J., Adams, M. W., and Kelly, R. M. (2008). Extremely thermophilic microorganisms for biomass conversion: status and prospects. *Curr. Opin. Biotechnol.* 19, 210–217. doi: 10.1016/j.copbio.2008.04.007
- Bomble, Y. J., Beckham, G. T., Matthews, J. F., Nimlos, M. R., Himmel, M. E., and Crowley, M. F. (2011). Modeling the self-assembly of the cellulosome enzyme complex. *J. Biol. Chem.* 286, 5614–5623. doi: 10.1074/jbc.M110.186031
- Borne, R., Bayer, E. A., Pagès, S., Perret, S., and Fierobe, H. P. (2013). Unraveling enzyme discrimination during cellulosome assembly independent of cohesin-dockerin affinity. *FEBS J.* 280, 5764–5779. doi: 10.1111/febs.12497
- Bothun, G. D., Knutson, B. L., Berberich, J. A., Strobel, H. J., and Nokes, S. E. (2004). Metabolic selectivity and growth of *Clostridium thermocellum* in continuous culture under elevated hydrostatic pressure. *Appl. Microbiol. Biotechnol.* 65, 149–157. doi: 10.1007/s00253-004-1554-1
- Brown, S. D., Guss, A. M., Karpinetis, T. V., Parks, J. M., Smolin, N., Yang, S., et al. (2011). Mutant alcohol dehydrogenase leads to improved ethanol tolerance in *Clostridium thermocellum*. *Proc. Natl. Acad. Sci. U.S.A.* 108, 13752–13757. doi: 10.1073/pnas.1102444108
- Brown, S. D., Lamed, R., Morag, E., Borovok, I., Shoham, Y., Klingeman, D. M., et al. (2012). Draft genome sequences for *Clostridium thermocellum* wild-type strain YS and derived cellulose adhesion-defective mutant strain AD2. *J. Bacteriol.* 194, 3290–3291. doi: 10.1128/JB.00473-12
- Brown, S. D., Raman, B., McKeown, C. K., Kale, S. P., He, Z., and Mielenz, J. R. (2007). "Construction and evaluation of a *Clostridium thermocellum* ATCC 27405 whole-genome oligonucleotide microarray," in *Applied Biochemistry and Biotechnology*, eds J. R. Mielenz, K. T. Klasson, W. S. Adney, and J. D. McMillan (Nashville, TN: Humana Press), 663–674.
- Burton, E., and Martin, V. J. (2012). Proteomic analysis of *Clostridium thermocellum* ATCC 27405 reveals the upregulation of an alternative transhydrogenase-malate pathway and nitrogen assimilation in cells grown on cellulose. *Can. J. Microbiol.* 58, 1378–1388. doi: 10.1139/cjm-2012-0412
- Carere, C. R., Cicek, N., Levin, D. B., Kalia, V., and Sparling, R. (2008). Pyruvate catabolism and hydrogen synthesis pathway genes of *Clostridium thermocellum* ATCC 27405. *Indian J. Microbiol.* 48, 252–266. doi: 10.1007/s12088-008-0036-z
- Carvalho, A. L., Dias, F. M. V., Prates, J. A. M., Nagy, T., Gilbert, H. J., and Fontes, C. M. G. A. (2003). Cellulosome assembly revealed by the crystal structure of the cohesin-dockerin complex. *Proc. Natl. Acad. Sci. U.S.A.* 100, 13809–13814. doi: 10.1073/pnas.1936124100
- Chen, F., and Dixon, R. A. (2007). Lignin modification improves fermentable sugar yields for biofuel production. *Nat. Biotechnol.* 25, 759–761. doi: 10.1038/nbt1316
- Cheng, X. Y., and Liu, C. Z. (2011). Hydrogen production via thermophilic fermentation of cornstalk by *Clostridium thermocellum*. *Energy Fuels* 25, 1714–1720. doi: 10.1021/ef2000344
- Demain, A. L., Newcomb, M., and Wu, J. D. (2005). Cellulase, *Clostridia*, and ethanol. *Microbiol. Mol. Biol. Rev.* 69, 124–154. doi: 10.1128/MMBR.69.1.124-154.2005
- Deng, Y., Olson, D. G., Zhou, J., Herring, C. D., Joe Shaw, A., and Lynd, L. R. (2013). Redirecting carbon flux through exogenous pyruvate kinase to achieve high ethanol yields in *Clostridium thermocellum*. *Metab. Eng.* 15, 151–158. doi: 10.1016/j.ymben.2012.11.006
- Dien, B., Cotta, M., and Jeffries, T. (2003). Bacteria engineered for fuel ethanol production: current status. *Appl. Microbiol. Biotechnol.* 63, 258–266. doi: 10.1007/s00253-003-1444-y

- Ding, S. Y., Liu, Y. S., Zeng, Y., Himmel, M. E., Baker, J. O., and Bayer, E. A. (2012). How does plant cell wall nanoscale architecture correlate with enzymatic digestibility? *Science* 338, 1055–1060. doi: 10.1126/science.1227491
- Dror, T. W., Morag, E., Rolider, A., Bayer, E. A., Lamed, R., and Shoham, Y. (2003a). Regulation of the cellosomal *celS* (*cel48A*) gene of *Clostridium thermocellum* is growth rate dependent. *J. Bacteriol.* 185, 3042–3048. doi: 10.1128/JB.185.10.3042-3048.2003
- Dror, T. W., Rolider, A., Bayer, E. A., Lamed, R., and Shoham, Y. (2003b). Regulation of expression of scaffoldin-related genes in *Clostridium thermocellum*. *J. Bacteriol.* 185, 5109–5116. doi: 10.1128/jb.185.17.5109-5116.2003
- Dror, T. W., Rolider, A., Bayer, E. A., Lamed, R., and Shoham, Y. (2005). Regulation of major cellosomal endoglucanases of *Clostridium thermocellum* differs from that of a prominent cellosomal xylanase. *J. Bacteriol.* 187, 2261–2266. doi: 10.1128/JB.187.7.2261-2266.2005
- Dumitache, A., Wolfaardt, G., Allen, G., Liss, S. N., and Lynd, L. R. (2013). Form and function of *Clostridium thermocellum* biofilms. *Appl. Environ. Microbiol.* 79, 231–239. doi: 10.1128/AEM.02563-12
- Egorova, K., and Antranikian, G. (2005). Industrial relevance of thermophilic Archaea. *Curr. Opin. Microbiol.* 8, 649–655. doi: 10.1016/j.mib.2005.10.015
- Ellis, L. D., Holwerda, E. K., Hogsett, D., Rogers, S., Shao, X., Tschaaplinski, T., et al. (2012). Closing the carbon balance for fermentation by *Clostridium thermocellum* (ATCC 27405). *Bioresour. Technol.* 103, 293–299. doi: 10.1016/j.biortech.2011.09.128
- Engel, P., Krull, S., Seiferheld, B., and Spiess, A. C. (2012). Rational approach to optimize cellulase mixtures for hydrolysis of regenerated cellulose containing residual ionic liquid. *Bioresour. Technol.* 115, 27–34. doi: 10.1016/j.biortech.2011.10.080
- Fang, H., and Xia, L. (2013). High activity cellulase production by recombinant *Trichoderma reesei* ZU-02 with the enhanced cellobiohydrolase production. *Bioresour. Technol.* 144, 693–697. doi: 10.1016/j.biortech.2013.06.120
- Feinberg, L., Foden, J., Barrett, T., Davenport, K. W., Bruce, D., Detter, C., et al. (2011). Complete genome sequence of the cellulolytic thermophile *Clostridium thermocellum* DSM1313. *J. Bacteriol.* 193, 2906–2907. doi: 10.1128/JB.00322-11
- Fernandes, A., Fontes, C., Gilbert, H., Hazlewood, G., Fernandes, T., and Ferreira, L. (1999). Homologous xylanases from *Clostridium thermocellum*: evidence for bi-functional activity, synergism between xylanase catalytic modules and the presence of xylan-binding domains in enzyme complexes. *Biochem. J.* 342, 105–110.
- Fleming, R., and Quinn, L. (1971). Chemically defined medium for growth of *Clostridium thermocellum*, a cellulolytic thermophilic anaerobe. *Appl. Microbiol.* 21, 967.
- Fontes, C. M., and Gilbert, H. J. (2010). Cellulosomes: highly efficient nanomachines designed to deconstruct plant cell wall complex carbohydrates. *Annu. Rev. Biochem.* 79, 655–681. doi: 10.1146/annurev-biochem-091208-085603
- Freier, D., Mothershed, C. P., and Wiegel, J. (1988). Characterization of *Clostridium thermocellum* JW20. *Appl. Environ. Microbiol.* 54, 204–211.
- Fu, C., Mielenz, J. R., Xiao, X., Ge, Y., Hamilton, C. Y., Rodriguez, M., et al. (2011). Genetic manipulation of lignin reduces recalcitrance and improves ethanol production from switchgrass. *Proc. Natl. Acad. Sci. U.S.A.* 108, 3803–3808. doi: 10.1073/pnas.1100310108
- Garcia-Martinez, D. V., Shinmyo, A., Madia, A., and Demain, A. L. (1980). Studies on cellulase production by *Clostridium thermocellum*. *Eur. J. Appl. Microbiol. Biotechnol.* 9, 189–197. doi: 10.1007/BF00504485
- Gefen, G., Anbar, M., Morag, E., Lamed, R., and Bayer, E. A. (2012). Enhanced cellulose degradation by targeted integration of a cohesin-fused β -glucosidase into the *Clostridium thermocellum* cellulosome. *Proc. Natl. Acad. Sci. U.S.A.* 109, 10298–10303. doi: 10.1073/pnas.1202747109
- Geng, A., He, Y., Qian, C., Yan, X., and Zhou, Z. (2010). Effect of key factors on hydrogen production from cellulose in a co-culture of *Clostridium thermocellum* and *Clostridium thermopalmarium*. *Bioresour. Technol.* 101, 4029–4033. doi: 10.1016/j.biortech.2010.01.042
- Ghoshlaghi, R., Scharer, J., Moo-Young, M., and Chou, C. (2009). Metabolic pathways of *Clostridia* for producing butanol. *Biotechnol. Adv.* 27, 764–781. doi: 10.1016/j.biotechadv.2009.06.002
- Gibson, L. J. (2012). The hierarchical structure and mechanics of plant materials. *J. R. Soc. Interface* 9, 2749–2766. doi: 10.1098/rsif.2012.0341
- Gilbert, H. J. (2007). Cellulosomes: microbial nanomachines that display plasticity in quaternary structure. *Mol. Microbiol.* 63, 1568–1576. doi: 10.1111/j.1365-2958.2007.05640.x
- Gold, N. D., and Martin, V. J. (2007). Global view of the *Clostridium thermocellum* cellulosome revealed by quantitative proteomic analysis. *J. Bacteriol.* 189, 6787–6795. doi: 10.1128/JB.00882-07
- Gupta, R. B., and Demirbas, A. (2010). *Gasoline, Diesel and Ethanol Biofuels from Grasses and Plants*. Cambridge; New York, NY: Cambridge University Press.
- Hall, M., Bansal, P., Lee, J. H., Realff, M. J., and Bommarius, A. S. (2010). Cellulose crystallinity—a key predictor of the enzymatic hydrolysis rate. *FEBS J.* 277, 1571–1582. doi: 10.1111/j.1742-4658.2010.07585.x
- Haruta, S., Cui, Z., Huang, Z., Li, M., Ishii, M., and Igarashi, Y. (2002). Construction of a stable microbial community with high cellulose-degradation ability. *Appl. Microbiol. Biotechnol.* 59, 529–534. doi: 10.1007/s00253-002-1026-4
- Hasunuma, T., Okazaki, F., Okai, N., Hara, K. Y., Ishii, J., and Kondo, A. (2013). A review of enzymes and microbes for lignocellulosic biorefinery and the possibility of their application to consolidated bioprocessing technology. *Bioresour. Technol.* 135, 513–522. doi: 10.1016/j.biortech.2012.10.047
- Hauser, L., Land, M., and Larimer, F. (2010). *Clostridium Thermocellum ATCC 27405 Analysis Files*. Available online at: <http://genome.ornl.gov/microbial/cthe/> (Accessed May 8, 2014).
- He, Q., Hemme, C. L., Jiang, H., He, Z., and Zhou, J. (2011). Mechanisms of enhanced cellulosic bioethanol fermentation by co-cultivation of *Clostridium* and *Thermoanaerobacter* spp. *Bioresour. Technol.* 102, 9586–9592. doi: 10.1016/j.biortech.2011.07.098
- Hemme, C. L., Mouttaki, H., Lee, Y. J., Zhang, G., Goodwin, L., Lucas, S., et al. (2010). Sequencing of multiple clostridial genomes related to biomass conversion and biofuel production. *J. Bacteriol.* 192, 6494–6496. doi: 10.1128/JB.01064-10
- Herrero, A., and Gomez, R. (1980). Development of ethanol tolerance in *Clostridium thermocellum*: effect of growth temperature. *Appl. Environ. Microbiol.* 40, 571–577.
- Hisano, H., Nandakumar, R., and Wang, Z. Y. (2009). Genetic modification of lignin biosynthesis for improved biofuel production. *In Vitro Cell. Dev. Biol. Plant* 45, 306–313. doi: 10.1007/s11627-009-9219-5
- Hörnemeyer, H. F., Tailliez, P., Millet, J., Girard, H., Bonn, G., Bobbleter, O., et al. (1988). Ethanol production by *Clostridium thermocellum* grown on hydrothermally and organosolv-pretreated lignocellulosic materials. *Appl. Microbiol. Biotechnol.* 29, 528–535. doi: 10.1007/BF00260980
- Hou, C. T., and Shaw, J. F. (2008). *Biocatalysis and Bioenergy*. Hoboken, NJ: Wiley.
- Hu, J., Arantes, V., and Saddler, J. (2011). The enhancement of enzymatic hydrolysis of lignocellulosic substrates by the addition of accessory enzymes such as xylanase: is it an additive or synergistic effect? *Biotechnol. Biofuels* 4, 1–14. doi: 10.1186/1754-6834-4-36
- Intanakul, P., Krairiksh, M., and Kitchaiya, P. (2003). Enhancement of enzymatic hydrolysis of lignocellulosic wastes by microwave pretreatment under atmospheric pressure. *J. Wood Chem. Technol.* 23, 217–225. doi: 10.1081/WCT-120021926
- Islam, R., Cicek, N., Sparling, R., and Levin, D. (2009). Influence of initial cellulose concentration on the carbon flow distribution during batch fermentation by *Clostridium thermocellum* ATCC 27405. *Appl. Microbiol. Biotechnol.* 82, 141–148. doi: 10.1007/s00253-008-1763-0
- Izquierdo, J. A., Sizova, M. V., and Lynd, L. R. (2010). Diversity of bacteria and glycosyl hydrolase family 48 genes in cellulolytic consortia enriched from thermophilic biocompost. *Appl. Environ. Microbiol.* 76, 3545–3553. doi: 10.1128/AEM.02689-09
- Johnson, E. A., Madia, A., and Demain, A. L. (1981). Chemically defined minimal medium for growth of the anaerobic cellulolytic thermophile *Clostridium thermocellum*. *Appl. Environ. Microbiol.* 41, 1060–1062.
- Johnson, E. A., Sakajoh, M., Halliwell, G., Madia, A., and Demain, A. L. (1982). Saccharification of complex cellulosic substrates by the cellulase system from *Clostridium thermocellum*. *Appl. Environ. Microbiol.* 43, 1125–1132.
- Kastelowitz, N., Sammond, D., Akahulta, M., Wu, H., Lin, P., Guss, A., et al. (2014). “Engineering more thermostable metabolic enzymes for improving CBP organisms,” in *36th Symposium on Biotechnology for Fuels and Chemicals* (Clearwater, FL: Society for Industrial Microbiology).
- Kato, S., Haruta, S., Cui, Z. J., Ishii, M., and Igarashi, Y. (2004). Effective cellulose degradation by a mixed-culture system composed of a cellulolytic *Clostridium* and aerobic non-cellulolytic bacteria. *FEMS Microbiol. Ecol.* 51, 133–142. doi: 10.1016/j.femsec.2004.07.015

- Koeck, D. E., Wibberg, D., Koellmeier, T., Blom, J., Jaenicke, S., Winkler, A., et al. (2013). Draft genome sequence of the cellulolytic *Clostridium thermocellum* wild-type strain BC1 playing a role in cellulosic biomass degradation. *J. Biotechnol.* 168, 62–63. doi: 10.1016/j.jbiotec.2013.08.011
- Krauss, J., Zverlov, V. V., and Schwarz, W. H. (2012). *In vitro* reconstitution of the complete *Clostridium thermocellum* cellulosome and synergistic activity on crystalline cellulose. *Appl. Environ. Microbiol.* 78, 4301–4307. doi: 10.1128/aem.07959-11
- Kumar, R., Hu, F., Sannigrahi, P., Jung, S., Ragauskas, A. J., and Wyman, C. E. (2013). Carbohydrate derived-pseudo-lignin can retard cellulose biological conversion. *Biotechnol. Bioeng.* 110, 737–753. doi: 10.1002/bit.24744
- Lalaurette, E., Thammannagowda, S., Mohagheghi, A., Maness, P. C., and Logan, B. E. (2009). Hydrogen production from cellulose in a two-stage process combining fermentation and electrohydrogenesis. *Int. J. Hydrogen Energy* 34, 6201–6210. doi: 10.1016/j.ijhydene.2009.05.112
- Lamed, R., Lobos, J., and Su, T. (1988). Effects of stirring and hydrogen on fermentation products of *Clostridium thermocellum*. *Appl. Environ. Microbiol.* 54, 1216–1221.
- Lamed, R., Setter, E., and Bayer, E. (1983). Characterization of a cellulose-binding, cellulase-containing complex in *Clostridium thermocellum*. *J. Bacteriol.* 156, 828–836.
- Lamed, R., and Zeikus, J. (1980). Ethanol production by thermophilic bacteria: relationship between fermentation product yields of and catabolic enzyme activities in *Clostridium thermocellum* and *Thermoanaerobium brockii*. *J. Bacteriol.* 144, 569–578.
- Lavarack, B. P., Griffin, G. J., and Rodman, D. (2002). The acid hydrolysis of sugarcane bagasse hemicellulose to produce xylose, arabinose, glucose and other products. *Biomass Bioenergy* 23, 367–380. doi: 10.1016/S0961-9534(02)00066-1
- Le Ruyet, P., Dubourguier, H., and Albagnac, G. (1984). Homoacetogenic fermentation of cellulose by a coculture of *Clostridium thermocellum* and *Acetogenium kivui*. *Appl. Environ. Microbiol.* 48, 893–894.
- Li, H. F., Knutson, B. L., Nokes, S. E., Lynn, B. C., and Flythe, M. D. (2012). Metabolic control of *Clostridium thermocellum* via inhibition of hydrogenase activity and the glucose transport rate. *Appl. Microbiol. Biotechnol.* 93, 1777–1784. doi: 10.1007/s00253-011-3812-3
- Linville, J. L., Rodriguez, M. Jr., Land, M., Syed, M. H., Engle, N. L., Tschaplinski, T. J., et al. (2013). Industrial robustness: understanding the mechanism of tolerance for the populus hydrolysate-tolerant mutant strain of *Clostridium thermocellum*. *PLoS ONE* 8:e78829. doi: 10.1371/journal.pone.0078829
- Lü, Y., Li, N., Yuan, X., Hua, B., Wang, J., Ishii, M., et al. (2013). Enhancing the cellulose-degrading activity of cellulolytic bacteria CTL-6 (*Clostridium thermocellum*) by co-culture with non-cellulolytic bacteria W2-10 (*Geobacillus* sp.). *Appl. Biochem. Biotechnol.* 171, 1578–1588. doi: 10.1007/s12010-013-0431-8
- Lu, Y., Zhang, Y.-H. P., and Lynd, L. R. (2006). Enzyme – microbe synergy during cellulose hydrolysis by *Clostridium thermocellum*. *Proc. Natl. Acad. Sci. U.S.A.* 103, 16165–16169. doi: 10.1073/pnas.0605381103
- Lv, W., and Yu, Z. (2013). Isolation and characterization of two thermophilic cellulolytic strains of *Clostridium thermocellum* from a compost sample. *J. Appl. Microbiol.* 114, 1001–1007. doi: 10.1111/jam.12112
- Lynd, L. R. (1996). Overview and evaluation of fuel ethanol from cellulosic biomass: technology, economics, the environment, and policy. *Annu. Rev. Energy Environ.* 21, 403–465. doi: 10.1146/annurev.energy.21.1.403
- Lynd, L. R., Grethlein, H. E., and Wolkin, R. H. (1989). Fermentation of cellulosic substrates in batch and continuous culture by *Clostridium thermocellum*. *Appl. Environ. Microbiol.* 55, 3131–3139.
- Lynd, L. R., van Zyl, W. H., McBride, J. E., and Laser, M. (2005). Consolidated bioprocessing of cellulosic biomass: an update. *Curr. Opin. Biotechnol.* 16, 577–583. doi: 10.1016/j.copbio.2005.08.009
- Lynd, L. R., Weimer, P. J., van Zyl, W. H., and Pretorius, I. S. (2002). Microbial cellulose utilization: fundamentals and biotechnology. *Microbiol. Mol. Biol. Rev.* 66, 506–577. doi: 10.1128/MMBR.66.3.506-577.2002
- McBee, R. (1948). The culture and physiology of a thermophilic cellulose-fermenting bacterium. *J. Bacteriol.* 56, 653–663.
- McBee, R. (1950). The anaerobic thermophilic cellulolytic bacteria. *Bacteriol. Rev.* 14, 51–63.
- McBee, R. (1954). The characteristics of *Clostridium thermocellum*. *J. Bacteriol.* 67, 505–506.
- Mitsuzawa, S., Kagawa, H., Li, Y., Chan, S. L., Paavola, C. D., and Trent, J. D. (2009). The rosettazyme: a synthetic cellulosome. *J. Biotechnol.* 143, 139–144. doi: 10.1016/j.biote.2009.06.019
- Mohr, G., Hong, W., Zhang, J., Cui, G.-Z., Yang, Y., Cui, Q., et al. (2013). A targetron system for gene targeting in thermophiles and its application in *Clostridium thermocellum*. *PLoS ONE* 8:e69032. doi: 10.1371/journal.pone.0069032
- Mori, Y. (1990). Characterization of a symbiotic coculture of *Clostridium thermohydrosulfuricum* YM3 and *Clostridium thermocellum* YM4. *Appl. Environ. Microbiol.* 56, 37–42.
- Nakayama, S., Kiyoshi, K., Kadokura, T., and Nakazato, A. (2011). Butanol production from crystalline cellulose by cocultured *Clostridium thermocellum* and *Clostridium saccharoperbutylacetonicum* N1-4. *Appl. Environ. Microbiol.* 77, 6470–6475. doi: 10.1128/AEM.00706-11
- Nataf, Y., Yaron, S., Stahl, F., Lamed, R., Bayer, E. A., Scheper, T. H., et al. (2009). Cellodextrin and laminaribiose ABC transporters in *Clostridium thermocellum*. *J. Bacteriol.* 191, 203–209. doi: 10.1128/jb.01190-08
- Ng, T. K., Ben-Bassat, A., and Zeikus, J. (1981). Ethanol production by thermophilic bacteria: fermentation of cellulosic substrates by cocultures of *Clostridium thermocellum* and *Clostridium thermohydrosulfuricum*. *Appl. Environ. Microbiol.* 41, 1337–1343.
- Ng, T. K., and Zeikus, J. G. (1981). Purification and characterization of an endoglucanase (1, 4-beta-D-glucan glucanohydrolase) from *Clostridium thermocellum*. *Biochem. J.* 199, 341–350.
- Olson, D. G., and Lynd, L. R. (2012a). Computational design and characterization of a temperature-sensitive plasmid replicon for gram positive thermophiles. *J. Biol. Eng.* 6, 1–10. doi: 10.1186/1754-1611-6-5
- Olson, D. G., and Lynd, L. R. (2012b). “Transformation of *Clostridium thermocellum* by electroporation,” in *Methods in Enzymology*, ed H. Gilbert (Waltham, MA: Academic Press), 317–330.
- Olson, D. G., McBride, J. E., Joe Shaw, A., and Lynd, L. R. (2012). Recent progress in consolidated bioprocessing. *Curr. Opin. Biotechnol.* 23, 396–405. doi: 10.1016/j.copbio.2011.11.026
- Olson, D. G., Tripathi, S. A., Giannone, R. J., Lo, J., Caiazza, N. C., Hogsett, D. A., et al. (2010). Deletion of the Cel48S cellulase from *Clostridium thermocellum*. *Proc. Natl. Acad. Sci. U.S.A.* 107, 17727–17732. doi: 10.1073/pnas.1003584107
- Orozco, A., Ahmad, M., Rooney, D., and Walker, G. (2007). Dilute acid hydrolysis of cellulose and cellulosic bio-waste using a microwave reactor system. *Process Saf. Environ. Prot.* 85, 446–449. doi: 10.1205/psep07003
- Poole, D. M., Morag, E., Lamed, R., Bayer, E. A., Hazlewood, G. P., and Gilbert, H. J. (1992). Identification of the cellulose-binding domain of the cellulose subunit S1 from *Clostridium thermocellum* YS. *FEMS Microbiol. Lett.* 99, 181–186.
- Puls, J., and Wood, T. M. (1991). The degradation pattern of cellulose by extracellular cellulases of aerobic and anaerobic microorganisms. *Bioresour. Technol.* 36, 15–19. doi: 10.1016/0960-8524(91)90096-3
- Raman, B., McKeown, C. K., Rodriguez, M., Brown, S. D., and Mielenz, J. R. (2011). Transcriptomic analysis of *Clostridium thermocellum* ATCC 27405 cellulose fermentation. *BMC Microbiol.* 11:134. doi: 10.1186/1471-2180-11-134
- Raman, B., Pan, C., Hurst, G. B., Rodriguez, M. Jr., McKeown, C. K., Lankford, P. K., et al. (2009). Impact of pretreated switchgrass and biomass carbohydrates on *Clostridium thermocellum* ATCC 27405 cellulosome composition: a quantitative proteomic analysis. *PLoS ONE* 4:e5271. doi: 10.1371/journal.pone.0005271
- Rani, K. S., Swamy, M., Sunita, D., Haritha, D., and Seenayya, G. (1996). Improved ethanol tolerance and production in strains of *Clostridium thermocellum*. *World J. Microbiol. Biotechnol.* 12, 57–60. doi: 10.1007/BF00327802
- Resch, M. G., Donohoe, B. S., Baker, J. O., Decker, S. R., Bayer, E. A., Beckham, G. T., et al. (2013). Fungal cellulases and complexed cellulosomal enzymes exhibit synergistic mechanisms in cellulose deconstruction. *Energy Environ. Sci.* 6, 1858–1867. doi: 10.1039/C3EE00019B
- Riederer, A., Takasuka, T. E., Makino, S.-I., Stevenson, D. M., Bukhman, Y. V., Elsen, N. L., et al. (2011). Global gene expression patterns in *Clostridium thermocellum* as determined by microarray analysis of chemostat cultures on cellulose or cellobiose. *Appl. Environ. Microbiol.* 77, 1243–1253. doi: 10.1128/AEM.02008-10
- Roberts, S. B., Gowen, C. M., Brooks, J. P., and Fong, S. S. (2010). Genome-scale metabolic analysis of *Clostridium thermocellum* for bioethanol production. *BMC Syst. Biol.* 4:31. doi: 10.1186/1752-0509-4-31

- Rydzak, T., Levin, D. B., Cicek, N., and Sparling, R. (2011). End-product induced metabolic shifts in *Clostridium thermocellum* ATCC 27405. *Appl. Microbiol. Biotechnol.* 92, 199–209. doi: 10.1007/s00253-011-3511-0
- Rydzak, T., McQueen, P. D., Krokhin, O. V., Spicer, V., Ezzati, P., Dwivedi, R. C., et al. (2012). Proteomic analysis of *Clostridium thermocellum* core metabolism: relative protein expression profiles and growth phase-dependent changes in protein expression. *BMC Microbiol.* 12:214. doi: 10.1186/1471-2180-12-214
- Saddler, J., and Chan, M. H. (1982). Optimization of *Clostridium thermocellum* growth on cellulose and pretreated wood substrates. *Eur. J. Appl. Microbiol. Biotechnol.* 16, 99–104.
- Sakka, K., Kishino, Y., Sugihara, Y., Jindou, S., Sakka, M., Inagaki, M., et al. (2009). Unusual binding properties of the dockerin module of *Clostridium thermocellum* endoglucanase CelJ (Cel9D-Cel44A). *FEMS Microbiol. Lett.* 300, 249–255. doi: 10.1111/j.1574-6968.2009.01788.x
- Shao, X., Jin, M., Guseva, A., Liu, C., Balan, V., Hogsett, D., et al. (2011a). Conversion for Avicel and AFEX pretreated corn stover by *Clostridium thermocellum* and simultaneous saccharification and fermentation: insights into microbial conversion of pretreated cellulosic biomass. *Bioresour. Technol.* 102, 8040–8045. doi: 10.1016/j.biortech.2011.05.021
- Shao, X., Raman, B., Zhu, M., Mielenz, J. R., Brown, S. D., Guss, A. M., et al. (2011b). Mutant selection and phenotypic and genetic characterization of ethanol-tolerant strains of *Clostridium thermocellum*. *Appl. Microbiol. Biotechnol.* 92, 641–652. doi: 10.1007/s00253-011-3492-z
- Shen, H., Pooyah, C. R., Ziebell, A., Tschaaplinski, T. J., Pattathil, S., Gjersing, E., et al. (2013). Enhanced characteristics of genetically modified switchgrass (*Panicum virgatum* L.) for high biofuel production. *Biotechnol. Biofuels* 6, 71–86. doi: 10.1186/1754-6834-6-71
- Shimon, L. J. W., Bayer, E. A., Morag, E., Lamed, R., Yaron, S., Shoham, Y., et al. (1997). A cohesin domain from *Clostridium thermocellum*: the crystal structure provides new insights into cellulosome assembly. *Structure* 5, 381–390. doi: 10.1016/S0969-2126(97)00195-0
- Sizova, M., Izquierdo, J., Panikov, N., and Lynd, L. (2011). Cellulose- and xylan-degrading thermophilic anaerobic bacteria from biocompost. *Appl. Environ. Microbiol.* 77, 2282–2291. doi: 10.1128/AEM.01219-10
- Sparling, R., Islam, R., Cicek, N., Carere, C., Chow, H., and Levin, D. B. (2006). Formate synthesis by *Clostridium thermocellum* during anaerobic fermentation. *Can. J. Microbiol.* 52, 681–688. doi: 10.1139/w06-021
- Spinnler, H. E., Lavigne, B., and Blachere, H. (1986). Pectinolytic activity of *Clostridium thermocellum*: its use for anaerobic fermentation of sugar beet pulp. *Appl. Microbiol. Biotechnol.* 23, 434–437. doi: 10.1007/BF02346055
- Stevenson, D. M., and Weimer, P. J. (2005). Expression of 17 genes in *Clostridium thermocellum* ATCC 27405 during fermentation of cellulose or cellobiose in continuous culture. *Appl. Environ. Microbiol.* 71, 4672–4678. doi: 10.1128/AEM.71.8.4672-4678.2005
- Tachaapaikoon, C., Kosugi, A., Pason, P., Waeonukul, R., Ratanakhanokchai, K., Kyu, K. L., et al. (2012). Isolation and characterization of a new cellulosome-producing *Clostridium thermocellum* strain. *Biodegradation* 23, 57–68. doi: 10.1007/s10532-011-9486-9
- Taherzadeh, M. J., and Karimi, K. (2007). Enzyme-based hydrolysis processes for ethanol from lignocellulosic materials: a review. *Bioresources* 2, 707–738. Available online at: http://ojs.cnr.ncsu.edu/index.php/BioRes/article/view/BioRes_2_4_707_738_Taherzadeh_Karimi_EzymeBased_Hydrol_Ethanol_Review
- Taylor, M. P., Eley, K. L., Martin, S., Tuffin, M. I., Burton, S. G., and Cowan, D. A. (2009). Thermophilic ethanogenesis: future prospects for second-generation bioethanol production. *Trends Biotechnol.* 27, 398–405. doi: 10.1016/j.tibtech.2009.03.006
- Timmons, M. D., Knutson, B. L., Nokes, S. E., Strobel, H. J., and Lynn, B. C. (2009). Analysis of composition and structure of *Clostridium thermocellum* membranes from wild-type and ethanol-adapted strains. *Appl. Microbiol. Biotechnol.* 82, 929–939. doi: 10.1007/s00253-009-1891-1
- Tracy, B. P., Jones, S. W., Fast, A. G., Indurthi, D. C., and Papoutsakis, E. T. (2012). *Clostridia*: the importance of their exceptional substrate and metabolic diversity for biofuel and biorefinery applications. *Curr. Opin. Biotechnol.* 23, 364–381. doi: 10.1016/j.copbio.2011.10.008
- Tripathi, S. A., Olson, D. G., Argyros, D. A., Miller, B. B., Barrett, T. F., Murphy, D. M., et al. (2010). Development of *pyrF*-based genetic system for targeted gene deletion in *Clostridium thermocellum* and creation of a *pta* mutant. *Appl. Environ. Microbiol.* 76, 6591–6599. doi: 10.1128/AEM.01484-10
- Tyurin, M. V., Desai, S. G., and Lynd, L. R. (2004). Electroporation of *Clostridium thermocellum*. *Appl. Environ. Microbiol.* 70, 883–890. doi: 10.1128/AEM.70.2.883-890.2004
- Tyurin, M. V., Sullivan, C. R., and Lynd, L. R. (2005). Role of spontaneous current oscillations during high-efficiency electroporation of thermophilic anaerobes. *Appl. Environ. Microbiol.* 71, 8069–8076. doi: 10.1128/AEM.71.12.8069-8076.2005
- Uversky, V. N., and Kataeva, I. A. (2006). *Cellulosome*. Hauppauge, NY: Nova Science Publishers.
- Van Der Veen, D., Lo, J., Brown, S. D., Johnson, C. M., Tschaaplinski, T. J., Martin, M., et al. (2013). Characterization of *Clostridium thermocellum* strains with disrupted fermentation end-product pathways. *J. Ind. Microbiol. Biotechnol.* 40, 725–734. doi: 10.1007/s10295-013-1275-5
- Vermerris, W. (2008). *Genetic Improvement of Bioenergy Crops*. New York, NY: Springer.
- Viikari, L., Vehmaanperä, J., and Koivula, A. (2012). Lignocellulosic ethanol: from science to industry. *Biomass Bioenergy* 46, 13–24. doi: 10.1016/j.biombioe.2012.05.008
- Viljoen, J., Fred, E., and Peterson, W. (1926). The fermentation of cellulose by thermophilic bacteria. *J. Agric. Sci.* 16, 1–17. doi: 10.1017/S0021859600088249
- Wei, H., Fu, Y., Magnusson, L., Baker, J. O., Maness, P. C., Xu, Q., et al. (2014). Comparison of transcriptional profiles of *Clostridium thermocellum* grown on cellobiose and pretreated yellow poplar using RNA-Seq. *Front. Microbiol.* 5:142. doi: 10.3389/fmicb.2014.00142
- Weimer, P., and Zeikus, J. (1977). Fermentation of cellulose and cellobiose by *Clostridium thermocellum* in the absence of *Methanobacterium thermoautotrophicum*. *Appl. Environ. Microbiol.* 33, 289–297.
- Wertz, J. L., and Bédué, O. (2013). *Lignocellulosic Biorefineries*. Lausanne: EPFL Press.
- Wiegel, J., and Dykstra, M. (1984). *Clostridium thermocellum*: adhesion and sporulation while adhered to cellulose and hemicellulose. *Appl. Microbiol. Biotechnol.* 20, 59–65.
- Wiegel, J., Mothershed, C. P., and Puls, J. (1985). Differences in xylan degradation by various noncellulolytic thermophilic anaerobes and *Clostridium thermocellum*. *Appl. Environ. Microbiol.* 49, 656–659.
- Williams, T. I., Combs, J. C., Lynn, B. C., and Strobel, H. J. (2007). Proteomic profile changes in membranes of ethanol-tolerant *Clostridium thermocellum*. *Appl. Microbiol. Biotechnol.* 74, 422–432. doi: 10.1007/s00253-006-0689-7
- Wilson, C. M., Rodriguez, M. Jr., Johnson, C. M., Martin, S. L., Chu, T. M., Wolfinger, R. D., et al. (2013a). Global transcriptome analysis of *Clostridium thermocellum* ATCC 27405 during growth on dilute acid pretreated Populus and switchgrass. *Biotechnol. Biofuels* 6, 179–197. doi: 10.1186/1754-6834-6-179
- Wilson, C. M., Yang, S., Rodriguez, M. Jr., Ma, Q., Johnson, C. M., Dice, L., et al. (2013b). *Clostridium thermocellum* transcriptomic profiles after exposure to furfural or heat stress. *Biotechnol. Biofuels* 6, 131–144. doi: 10.1186/1754-6834-6-131
- Xu, J., Crowley, M. F., and Smith, J. C. (2009a). Building a foundation for structure-based cellulosome design for cellulosic ethanol: insight into cohesin-dockerin complexation from computer simulation. *Protein Sci.* 18, 949–959. doi: 10.1002/pro.105
- Xu, Q., Singh, A., and Himmel, M. E. (2009b). Perspectives and new directions for the production of bioethanol using consolidated bioprocessing of lignocellulose. *Curr. Opin. Biotechnol.* 20, 364–371. doi: 10.1016/j.copbio.2009.05.006
- Yee, K. L., Rodriguez, M. Jr., Tschaaplinski, T. J., Engle, N. L., Martin, M. Z., Fu, C., et al. (2012). Evaluation of the bioconversion of genetically modified switchgrass using simultaneous saccharification and fermentation and a consolidated bioprocessing approach. *Biotechnol. Biofuels* 5, 81–93. doi: 10.1186/1754-6834-5-81
- Zeng, H. (2013). *Polymer Adhesion, Friction, and Lubrication*. Hoboken, NJ: Wiley.
- Zhang, X., Xu, C., and Wang, H. (2007a). Pretreatment of bamboo residues with *Coriolus versicolor* for enzymatic hydrolysis. *J. Biosci. Bioeng.* 104, 149–151. doi: 10.1263/jbb.104.149
- Zhang, X., Yu, H., Huang, H., and Liu, Y. (2007b). Evaluation of biological pretreatment with white rot fungi for the enzymatic hydrolysis of bamboo culms. *Int. Biodeterior. Biodegradation* 60, 159–164. doi: 10.1016/j.ibiod.2007.02.003
- Zhang, Y. H. P. (2011). What is vital (and not vital) to advance economically-competitive biofuels production. *Process Biochem.* 46, 2091–2110.

- Zhang, Y. H. P., and Lynd, L. R. (2005). Cellulose utilization by *Clostridium thermocellum*: bioenergetics and hydrolysis product assimilation. *Proc. Natl. Acad. Sci. U.S.A.* 102, 7321–7325. doi: 10.1073/pnas.0408734102
- Zhao, X., Zhang, L., and Liu, D. (2012). Biomass recalcitrance. Part I: the chemical compositions and physical structures affecting the enzymatic hydrolysis of lignocellulose. *Biofuels Bioproducts Biorefining* 6, 465–482. doi: 10.1002/bbb.1331
- Zhou, J., Olson, D. G., Argyros, D. A., Deng, Y., Van Gulik, W. M., Van Dijken, J. P., et al. (2013). Atypical Glycolysis in *Clostridium thermocellum*. *Appl. Environ. Microbiol.* 79, 3000–3008. doi: 10.1128/aem.04037-12
- Zuroff, T. R., and Curtis, W. R. (2012). Developing symbiotic consortia for lignocellulosic biofuel production. *Appl. Microbiol. Biotechnol.* 93, 1423–1435. doi: 10.1007/s00253-011-3762-9
- Zverlov, V. V., Kellermann, J., and Schwarz, W. H. (2005a). Functional subgenomics of *Clostridium thermocellum* cellulosomal genes: identification of the major catalytic components in the extracellular complex and detection of three new enzymes. *Proteomics* 5, 3646–3653. doi: 10.1002/pmic.200401199
- Zverlov, V. V., Schantz, N., Schmitt-Kopplin, P., and Schwarz, W. H. (2005b). Two new major subunits in the cellulosome of *Clostridium thermocellum*: xyloglucanase Xgh74A and endoxylanase Xyn10D. *Microbiology* 151, 3395–3401. doi: 10.1099/mic.0.28206-0

Conflict of Interest Statement: The authors declare that the research was conducted in the absence of any commercial or financial relationships that could be construed as a potential conflict of interest.

Received: 05 June 2014; accepted: 28 July 2014; published online: 26 August 2014.

Citation: Akinosh H, Yee K, Close D and Ragauskas A (2014) The emergence of *Clostridium thermocellum* as a high utility candidate for consolidated bioprocessing applications. *Front. Chem.* 2:66. doi: 10.3389/fchem.2014.00066

This article was submitted to Chemical Biology, a section of the journal *Frontiers in Chemistry*.

Copyright © 2014 Akinosh, Yee, Close and Ragauskas. This is an open-access article distributed under the terms of the Creative Commons Attribution License (CC BY). The use, distribution or reproduction in other forums is permitted, provided the original author(s) or licensor are credited and that the original publication in this journal is cited, in accordance with accepted academic practice. No use, distribution or reproduction is permitted which does not comply with these terms.



Delivery of chemical cargo to endogenous proteins on live cells

James J. Chambers *

Department of Chemistry, Program in Neuroscience and Behavior, University of Massachusetts, Amherst, MA, USA

*Correspondence: chambers@chem.umass.edu

Edited by:

Carissa M. Soto, Naval Research Laboratory, USA

Reviewed by:

Matthew Robert Pratt, University of Southern California, USA

Keywords: fluorescent tagging, protein trafficking, fluorescence microscopy, ligand-targeted delivery, traceless labeling

During the past two decades, our collective mastery of gene manipulation, delivery, and fluorescent fusion protein expression has been astounding and has enabled never before dreamed of new lines of research. These advances, coupled with progress in the collection and analysis of microscopy data, have allowed the scientific community to detect proteins in live cells with resolution that was unthinkable not long ago. The confluence of protein engineering and advanced microscopy has enabled us to observe cellular processes at the single molecule level and to begin unraveling the mysteries of cellular biochemistry and dynamics. These advances, however, require delivery of a contrast agent to the subject organism which can sometimes lead to untoward effects and potentially confounded results. Here, I present an opinion on the need to improve and deploy new strategies that allow for the silent tagging of endogenous proteins with contrast agents.

WHERE ART THOU, PROTEIN OF INTEREST?

Visualization of cells has been enabled by the use of simple organic and inorganic dyes. The results of staining provides the ability to differentiate cell types (e.g., hematoxylin vs. eosin stain) and sometimes offers glimpses of complex cell connectivity (e.g., chromium/silver Golgi stain). In the case of brain tissue, these stains can provide insight into neuronal connectivity (Cajal, 1894). Of course, the utility of these simple dyes and stains is limited in scope to revealing snapshots in time since they require fixation and sometimes development before imaging can be performed.

Arguably, the most difficult challenge facing biology and medicine is the delivery of contrast agents to the brain for the purpose of visualizing the development, plasticity, dysfunction, and degeneration in live neural tissue. The majority of what we know about brain dysfunction comes from tissue snapshots collected from post-mortem samples. These data are robust and offer many insights into biochemical and morphological underpinnings of disease, but the data that these methods can reveal is, by definition, temporally limited to the moment the fixative impregnates the tissue. The detection of changes in cell morphology or, of more relevance to this opinion, responsive dynamic movements of proteins in various subcellular compartments, are lost once the fixative is added.

HERE, PROTEIN OF INTEREST, CAN YOU HOLD THIS?

Without question, the field of live cell fluorescence microscopy would be stalled if it weren't for the relatively recent discovery and exploit of natural fluorescent proteins and the boon in molecular biology and genetic delivery strategies (Giepmans et al., 2006). At first, it was the now famous green fluorescent protein from *Aequorea victoria*. Once the genetic code for GFP was sequenced and packaged into an expression vector, the genie was out of the bottle. One would be hard-pressed now to find any lab that works on questions in cell biology that does not have at least one plasmid containing some form of a boutique GFP variant.

In parallel to the explosion in popularity of GFP and variants thereof, there continues to be the development of

new, organic based fluorescent molecules (Mutze et al., 2012). Just when it seems that chemists have exhausted the diversity of chemical and structural space to produce new fluorophores, new ones come along with different properties. These new fluorophores offer combinations of fundamental photophysical properties; some are long-lasting, some are bright (high quantum yield), and some have large Stokes shifts while others photobleach easily, are dim, and excitation and emission wavelengths are not well-separated. However, the old adage, in adapted form, holds here: One molecule's flaw is another molecule's feature. For instance, fast photobleaching chromophores, if photo-reversible, are vital to single molecule imaging techniques used in stochastic optical reconstruction microscopy (STORM imaging) in which molecules are bleached and then a small subset is stochastically turned back on to reveal their sub-diffraction position in space. It is clear that the menu of fluorophores is akin to selecting a fine wine; to make an informed decision, one must understand and appreciate the nuances of the available options.

HOW DO WE DELIVER THESE CONTRAST AGENTS TO THE PROTEIN OF INTEREST?

The two main methods in use today to deliver fluorescent chromophores to protein targets of interest are to use genetic fusion modification of the target itself or to employ a non-covalent delivery vehicle such as an antibody that has been raised to recognize a specific hapten on the target molecule. Both of these methods are logically trivial and are routine in many cell biology laboratories.

With currently available commercial technology, generation of a fusion protein containing the target of interest is simple and there are myriad transfection formulations available to deliver the generated plasmid to even the most difficult to transfect cell types (in addition, of course, there are virally-mediated delivery and transgenic strategies). The range of colors for protein-based fluorophores is seemingly infinite, allowing multiplexed experiments (Giepmans et al., 2006) as well as genetically encoded, photoactivatable proteins for single particle tracking of parts of organelles (Manley et al., 2008).

Antibody based delivery of contrast agents has been used extensively in cell biology studies. With advances in synthetic chromophores and new methods for the covalent attachment to antibodies, delivery of these chromophores to targets on live cell surfaces is also becoming routine. The exquisite specificity of the antibody method, coupled with the diversity of commercially available sources for pre-stained antibodies, makes this method very attractive when embarking on a new study.

With all of the upsides of the genetic and antibody methods, there are some potential pitfalls and caveats that the researcher must be aware of (Figure 1). For instance, with fusion proteins and transfection, it is difficult to specifically control the expression level of the fusion protein. This can sometimes result in confounded results, especially in cases where the native protein is normally tightly controlled by the cell. I would postulate that more examples of this confound have been detected, but not reported due to the nature of the null result. In the neuroscience community, specific examples of this problem have been observed in the fusion expression of certain ion channels including the AMPA subtype of glutamate receptors. The delicate balance of expression level and subcellular location is likely one of the most important functions in maintaining communication between two connected neurons. The interplay of synaptic scaling, both to enhance and diminish communication, is essential in both the developing and developed nervous system (Jackson et al., 2011; Bats et al., 2012; Opazo et al., 2012; Lambo and Turrigiano, 2013).

Further, the insertion of the fluorescent protein within a native protein can be difficult without severe perturbations of the protein and/or proper protein targeting, especially in mammalian systems (Baker et al., 2007). More importantly, over-expression of tagged-monomers of protein receptor subunits has been observed to bias receptor subtype composition thus confounding experimental results (Bredt and Nicoll, 2003). However, these issues can be circumvented in genetically-tractable organisms by performing knock-out/knock-in genetics so that the native levels of the protein are maintained as close as possible to the wild-type state.

The antibody method of labeling native proteins, by contrast, many times requires the addition of large multivalent molecules as a primary antibody and then multiple molecules of a similarly-sized secondary antibody to track the movement of receptors. While this method offers the benefit of exquisite specificity due to the multivalent and immunologically optimized interaction with the target, the large size of typical primary antibodies in addition to the size of typical secondary antibodies may impose unforeseen consequences when one would like to study *natural* protein movements on the cell surface. Additionally, when studying proteins that may move into or out of the synapse, the antibody method may be size-limited as to what it can tell us regarding natural movements of receptors and their movement into or out of the synapse (Dahan et al., 2003).

A COMPROMISE BETWEEN GENETICS AND SIZE

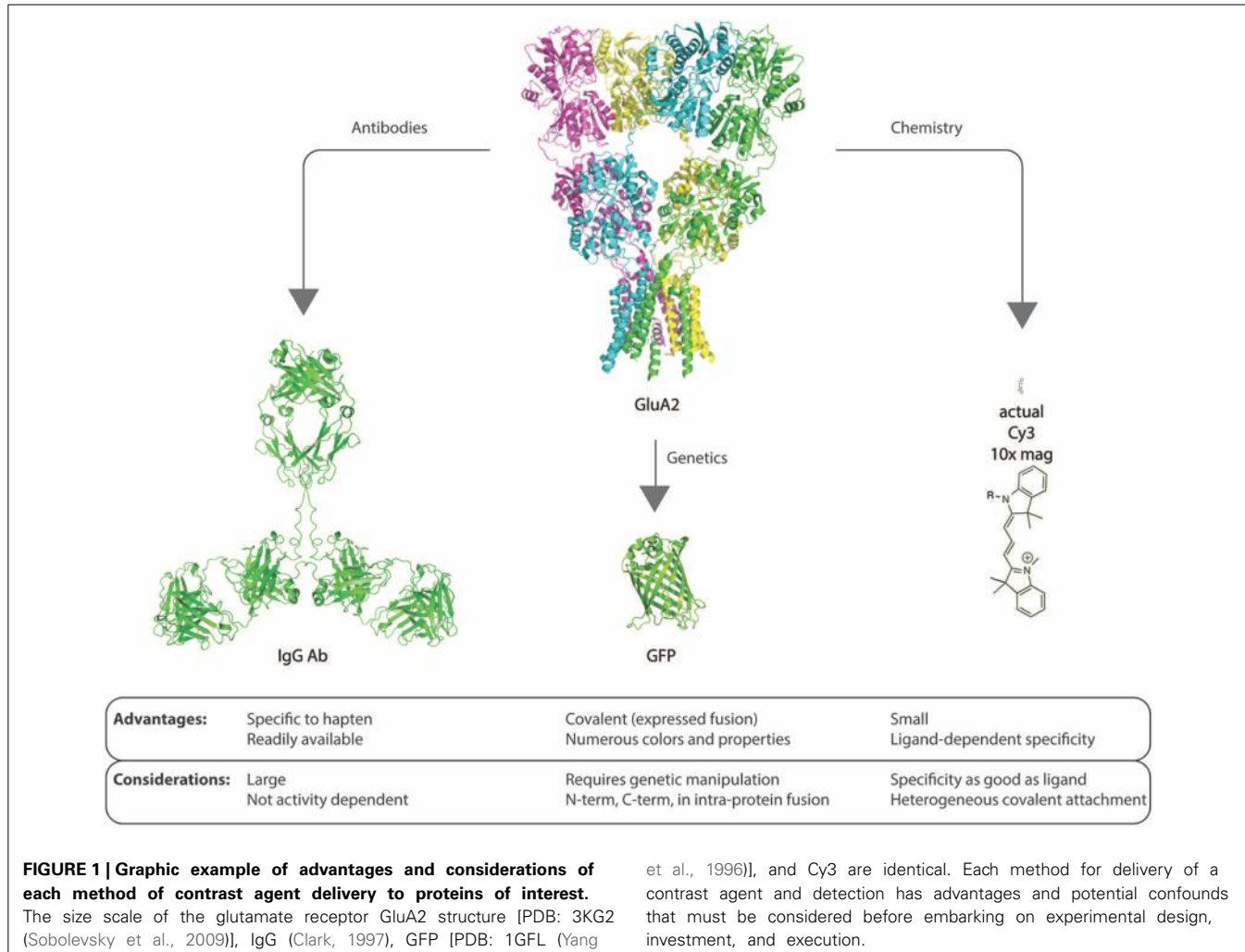
Small affinity tags that specifically bind a fluorescent probe, sometimes as small as a single cysteine amino acid, can be used to covalently attach a fluorophore to a receptor (Griffin et al., 1998; Marks et al., 2004; McCann et al., 2005). In addition, new gene editing strategies (Sun and Zhao, 2013) hold great promise for installing either short sequence motifs that can be recognized by an exogenously applied chemical entity (e.g., FlAsH, ReAsH, or RhoBo Adams and Tsien, 2008; Halo et al., 2009) or for the directed mutation of underlying sequences that can be modified to produce

consensus sequences for a variety of post-translational modifying enzymes (Lin and Wang, 2008).

A DIFFERENT SOLUTION

A number of academic laboratories have been developing ligand-targeted delivery for contrast enhancement cargo (Cha et al., 2005; Vytla et al., 2011; Ishida et al., 2013). At the core of these strategies is the ligand which directs the cargo to the right place. By employing medicinal chemistry literature and fundamental knowledge of binding energies, tethered pharmacophores are being developed to allow for the ligand to direct the sometimes-covalent probe to the target protein or receptor. This is where specificity becomes difficult at times. Because targeting of the receptor is reliant on the ligand, the best-case scenario is one in which the tethered ligand only binds to the intended target. In reality, many pharmacophores are believed to be specific at a certain concentration, but off-target competitive and allosteric sites are always rife in the milieu of a cell or tissue. These are in addition to random collisions that can result in covalent modification. Methods to test the specificity of a ligand-directed probe include competitive blockage of labeling, use of orthogonal readouts (biochemical activity, electrophysiology, binding interaction reporters, etc.). In the end, however, it is difficult, if not impossible, to ever definitively determine that a new probe molecule is 100% specific for a desired target. While we can screen the known off-site interactions, the real problem is that there are likely unknown unknowns lurking on the cells and tissue that result in off-target labeling.

One strategy that we have been developing allows for non-invasive modification of protein receptors with a small molecular weight fluorophore for imaging experiments. The strategy may be likened to a molecular-scale bur that secretly sticks to a receptor and provides a read-out of receptor location. Our probes harbor a ligand (agonist, antagonist, or any other ligand that maintains affinity for the target protein) for targeting specificity, a fluorescent dye for optical monitoring of the receptor, and a promiscuous electrophilic group for covalent coupling to the target receptor. In addition, we



have also engineered the probe system so that the ligand can be excised from the coupled system via simple and efficient photolysis of the structural core (Vytla et al.). After photolysis, the coupled fluorescent probe/receptor complex consists of a non-liganded receptor that has a small fluorescent probe stuck to its side. This allows for time-resolved tracking of endogenous receptors that can continue to function in their native environment and respond to endogenous ligands and then signal normally. This has allowed us to now track labeled receptors on live neurons and monitor their movements in response to stimuli. In order to track receptor molecules in their native state, it is important to relieve persistently-agonized or antagonized receptors and avoid changes to the receptor that are accompanied by ligand

binding. Agonist-induced conformational changes of some receptors, such as the glutamate receptors, have been shown to induce clathrin-mediated endocytosis of the receptors or differential trafficking of these receptors (Nong et al., 2004; Malinow et al., 2005; Dhami and Ferguson, 2006). In addition to agonist-induced changes, antagonist-induced alterations in receptor trafficking have also been described (Carroll et al., 2001).

DESIRABLE PROPERTIES FOR DELIVERY OF CONTRAST AGENTS TO PROTEINS IN CELLS:

TRACELESS

The protein target, the cell, and the observer should detect no difference between the unlabeled (native state) and the labeled form of the target protein. Depending on the protein target, evidence

of lack of perturbation may be difficult to prove.

SPECIFIC

The delivery of the contrast agent to the protein of interest should be as specific as possible. Off target labeling will confound downstream results and should be avoided at all costs.

HIGH CONTRAST

The contrast agent that is delivered should be easy to detect from background signal. For instance, a high quantum efficiency fluorophore should be employed in the case of fluorescence microscopy.

LONG TERM PROSPECTS FOR TRACELESS LABELING

Traceless delivery of contrast agents to endogenous proteins is the logical next

step in garnering an unperturbed view of the routines of proteins in live cells. We, and others, continue to develop new pharmacophores to enable ligand-directed labeling of endogenous proteins. During the next few years, it will be interesting to compare chemically-enabled traceless labeling with the other two main methods of protein detection; fluorescent fusion protein expression and antibody-based tracking. I suspect there will always be a trade off between availability of reagents, ease of use, and financial considerations that will dictate which of these now three methods one will choose for a given experiment.

REFERENCES

- Adams, S. R., and Tsien, R. Y. (2008). Preparation of the membrane-permeant biarsenicals FlAsH-EDT2 and ReAsH-EDT2 for fluorescent labeling of tetracysteine-tagged proteins. *Nat. Protoc.* 3, 1527–1534. doi: 10.1038/nprot.2008.144
- Baker, B. J., Lee, H., Pieribone, V. A., Cohen, L. B., Isacoff, E. Y., Knopf, T., et al. (2007). Three fluorescent protein voltage sensors exhibit low plasma membrane expression in mammalian cells. *J. Neurosci. Methods* 161, 32–38. doi: 10.1016/j.jneumeth.2006.10.005
- Batts, C., Soto, D., Studniarczyk, D., Farrant, M., and Cull-Candy, S. G. (2012). Channel properties reveal differential expression of TARPed and TARPress AMPARs in stargazer neurons. *Nat. Neurosci.* 15, 853–861. doi: 10.1038/nn.3107
- Bredt, D. S., and Nicoll, R. A. (2003). AMPA receptor trafficking at excitatory synapses. *Neuron* 40, 361–379. doi: 10.1016/S0896-6273(03)00640-8
- Cajal, S. R. Y. (1894). The croonian lecture: la fine structure des centres nerveux. *Proc. R. Soc. Lond.* 55, 444–468. doi: 10.2307/115494
- Carroll, R. C., Beattie, E. C., Von Zastrow, M., and Malenka, R. C. (2001). Role of AMPA receptor endocytosis in synaptic plasticity. *Nat. Rev. Neurosci.* 2, 315–324. doi: 10.1038/35072500
- Cha, J. H., Zou, M. F., Adkins, E. M., Rasmussen, S. G., Loland, C. J., Schoenenberger, B., et al. (2005). Rhodamine-labeled 2beta-carbomethoxy-3beta-(3,4-dichlorophenyl)tropane analogues as high-affinity fluorescent probes for the dopamine transporter. *J. Med. Chem.* 48, 7513–7516. doi: 10.1021/jm050431y
- Clark, M. R. (1997). “IgG effector mechanisms,” in *Antibody Engineering*, ed. J. D. Capra (Basel: Karger), 88–110.
- Dahan, M., Levi, S., Luccardini, C., Rostaing, P., Riveau, B., and Triller, A. (2003). Diffusion dynamics of glycine receptors revealed by single-quantum dot tracking. *Science* 302, 442–445. doi: 10.1126/science.1088525
- Dhami, G. K., and Ferguson, S. S. G. (2006). Regulation of metabotropic glutamate receptor signaling, desensitization and endocytosis. *Pharmacol. Ther.* 111, 260–271. doi: 10.1016/j.pharmthera.2005.01.008
- Giepmans, B. N., Adams, S. R., Ellisman, M. H., and Tsien, R. Y. (2006). The fluorescent toolbox for assessing protein location and function. *Science* 312, 217–224. doi: 10.1126/science.1124618
- Griffin, B. A., Adams, S. R., and Tsien, R. Y. (1998). Specific covalent labeling of recombinant protein molecules inside live cells. *Science* 281, 269–272. doi: 10.1126/science.281.5374.269
- Halo, T. L., Appelbaum, J., Hobert, E. M., Balkin, D. M., and Schepartz, A. (2009). Selective recognition of protein tetraserine motifs with a cell-permeable, pro-fluorescent bis-boronic acid. *J. Am. Chem. Soc.* 131, 438–439. doi: 10.1021/ja807872s
- Ishida, M., Watanabe, H., Takigawa, K., Kurishita, Y., Oki, C., Nakamura, A., et al. (2013). Synthetic self-localizing ligands that control the spatial location of proteins in living cells. *J. Am. Chem. Soc.* 135, 12684–12689. doi: 10.1021/ja4046907
- Jackson, A. C., Milstein, A. D., Soto, D., Farrant, M., Cull-Candy, S. G., and Nicoll, R. A. (2011). Probing TARP modulation of AMPA receptor conductance with polyamine toxins. *J. Neurosci.* 31, 7511–7520. doi: 10.1523/JNEUROSCI.6688-10.2011
- Lambo, M. E., and Turrigiano, G. G. (2013). Synaptic and intrinsic homeostatic mechanisms cooperate to increase L2/3 pyramidal neuron excitability during a late phase of critical period plasticity. *J. Neurosci.* 33, 8810–8819. doi: 10.1523/JNEUROSCI.4502-12.2013
- Lin, M. Z., and Wang, L. (2008). Selective labeling of proteins with chemical probes in living cells. *Physiology (Bethesda)* 23, 131–141. doi: 10.1152/physiol.00007.2008
- Malinow, R., Rumpel, S., Zador, A., and Ledoux, J. (2005). AMPA receptor trafficking and GluR1 - Response. *Science* 310, 234–235. doi: 10.1126/science.310.5746.234
- Manley, S., Gillette, J. M., Patterson, G. H., Shroff, H., Hess, H. F., Betzig, E., et al. (2008). High-density mapping of single-molecule trajectories with photoactivated localization microscopy. *Nat. Methods* 5, 155–157. doi: 10.1038/nmeth.1176
- Marks, K. M., Braun, P. D., and Nolan, G. P. (2004). A general approach for chemical labeling and rapid, spatially controlled protein inactivation. *Proc. Natl. Acad. Sci. U.S.A.* 101, 9982–9987. doi: 10.1073/pnas.0401609101
- McCann, C. M., Bareyre, F. M., Lichtman, J. W., and Sanes, J. R. (2005). Peptide tags for labeling membrane proteins in live cells with multiple fluorophores. *Biotechniques* 38, 945–952. doi: 10.2144/05386IT02
- Mutze, J., Iyer, V., Macklin, J. J., Colonell, J., Karsh, B., Petrasek, Z., et al. (2012). Excitation spectra and brightness optimization of two-photon excited probes. *Biophys. J.* 102, 934–944. doi: 10.1016/j.bpj.2011.12.056
- Nong, Y., Huang, Y. Q., and Salter, M. W. (2004). NMDA receptors are movin’ in. *Curr. Opin. Neurobiol.* 14, 353–361. doi: 10.1016/j.conb.2004.05.001
- Opazo, P., Sainlos, M., and Choquet, D. (2012). Regulation of AMPA receptor surface diffusion by PSD-95 slots. *Curr. Opin. Neurobiol.* 22, 453–460. doi: 10.1016/j.conb.2011.10.010
- Sobolevsky, A. I., Rosconi, M. P., and Gouaux, E. (2009). X-ray structure, symmetry and mechanism of an AMPA-subtype glutamate receptor. *Nature* 462, 745–756. doi: 10.1038/nature08624
- Sun, N., and Zhao, H. (2013). Transcription activator-like effector nucleases (TALENs): a highly efficient and versatile tool for genome editing. *Biotechnol. Bioeng.* 110, 1811–1821. doi: 10.1002/bit.24890
- Vytla, D., Combs-Bachmann, R. E., Hussey, A. M., Hafez, I., and Chambers, J. J. (2011). Silent, fluorescent labeling of native neuronal receptors. *Org. Biomol. Chem.* 9, 7151–7161. doi: 10.1039/c1ob05963g
- Yang, F., Moss, L. G., and Phillips, G. N. Jr. (1996). The molecular structure of green fluorescent protein. *Nat. Biotechnol.* 14, 1246–1251. doi: 10.1038/nbt1096-1246

Received: 17 February 2014; accepted: 24 February 2014; published online: 12 March 2014.

Citation: Chambers JJ (2014) Delivery of chemical cargo to endogenous proteins on live cells. *Front. Chem.* 2:11. doi: 10.3389/fchem.2014.00011

This article was submitted to Chemical Biology, a section of the journal *Frontiers in Chemistry*.

Copyright © 2014 Chambers. This is an open-access article distributed under the terms of the Creative Commons Attribution License (CC BY). The use, distribution or reproduction in other forums is permitted, provided the original author(s) or licensor are credited and that the original publication in this journal is cited, in accordance with accepted academic practice. No use, distribution or reproduction is permitted which does not comply with these terms.



Non-standard amino acid incorporation into proteins using *Escherichia coli* cell-free protein synthesis

Seok Hoon Hong^{1,2}, Yong-Chan Kwon^{1,2} and Michael C. Jewett^{1,2,3,4*}

¹ Chemical and Biological Engineering, Northwestern University, Evanston, IL, USA

² Chemistry of Life Processes Institute, Northwestern University, Evanston, IL, USA

³ Robert H. Lurie Comprehensive Cancer Center, Northwestern University, Chicago, IL, USA

⁴ Institute of Bionanotechnology in Medicine, Northwestern University, Chicago, IL, USA

Edited by:

Carissa M. Soto, Naval Research Laboratory, USA

Reviewed by:

Irina Bakunina, Russian Academy of Sciences, Russia

Wenshe R. Liu, Texas A&M University, USA

***Correspondence:**

Michael C. Jewett, Chemical and Biological Engineering, Northwestern University, 2145 Sheridan Road, Tech E-136, Evanston, IL 60208-3120, USA
e-mail: m-jewett@northwestern.edu

Incorporating non-standard amino acids (NSAAs) into proteins enables new chemical properties, new structures, and new functions. In recent years, improvements in cell-free protein synthesis (CFPS) systems have opened the way to accurate and efficient incorporation of NSAAs into proteins. The driving force behind this development has been three-fold. First, a technical renaissance has enabled high-yielding (>1 g/L) and long-lasting (>10 h in batch operation) CFPS in systems derived from *Escherichia coli*. Second, the efficiency of orthogonal translation systems (OTSS) has improved. Third, the open nature of the CFPS platform has brought about an unprecedented level of control and freedom of design. Here, we review recent developments in CFPS platforms designed to precisely incorporate NSAAs. In the coming years, we anticipate that CFPS systems will impact efforts to elucidate structure/function relationships of proteins and to make biomaterials and sequence-defined biopolymers for medical and industrial applications.

Keywords: non-standard amino acids, cell-free protein synthesis, synthetic biology, sequence-defined polymers, genome engineering

INTRODUCTION

The incorporation of non-standard amino acids (NSAAs) into proteins and (poly)peptide-based materials is a key emerging application area in synthetic biology (Liu and Schultz, 2010; Hoesl and Budisa, 2012). In recent years, efforts to incorporate NSAAs using cell-free protein synthesis (CFPS) systems based on *Escherichia coli* have grown significantly. In this mini-review, we discuss these efforts, beginning with a description of the molecular basis for NSAA incorporation in *E. coli* using orthogonal translation systems (OTSS). We then describe CFPS and recent improvements in NSAA incorporation in crude cell extract as well as reconstituted systems of purified components. Finally, we discuss emerging frontiers and opportunities for CFPS.

NSAA INCORPORATION

To date, over 100 OTSSs have been established for site-specific incorporation of NSAAs into proteins (O'Donoghue et al., 2013). Site-specific NSAA incorporation has been used to expand our understanding of biological systems by enabling studies of protein structure and dynamics with unique IR and X-ray diffraction signatures, fluorescent probes, and photocages (Liu and Schultz, 2010). In other examples, cross-linkable NSAAs have been incorporated to characterize protein-protein and protein-nucleic acid interactions (Liu and Schultz, 2010). In addition to expanding the chemistry of biomolecular systems, NSAA technology has also enabled researchers to mimic post-translational modifications of eukaryotic proteins in bacterial protein expression systems. In an exemplary model, site-specific acetylation of recombinant histones by genetically encoding acetyl-lysine (AcK)

elucidated new mechanistic understanding (Neumann et al., 2009).

Beyond fundamental science, NSAA incorporation has also opened the way to novel biopolymer materials, enzymes, and therapeutics which are difficult—if not impossible—to create by other means. Antibody drug conjugates (Zimmerman et al., 2014), modified human therapeutics (Cho et al., 2011), tethered enzymes (Smith et al., 2013), protein polymers (Albayrak and Swartz, in press), phosphoproteins (Park et al., 2011), and selenoproteins (Bröcker et al., 2014) showcase the power of NSAA incorporation. In one example, pegylated human growth hormone showed improved potency and reduced injection frequency (Cho et al., 2011). In another case, an Anti-Her2 antibody bearing *p*-acetyl-L-phenylalanine enabled precise control of conjugation site and stoichiometry for selective and efficient conjugation to an anti-cancer drug resulting in enhanced tumor regression (Axup et al., 2012). These and other recent breakthroughs highlight exciting opportunities for expanding the chemistry of life.

To incorporate NSAAs site-specifically into proteins, OTSSs require (re-)assignment of codons to NSAAs, NSAA-transfer RNA (tRNA) substrates, and ribosome selection of these non-natural substrates into the catalytic center. So far, ribosome accommodation of NSAAs has not been the limiting factor. Rather, strategies to provide for efficient and accurate incorporation of NSAA-tRNA substrates have been the biggest challenge. In practice, this is usually achieved by using orthogonal tRNA (o-tRNA)/aminoacyl-tRNA synthetase (o-aaRS) pairs from phylogenetically distant organisms (Kim et al., 2013). For example, an engineered tRNA^{Tyr}_{CUA}/TyrRS pair derived from *Methanocaldococcus jannaschii* is used frequently for NSAA

incorporation (Wang et al., 2001). More recent expansions of the technology have used variants of the pyrrolysine translation system, tRNA_{CUA}^{PyL}/PylRS from *Methanosarcinaceae* species (Polycarpo et al., 2006; Wang et al., 2012c). There are many seminal works of orthogonal pairs that have been developed for NSAA incorporation to help drive the field forward (Hughes and Ellington, 2010; Wan et al., 2010; Young et al., 2011; Bianco et al., 2012; Wang et al., 2012a,b; Ko et al., 2013; Lee et al., 2013; Niu et al., 2013; Bröcker et al., 2014; Ma et al., 2014). For codon selection, researchers tend to incorporate NSAAAs in response to a non-sense stop codon or quadruplet codon (Wang et al., 2007; Neumann et al., 2010; Niu et al., 2013). The amber codon (TAG) has been the most widely used, because of its low frequency as a stop signal compared to other stop codons (TAA, TGA) (Hoesl and Budisa, 2012).

Figure 1 shows a cartoon representation of an OTS for amber suppression. It also highlights the systems biology challenges associated with NSAA incorporation (O'Donoghue et al., 2013). The orthogonal synthetases have poor catalytic efficiency (Tanrikulu et al., 2009; Nehring et al., 2012; Umehara et al., 2012). Elongation Factor Tu (EF-Tu) has a limited capability to incorporate bulky or charged NSAAAs (Park et al., 2011; O'Donoghue et al., 2013). The presence of release factor 1 (RF1) can cause early termination of proteins when using amber suppression technology (Johnson et al., 2011; Hong et al., 2014). Recent advances have addressed some of these challenges by improving NSAA incorporation efficiency by engineering o-tRNA (Young et al., 2010; Chatterjee et al., 2012), o-aaRS (Liu et al., 1997; Chatterjee et al., 2012), or EF-Tu (Doi et al., 2007; Park et al., 2011) as well as controlling transcription and translation rate (Young et al., 2010; Chatterjee et al., 2013), and removing RF1 competition (Mukai et al., 2010; Johnson et al., 2011; Loscha et al., 2012; Lajoie et al., 2013). While further efforts to re-engineer translation are still needed, these improvements are accelerating rapid growth in synthetic biology efforts to "upgrade protein synthesis" (O'Donoghue et al., 2013). The bulk of this work is being carried out *in vivo*; however, complementary *in vitro* systems are also emerging, which we focus on below.

CELL-FREE PROTEIN SYNTHESIS

CFPS is the synthesis of proteins *in vitro* without using intact, living cells (Jewett et al., 2008; Caschera and Noireaux, 2014). Over the last 50 years, CFPS systems have significantly advanced our ability to understand, exploit, and expand the capabilities of biological systems (Carlson et al., 2012; Swartz, 2012; Murray and Baliga, 2013). As a complement to *in vivo* systems, CFPS systems offer some interesting benefits. First, the open environment of the reaction allows the user to directly influence the biochemical systems of interest and as a result, new components can be added or synthesized and can be maintained at precise concentrations (**Figure 2**). For example, NSAAAs that do not enter the cell can be utilized in CFPS. Second, cell-free systems are not constrained by cell-viability requirements, allowing protein synthesis to proceed with otherwise toxic reagents or protein products. Third, CFPS systems can use linear DNA fragments (e.g., PCR products) for a target gene expression, which avoids time-consuming gene cloning steps commonly required for *in vivo* protein synthesis.

Finally, from a biomanufacturing perspective, cell-free systems separate catalyst synthesis (cell growth) from catalyst utilization (protein production) (Swartz, 2012). This concept represents a significant departure from cell-based processes that rely on microscopic cellular "reactors."

Although CFPS technologies offer many exciting advantages, challenges remain that provide opportunity for improvement. For example, CFPS platforms still have few examples industrially. In addition, cell lysis procedures can be difficult to standardize, leading to different extract performance and limited reaction scales for academic research labs. Thus, while protein yields (mg/L) are often higher in CFPS, the total amount of protein purified from cells in research labs is typically more because the reaction scales are greater. Despite these challenges, the advantages of CFPS are stimulating new application areas. Dominant amongst these are high-throughput protein production (Calhoun and Swartz, 2005; Swartz, 2012; Catherine et al., 2013; Chappell et al., 2013; Murray and Baliga, 2013), clinical manufacture of protein therapeutics (Murray and Baliga, 2013), genetic circuit optimization (Shin and Noireaux, 2012), the construction of synthetic ribosomes (Jewett et al., 2013), and incorporation of NSAAAs (Goerke and Swartz, 2009; Bundy and Swartz, 2010; Ugwumba et al., 2010; Mukai et al., 2011; Ugwumba et al., 2011; Loscha et al., 2012; Albayrak and Swartz, 2013a; Hong et al., 2014; Shrestha et al., 2014).

CRUDE EXTRACT-BASED CFPS FOR NSAA INCORPORATION

Efforts to use crude extract-based CFPS for the production of proteins containing single and multiple NSAAAs are rapidly increasing. Key advances have centered on optimizing the performance of OTSs, expressing the OTS components in the source strain to create one-pot reactions, and removing RF1 competition.

OTS OPTIMIZATION

The Swartz group has made marked contributions to CFPS development for high yielding NSAA incorporation (Goerke and Swartz, 2009; Bundy and Swartz, 2010). Showcasing the freedom of design in adjusting cell-free system components by direct addition to the reaction, their approach typically adds the NSAA and its purified o-aaRS directly to the reaction, while the o-tRNA is expressed during the cell growth prior to making the extract. As compared to *in vivo* systems, an advantage of this approach is that the toxicity associated with overexpressing the o-tRNA and o-aaRS is not observed. This is because the OTS elements are sequestered from each other until the protein synthesis reaction. Another advantage is that NSAAAs with low solubility or poor transport characteristics can be used. For example, the tyrosine analog *p*-propargyloxy-L-phenylalanine (pPaF), which can be used in site-specific bioconjugation with the copper-catalyzed azide-alkyne cycloaddition, has low solubility. This is a known limitation *in vivo*. However, site-specific pPaF incorporation in the CFPS reaction was improved ~27-fold (as based on protein yield) for producing a modified protein when compared to previous *in vivo* approach (Bundy and Swartz, 2010).

Cell-free systems are not only useful for making protein product but also for assessing the catalytic efficiency of the

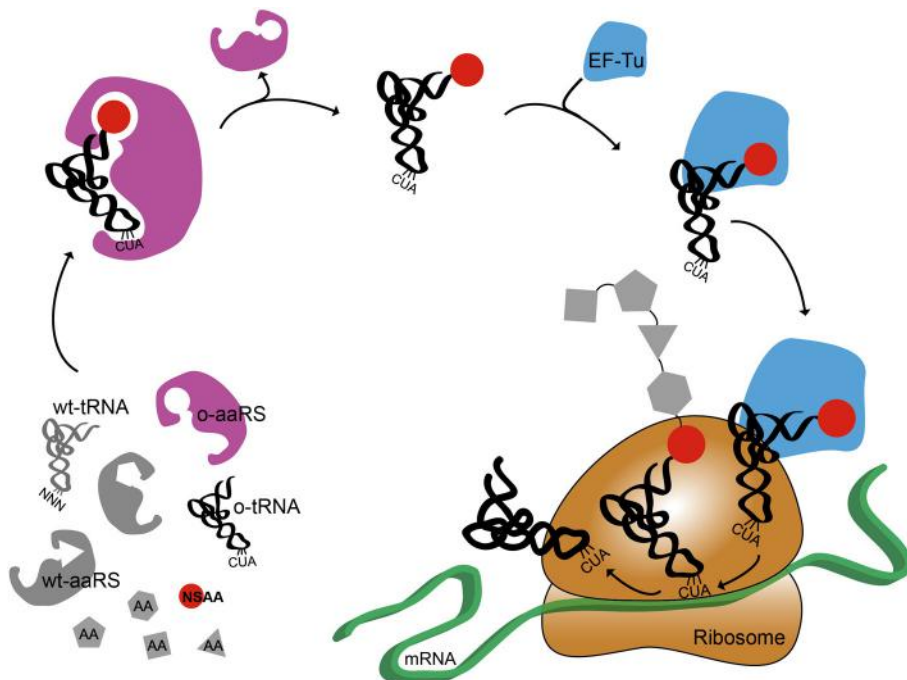


FIGURE 1 | Schematic representation of non-standard amino acid incorporation using an orthogonal translation system.

Orthogonal aminoacyl tRNA synthetase, o-aaRS; orthogonal tRNA, o-tRNA; wild-type aminoacyl tRNA synthetase, wt-aaRS; wild-type

tRNA, wt-tRNA; elongation factor Tu, EF-Tu; non-standard amino acid, NSAA. Anti-codon sequence on wt-tRNA is NNN, where N is A, C, G, or U. Anti-amber codon sequence on o-tRNA is CUA.

OTSs. A growing number of studies, for example, have shown that o-aaRSs are poor catalysts, up to 1000 times worse than natural aminoacyl tRNA synthetases, mainly due to the fact that the evolution of the orthogonal pairs occurs under high concentrations of non-standard amino acids (Tanrikulu et al., 2009; Nehring et al., 2012; Umehara et al., 2012; Albayrak and Swartz, 2013b). Future efforts for improving site-specific NSAA incorporation will require the development of o-aaRSs with higher catalytic rates and stronger affinity for the o-tRNAs. One approach to achieve such desired properties is to find strategies to remove fitness and the health of the cell on evolutionary outcomes. Ellington's lab recently published such an approach, compartmentalized partnered replication (Ellefson et al., 2014), but there are other opportunities as well.

In the meantime, NSAA incorporation in cell-free systems is being improved by increasing the amount of o-tRNA and o-aaRS in the CFPS reaction. One approach to achieving increased o-tRNA levels was pioneered by Albayrak and Swartz (2013a) and validated by Hong et al. (2014). Namely, the o-tRNA is co-produced in the CFPS reaction as a transzyme construct. The transzyme construct is a DNA fragment containing hammer-head ribozyme sequence between T7-controlled promoter and o-tRNA sequences. Upon transcription, the hammer-head ribozyme cleaves 5'-end of tRNA liberating active tRNA into the reaction (Fechter et al., 1998) and thereby increased o-tRNA is supplied to the CFPS reaction. With the transzyme technology, up to 0.9–1.7 mg/mL of a modified protein containing NSAA was produced (Albayrak and Swartz, 2013a) and multiple site NSAA incorporation was improved (Hong et al., 2014). As another approach, there

are efforts to co-express all the OTS components in the source strain. While there are potential concerns of expressing both the o-tRNA and the o-aaRS in the source strain prior to lysis, Bundy and colleagues recently showed that this was not only possible, but improved CFPS yields of a modified protein (Smith et al., 2014). As an alternative approach, natural amino acids have been depleted from crude extracts to allow for the incorporation of NSAA analogs (Singh-Blom et al., 2014).

REMOVING RF1 COMPETITION

NSAA incorporation using amber codon suppression is limited by RF1 competition (Lajoie et al., 2013). The presence of RF1 causes the production of truncated protein and low yields of protein product in the case of multiple identical site-specific NSAA incorporation (Park et al., 2011; Hong et al., 2014). Deletion of RF1 is lethal in native biological systems. However, this limitation was recently addressed by making a more promiscuous release factor 2 (Johnson et al., 2011, 2012), and genome engineering (Mukai et al., 2010; Heinemann et al., 2012; Ohtake et al., 2012). Most notably, the development of the first genetically recoded *E. coli* strain was completed; all 321 TAG stop codons were reassigned to synonymous TAA codons allowing the deletion of RF1 without observing growth defects (Lajoie et al., 2013).

With RF1-deficient *E. coli* strains at hand, efforts are underway to utilize these strains *in vivo* for improved production of proteins with NSAs, but also to develop RF1-deficient CFPS systems. In one example, human histone H4 protein was produced with site-specific incorporation of AcK at four amber sites by using a RF1-deficient cell extract (Mukai et al., 2011). In another

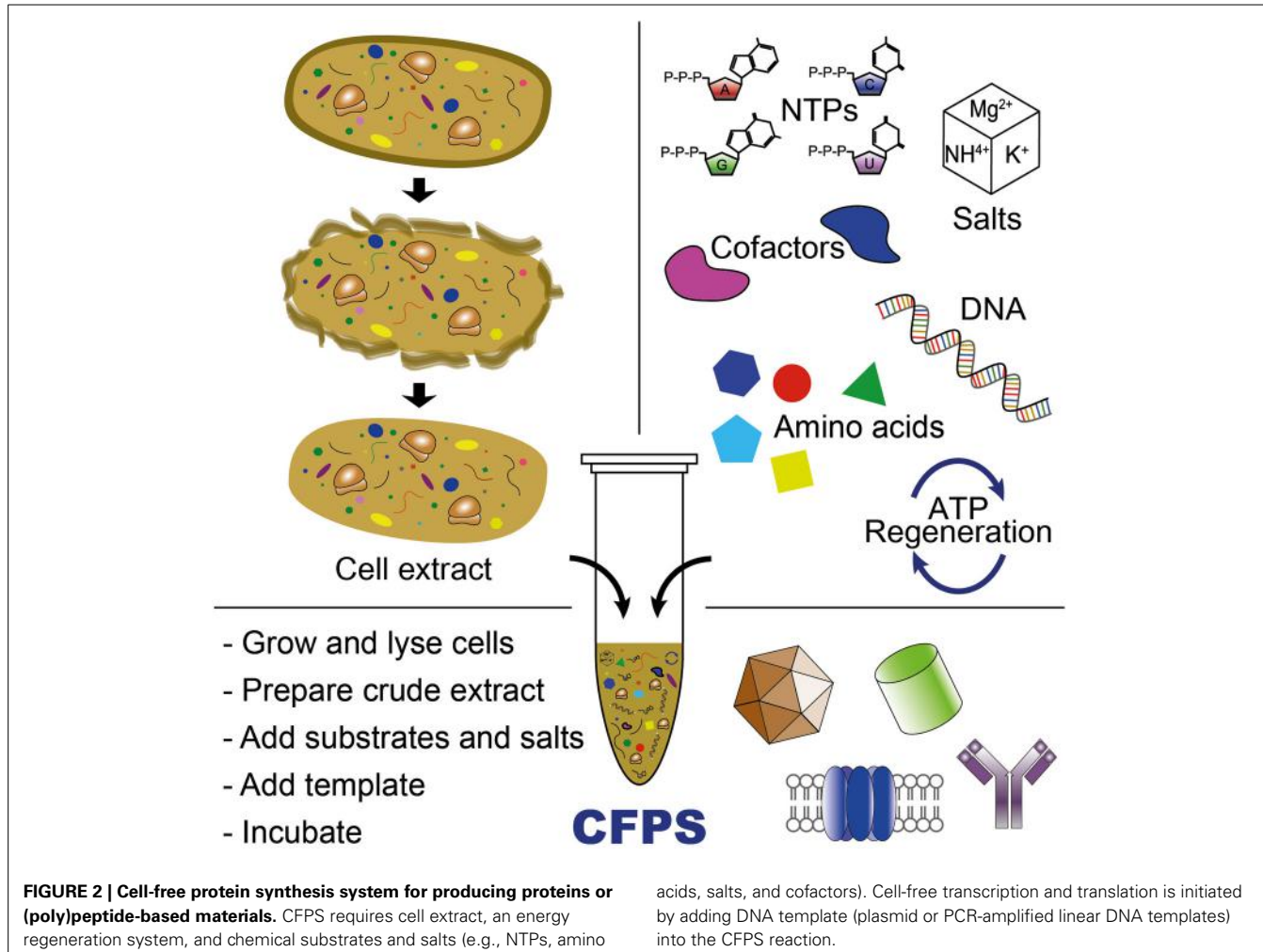


FIGURE 2 | Cell-free protein synthesis system for producing proteins or (poly)peptide-based materials. CFPS requires cell extract, an energy regeneration system, and chemical substrates and salts (e.g., NTPs, amino

acids, salts, and cofactors). Cell-free transcription and translation is initiated by adding DNA template (plasmid or PCR-amplified linear DNA templates) into the CFPS reaction.

case, the effect of RF1 deletion was systematically assessed for single and multiple site pPaF incorporation using cell extracts from genetically recoded *E. coli* with or without RF1 (Hong et al., 2014). The production of modified soluble superfolder green fluorescent protein (sfGFP) containing pPaF was 2.5-fold higher in the RF1-deficient cell extract compared to the RF1-present cell extract. The authors showed that the yield improvement was due to an increase in full-length modified sfGFP synthesis, observing a shift from 20% full-length product (with RF1) to 80% full-length product (without RF1). In a complementary approach, RF1-depleted cell extracts were constructed from selective removal of a RF1 variant tagged with chitin-binding domains (Loscha et al., 2012) or His-tag (Gerrits et al., 2007). Looking forward, we anticipate that RF1-deficient *E. coli* strains will become an important chassis for NSAA incorporation.

RECONSTITUTED *IN VITRO* TRANSLATION FOR NSAA INCORPORATION

Although crude extract-based CFPS systems have shown tremendous growth, there are limitations to the number of open coding channels available because one must grow *E. coli* to obtain cellular lysate. To address this limitation, researchers have turned to

purified translation systems, such as the PURE system (protein synthesis using purified recombinant elements) (Shimizu et al., 2001). Since the user defines all of the elements in the PURE system, single or multiple components (e.g., tRNA, aaRS) can be omitted, increased, or decreased according to the experimental purpose (Hirao et al., 2009). This enables highly efficient sense and non-sense suppression and provides unmatched flexibility for genetic code reprogramming to incorporate NSAAs (Shimizu et al., 2005). Efforts using purified translation for NSAA incorporation have mainly centered on the production, screening, and selection of peptidomimetic, or non-standard peptides (Josephson et al., 2005; Tan et al., 2005; Hartman et al., 2007; Passioura and Suga, 2013). As an exemplary illustration, peptidomimetic synthesis was achieved by adding pre-aminoacylated tRNA with NSAA corresponding to sense codons in the reconstituted translation system lacking aaRS activities (Forster et al., 2003). In an alternative approach, Suga's group has leveraged the highly flexible tRNA acylation Flexizyme technology. Flexizyme is an artificial ribozyme that was developed to charge virtually any amino acid onto any tRNA *in vitro*, allowing the synthesis of proteins and short peptides containing multiple distinct NSAAs (Murakami et al., 2006; Ohuchi et al., 2007). A drug discovery

pipeline has been enabled by combining a modified reconstituted translation system with Flexizyme technology (Goto et al., 2011) for the development of small peptides (Passioura and Suga, 2013), such as macrocyclic peptides (Hayashi et al., 2012; Morimoto et al., 2012). In yet a different approach, Szostak's work has demonstrated the ability to incorporate numerous amino acid analogs using the endogenous machinery. Strikingly, the natural aaRS machinery tolerates many kinds of side chain derivatives, such as α,α disubstituted, *N*-methyl and α -hydroxy derivatives (Hartman et al., 2007). Even D-amino acids have been shown to be compatible with polypeptide elongation (Fujino et al., 2013).

Although PURE translation is a powerful research tool, the cost of the PURE system is prohibitive for most commercial applications. For example, when compared to crude extract-based CFPS systems, which have been scaled to 100 L (Zawada et al., 2011), the PURE system costs \sim 1000 times more on a milligram protein produced/\$ basis (Hong et al., 2014) and yields lower protein titers than the crude extract-based CFPS system (Lee et al., 2012; Hong et al., 2014). Hence, an important design decision for producing proteins with NSAs using cell-free systems is choosing between a crude extract and a purified system.

EMERGING APPLICATIONS

Marked advancements in productivity, improvements in OTS efficiency, and increases in the ability to incorporate multiple identical NSAs (in crude extracts) and multiple distinct NSAs (in the PURE system) are rapidly expanding the possible applications of CFPS systems. In this section, we highlight several emerging applications made possible by these advances. These include the production of protein-based materials and therapeutics.

PROTEIN-BASED MATERIALS

NSAA incorporation is being applied to create new types of sequence-defined polymers for versatile applications in biomaterials synthesis. In an illustrative example, Albayrak and Swartz reported direct polymerization of proteins containing two or three copies of site-specifically incorporated NSAs that allows copper-catalyzed azide-alkyne cycloaddition to form linear or branched protein polymers (Albayrak and Swartz, in press).

THERAPEUTICS

NSAA incorporation is being applied to (i) clinical scale production of protein therapeutics and vaccines, (ii) discovery of novel biologics through ribosome display methods (Murray and Baliga, 2013), and (iii) structure/function studies to identify protein inhibitors. Swartz and colleagues, for example, have developed a novel pipeline for the production of decorated virus-like particles that could function as potential vaccines and imaging agents (Lu et al., 2013). In another example, Sutro Biopharma has demonstrated the synthesis of site-specific antibody drug conjugates (ADCs) (Zimmerman et al., 2014). Their ADCs, which were synthesized at \sim 250 μ g/mL titers, proved potent in cell cytotoxicity assays. Rather than producing a therapeutic using CFPS, Ugwumba et al. utilized the NSAA 7-(hydroxy-coumarin-4-yl) ethylglycine to structurally probe a protein from the West Nile Virus to identify novel inhibitors (Ugwumba et al., 2011). Collectively, these recent reports highlight the utility of CFPS for

producing novel vaccines and therapeutics, as well for serving as a rapid and attractive tool in drug discovery.

CONCLUSION AND OUTLOOK

CFPS has emerged as a promising approach to enable site-specific incorporation of NSAs into proteins and bio-based polymers. With the ability to select peptides and proteins for novel drugs in the PURE system and advent of scalable CFPS from crude extract systems, we anticipate significant growth in the field in years to come. Immediate challenges are (i) the evolution of more efficient OTSs (ii) new codons that can be assigned to NSAs, and (iii) the development of genetically recoded organisms for preparing highly active cellular extracts. Addressing these challenges and continuing to lower costs will expand the scale and scope of cell-free biology, providing a transformative toolbox that enables new frontiers in synthetic biology.

ACKNOWLEDGMENTS

This work was supported by the National Science Foundation (MCB-0943393), the Office of Naval Research (N00014-11-1-0363), the DARPA YFA Program (N66001-11-1-4137), the Army Research Office (W911NF-11-1-044), the NSF Materials Network Grant (DMR - 1108350), the DARPA Living Foundries Program (N66001-12-C-4211), the David and Lucile Packard Foundation (2011-37152), and the Chicago Biomedical Consortium with support from the Searle Funds at the Chicago Community Trust for support. We thank Dr. Javin Oza for critical reading of the manuscript.

REFERENCES

- Albayrak, C., and Swartz, J. R. (2013a). Cell-free co-production of an orthogonal transfer RNA activates efficient site-specific non-natural amino acid incorporation. *Nucleic Acids Res.* 41, 5949–5963. doi: 10.1093/nar/gkt226
- Albayrak, C., and Swartz, J. R. (2013b). Using *E. coli*-based cell-free protein synthesis to evaluate the kinetic performance of an orthogonal tRNA and aminoacyl-tRNA synthetase pair. *Biochem. Biophys. Res. Commun.* 431, 291–295. doi: 10.1016/j.bbrc.2012.12.108
- Albayrak, C., and Swartz, J. R. (in press). Direct polymerization of proteins. *ACS Synth. Biol.* doi: 10.1021/sb400116x
- Axup, J. Y., Bajjuri, K. M., Ritland, M., Hutchins, B. M., Kim, C. H., Kazane, S. A., et al. (2012). Synthesis of site-specific antibody-drug conjugates using unnatural amino acids. *Proc. Natl. Acad. Sci. U.S.A.* 109, 16101–16106. doi: 10.1073/pnas.1211023109
- Bianco, A., Townsley, F. M., Greiss, S., Lang, K., and Chin, J. W. (2012). Expanding the genetic code of *Drosophila melanogaster*. *Nat. Chem. Biol.* 8, 748–750. doi: 10.1038/nchembio.1043
- Bröcker, M. J., Ho, J. M. L., Church, G. M., Söll, D., and O'Donoghue, P. (2014). Recoding the genetic code with selenocysteine. *Angew. Chem. Int. Ed. Engl.* 53, 319–323. doi: 10.1002/anie.201308584
- Bundy, B. C., and Swartz, J. R. (2010). Site-specific incorporation of *p*-propargyloxyphenylalanine in a cell-free environment for direct protein-protein click conjugation. *Bioconjug. Chem.* 21, 255–263. doi: 10.1021/bc9002844
- Calhoun, K. A., and Swartz, J. R. (2005). Energizing cell-free protein synthesis with glucose metabolism. *Biotechnol. Bioeng.* 90, 606–613. doi: 10.1002/bit.20449
- Carlson, E. D., Gan, R., Hodgman, C. E., and Jewett, M. C. (2012). Cell-free protein synthesis: applications come of age. *Biotechnol. Adv.* 30, 1185–1194. doi: 10.1016/j.biotechadv.2011.09.016
- Caschera, F., and Noireaux, V. (2014). Synthesis of 2.3 mg/ml of protein with an all *Escherichia coli* cell-free transcription-translation system. *Biochimie* 99, 162–168. doi: 10.1016/j.biochi.2013.11.025
- Catherine, C., Lee, K.-H., Oh, S.-J., and Kim, D.-M. (2013). Cell-free platforms for flexible expression and screening of enzymes. *Biotechnol. Adv.* 31, 797–803. doi: 10.1016/j.biotechadv.2013.04.009

- Chappell, J., Jensen, K., and Freemont, P. S. (2013). Validation of an entirely *in vitro* approach for rapid prototyping of DNA regulatory elements for synthetic biology. *Nucleic Acids Res.* 41, 3471–3481. doi: 10.1093/nar/gkt052
- Chatterjee, A., Sun, S. B., Furman, J. L., Xiao, H., and Schultz, P. G. (2013). A versatile platform for single- and multiple-unnatural amino acid mutagenesis in *Escherichia coli*. *Biochemistry* 52, 1828–1837. doi: 10.1021/bi4000244
- Chatterjee, A., Xiao, H., and Schultz, P. G. (2012). Evolution of multiple, mutually orthogonal prolyl-tRNA synthetase/tRNA pairs for unnatural amino acid mutagenesis in *Escherichia coli*. *Proc. Natl. Acad. Sci. U.S.A.* 109, 14841–14846. doi: 10.1073/pnas.1212454109
- Cho, H., Daniel, T., Buechler, Y. J., Litzinger, D. C., Maio, Z., Putnam, A.-M. H., et al. (2011). Optimized clinical performance of growth hormone with an expanded genetic code. *Proc. Natl. Acad. Sci. U.S.A.* 108, 9060–9065. doi: 10.1073/pnas.1100387108
- Doi, Y., Ohtsuki, T., Shimizu, Y., Ueda, T., and Sisido, M. (2007). Elongation factor Tu mutants expand amino acid tolerance of protein biosynthesis system. *J. Am. Chem. Soc.* 129, 14458–14462. doi: 10.1021/ja075557u
- Ellefson, J. W., Meyer, A. J., Hughes, R. A., Cannon, J. R., Brodbelt, J. S., and Ellington, A. D. (2014). Directed evolution of genetic parts and circuits by compartmentalized partnered replication. *Nat. Biotechnol.* 32, 97–101. doi: 10.1038/nbt.2714
- Fechter, P., Rudinger, J., Giegé, R., and Théobald-Dietrich, A. (1998). Ribozyme processed tRNA transcripts with unfriendly internal promoter for T7 RNA polymerase: production and activity. *FEBS Lett.* 436, 99–103. doi: 10.1016/S0014-5793(98)01096-5
- Forster, A. C., Tan, Z., Nalam, M. N. L., Lin, H., Qu, H., Cornish, V. W., et al. (2003). Programming peptidomimetic syntheses by translating genetic codes designed *de novo*. *Proc. Natl. Acad. Sci. U.S.A.* 100, 6353–6357. doi: 10.1073/pnas.1132122100
- Fujino, T., Goto, Y., Suga, H., and Murakami, H. (2013). Reevaluation of the d-amino acid compatibility with the elongation event in translation. *J. Am. Chem. Soc.* 135, 1830–1837. doi: 10.1021/ja309570x
- Gerrits, M., Strey, J., Claußnitzer, I., Groll, U. V., Schäfer, F., Rimmele, M., et al. (2007). “Cell-free synthesis of defined protein conjugates by site-directed cotranslational labeling,” in *Cell-Free Protein Expression*, eds W. Kudlicki, F. Katzen, and R. Bennett (Austin, TX: Landes Bioscience), 166–180.
- Goerke, A. R., and Swartz, J. R. (2009). High-level cell-free synthesis yields of proteins containing site-specific non-natural amino acids. *Biotechnol. Bioeng.* 102, 400–416. doi: 10.1002/bit.22070
- Goto, Y., Katoh, T., and Suga, H. (2011). Flexizymes for genetic code reprogramming. *Nat. Protoc.* 6, 779–790. doi: 10.1038/nprot.2011.331
- Hartman, M. C. T., Josephson, K., Lin, C.-W., and Szostak, J. W. (2007). An expanded set of amino acid analogs for the ribosomal translation of unnatural peptides. *PLoS ONE* 2:e972. doi: 10.1371/journal.pone.0000972
- Hayashi, Y., Morimoto, J., and Suga, H. (2012). *In vitro* selection of anti-Akt2 thioether-macrocyclic peptides leading to isoform-selective inhibitors. *ACS Chem. Biol.* 7, 607–613. doi: 10.1021/cb200388k
- Heinemann, I. U., Rovner, A. J., Aerni, H. R., Rogulina, S., Cheng, L., Olds, W., et al. (2012). Enhanced phosphoserine insertion during *Escherichia coli* protein synthesis via partial UAG codon reassignment and release factor 1 deletion. *FEBS Lett.* 586, 3716–3722. doi: 10.1016/j.febslet.2012.08.031
- Hirao, I., Kanamori, T., and Ueda, T. (2009). “Cell-free synthesis of proteins with unnatural amino acids. The PURE system and expansion of the genetic code,” in *Protein Engineering*, eds C. Körber and U. Rajbhandary (Heidelberg: Springer Berlin), 271–290.
- Hoesl, M. G., and Budisa, N. (2012). Recent advances in genetic code engineering in *Escherichia coli*. *Curr. Opin. Biotechnol.* 23, 751–757. doi: 10.1016/j.copbio.2011.12.027
- Hong, S. H., Ntai, I., Haimovich, A. D., Kelleher, N. L., Isaacs, F. J., and Jewett, M. C. (2014). Cell-free protein synthesis from a release factor 1 deficient *Escherichia coli* activates efficient and multiple site-specific nonstandard amino acid incorporation. *ACS Synth. Biol.* doi: 10.1021/sb400140t. [Epub ahead of print].
- Hughes, R. A., and Ellington, A. D. (2010). Rational design of an orthogonal tryptophanyl nonsense suppressor tRNA. *Nucleic Acids Res.* 38, 6813–6830. doi: 10.1093/nar/gkq521
- Jewett, M. C., Calhoun, K. A., Voloshin, A., Wuu, J. J., and Swartz, J. R. (2008). An integrated cell-free metabolic platform for protein production and synthetic biology. *Mol. Syst. Biol.* 4, 220. doi: 10.1038/msb.2008.57
- Jewett, M. C., Fritz, B. R., Timmerman, L. E., and Church, G. M. (2013). *In vitro* integration of ribosomal RNA synthesis, ribosome assembly, and translation. *Mol. Syst. Biol.* 9, 678. doi: 10.1038/msb.2013.31
- Johnson, D. B. F., Wang, C., Xu, J., Schultz, M. D., Schmitz, R. J., Ecker, J. R., et al. (2012). Release factor one is nonessential in *Escherichia coli*. *ACS Chem. Biol.* 7, 1337–1344. doi: 10.1021/cb300229q
- Johnson, D. B. F., Xu, J., Shen, Z., Takimoto, J. K., Schultz, M. D., Schmitz, R. J., et al. (2011). RF1 knockout allows ribosomal incorporation of unnatural amino acids at multiple sites. *Nat. Chem. Biol.* 7, 779–786. doi: 10.1038/nchembio.657
- Josephson, K., Hartman, M. C. T., and Szostak, J. W. (2005). Ribosomal synthesis of unnatural peptides. *J. Am. Chem. Soc.* 127, 11727–11735. doi: 10.1021/ja0515809
- Kim, C. H., Axup, J. Y., and Schultz, P. G. (2013). Protein conjugation with genetically encoded unnatural amino acids. *Curr. Opin. Chem. Biol.* 17, 412–419. doi: 10.1016/j.cbpa.2013.04.017
- Ko, J.-h., Llopis, P. M., Heinritz, J., Jacobs-Wagner, C., and Söll, D. (2013). Suppression of amber codons in *Caulobacter crescentus* by the orthogonal *Escherichia coli* histidyl-tRNA synthetase/tRNA^{His} Pair. *PLoS ONE* 8:e83630. doi: 10.1371/journal.pone.0083630
- Lajoie, M. J., Rovner, A. J., Goodman, D. B., Aerni, H.-R., Haimovich, A. D., Kuznetsov, G., et al. (2013). Genomically recoded organisms expand biological functions. *Science* 342, 357–360. doi: 10.1126/science.1241459
- Lee, K. B., Kim, H.-C., Kim, D.-M., Kang, T. J., and Suga, H. (2012). Comparative evaluation of two cell-free protein synthesis systems derived from *Escherichia coli* for genetic code reprogramming. *J. Biotechnol.* 164, 330–335. doi: 10.1016/j.jbiotec.2013.01.011
- Lee, S., Oh, S., Yang, A., Kim, J., Söll, D., Lee, D., et al. (2013). A facile strategy for selective incorporation of phosphoserine into histones. *Angew. Chem. Int. Ed. Engl.* 52, 5771–5775. doi: 10.1002/anie.201300531
- Liu, C. C., and Schultz, P. G. (2010). Adding new chemistries to the genetic code. *Annu. Rev. Biochem.* 79, 413–444. doi: 10.1146/annurev.biochem.052308.105824
- Liu, D. R., Magliery, T. J., Pastrnak, M., and Schultz, P. G. (1997). Engineering a tRNA and aminoacyl-tRNA synthetase for the site-specific incorporation of unnatural amino acids into proteins *in vivo*. *Proc. Natl. Acad. Sci. U.S.A.* 94, 10092–10097. doi: 10.1073/pnas.94.19.10092
- Loscha, K. V., Herlt, A. J., Qi, R., Huber, T., Ozawa, K., and Otting, G. (2012). Multiple-site labeling of proteins with unnatural amino acids. *Angew. Chem. Int. Ed. Engl.* 51, 2243–2246. doi: 10.1002/anie.201108275
- Lu, Y., Welsh, J. P., Chan, W., and Swartz, J. R. (2013). *Escherichia coli*-based cell free production of flagellin and ordered flagellin display on virus-like particles. *Biotechnol. Bioeng.* 110, 2073–2085. doi: 10.1002/bit.24903
- Ma, Y., Biava, H., Contestabile, R., Budisa, N., and di Salvo, M. L. (2014). Coupling bioorthogonal chemistries with artificial metabolism: intracellular biosynthesis of azidohomoalanine and its incorporation into recombinant proteins. *Molecules* 19, 1004–1022. doi: 10.3390/molecules19011004
- Morimoto, J., Hayashi, Y., and Suga, H. (2012). Discovery of macrocyclic peptides armed with a mechanism-based warhead: isoform-selective inhibition of human deacetylase SIRT2. *Angew. Chem. Int. Ed. Engl.* 51, 3423–2427. doi: 10.1002/anie.201108118
- Mukai, T., Hayashi, A., Irahara, F., Sato, A., Ohtake, K., Yokoyama, S., et al. (2010). Codon reassignment in the *Escherichia coli* genetic code. *Nucleic Acids Res.* 38, 8188–8195. doi: 10.1093/nar/gkq707
- Mukai, T., Yanagisawa, T., Ohtake, K., Wakamori, M., Adachi, J., Hino, N., et al. (2011). Genetic-code evolution for protein synthesis with non-natural amino acids. *Biochem. Biophys. Res. Commun.* 411, 757–761. doi: 10.1016/j.bbrc.2011.07.020
- Murakami, H., Ohta, A., Ashigai, H., and Suga, H. (2006). A highly flexible tRNA acylation method for non-natural polypeptide synthesis. *Nat. Methods* 3, 357–359. doi: 10.1038/nmeth877
- Murray, C. J., and Baliga, R. (2013). Cell-free translation of peptides and proteins: from high throughput screening to clinical production. *Curr. Opin. Chem. Biol.* 17, 420–426. doi: 10.1016/j.cbpa.2013.02.014
- Nehring, S., Budisa, N., and Wiltschi, B. (2012). Performance analysis of orthogonal pairs designed for an expanded eukaryotic genetic code. *PLoS ONE* 7:e31992. doi: 10.1371/journal.pone.0031992
- Neumann, H., Hancock, S. M., Buning, R., Routh, A., Chapman, L., Somers, J., et al. (2009). A method for genetically installing site-specific acetylation in

- recombinant histones defines the effects of H3 K56 acetylation. *Mol. Cell* 36, 153–163. doi: 10.1016/j.molcel.2009.07.027
- Neumann, H., Wang, K., Davis, L., Garcia-Alai, M., and Chin, J. W. (2010). Encoding multiple unnatural amino acids via evolution of a quadruplet-decoding ribosome. *Nature* 464, 441–444. doi: 10.1038/nature08817
- Niu, W., Schultz, P. G., and Guo, J. (2013). An expanded genetic code in mammalian cells with a functional quadruplet codon. *ACS Chem. Biol.* 8, 1640–1645. doi: 10.1021/cb4001662
- O'Donoghue, P., Ling, J., Wang, Y.-S., and Söll, D. (2013). Upgrading protein synthesis for synthetic biology. *Nat. Chem. Biol.* 9, 594–598. doi: 10.1038/nchembio.1339
- Ohtake, K., Sato, A., Mukai, T., Hino, N., Yokoyama, S., and Sakamoto, K. (2012). Efficient decoding of the UAG triplet as a full-fledged sense codon enhances the growth of a *prfA*-deficient strain of *Escherichia coli*. *J. Bacteriol.* 194, 2606–2613. doi: 10.1128/JB.00195-12
- Ohuchi, M., Murakami, H., and Suga, H. (2007). The flexizyme system: a highly flexible tRNA aminoacylation tool for the translation apparatus. *Curr. Opin. Chem. Biol.* 11, 537–542. doi: 10.1016/j.cbpa.2007.08.011
- Park, H.-S., Hohn, M. J., Umehara, T., Guo, L.-T., Osborne, E. M., Benner, J., et al. (2011). Expanding the genetic code of *Escherichia coli* with phosphoserine. *Science* 333, 1151–1154. doi: 10.1126/science.1207203
- Passioura, T., and Suga, H. (2013). Flexizyme-mediated genetic reprogramming as a tool for noncanonical peptide synthesis and drug discovery. *Chem. Eur. J.* 19, 6530–6536. doi: 10.1002/chem.201300247
- Polycarpo, C. R., Herring, S., Béribé, A., Wood, J. L., Söll, D., and Ambrogelly, A. (2006). Pyrrolysine analogues as substrates for pyrrolysyl-tRNA synthetase. *FEBS Lett.* 580, 6695–6700. doi: 10.1016/j.febslet.2006.11.028
- Shimizu, Y., Inoue, A., Tomari, Y., Suzuki, T., Yokogawa, T., Nishikawa, K., et al. (2001). Cell-free translation reconstituted with purified components. *Nat. Biotechnol.* 19, 751–755. doi: 10.1038/90802
- Shimizu, Y., Kanamori, T., and Ueda, T. (2005). Protein synthesis by pure translation systems. *Methods* 36, 299–304. doi: 10.1016/j.ymeth.2005.04.006
- Shin, J., and Noireaux, V. (2012). An *E. coli* cell-free expression toolbox: application to synthetic gene circuits and artificial cells. *ACS Synth. Biol.* 1, 29–41. doi: 10.1021/sb200016s
- Shrestha, P., Smith, M. T., and Bundy, B. C. (2014). Cell-free unnatural amino acid incorporation with alternative energy systems and linear expression templates. *New Biotechnol.* 31, 28–34. doi: 10.1016/j.nbt.2013.09.002
- Singh-Blom, A., Hughes, R. A., and Ellington, A. D. (2014). An amino acid depleted cell-free protein synthesis system for the incorporation of non-canonical amino acid analogs into proteins. *J. Biotechnol.* 178, 12–22. doi: 10.1016/j.jbiotec.2014.02.009
- Smith, M. T., Hawes, A. K., Shrestha, P., Rainsdon, J. M., Wu, J. C., and Bundy, B. C. (2014). Alternative fermentation conditions for improved *Escherichia coli*-based cell-free protein synthesis for proteins requiring supplemental components for proper synthesis. *Process Biochem.* 49, 217–222. doi: 10.1016/j.procbio.2013.10.012
- Smith, M. T., Wu, J. C., Varner, C. T., and Bundy, B. C. (2013). Enhanced protein stability through minimally invasive, direct, covalent, and site-specific immobilization. *Biotechnol. Prog.* 29, 247–254. doi: 10.1002/bptr.1671
- Swartz, J. R. (2012). Transforming biochemical engineering with cell-free biology. *AIChE J.* 58, 5–13. doi: 10.1002/aic.13701
- Tan, Z., Blacklow, S. C., Cornish, V. W., and Forster, A. C. (2005). *De novo* genetic codes and pure translation display. *Methods* 36, 279–290. doi: 10.1016/j.ymeth.2005.04.011
- Tanrikulu, I. C., Schmitt, E., Mechulam, Y., Goddard, W. A., and Tirrell, D. A. (2009). Discovery of *Escherichia coli* methionyl-tRNA synthetase mutants for efficient labeling of proteins with azidonorleucine *in vivo*. *Proc. Natl. Acad. Sci. U.S.A.* 106, 15285–15290. doi: 10.1073/pnas.0905735106
- Ugwumba, I. N., Ozawa, K., de la Cruz, L., Xu, Z.-Q., Herlt, A. J., Hadler, K. S., et al. (2011). Using a genetically encoded fluorescent amino acid as a site-specific probe to detect binding of low-molecular-weight compounds. *Assay Drug Dev. Technol.* 9, 50–57. doi: 10.1089/adt.2010.0306
- Ugwumba, I. N., Ozawa, K., Xu, Z.-Q., Ely, F., Foo, J.-L., Herlt, A. J., et al. (2010). Improving a natural enzyme activity through incorporation of unnatural amino acids. *J. Am. Chem. Soc.* 133, 326–333. doi: 10.1021/ja104166g
- Umehara, T., Kim, J., Lee, S., Guo, L.-T., Söll, D., and Park, H.-S. (2012). *N*-Acetyl lysyl-tRNA synthetases evolved by a CcdB-based selection possess *N*-acetyl lysine specificity *in vitro* and *in vivo*. *FEBS Lett.* 586, 729–733. doi: 10.1016/j.febslet.2012.01.029
- Wan, W., Huang, Y., Wang, Z., Russell, W. K., Pai, P.-J., Russell, D. H., et al. (2010). A facile system for genetic incorporation of two different noncanonical amino acids into one protein in *Escherichia coli*. *Angew. Chem. Int. Ed. Engl.* 49, 3211–3214. doi: 10.1002/anie.201000465
- Wang, F., Niu, W., Guo, J., and Schultz, P. G. (2012a). Unnatural amino acid mutagenesis of fluorescent proteins. *Angew. Chem. Int. Ed. Engl.* 51, 10132–10135. doi: 10.1002/anie.201204668
- Wang, K., Neumann, H., Peak-Chew, S. Y., and Chin, J. W. (2007). Evolved orthogonal ribosomes enhance the efficiency of synthetic genetic code expansion. *Nat. Biotechnol.* 25, 770–777. doi: 10.1038/nbt1314
- Wang, L., Brock, A., Herberich, B., and Schultz, P. G. (2001). Expanding the genetic code of *Escherichia coli*. *Science* 292, 498–500. doi: 10.1126/science.1060077
- Wang, Y.-S., Fang, X., Chen, H.-Y., Wu, B., Wang, Z. U., Hilley, C., et al. (2012b). Genetic incorporation of twelve *meta*-substituted phenylalanine derivatives using a single pyrrolysyl-tRNA synthetase mutant. *ACS Chem. Biol.* 8, 405–415. doi: 10.1021/cb300512r
- Wang, Y.-S., Fang, X., Wallace, A. L., Wu, B., and Liu, W. R. (2012c). A rationally designed pyrrolysyl-tRNA synthetase mutant with a broad substrate spectrum. *J. Am. Chem. Soc.* 134, 2950–2953. doi: 10.1021/ja211972x
- Young, D. D., Young, T. S., Jahnz, M., Ahmad, I., Spraggon, G., and Schultz, P. G. (2011). An evolved aminoacyl-tRNA synthetase with atypical polysubstrate specificity. *Biochemistry* 50, 1894–1900. doi: 10.1021/bi101929e
- Young, T. S., Ahmad, I., Yin, J. A., and Schultz, P. G. (2010). An enhanced system for unnatural amino acid mutagenesis in *E. coli*. *J. Mol. Biol.* 395, 361–374. doi: 10.1016/j.jmb.2009.10.030
- Zawada, J. F., Yin, G., Steiner, A. R., Yang, J., Naresh, A., Roy, S. M., et al. (2011). Microscale to manufacturing scale-up of cell-free cytokine production—a new approach for shortening protein production development timelines. *Biotechnol. Bioeng.* 108, 1570–1578. doi: 10.1002/bit.23103
- Zimmerman, E. S., Heibeck, T. H., Gill, A., Li, X., Murray, C. J., Madlansacay, M. R., et al. (2014). Production of site-specific antibody-drug conjugates using optimized non-natural amino acids in a cell-free expression system. *Bioconjug. Chem.* 25, 351–361. doi: 10.1021/bc400490z
- Conflict of Interest Statement:** The authors declare that the research was conducted in the absence of any commercial or financial relationships that could be construed as a potential conflict of interest.
- Received:** 15 March 2014; **accepted:** 19 May 2014; **published online:** 10 June 2014.
- Citation:** Hong SH, Kwon Y-C and Jewett MC (2014) Non-standard amino acid incorporation into proteins using *Escherichia coli* cell-free protein synthesis. *Front. Chem.* 2:34. doi: 10.3389/fchem.2014.00034
- This article was submitted to Chemical Biology, a section of the journal *Frontiers in Chemistry*.
- Copyright © 2014 Hong, Kwon and Jewett. This is an open-access article distributed under the terms of the Creative Commons Attribution License (CC BY). The use, distribution or reproduction in other forums is permitted, provided the original author(s) or licensor are credited and that the original publication in this journal is cited, in accordance with accepted academic practice. No use, distribution or reproduction is permitted which does not comply with these terms.